THE UNIVERSITY
of EDINBURGH

This thesis has been submitted in fulfilment of the requirements for a postgraduate degree (e.g. PhD, MPhil, DClinPsychol) at the University of Edinburgh. Please note the following terms and conditions of use:

This work is protected by copyright and other intellectual property rights, which are retained by the thesis author, unless otherwise stated.
A copy can be downloaded for personal non-commercial research or study, without prior permission or charge.
This thesis cannot be reproduced or quoted extensively from without first obtaining permission in writing from the author.
The content must not be changed in any way or sold commercially in any format or medium without the formal permission of the author.
When referring to this work, full bibliographic details including the author, title, awarding institution and date of the thesis must be given.

Modelling and Optimisation of Energy Systems with Thermal Energy Storage

Renaldi

Doctor of Philosophy

The University of Edinburgh

2018

Lay Summary

Our energy system is currently undergoing a major transitional change from fossil fuels-dominated towards low-carbon and renewable energy-based system. Climate change and security of energy supply are among the main reasons behind this movement. Naturally, numerous challenges are unavoidable considering the massive scale of the change.

One particular challenge is to overcome the intermittent or even uncertain characteristic of several renewable energy sources. For example, solar energy is available during the day, while typical household energy consumption peaks in the morning and evening. In the case of wind and ocean wave energy, their availability may not coincide with the energy demand. A solution to this problem is to use energy storage equipment.

Thermal energy or heat storage is selected as the studied energy storage technology in this thesis. It is because heating has a significant share in the UK energy consumption, with up to triple the size of electricity demand during the winter period compared to the summer. Therefore, the transition to low-carbon and renewable energy in the heating sector is imperative if significant progress is to be made in the whole energy system. Furthermore, thermal energy storage can also be implemented as a seasonal storage, for example, to store solar energy in the summer for heating in the winter.

Nevertheless, the use of energy storage will increase the complexity of designing and operating an energy system. It is because rather than simply matching the supply and demand of energy, the questions now become more open-ended: when should we store the energy? what size of storage needs to be installed? and where should it be placed?

This thesis focuses on two interrelated topics: (i) how thermal energy storage contributes towards renewable-based domestic heating systems, and (ii) how design tools can be adapted so they can manage the increasing complexity that comes with the inclusion of thermal energy storage. These topics are analysed and discussed using two illustrative case studies. The first case study represents a residential heating system, while the second case study illustrates a community heating system.

Abstract

One of the main challenges in the implementation of renewable energy is the mismatch between supply and demand. Energy storage has been identified as one of the solutions to the mismatch problem. Among various storage technologies, thermal energy storage (TES) is foreseen to have a significant role to achieve a low carbon energy systems because of the large share of thermal energy demand and its relatively low cost. However, integrating TES into energy systems requires careful design and implementation since otherwise potential financial and environmental savings may not be achieved.

Computational-based design tools are ubiquitous in the design process of modern energy systems and can be broadly categorised into two methodologies: optimisation and simulation. In both cases, designing an energy system with storage technology is significantly more complicated than those without, mainly due to the coupling of variables between time steps.

This thesis is concerned with two facets of the application of TES in energy systems. First, the role of TES in improving the performance of renewable-based domestic heating systems. Second, the implementation of optimisation and simulation tools in the design of energy systems with integrated TES. They are addressed by examining two case studies that illustrate the spatial and temporal variance of energy systems: a single dwelling heat pump system with a hot water tank, and a solar district heating system with a borehole thermal energy storage.

In the single dwelling case study, the technical and financial benefits of TES installation in a heat pump system are illustrated by the optimisation model. A simulation model which utilises the optimisation results is developed to assess the accuracy of the optimisation results and the potential interaction between the two methodologies.

The solar district heating case study is utilised to highlight the potential of a time decomposition technique, the multiple time grids method, in reducing the computational time in the operational optimisation of the system. Furthermore, the case study is also employed to illustrate the potential of installing a similar system in the UK. The latter study was performed by developing a validated simulation model of the solar district heating system.

The findings of the analyses reported in this thesis exemplify the potential of TES in a domestic and community-level heating system in the UK. They also provide a basis for recommendations on the improved use of optimisation and simulation tools in the design process of energy systems.

Acknowledgements

This is the part of the thesis in which one is allowed to waffle. I (over)indulge this opportunity, so here I go.

First and foremost, I would like to thank my PhD supervisor, Dr. Daniel Friedrich, for his guidance, knowledge, patience, and for believing in me. I cannot ask for a better role model on how to be a good researcher in general and an early-career academic in particular. Our weekly meeting is something that I always look forward to, be it to report research progress (or the lack of it), bounce new ideas, debugging a piece of code, and sharing conference experience. From the Skype interview for the PhD position up to reviewing and submitting this thesis, from discussing linear programming and district heating simulation up to *hagelslag* and Pearl Jam, it has been a great pleasure to work with you in the past 3.5+ years. And yes, I have been a very happy student indeed.

My gratitude also goes to my second supervisor, Dr. Aristides Kiprakis. His comments and suggestions on my work are always spot-on. I am also grateful to Prof. Win Rampen for assessing my first year report and presentation. I would also thank Prof. Markus Mueller, the head of Institute for Energy Systems, for supporting me in my travel scholarship application and for being a good leader for all of us in IES. During the course of my PhD, I have been involved in tutoring Energy Systems 4 on two different occasions. For this, I thank Dr. Hannah Chalmers for giving me the opportunity.

While still in the academics part of this acknowledgement, I would like to send my gratitude to several academics who have set good examples for me over the years during my academic journey: Prof. Yatna Yuwana Martawirya and Prof. Pulung Nurprasetio (Bandung Institute of Technology, Indonesia) for all your support since I was an undergrad student many years ago; Dr. Camilo Rindt (Eindhoven University of Technology, Netherlands) for guiding me in my first steps in sustainable energy research and for your kind support even long after I graduated from TU/e; Dr. Giuseppe Ingarao (University of Palermo, Italy) for all the support and suggestions in recent years.

I have spent most of my PhD years in the Power Lab, where my officemates and I enjoyed the secluded, (mostly) quite, and spacious workplace. Obviously, my officemates deserve a dedicated paragraph in this section. Thank you: Will Ubani for all the help, jokes, serious discussions, LaTeX-buddy, and of course, the ultimate milkman story (I should say "we" thank you for this one). Marios Sousounis for all the lunches and source of early fatherhood tips, including a hands-on tutorial on putting up an infant car-seat. Hawwoi Chuan for anecdotes around the alternative way to find funding, you should

write a book about this, Howy. J.P. Echenique for his overall wisdom, being the most senior student and all, not to mention the best desk in the lab. Leong-Kit Gan for the second best desk in the lab, which I occupied for only seven months. Xiaoyun Rong for tips on buying a good chair for work. Ricardo Lopez for keep asking me to go for lunch, and vice-versa, until we realised that our lunch time was not compatible. Jan Bernholz for all the walks and talks. Damiano D'Aguanno for all the discussions around movies, the usual stuff, and, well to some extent, research. Chuan Qin for illustrating how fast one year could go by. Jesús Lizana for being the only other thermal guy in the room, before Serguey Maximov arrived. Syahin Zaini for sharing the night- and weekend-shift in Alrick 2.2 during the wrapping up of this thesis. And finally, thanks to Douglas Carmichael for keeping all of us safe in the lab.

Being a part of IES has exposed me to all spectrum of energy research, along with their researchers. Thank you, Ruben Bravo for our research and life-related chit chat whenever we bumped into each other, be it Faraday's kitchen, Mayfield Road, Tesco, and even Cameron Toll. Thomas Spitz, thanks a lot for all your help over the years, I learn that moving can become quite a competitive feat. Krisna Pawitan, my only fellow countryman in IES, it's been good to know that I can speak my mother tongue at work every now and then. Maggie Creed for introducing me to Lessells travel scholarship and helping me in my application. I would also like to send my gratitude to the IES seminar team who have done a great job in keeping us doing a research-related activity on Friday lunch time. During my time at IES, this means saying thanks to: Susan Tully, Anna Dunbar, Joe Burchell, Monika Kreitmair, Alex Kleidaras, Nicola Speranza, Ben McGilton, Kevin Kails, and Ross Calvert.

During my graduate years, I have crossed paths with remarkable people who I believe contributed to the way I work on my PhD research and write this thesis, in one way or another. Dimitrios Petalios and Maria Baka, for both of you I will simply say: *Euxaristo poly, teman-teman.* Yelin Deng, Dimos Paraskevas, Yansong Guo, and Karel Kellens, thank you for all the discussions on LCA, energy, and resource efficiency. Jaime Undurraga, for all the Dutch practice and music quiz, as well as the exemplary acknowledgement section of your thesis, which style I copied over here. I would also like to send a big thank you to Mattia Vallerio, Carlo Annaratone, Koosha Paridel, Enrico Di Lello, and Eirini Velliou.

Being abroad for so many years, there have been those old friends whose companionship transcends the distance. Thank you: Adriansyah, for the friendship, second opinions, and of course, metal. Wayan Santika, for the camaraderie during our time at SET TU/e and beyond, good luck with your PhD, beh. Pak Taufik, for the question mark message and De Metafoor forum. Thanks are also due to these people who shared the start of my postgraduate journey: Agni Yudo, Samuel Louvan, Arya Adriansyah, Grant Kesuma,

and Jimmy Syafrizal.

My parents have given me the constant and unquestionable support throughout my life, *Terimakasih, Bapak, Ibu.* My sister, Finda, thank you for sharing the same sense of humour. I would also like to acknowledge my late grandmother for her relentless support. *Dank u wel, Oma. Ik hoop dat ik je trots heb gemaakt.*

My dear wife, Marisza, where do I even begin? It is beyond me how I would be able to do all of this without your love and support. You have seen and shared the highs, you have witnessed and withstand the lows. Thank you for everything. After your patience in listening to thermal energy storage, optimisation, and simulation in the past 3.5 years, it is my turn to hear about periodontal diseases, mixed-method, and dental public health.

The last person in this section is also the youngest: my daughter, Minerva. Joining us exactly on the last day of my third PhD year, you are definitely the accelerator in the process of writing-up this thesis. Although you are way too young to understand it now, I hope someday this thesis could become my example to you in illustrating the importance of perseverance, self-belief, and doing what you love in life. For now, let's stick to how Betty the baby gorilla goes bananas in her pyjamas.

Edinburgh, October 2017

Renaldi

Declaration

I declare that this thesis was composed by myself, that the work contained herein is my own except where explicitly stated otherwise in the text, and that this work has not been submitted for any other degree or professional qualification except as specified.

Renaldi

Contents

List of Figures

List of Tables

List of Symbols

δ^i	Time step size of equipment i	[h]
ϵ^i	Time point set of equipment i	[-]
η^i	Efficiency of equipment i	[-]
$\psi^j_{ch,t}$	Binary charge status of storage j at time step t	[-]
$\psi^j_{dch,t}$	Binary discharge status of storage j at time step t	[-]
τ	Time of the cash flow	[year]
ζ^i_t	Binary operational status of equipment i at time step t	[-]
ϕ^j	Loss fraction of storage j	[%]
A	Surface area	[m^2]
c_p	Specific heat capacity	[kJ/(kg·K)]
C_{inv}	Investment cost	[£, €, or $]
C^i_{inv}	Investment cost of equipment i	[£, €, or $]
C^i_{in}	Input energy cost of equipment i	[£, €, or $/kWh]
C_{opr}	Operational cost	[£, €, or $]
C_{tot}	Total cost	[£, €, or $]
G_T	Solar irradiance at the surface	[W/m^2]
HH	Heating hours	[h]
k_1	First signature variable in synthetic heat demand equation	[kW/°C]
k_2	Second signature variable in synthetic heat demand equation	[kW]
LF_{min}	Minimum load factor	[-]
$\dot{m}$	Mass flow rate	[kg/s]
$P^i_{in,t}$	Electrical power input to equipment i at time step t	[kW]
$\dot{Q}^i_{nom}$	Nominal capacity of equipment i	[kW]
$\dot{Q}_t$	Rate of thermal energy at time step t	[kW]
Q^{DEM}_{annual}	Annual heat demand	[kWh]
$Q^j_{sto,t}$	Energy content of storage j at time step t	[kWh]

Q^j_{max}	Maximum storage capacity of storage j	[kWh]
$\dot{Q}^j_{ch,t}$	Rate of energy charged to storage j at time step t	[kW]
$\dot{Q}^j_{ch,max}$	Maximum charge rate of storage j	[kW]
$\dot{Q}^j_{dch,t}$	Rate of energy discharged from storage j at time step t	[kW]
$\dot{Q}^j_{dch,max}$	Maximum discharge rate of storage j	[kW]
R	Revenue	[£, €, or $]
r	Discount rate	[%]
SOC^j_t	State of charge of storage j at time step t	[kWh]
t^{ac}	Active time	[h]
t^{ic}	Inactive time	[h]
T_{ext}	External air temperature	[°C]
T_{in}	Inlet temperature	[K]
T_{lift}	Temperature lift in a heat pump	[°C]
T_{out}	Outlet temperature	[K]
T^{ac}_{thld}	Threshold temperature during active time	[°C]
T^{ic}_{thld}	Threshold temperature during inactive time	[°C]
y_i	Discrete variable to show installation status of equipment i	[-]

List of Abbreviations

ATES	Aquifer Thermal Energy Storage
BOI	Boiler
BTES	Borehole Thermal Energy Storage
CHP	Combined Heat and Power
COP	Coefficient of Performance
DEM	Heat Demand
DHW	Domestic Hot Water
DLSC	Drake Landing Solar Community
DLSP	Drake Landing Set-Point
E7	Economy 7
E10	Economy 10
GA	Genetic Algorithm
GHG	Greenhouse Gases
HP	Heat Pump
HX	Heat Exchanger
IP	Integer Programming
LCOE	Levelised Cost of Energy
LP	Linear Programming
LTS	Long Term Storage
MILP	Mixed Integer Linear Programming
MINLP	Mixed Integer Non-Linear Programming
MKEP	Milton Keynes Energy Park
MNU	Multiple Non-Uniform
MU	Multiple Uniform
NLP	Non-Linear Programming
PCM	Phase Change Materials
PSO	Particle Swarm Optimisation
PTES	Pit-water Thermal Energy Storage
RH	Resistive Heater
RHI	Renewable Heat Incentive
SBS	Scottish Building Standard
SCO	Solar Collector
SF	Solar Fraction

SNU	Single Non-Uniform
SPF	Seasonal Performance Factor
ST	Solar Thermal
STS	Short Term Storage
SU	Single Uniform
TES	Thermal Energy Storage
TRNSYS	Transient System Simulation Tool
TTES	Tank Thermal Energy Storage

Chapter 1

Introduction

1.1 Overview

Thermal energy provision has a significant share in the total final energy use worldwide. In 2010, space heating alone represented 32-34% of the global final energy consumption in both residential and commercial building sectors (Lucon *et al.*, 2014). If water heating and cooling are included, these shares increase to 58% and 52% for residential and commercial sectors, respectively. A similar situation also occurs in the UK, where thermal energy (heat) corresponds to 45% of the overall energy consumption end use (Department of Business, Energy Industrial Strategy, 2017b). From this heat demand, space heating has the largest share of 68%, followed by industrial process use (14%), and water heating (10%). Fossil fuels remain the main primary energy source to satisfy the UK heat demand with approximately 80% share in 2016, with natural gas as the largest contributor (Department of Business, Energy Industrial Strategy, 2017b).

The UK and Scottish Government have acknowledged the importance of the decarbonisation of the heating sector towards achieving the Carbon Budget targets set in the Climate Change Act, i.e. net carbon account in 2050 is at least 80% lower than the 1990 baseline (Crown, 2008). This recognition has been implemented by the current and forthcoming heat-specific policies, e.g. Heat Policy Statement (The Scottish Government, 2015)).

One option to achieve heat decarbonisation is to use renewable-based heating systems, such as utilising solar thermal energy and electricity generated from renewable sources. However, supply-demand mismatch due to the daily and seasonal variation of most renewable sources can limit the potential impacts of this effort. Storing the energy in thermal energy storage (TES) can help to alleviate the mismatch problem by providing a buffer between supply and demand. At present, TES solution is also cheaper than storing electricity in batteries for the same energy to power ratio (World Energy Council, 2016).

The most common TES technology in the UK is the domestic hot water tank, with installations in approximately 14 million households, which gives a maximum combined

storage capacity of around 80 GWh (Taylor *et al.*, 2012). Most of them were introduced in the 1970s due to the requirement for systems with non-condensing boilers. As domestic heating systems progress with the now widely installed condensing boilers, the installation of this type of TES has been declining (Institution of Mechanical Engineers, 2014). However, there has been renewed interests in domestic TES technology, including hot water tanks, due to their potential role in heat decarbonisation strategies, such as heat electrification through heat pumps and its corresponding demand side management capabilities (Hewitt, 2012; Arteconi *et al.*, 2013).

Given that TES installation corresponds to extra investment cost for the user, along with extra space requirement, its benefits have to be well-founded and include the financial consideration from the perspective of the users. Otherwise, the potential of domestic TES in decarbonising the heating system may not be realised.

In addition to short-term TES, such as domestic hot water tanks with operating cycle on a daily or several days basis, long-term TES technology has also been shown to contribute to the increase in renewable-based heating systems, particularly with solar district heating systems in Europe (Perez-Mora *et al.*, 2017). They have monthly up to seasonally operating cycle, for instance, to store the abundant solar energy in the summer to be used later in the winter. The potential application of long-term TES in the UK, particularly for district heating system, has been briefly mentioned in several recent reports (Eames *et al.*, 2014; Radcliffe and Li, 2015).

For a large installation integrated with long-term TES, it is imperative to move beyond qualitative discussions in assessing its feasibility. A quantitative assessment can provide not only numbers to different metrics, but also inform policymaking to ensure the resulting policies to foster the technology deployment are well-substantiated.

Integrating TES into energy systems requires careful design and implementation since otherwise potential financial and environmental savings may not be achieved. Computational design tools are ubiquitous in the design process of modern energy systems. These range from relatively simple spreadsheet-based tools for a quick feasibility assessment up to the more complex numerical method-based tools for in-depth evaluations. These tools can be broadly categorised into two methodologies: optimisation and simulation. Optimisation aims to find the best solution to the design problem, typically employing highly simplified models of reality. Simulation, on the other hand, seeks to describe the physical phenomena of interest involved in the system, usually using models closer to reality than in optimisation. Although typically performed separately, there are several possibilities to link between the two methodologies, with the aim of harnessing their strengths while minimising their respective drawbacks.

Regardless of the methodologies, designing an energy system with integrated storage

technology is invariably more complicated than those without, mainly due to the coupling of variables between time-steps. For instance, in an optimisation, the decision to charge or discharge a storage within a time step will affect the operational decision of the time steps. In a simulation, additional control assumptions have to be defined to ensure the added flexibility due to storage is appropriately considered. As the designed energy systems grow, either spatially, temporally, or both, this increasing complexity has to be managed carefully to preserve the tractability of the model and avoid excessive computational time.

In order to quantitatively assess the technical and financial performance of TES in the scope of heat decarbonisation in the UK, optimisation and simulation tools can be utilised in analysing the considered energy systems. This thesis explores the potential role of short- and long-term TES in the UK by using both optimisation and simulation tools, and develops a method to limit the increasing problem complexity which arises due to the presence of energy storage technology.

1.2 Aims and objectives

The aims of this thesis are twofold. Firstly, to investigate the potential role of thermal energy storage in facilitating domestic heat decarbonisation in the UK. Secondly, to evaluate two design tools, namely optimisation and simulation, in designing energy systems with thermal energy storage.

The following objectives form a pathway to fulfilling the thesis aims:

1. To explore how thermal energy storage contributes to improving the performance of renewable-based domestic heating systems in the UK.
2. To investigate the feasibility of long-term thermal energy storage to address the seasonal mismatch between solar energy and heat demand in the UK.
3. To examine the role of optimisation and simulation in designing thermal systems on a residential and community level.
4. To evaluate methods to manage increasing complexity in optimising and simulating energy systems with thermal energy storage.

1.3 Contribution to knowledge

The work presented in this thesis focuses on thermal systems simulation and optimisation, with perspective from energy systems, mechanical engineering, and mathematical optimisation. Although the analyses performed in this thesis are based on specific case studies, the methodologies presented could be applied to other similar energy systems. The following results can be considered an original contribution to knowledge:

- **The design and operational optimisation of thermal energy storage integration in a residential heat pump heating system.** Heat pump and thermal energy storage are one of the potential combinations to lower the carbon intensity of residential heating systems. Design and operational optimisation of such system was performed to identify the influence of electricity time-of-use tariff and a policy-based financial incentive in improving the financial performance.
- **The evaluation of a potential interaction between the optimisation and simulation methodology.** A simulation model which uses the results from optimisation is developed based on the residential heating system case study. The results of simulation and optimisation are compared and further assessed.
- **The implementation of a temporal decomposition technique in the operational optimisation of an energy system.** A complexity reduction method called the multiple time grids is implemented in the operational optimisation of a community-sized energy system. It is shown that the multiple time grids method can significantly reduce computational time of the problem while maintaining an acceptable level of accuracy.
- **The techno-economic evaluation of a solar district heating system in UK locations.** Feasibility of a solar district heating system in UK locations has been quantified using a validated simulation model. The results illustrate that a solar district heating system is technically feasible to be implemented in the UK. The relatively lower solar fraction can be offset by installing long-term storage and implementing the system to supply new-built houses with better energy performance than older homes.

It is expected that the methodologies and analyses presented in this thesis will be pertinent to those engaged in energy systems research, energy policy making, and others involved in the planning, design and operation of residential and community-level energy systems.

1.4 Thesis structure

The thesis consists of seven chapters, with necessary appendices.

Chapter 2 gives an overview of energy systems and thermal energy storage. The chapter discusses potential contributions of thermal energy storage in the present and future energy systems. Furthermore, the optimisation and simulation approach in the design of energy systems are briefly reviewed. The chapter ends with the identified knowledge gaps, which are addressed further in the thesis.

Chapter 3 presents the general methodology used in the thesis. A generic energy system is employed to illustrate both the optimisation and simulation model. A method to generate synthetic heat demand profiles is also explained. The chapter also includes information on the modelling tools used throughout the thesis.

Chapter 4 describes how optimisation and simulation can be applied in the design of a residential heating system, which main equipment includes heat pump and hot water storage tank. The influence of renewable heat incentive (RHI) subsidy on the total cost of different system configurations are also shown using the optimisation results. The comparative interaction between optimisation and simulation, as described in Chapter 2, is analysed using the results of both optimisation and simulation studies.

Chapter 5 focuses on the implementation of the multiple time grids approach in the operational optimisation of an energy system. It is applied in the optimisation of a case study, Drake Landing Solar Community district heating system. The influence of using multiple time grids on computational time and accuracy of results are elaborated further in the chapter.

Chapter 6 details how a simulation model can be employed to investigate the techno-economic feasibility of a solar district heating system in the UK. A validated simulation model of Drake Landing Solar Community is developed and formed the basis of the techno-economic study performed in this chapter. Systems performance in UK locations are reported, as well as the comparison with benchmark values. A parametric study shows the influence of different parameters on the performance metrics of the system.

Chapter 7 summarises the results obtained in this thesis, and recommends potential directions for future work.

Chapter 2

Energy systems and thermal energy storage

2.1 Introduction

Energy systems consist of all components related to the production, conversion, delivery, and use of energy (Intergovernmental Panel on Climate Change, 2014). The forms of energy involved include primary energy (e.g. coal, crude oil, natural gas, and renewable sources) and secondary energy form (e.g. fuel products, electricity, and heat). Energy systems can range in scope according to its spatial characteristic, ranging from building, local, municipal, regional, national, and global level. At the global level, energy systems study is typically concerned about the supply chain of primary energy resources. At the national level, electricity and natural gas network are two examples of main energy systems. At the local and municipal level, other vectors such as heat might be considered, together with individual building energy demand. At the building level, occupants use profile and comfort play significant roles in energy system design and operation.

The supply sector in energy systems remains the largest contributor to global greenhouse gas (GHG) emissions (Bruckner *et al.*, 2014). As defined in the IPCC report, the energy supply sector includes all energy extraction, conversion, storage, transmission, and distribution processes that deliver final energy to the end-use sectors (Bruckner *et al.*, 2014). In the UK, the energy supply sector was responsible for 29% of GHG emissions in 2015 (Department of Business, Energy Industrial Strategy, 2017a). This is mainly due to the use of coal and natural gas in electricity production. In absolute terms, the UK energy supply GHG emissions have experienced a 48% reduction between 1990 and 2015 (Department of Business, Energy Industrial Strategy, 2017a). This is attributed to efficiency improvements, fuel switching from coal to natural gas, and the growth of renewable energy technologies. Renewable energy contributed around 22% and 6% to 2015 UK electricity and heat generation, respectively (Department of Business, Energy Industrial Strategy, 2016). These values need to be increased in order to further reduce the GHG emissions of energy supply, especially if the Climate Change Act target to reduce emissions by at least 80% by 2050 is to be met (Committee on

Climate Change, 2017).

One of the main challenges in the implementation of renewable energy is the mismatch between supply and demand. For example, solar energy supply has its peak during the day, while both residential electricity (for photovoltaic) and heat (for solar thermal) demand are typically peaking in the morning and early evening. Fig. 2.1 illustrates this issue using the gas consumption per heated floor area of a house in the Milton Keynes Energy Park development and the corresponding solar irradiance on a horizontal plane. Similar situations can also occur in the case of wind energy when periods of low wind availability coincide with high demand.

Furthermore, the mismatch can be present not only in an hourly and daily timescale but also monthly and seasonally. Fig. 2.2 shows the seasonal variation of heat demand and solar energy for the same house as in Fig. 2.1. The heat demand is highest during the winter and lowest during the summer, while the opposite is true for the solar energy.

Energy storage has been identified as one of the solutions to the mismatch problem. It allows decoupling between energy supply and demand by providing a buffer to store the surplus energy produced. Energy vectors that can be stored with currently available technologies include electrical, mechanical, thermal, and chemical energy. In addition to the form of the stored energy, storage technologies can also be categorised and mapped based on their capacity and temporal characteristics, e.g. discharge time, as illustrated in Fig. 2.3.

Fig. 2.3 also shows the demand applications relative to the current and emerging storage technologies. Regarding heat demand and thermal storage, it is interesting to note that there is already an overlap between household peaking demand and domestic hot water storage, as well as between community seasonal space heating demand and underground storage. Furthermore, the UK aggregate domestic hot water storage capacity is within the range of wind power variability. This illustrates the potential role of domestic hot water storage and other thermal energy storage technologies in demand side modelling of electric power networks.

In order to get a better view on the scale of daily energy demand, it is useful to see the electricity and heat demand profile over a time horizon, as shown in Fig. 2.4 for the case of United Kingdom. Here the natural gas demand was used as a proxy for heat demand as most of the heat demand in the UK are covered by natural gas boilers. It can be seen that the daily heat demand is significantly larger than the electricity demand for most of the time in a year. Furthermore, the heat demand exhibits a seasonal pattern with high demand in the winter and low in the summer. On the other hand, the electricity demand is relatively stable over the year. This seasonal variation of heat demand is currently managed through the gas grid and gas storage. If the heating sector is going

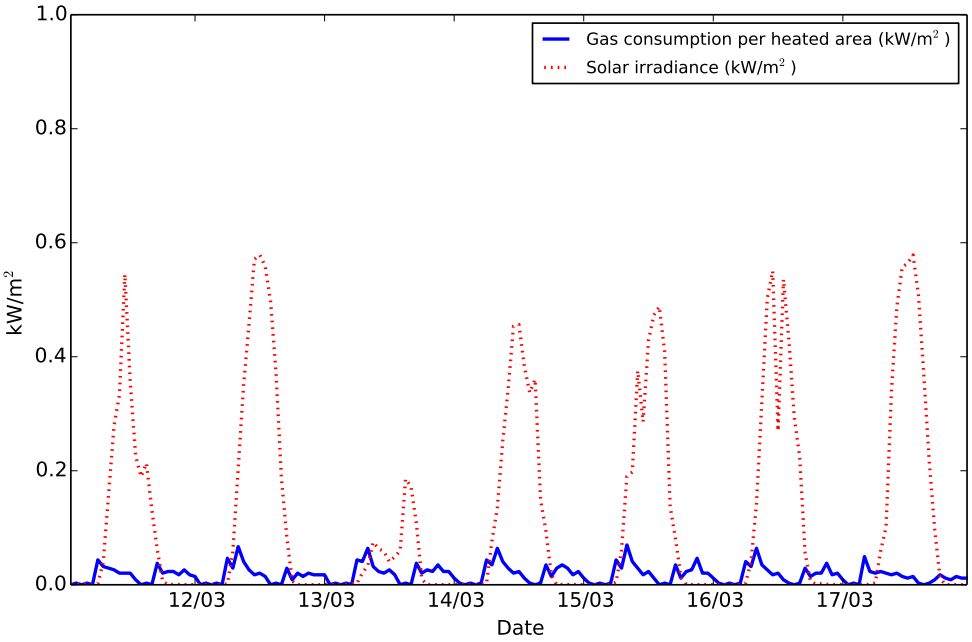

Figure 2.1: Gas consumption per heated area and incident solar irradiance on a horizontal plane profile for a week in the case of a house in the Milton Keynes Energy Park. Plotted data were based on house MK0805 during year 1990 (UK Energy Research Centre, 2015). Average heated floor area of 104.8 m^2 was used in calculating the gas consumption per heated area (Summerfield *et al.*, 2007).

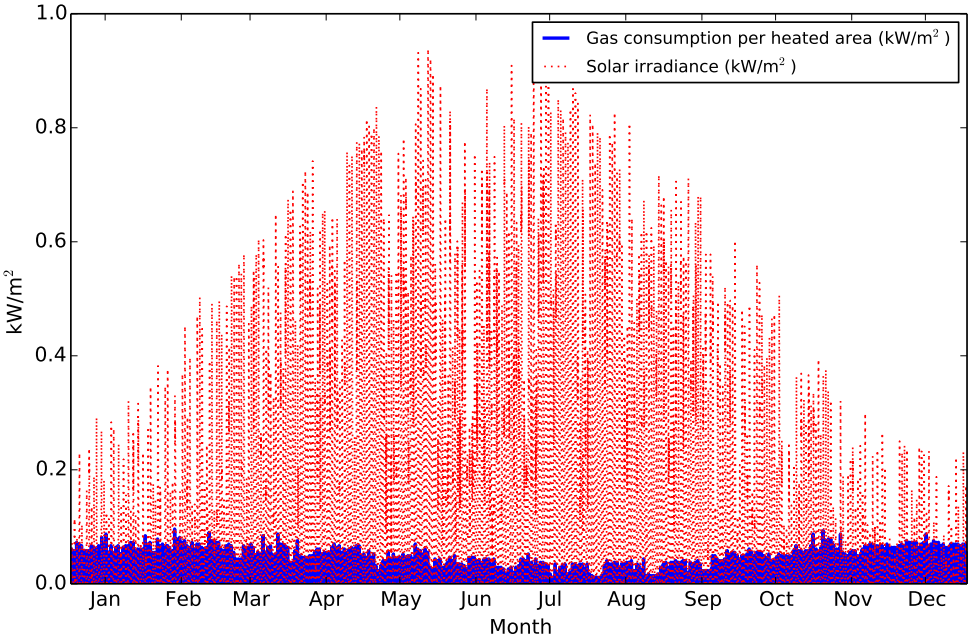

Figure 2.2: Gas consumption per heated area and incident solar irradiance on a horizontal plane profile for a year in the case of a house in the Milton Keynes Energy Park. Plotted data were based on house MK0805 during year 1990 (UK Energy Research Centre, 2015). Average heated floor area of 104.8 m^2 was used in calculating the gas consumption per heated area (Summerfield *et al.*, 2007).

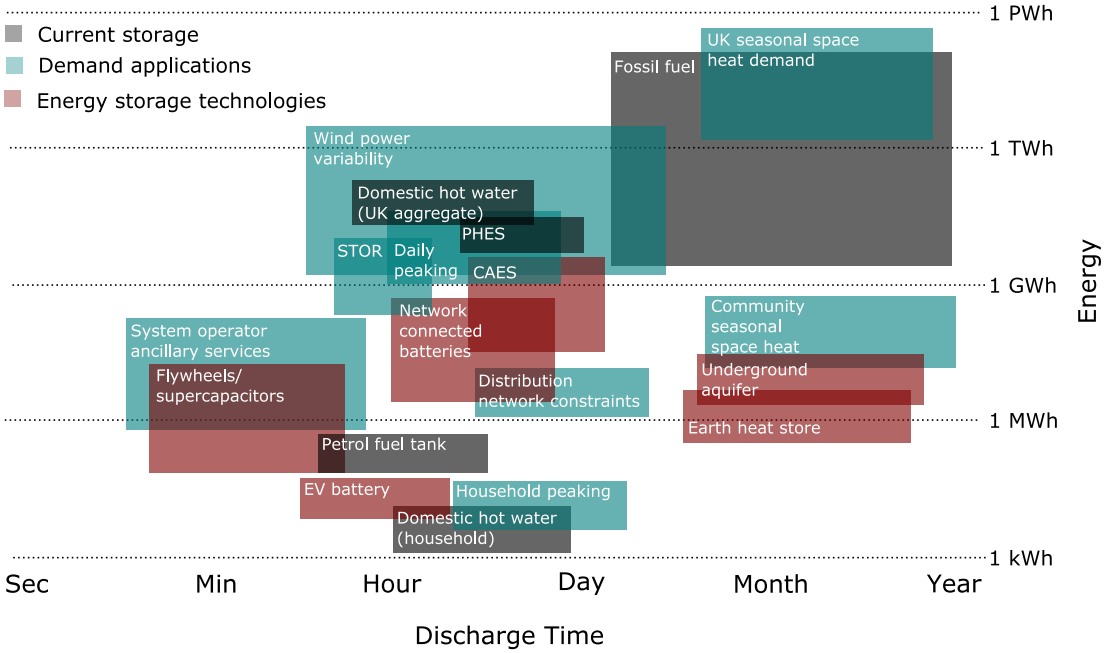

Figure 2.3: Capacities and discharge times for various storage technologies and demand applications. CAES: Compressed Air Energy Storage; PHES: Pumped Hydroelectric Energy Storage; EV: Electric Vehicles (Adapted from ((Institution of Mechanical Engineers, 2014)))

to be decarbonised through an increase in renewable-based heat sources, the seasonal variation has to be managed through other means.

It should be noted that the emerging storage technologies shown in Fig. 2.3 have different technological maturity level. This is shown in Fig. 2.5 for various electrical and thermal energy storage technologies. It is clear that most TES technologies are quite mature and located in either demonstration or commercialisation stage, except for thermochemical energy storage. This also means that the cost of most TES technologies is lower than other potential technologies which are still in the earlier stage of maturity, such as batteries and compressed air energy storage (CAES). Furthermore, although Pump Hydro Energy Storage (PHES) has lower capital requirement times technology risk than most TES, it is limited by the geographical situation, as also the case in CAES. TES, on the other hand, has little geographical limitations and can be deployed in a more distributed way.

Therefore, given the importance and inherent characteristics of heat demand and combined with its benefits over other storage technologies, it is clear that TES has a significant potential to contribute towards a low carbon energy systems. Due to the vast array of TES technologies, they can be implemented on a different level of energy systems and can have various roles.

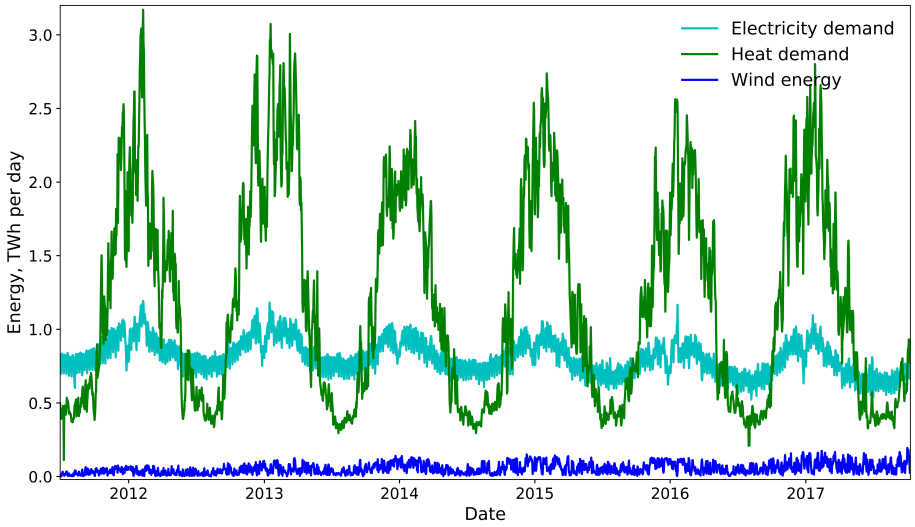

Figure 2.4: Daily energy demand profile of the United Kingdom over the last 6 years (July 2012 - June 2017). Non-daily metered gas consumption profile acts as a proxy for the heat demand profile (Source: Daniel Friedrich).

2.2 Thermal energy storage in energy systems

2.2.1 Types of thermal energy storage

Thermal energy storage technologies are classified into three categories according to their energy retaining mechanism: sensible, latent, and thermochemical (Cabeza, 2014). Figure 2.6 illustrates this classification along with several examples. The energy density of some of the examples is given in Table 2.1. From this table, it is clear that thermochemical storage has significantly larger energy density than sensible and latent storage. However, it should be noted that for the given case of hydrogen as a thermochemical storage, the weight of storage tank is not included in the table. This may influence the technical and financial feasibility of the technology in comparison with the other options.

Sensible TES stores the thermal energy in the form of temperature change of the storage material. The most common storage material is water. Due to its low cost and non-toxic materials, sensible storage has been widely used, both in domestic and industrial applications. Nevertheless, its main drawback is the relatively low volumetric heat capacity which can limit its application in areas where space is a premium. In addition to water, other materials used as a sensible storage material include high-density bricks, rocks, concrete, and soil.

In latent TES, the energy is stored as the latent energy required or released during

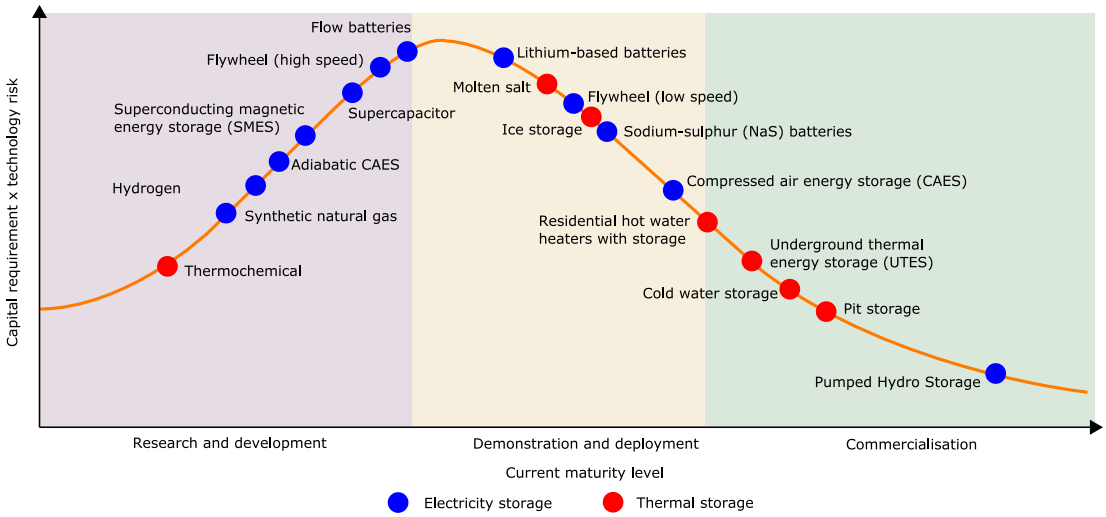

Figure 2.5: Maturity levels of different storage technologies (Adapted from (International Energy Agency, 2014)).

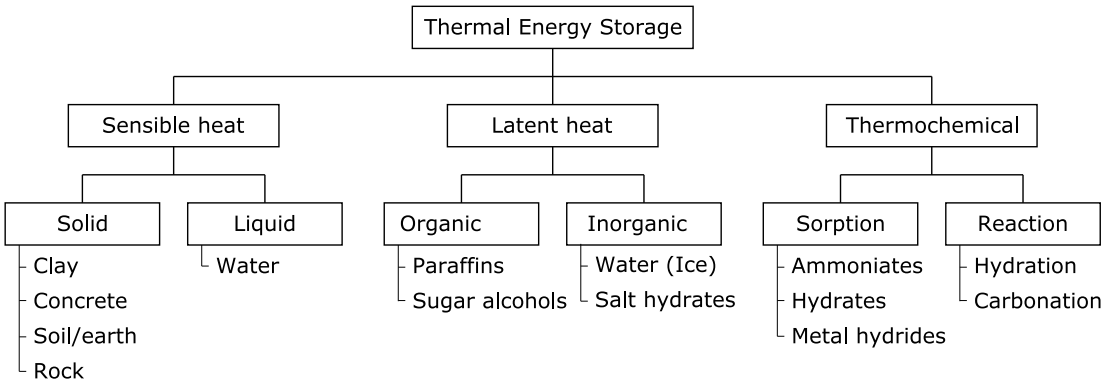

Figure 2.6: Thermal energy storage classification

the phase change of the storage material (Phase Change Material - PCM). Typical examples include ice storage for cooling purpose and PCM-integrated building walls. In comparison to sensible TES, latent TES has higher volumetric heat capacity and isothermal behaviour during charging and discharging. The higher energy density makes it attractive in space-constrained applications since latent TES will have a smaller footprint than sensible TES for the same storage capacity. Such applications include the domestic heating system, where a hot water storage tank can occupy significant space in an already space-constrained flat. The isothermal behaviour is useful for temperature control and energy management applications, such as electronics cooling (Wang and Baldea, 2013). Nevertheless, latent TES also has its drawbacks, such as its relatively higher cost than sensible TES, toxic and corrosive nature of some PCMs, low thermal conductivity, phase-separation, and sub-cooling problem (Cabeza, 2014).

The last type, thermochemical TES, utilises reversible chemical reactions or sorption

Table 2.1: Energy density of different types of thermal energy storage technology (Adapted from (Cabeza, 2014)).

Type of TES	Material	Energy stored (MJ/m^3)	Energy stored (kJ/kg)	Comments
Sensible heat	Granite	50	17	$\Delta T = 20$ °C
	Water	84	84	$\Delta T = 20$ °C
Latent heat	Water	306	330	$T_{melt} = 0$ °C
	Paraffins	180	200	$T_{melt} = 5$–130 °C
	Salt hydrates	300	200	$T_{melt} = 5$–130 °C
	Salt	600–1500	300–700	$T_{melt} = 300$–800 °C
Thermochemical	H2 gas (oxidation)	11	120000	300 K, 1 bar
	H2 gas (oxidation)	2160	120000	300 K, 200 bar
	H2 liquid (oxidation)	8400	120000	20 K, 1 bar
	Fossil gas	32	–	300 K, 1 bar
	Gasoline	33000	43200	–
Electrical storage	Zn/Mn oxide battery	–	180	–
	Pb battery	–	70–180	–

to store thermal energy. An endothermic/exothermic reaction involved in chemical reactions-type thermochemical TES is shown in Eq. 2.1. A and B are the reactants, while AB and ΔH_R are the products and associated enthalpy of reaction, respectively. The latter is the one utilised in the storage of thermal energy in thermochemical TES. The charging process is correlated with the endothermic process which shifts the equilibrium to the left, while the discharging process occurs with the reverse exothermic reaction.

$$A + B \rightleftarrows AB + \Delta H_R \tag{2.1}$$

Compared with the other two TES types, thermochemical TES has the highest storage density (Table 2.1), as well as relatively low storage losses. This makes it a prominent candidate for long-term or seasonal storage. However, as shown in Fig. 2.5, thermochemical TES is still in its infancy with more fundamental research to be done before it can become a cost-competitive alternative to other TES technologies.

Among the three types, sensible TES in the form of hot water tank storage remains

the most commonly found installation in energy systems ranging from residential heating to district heating system. In the UK, the maximum combined storage capacity of residential hot water tanks is approximately 80 GWh (Taylor *et al.*, 2012). The popularity of hot water tanks is mainly because it is required in a system without combi-boilers, which was the common set-up in the 1970s. The technology has recently been considered to have significant potentials in low-carbon energy systems, as discussed further in Subsection 2.2.2.

Essentially, hot water tanks are based on water contained in stainless steel, concrete or plastic tanks. Other typical components in a hot water tank include heat exchanger coils, resistive heating elements, and stratification enhancement devices (Cabeza, 2014). The latter are usually installed to encourage and maintain thermal stratification within the tank and can take form as baffle plates or multiple inlets, among others. Despite being an already mature technology, research is still performed on improving the operational performance of hot water tanks, for example in solar-assisted heat pump systems (Banister and Collins, 2015), wall material (Armstrong *et al.*, 2014b), and balancing thermal and sanitary performance (Armstrong *et al.*, 2014a).

Furthermore, hot water tanks are also more affordable and easier to maintain compared to other TES technologies. For example, the cost of sensible TES materials can be less than £5/kWh, while the value is up to £50/kWh and above £100/kWh for latent and thermochemical materials, respectively (Radcliffe and Li, 2015).

In general, the cost of TES systems depends on the specific application and operational profile, e.g. the number of storage cycles. Table 2.2 shows this dependency using a simplified calculation assuming a hypothetical TES system with 100 kWh capacity, thermal energy price of €0.05/kWh, and investment return time of five years (Hauer, 2013). For instance, if the 100 kWh storage is to be used as a seasonal storage with one cycle per year, it means that in five years the storage would save 500 kWh of thermal energy. This corresponds to €25 based on the assumed thermal energy price. Thus, in order to ensure the five years investment return time, the maximum allowed investment cost is €25/100 kWh = €0.25/kWh. This value is only viable if a cheap sensible TES is implemented as the seasonal storage. Nevertheless, it should be noted that the storage volume has been given limited consideration in the reported table.

Different than the temporal cycle of a short-term storage such as residential hot water tank, which typically ranges from hours to days, long-term storage has a temporal cycle in the scale of months or even seasons. This is particularly useful, for example, to store solar thermal energy available in the summer to be used later in the winter (Ochs *et al.*, 2009; Rad and Fung, 2016). In the subsequent part of this thesis, the term seasonal TES and long-term TES are used interchangeably.

Table 2.2: Energy and economic savings of TES systems as a function of storage cycles per year (Hauer, 2013)

	Cycles per year	5 year energy savings (kWh)	5 year economic savings (€)	Investment cost (€/kWh)
Seasonal storage	1	500	25	0.25
Daily storage	300	150000	7500	75
Short-term storage (3 cycles/day)	900	450000	22500	225
Buffer storage (10 cycles/day)	3000	1500000	75000	750

Similar with short-term TES, the most commonly installed long-term TES to date is the sensible type, while latent and thermochemical storage are still in the development phase (Xu *et al.*, 2014). Figure 2.7 illustrates four typical long-term sensible TES installation: large tank, pit-water, aquifer, and borehole storage. The working principle of the underground tank and pit-water storage are the same as a residential hot water tank, where a thermally stratified body of water is used as a storage medium. In aquifer storage, a naturally present underground aquifer acts as the storage medium. Borehole storage uses soil as the storage medium, with a working fluid flowing in a closed-loop heat exchanger.

These four long-term TES have their advantages and limitations. For instance, specific geological conditions are required for BTES and ATES due to their reliance on naturally available soil and aquifer. This is not the case for TTES and PTES which can be built almost anywhere. Moreover, TTES and PTES have higher volumetric thermal capacity than ATES and BTES, with the latter having the lowest volumetric thermal capacity ranging from 15 to 30 kWh/m^3 depending on the ground properties (Ochs *et al.*, 2009).

At present, most long-term TES are installed as a part of district heating systems. The ”Solarthermie 2000” and ”Solarthermie 2000plus” projects in Germany, for example, have designed and built solar district heating system demonstration projects which tested all four types of long-term storage illustrated in Fig. 2.7 (Ochs *et al.*, 2009). Seasonal storage has also been deployed in various district heating installations in Denmark, for example pit-water storage in Marstal and Dronninglund, and borehole storage in Braedstrup. In Canada, the Drake Landing Solar Community (DLSC) is the first solar district heating system in North America, and it includes a BTES as the seasonal storage (Sibbitt *et al.*, 2012).

One of the important outcomes of all these projects is the cost curve of the seasonal

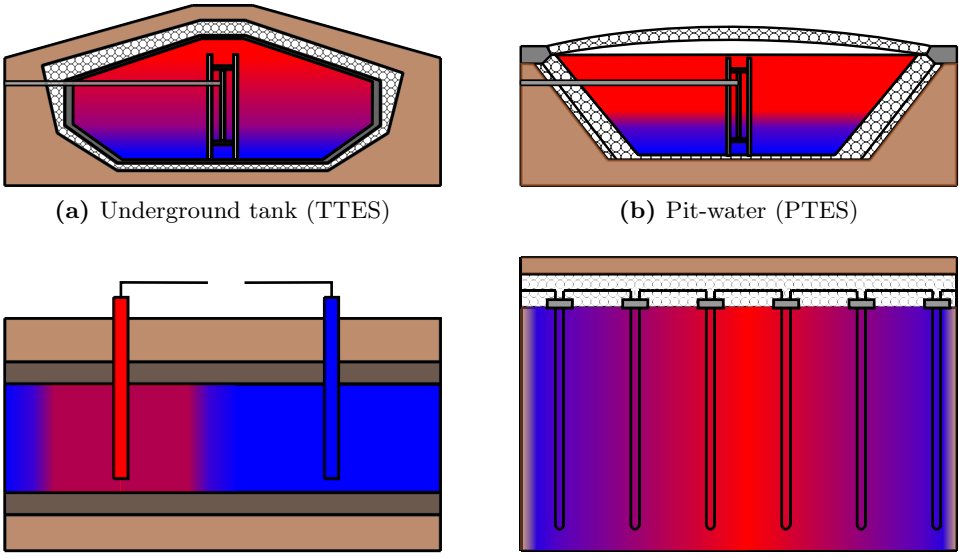

(a) Underground tank (TTES)

(b) Pit-water (PTES)

(c) Aquifer (ATES)

(d) Borehole (BTES)

Figure 2.7: Typical long-term TES. The illustrations show higher (red) and lower temperature (blue) region in the storage medium, along with the soil/ground (brown) and insulation (white).

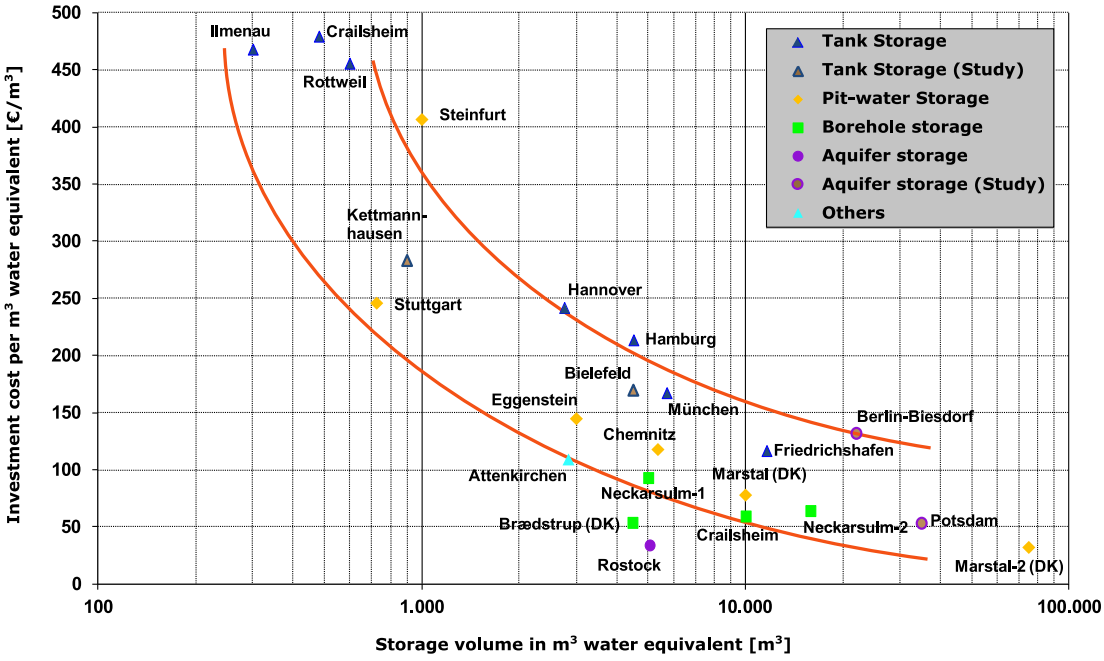

Figure 2.8: Cost of seasonal storage (Solites, 2014).

storage, as displayed in Fig. 2.8. It shows the investment cost per m^3 water equivalent of long-term storage as a function of its storage volume in water equivalent. The water equivalent is the corresponding water volume to store the same amount of thermal energy (Pavlov and Olesen, 2012). This concept is particularly useful to compare the non-water-based storage medium, such as in BTES, with the water-based storage technologies. The two continuous regression lines in Fig. 2.8 correspond to the lower and upper limit of the investment cost. It is interesting to note that BTES has relatively lower investment cost for all considered installations, i.e. Neckarsulm, Crailsheim, and Braedstrup, while most of the TTES are closer to the upper regression line. The relatively higher cost of TTES and PTES can be attributed to the construction costs of both types which typically include ground excavation.

2.2.2 Role of thermal energy storage in energy systems

In future energy systems with highly interlinked energy vectors, e.g. electricity and heat, the role of thermal energy storage is foreseen to expand beyond the context of domestic energy cost saving through the use of off-peak electricity, as has been the case in the UK for decades.

By its ability to decouple supply and demand, thermal storage has a central role in increasing the installation of **renewable-based heating systems**. These include heat pumps, solar thermal collectors, micro-CHP, and district heating schemes.

Several studies have shown the potential role of thermal energy storage in **demand-side management** programs. In principle, the idea is to use the energy buffer provided by TES to shift the electricity load, for example from peak to off-peak hours in an electrified heating system. For example, the combination of heat pump and thermal storage has been widely investigated as a promising tool for load shifting (Hewitt, 2012; Arteconi *et al.*, 2013; Kelly *et al.*, 2014). The same technological combination can also have impacts on increasing wind power utilisation and providing cost-effective fuel saving in the context of large-scale installation in the system (Hedegaard *et al.*, 2012; Hedegaard and Balyk, 2013). In addition to heat pumps, electric heating can also be implemented for active demand response in combination with thermal storage (Patteeuw *et al.*, 2015).

Besides active storage equipment, passive storage technology can also play an important role in improving the building energy systems, particularly in **reducing the heating/cooling demand**. Passive storage is mostly associated with the thermal capacitance of the building itself. Optimal control for both active (TES) and passive storage (Building thermal inertia) has been shown to produce greater cost savings than a separate, individual control system (Henze *et al.*, 2004). In a district heating system, it is also possible to utilise the connected buildings as storage by periodically overheating

and underheating them (Kensby *et al.*, 2014). Passive storage can also be enhanced by integrating storage materials (PCM) within the building walls (Soares *et al.*, 2013).

Another key characteristic of energy systems which can be improved by thermal storage is **flexibility**. The flexibility of a district heating system with CHP and TES was investigated for different equipment size and configuration, i.e. centralised vs distributed storage (Nuytten *et al.*, 2013). It was found that for the investigated case, increasing CHP power does not result in more flexibility, while TES size has a linear influence on flexibility. Furthermore, the scenario with distributed TES only has a fraction of the flexibility of the centralised case. This is because in the distributed case, the CHP operation is dictated by the customer with the highest instantaneous heat demand.

The operational flexibility of energy systems at building level has also been studied (Stinner *et al.*, 2016). In the study, the authors proposed a flexibility quantification method for building energy systems and used it to compare the flexibility of systems with heat pumps and CHP in combination with TES. It was concluded that the sizing of the heat generator determines if the systems can offer flexibility at all, while the TES size influences the duration of the flexibility.

As briefly discussed in the previous section, thermal storage also has the ability to act as a **seasonal storage**. With growing number of installations around the world, the role of TES as a seasonal storage has been subjected to a number of review studies (Novo *et al.*, 2010; Pinel *et al.*, 2011; Pavlov and Olesen, 2012; Xu *et al.*, 2014; Hesaraki *et al.*, 2015).

On the industrial and grid level, thermal storage technology is also a viable option for storing energy in several applications. In industrial plants, improving energy performance by **waste heat recovery** has been widely acknowledged as a feasible measure. Nevertheless, the demand for heating does not always coincide with the processes producing the waste heat; thus, storing the waste heat could help in solving this problem (Miró *et al.*, 2016). As an example, a TES system which stores waste heat from an industrial plant in BTES is currently being tested in Sweden (Nordell *et al.*, 2016). Recently, the potential of thermal storage as **electricity grid level storage** has gained interests from academic and industrial sectors. For example, pumped thermal electricity storage technology can store electrical energy by converting it into sensible heat, using the Joule-Brayton and its reverse cycle during discharging and charging, respectively (White *et al.*, 2013; McTigue *et al.*, 2015).

From the overview of the role of TES, it is obvious that the future potential use of thermal energy storage involves different time scales, energy vectors, equipment, and stakeholders. Naturally, this increases the complexity involved in designing and operating the energy systems. Thus, optimisation-based design and operation are important

to ensure the benefits of integrating storage are achieved.

2.2.3 Thermal energy storage in the UK and Scotland

The current condition and prospective role of thermal energy storage in the UK have been recently reported by several institutions (Taylor *et al.*, 2012; Institution of Mechanical Engineers, 2014; Eames *et al.*, 2014; Radcliffe and Li, 2015). At present, most TES installations in the UK are domestic hot water tanks, while seasonal storage installations are very limited. Nevertheless, the potential contributions of seasonal thermal storage have been acknowledged in the aforementioned reports, although mainly in qualitative nature and without techno-economic analysis.

One of the barriers to deployment of TES technologies is the technology cost and performance. In the case of seasonal storage, it needs to be large to make it cost competitive, due to the low number of charge/discharge cycle (Eames *et al.*, 2014). Therefore, the currently available technology is only attractive in a relatively large heat delivery systems, e.g. district heating systems. One potential application is for district heating systems to use heat pumps in combination with underground storage to enhance winter time COP (Eames *et al.*, 2014). A similar proposition of storing electrical energy over a period of months using seasonal TES is also mentioned in the report of TES potential in Scotland (Radcliffe and Li, 2015). Another proposition is to repurpose disused shale gas wells for medium depth BTES (Westaway, 2016). However, more research is required to assess the life cycle impacts of such installation, since they may offset the benefits of the storage technology.

So far, the benefits and challenges of seasonal TES in its most viable application, i.e. district heating systems, have been only discussed in a qualitative manner, while ***quantitative evaluations of an energy system with seasonal storage in the UK*** are still very limited in the literature. This gap can be addressed, for example, by performing a simulation study on an existing system. The influence of UK-specific parameters, e.g. weather, demand profiles, and fuel costs, on the applicability of such system can then be studied further.

2.3 Energy systems optimisation and simulation

2.3.1 Conceptual levels of energy systems optimisation

Energy systems optimisation can be divided into three conceptual levels (Frangopoulos *et al.*, 2002):

- **Synthesis optimisation** defines the type of components utilised in the system and the connections between them. The superstructure of an energy system is determined at this level.
- **Design optimisation** finds the optimal specifications, e.g. rated capacity and size, of the components selected in the synthesis optimisation.
- **Operational optimisation** identifies the operational profiles of components along the simulated time period, while the system synthesis and design are given from the previous two optimisation levels. The operational profiles include, for example, ON/OFF status of an equipment and charge/discharge decision of a storage.

Fig. 2.9 illustrates these conceptual levels. As described earlier, all three levels are highly coupled and, ideally, have to be solved simultaneously. Performing optimisation at a certain level normally requires work to be done on the lower levels, while results from higher levels are used as an input. For instance, the synthesis optimisation of an energy system has to involve some form of design and operational optimisation, since otherwise the system cannot be evaluated. In another spectrum, the operational optimisation of an energy system is typically performed on a given design and superstructure. Clearly, the higher the optimisation level, the more difficult it becomes to solve the problem as the design space increases significantly.

Due to this increasing complexity, most studies in the literature are typically focusing on one or two optimisation levels, while the third level is considered as a given or modelled in a highly simplified way. For example, Voll proposed an automated synthesis optimisation framework which covers synthesis and design level in detail. In order to limit the complexity, time steps in the operational level were aggregated into six time steps to represent one year of operation (Voll, 2013). On the other hand, there are optimisation frameworks that are focused on design and operational level, while assuming the superstructure of the system as a given, e.g. EnergyHub method (Evins *et al.*, 2014).

The optimisation problems studied in this thesis are limited to the design and operational level. In all cases, the superstructure of the energy system is given. This limitation is considered because the objectives of the thesis can be achieved without considering the synthesis level of optimisation, as described at the end of this chapter. An example of design and operational optimisation is given in Chapter 4, while a focused investigation on an operational optimisation problem is treated in Chapter 5.

Regardless of the conceptual level, optimisation problems are formulated according to their characteristics (e.g. linear or non-linear), number of objectives (e.g. single or multi-objective), and solved using the available algorithms (i.e. deterministic or metaheuristics). Furthermore, the types of components involved in the optimisation

can also influence the formulations. For example, the presence of storage may affect the selection of the temporal representation of the problem, and add extra constraints which have to be included to capture the storage behaviour.

2.3.2 Methods in energy systems optimisation

Mathematical optimisation aims to determine the values of decision variables that minimise (or maximise) an objective function. The relations between decision variables are represented by the objective function and equality and inequality constraints. The general form of a single-objective optimisation problem is shown in Eq. 2.2, where x is the vector of decision variables, f is the objective function, and h and g are the vector of equality and inequality constraints functions, respectively.

$$\begin{aligned} \min_{x} \quad & f(x), \\ \text{s.t.} \quad & h(x) = 0, \\ & g(x) \leq 0, \end{aligned} \tag{2.2}$$

Following the notation in (Frangopoulos *et al.*, 2002), the independent decision variables in Eq. 2.2 can be categorised into three sets which correspond to the optimisation level.

$$x \equiv (v, w, z) \tag{2.3}$$

where

- v is a set of variables for operational optimisation, e.g. heat transfer rate, mass flow rates, and temperature of streams.
- w is a set of variables for design optimisation, e.g. nominal capacity of the equipment.
- z is a set of variables for synthesis optimisation, e.g. existence of components and connections between them.

Taking into account these sets, the general objective function in Eq. 2.2 can be written specifically for the considered optimisation level, as shown in Eq. 2.4. Subscript s, d, and o correspond to synthesis, design, and operational level of optimisation, respectively.

$$\min_{v,w,z} \quad f_{sdo}(v, w, z) \qquad \text{"Synthesis, Design, and Operational"} \tag{2.4a}$$

$$\min_{v,w} \quad f_{do}(v, w) \qquad \text{"Design and Operational"} \tag{2.4b}$$

$$\min_{v} \quad f_{o}(v) \qquad \text{"Operational"} \tag{2.4c}$$

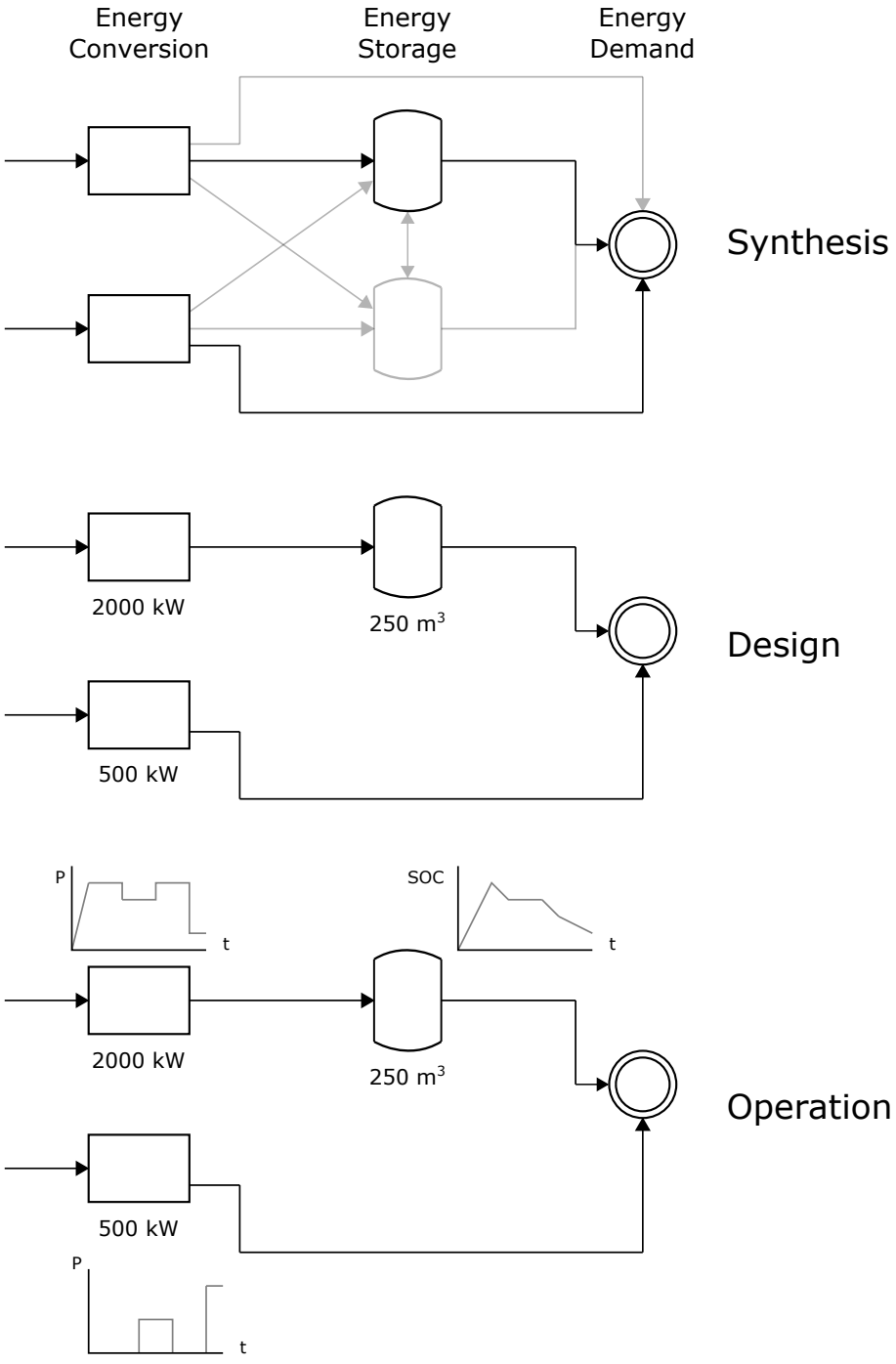

Figure 2.9: Conceptual levels of energy systems optimisation: Synthesis, Design, and Operation. Synthesis optmisation determines the installed components and their interconnections. The shaded lines in the synthesis level illustrates the unselected components and connections. Design optimisation defines the sizing of components. Operational optimisation finds the best operational profiles for all components.

Depending on the linearity of the objective function and the constraints, along with the continuous / discrete nature of the decision variables, optimisation problems are categorised as linear programming (LP), nonlinear programming (NLP), integer programming (IP), mixed-integer linear programming (MILP), and mixed-integer nonlinear programming (MINLP).

Methodologies for systematic energy and process systems optimisation have been extensively studied and reviewed in the literature (e.g. (Frangopoulos *et al.*, 2002; Biegler and Grossmann, 2004; Grossmann and Guillén-Gosálbez, 2010; Olsthoorn *et al.*, 2016)). The methodologies are typically categorised into two types: deterministic and (meta)heuristics methods.

Deterministic methods

Algorithms within this category implement a predetermined search pattern to find the solution and provide the theoretical guarantee that the solution is the global optimum, as opposed to a local one. The *simplex algorithm* is one of the most well-known algorithms in this category. It solves LP problems by following the edges of the feasible region until the vertex with optimal objective value is reached. Another popular algorithm to solve LP problems is the *interior point method*. In contrast with the simplex algorithm, the interior point algorithm finds the optimal solution to an LP problem by moving through the interior of the feasible region.

For IP and MILP problems, algorithms in the deterministic category include the *cutting plane* and the *branch-and-bound* methods (Land and Doig, 1960). Different variants and combinations of these two methods have also been developed, such as the *branch-and-cut* method. In solving the IP or MILP problems, these methods start by solving the LP relaxation of the problems. This is performed by replacing the integer constraint by weaker constraint, for example prescribing $0 \leq x_i \leq 1$ instead of $x_i \in \{0, 1\}$. In the cutting plane method, the algorithm then adds further linear constraints that drive the solution towards integer values. In the branch-and-bound method, the problem is branched into subproblems for each relaxed variable of the generated LP relaxation solutions. The objective function values of the subproblems then represent lower bounds of the optimal objective value for the case of minimisation. The algorithm then decides if a subproblem is discarded or considered further. This process continues until global optimality is reached or a termination condition is met. The latter is typically known as the optimality gap of the problem and defined as the difference between the best feasible solution so far and the best known lower bound. Popular solvers for IP and MILP optimisation include CPLEX (IBM, 2017), Gurobi (Gurobi Optimization, Inc., 2017), GLPK (Makhorin, 2012), and CBC (COIN-OR, 2017).

Various algorithms have also been developed to solve (MI)NLP problems (Biegler, 2010), for example IPOPT (Andreas and Biegler, 2006), BARON (Tawarmalani and Sahinidis, 2005), Bonmin (Bonami *et al.*, 2008) and ANTIGONE (Misener and Floudas, 2014). Although most engineering problems are non-linear in nature, formulating and solving their optimisation problem as (MI)NLP problems mean that, given the current state of (MI)NLP algorithms, the solution is not guaranteed to be the global optimal solution. Even if such guarantee is not of paramount importance, the computational cost of (MI)NLP algorithms is still relatively high. Therefore, it is generally advised that, if possible, non-linearities should be avoided or reformulated as linear constraints in the formulation of mathematical programming problems (Klatt and Marquardt, 2009; Grossmann, 2012).

A comparison of the result and computational time between MILP and MINLP problem for an energy system synthesis optimisation was reported by Voll (Voll, 2013). The test problem was an industrial energy system that satisfies heating and cooling demands in the range of 1.2 - 4.3 MW. The objective of the test problem was to determine the size of energy conversion equipment that maximises the negative Net Present Value (NPV) of the system. The test problem sizes and summary of results are reproduced in Table 2.3 and 2.4, respectively. It can be seen from Table 2.4 that the MILP-CPLEX formulation was able to obtain a solution close to the MINLP-BARON with a computational time of 0.1% of the MINLP. The MINLP formulation even exceeded the time limit when it was not initialised with the MILP solution. This example illustrates how MILP formulation can give a satisfactory solution with fast computational time relative to MINLP.

Stochastic methods

Stochastic optimisation methods, also known as (meta)heuristic methods, are mostly based on physical analogies in generating test points toward an equilibrium condition (Grossmann and Biegler, 2004). By iteratively trying to improve the solution using the relevant analogy, these methods do not have to analyse the mathematical structure of the problem. Thus, only relatively little prior knowledge of the problem is required. Another advantage of stochastic methods is the relative ease of implementation (Grossmann and Biegler, 2004). The major drawbacks of stochastic methods include non-

Table 2.3: Problem size for MILP and MINLP formulations of a test case in (Voll, 2013)

	MILP problem	MINLP problem
constraints	4116	712
continuous variables	3030	506
binary variables	328	56

Table 2.4: Comparison of objective values and computational times between MILP and MINLP formulations for synthesis optimisation of a test case (Voll, 2013). CPU times given in h:mm:ss (t_∞: time limit of 48 hours reached, optimisation aborted). Relative optimality gap: 0%. B: Boiler, CHP: Combined heat and power, TC: turbo-driven compression chiller, AC: absorption chiller.

	NPV	CPU	Solution structure (equipment sizing in kW)							
	M€	time	B1	B2	CHP1	CHP2	TC1	TC2	AC1	AC2
MILP										
CPLEX	–7.24	00:01:28	1900	100	2300	0	1900	840	370	0
MINLP (trivial initial solution)										
Bonmin	–11.76	01:41:15	2160	100	3200	800	1170	0	3380	0
BARON		t_∞								
MINLP (initialised with MILP solution)										
Bonmin	–10.96	00:16:49	650	0	3200	1110	2820	0	2660	0
BARON	–7.11	23:12:11	1900	280	2120	0	1900	800	410	0

guaranteed optimality and slow convergence. Prominent examples include simulated annealing, particle swarm, and evolutionary algorithms.

Evolutionary algorithms use biological evolution as the physical analogy in generating test points. A widely used evolutionary algorithm in the field of energy systems optimisation is the genetic algorithm (GA) (Holland and Reitman, 1977). It works by iteratively going through a population of candidate solutions and evaluating the objective function value of these candidates. Between each iteration, the prospective solutions are improved by different mechanisms, i.e. mutation, crossover, inversion, and selection. The algorithm terminates when a satisfactory objective function value or a maximum number of iterations has been reached.

One of the advantages of stochastic optimisation methods is their straightforward applicability on multi-objective optimisation problems. Stochastic algorithms have been used in numerous multi-objective optimisation of energy systems. For instance, a variation of evolutionary algorithms has been utilised in the design and operational optimisation of multi-vectors energy systems (Fazlollahi *et al.*, 2012). In the study, two objectives were considered, namely total cost and CO_2 emission. A Pareto frontier was generated, from which the designer can select the most suitable design. The study also compared the performance of the evolutionary algorithm with the MILP with integer cut constraints model and concluded that the evolutionary algorithm is more suited for handling the multi-objective optimisation. However, the MILP model requires less computational effort than the evolutionary algorithm.

Hybrid methods

Energy systems optimisation problems can be solved either simultaneously or sequentially. In the simultaneous approach, optimisation problems on all levels shown in Fig. 2.9 are solved together in one formulation. It is clear that this approach will produce a relatively large size and non-linear problem. The disadvantages of MINLP and metaheuristics algorithms discussed earlier would make their implementation in the simultaneous optimisation still prohibitive in most cases.

In order to overcome this issue, the sequential approach can be followed and has been widely implemented in the literature. In this approach, each optimisation level is solved in a relatively independent manner, typically with different algorithms and/or with a reduced-order version of the lower level problem. For example, synthesis optimisation can be performed with coarser demand profile to limit the size of the operational optimisation problem (Voll, 2013). Another widely used strategy in the sequential approach is implementing metaheuristic algorithms to solve the highly non-linear level and (MI)LP to solve the lower level optimisation. Such a hybrid method has been shown to be effective in solving inherently non-linear energy systems optimisations (Fazlollahi, 2014; Rager, 2015).

2.3.3 Optimisation of energy systems with thermal energy storage

The literature on energy systems optimisation spans across different fields of applications (e.g. thermal, electrical, and chemical), various optimisation methods (e.g. deterministic, stochastic, and hybrid framework), and different objective functions (e.g. thermodynamic, economic, environmental, and multi-objective). In order to limit the overview, the following paragraphs focus on optimisation studies that include thermal energy storage. The spatial characteristic in the studies is also limited to building and district-level. This is because, at present, these two levels have the highest level of implementation potential for both short- and long-term thermal energy storage technology.

Building energy system

Studies on the optimisation of building energy systems have been recently focusing on the integration of renewable technologies, such as heat pump, solar thermal, micro combined heat and power (CHP), and fuel cells. This is because most of these technologies are less-developed and in turn, generally costlier than the incumbent technology, such as gas boilers. Furthermore, some of them could also interact with more than one energy vector. As an example, heat pump and micro-CHP are coupling the electricity and heating energy vector. Besides the added complexity, this can also be considered

as opportunities for overall system improvement. Therefore, designing and operating the system optimally is important to ensure the benefits of these renewable systems. Examples of optimisation studies on building energy systems, both residential and commercial, are given in the following paragraphs.

The integration of solar thermal technology in building energy systems have been widely studied in the literature. Most of the optimisation studies focus on the sizing and operation of the solar collector and TES equipment, with economic and/or environmental objectives in mind. Various algorithms have been implemented for this problem, for example genetic algorithm, particle swarm optimisation (Bornatico *et al.*, 2012), and hybrid algorithms (Cheng Hin and Zmeureanu, 2014). A MILP formulation has also been developed for the design and operational optimisation of a solar domestic hot water system (Omu *et al.*, 2016).

Residential CHP systems with integrated storage have also been subjected to optimisation studies in the literature. For example, using a MILP optimisation model, Wakui and Yokoyama investigated the optimal design of a residential cogeneration system which includes a CHP unit, a thermal storage tank, a gas boiler and auxiliary devices (Wakui and Yokoyama, 2014).

It is known that the benefits of optimisation-based design increase as the systems become more complex. In the case of building energy system, this means accounting for various types of generation, storage, and distribution equipment. For instance, a MILP-based framework to optimise the design and operation of building energy system has been developed by Ashouri et al. (Ashouri *et al.*, 2013). Within the framework, generic equipment models were used to describe energy conversion and storage equipment, along with their predefined connections. Using a similar approach, Fux et al. considered the control aspect in their study of a stand-alone building energy system (Fux *et al.*, 2013). In another study, the results of a MILP-based residential energy systems optimisation tool has been compared with a commercial design tool (HOMER) (Lauinger *et al.*, 2016). In the investigated case, the MILP-based tool produced a similar solution in significantly less time.

In reality, the design and operation of building energy systems are highly coupled with the design of the building itself. Several studies have taken this into account in the optimisation of building energy systems. In one study, a multi-level optimisation model, combining GA, MILP, and building energy simulation program, was developed to optimise building design and energy system sizing and operation (Evins *et al.*, 2016). In another study, the building model was developed within the MILP formulation rather than using an external simulation program (Schütz *et al.*, 2017).

District energy system

The design of district energy systems is generally more complex than those of buildings due to the larger scale, wider design space, and higher variety of demand profiles. Therefore, optimisation of these systems has been widely studied, particularly in recent years with the increasing implementation of microgrids and district heating systems. As in building level studies, various model formulations and algorithms have been used to optimise district energy systems.

Different studies have included TES equipment in district energy systems optimisation. For example, several authors used an optimisation framework to examine the influence of TES in CHP-based district heating systems (Söderman and Pettersson, 2006; Christidis *et al.*, 2012; Raine *et al.*, 2014). In such an arrangement, studies typically focus on increasing the benefits of CHP dual productions, i.e. electricity and heat, by using the optimal sizing and operation of TES. The influence of external factors, such as fuel and electricity costs variation, can then be examined using the optimisation model. Daily TES as part of a more general district energy system was also considered in the multi-objectives and multi-period optimisation framework of Fazlollahi et al., in which the storage tank was discretised into a finite number of temperature levels (Fazlollahi *et al.*, 2014a). The work has been extended by including a seasonal tank storage in the optimisation problem (Rager, 2015).

In the context of systems-level optimisation, seasonal TES has also been included in various studies, despite it being not as common as short-term TES. One early study on the optimisation of district heating with seasonal storage investigated a solar heating system with heat pump and a cylindrical rock cavern as the seasonal storage (Lund, 1984). In another study, the optimisation of a solar district heating system included more production equipment, such as condensing boilers, heat pumps, and CHP, while TTES was considered as the seasonal storage (Lindenberger *et al.*, 2000). Tveit et al. examined the non-linear off-design characteristics in the optimisation of CHP-based district heating systems equipped with long-term TES (Tveit *et al.*, 2009). In addition to TTES, optimisation studies of systems with PTES (Dominković *et al.*, 2015) and BTES (Prasanna and Dorer, 2017) have also been reported in the literature.

Complexity due to storage equipment

As briefly mentioned in Subsection 2.3.1, the inclusion of storage can increase the problem complexity in all three levels of energy systems optimisation. The spatial placement of storage and its connection with other equipment can be considered as extra problems on the synthesis level (Fig. 2.10(a)). For instance, it has been reported that the location of TES and the separation of short- and long-term TES are crucial aspects that influence the performance of a neighbourhood-scale district heating system (Hsieh *et al.*, 2017).

At the design level, the trade-off between energy conversion equipment rating and storage size need to be considered. Extra equipment also means a decision has to be made on its model complexity, taking into account the balance between accuracy and computational time (Fig. 2.10(b)). This trade-off has recently been reported for the case of domestic hot water tank (Schütz *et al.*, 2015). In the study, the authors compared different options to linearise the non-linearity which arises from the consideration of stratification in a hot water tank. All of the studied linearisation approaches produced optimisation runs with higher computational time relative to the capacity model (non-stratified). The study was limited to the operational optimisation of a CHP-based residential heating system over a relatively short time horizon, i.e. two days. Therefore, it is clear that for a longer time horizon, the most accurate linearisation, i.e. binary reformulation, would be too time consuming to be implemented.

Furthermore, the presence of storage couples the decision between time steps on the operational optimisation level. This issue is exacerbated when two types of storage with different temporal characteristics are present in the system, e.g. short- and long-term storage in a solar district heating system as illustrated on the right hand side of Fig. 2.10(c). The temporal aspect of energy system optimisation is typically modelled using the coarsest time step size able to properly capture the behaviour of all equipment. For a system with short-term TES, this means using hourly or other sub-daily time steps in modelling the whole system. This becomes problematic in a system with short- and long-term TES because in order to evaluate the performance of the latter, a multi-year time horizon is normally required, and using hourly time step will significantly increase the problem size.

Several options can be considered to manage the increasing complexity of an optimisation problem due to storage. For example, a simpler problem formulation can be used instead of a more realistic, but significantly more difficult to solve formulation. This approach has been discussed in Subsection 2.3.2, with the preference of a MILP over a MINLP formulation. Another option is to use decomposition methods to further simplify the optimisation problem.

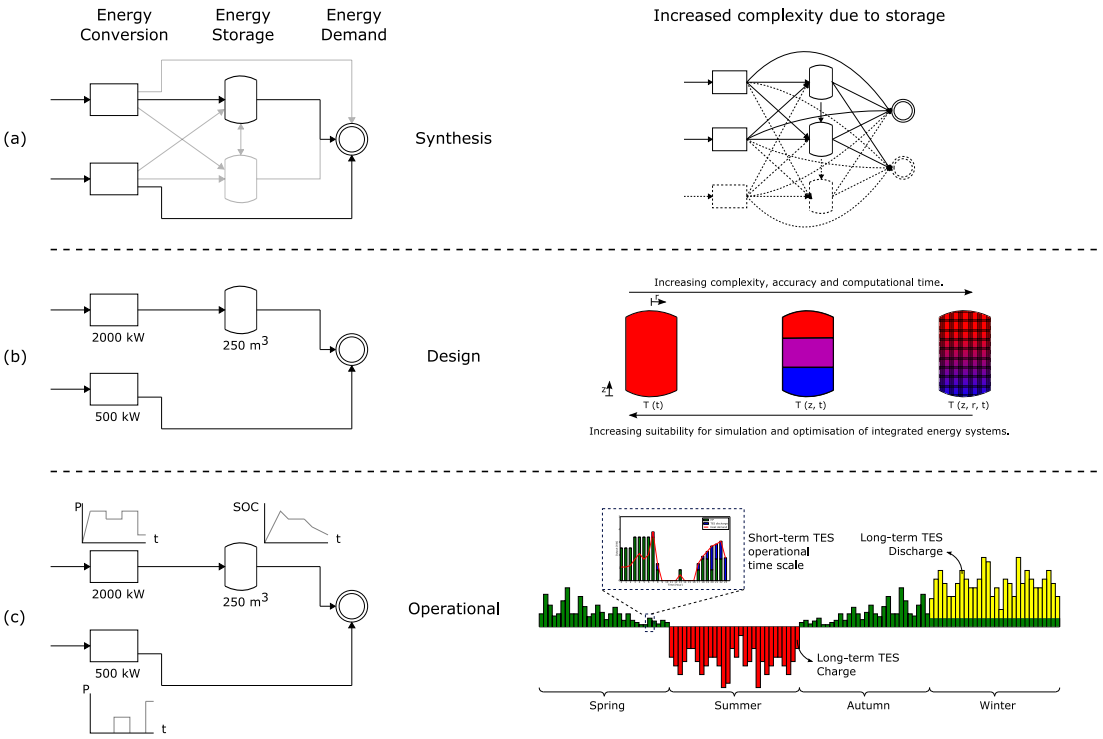

Figure 2.10: Increased complexity due to TES on (a) synthesis, (b) design, and (c) operational optimisation level.

2.3.4 Optimisation problem decomposition

Due to the complexity of the integrated optimisation problem, decomposition is typically performed in order to solve the problem within acceptable time and resources utilisation. Various forms of decomposition can be categorised into three principal types: conceptual, physical, and time decomposition (Frangopoulos *et al.*, 2002).

In conceptual decomposition, the three levels of optimisation (Fig. 2.9) are performed separately, with pre-defined relations or nesting between them. For example, a synthesis optimisation can be performed with limited time steps and then the resulting superstructure is used in the design and operational optimisation which implements finer time steps. Different optimisation methods can also be used at different levels, e.g. stochastic on the design level and deterministic on the operational level (Fazlollahi *et al.*, 2012).

Physical decomposition reduces the problem complexity by creating sub-problems based on the physical components of the energy systems. This is particularly useful when the systems can be divided into semi-independent sub-components that communicates with each other through a set of variables. One example is the process synthesis, heat integration and utility plant sub-system in a chemical plant design (Papoulias and Grossmann, 1983; Murat Sen *et al.*, 2015). Furthermore, models of different com-

plexity can be used to describe a component in energy systems. Some of the widely implemented assumptions in this approach include constant equipment efficiencies, predefined charge/discharge control for energy storage, and zero heat loss in distribution pipes.

Time decomposition approach focuses on how the time horizon and time interval are modelled in the operational optimisation problem. Typically, a defined time horizon is discretised into fixed-size intervals in which the optimisation problem is solved as a quasi-stationary problem. For instance, an optimisation to determine the operational profile over the course of a day can be performed in hourly or sub-hourly intervals. Time decomposition approach is described further in the following paragraphs.

Time decomposition

Determining the most suitable time step size in an optimisation is highly dependent on the temporal nature of the problem. For example, an industrial energy system with relatively constant demand can be modelled with quarterly time step without significant impact on the accuracy (Voll, 2013), while a micro-grid needs to be modelled with sub-hourly time step in order to properly capture the peak demand (Hawkes and Leach, 2005). Furthermore, it has been shown that using different time resolutions on the same problem could produce different results (Hawkes and Leach, 2005; Wakui and Yokoyama, 2015).

In the case of designing a residential heating system, the hourly time step is the most commonly used time discretisation in the literature. This can be attributed to the relatively slower rate of heat demand, except for the domestic hot water (DHW) demand. Although hourly time step is found to be acceptable in most cases, its implementation on larger systems and longer time horizon could still produce a significantly larger and more difficult problem to solve. One solution to this issue is by using typical periods to reduce the size of the problem. Different methodologies to generate typical periods (days, weeks, year) have been proposed in the literature. Several of these methodologies are briefly discussed in the following paragraphs.

The most straightforward way to generate typical periods is by empirical grouping or selection of the representative periods. For example, demand data can be reduced by performing grouping of months to seasons and hours to intraday periods (Mavrotas *et al.*, 2010). In another example, a graphical tool was used to select typical days which can reproduce the cumulative energy demand profile over the whole year (Ortiga *et al.*, 2011). Aside from the obvious peak days, the empirical selection of typical periods is less systematic and prone to the subjectivity of the user.

This issue of subjectivity has been minimised by more systematic methodologies re-

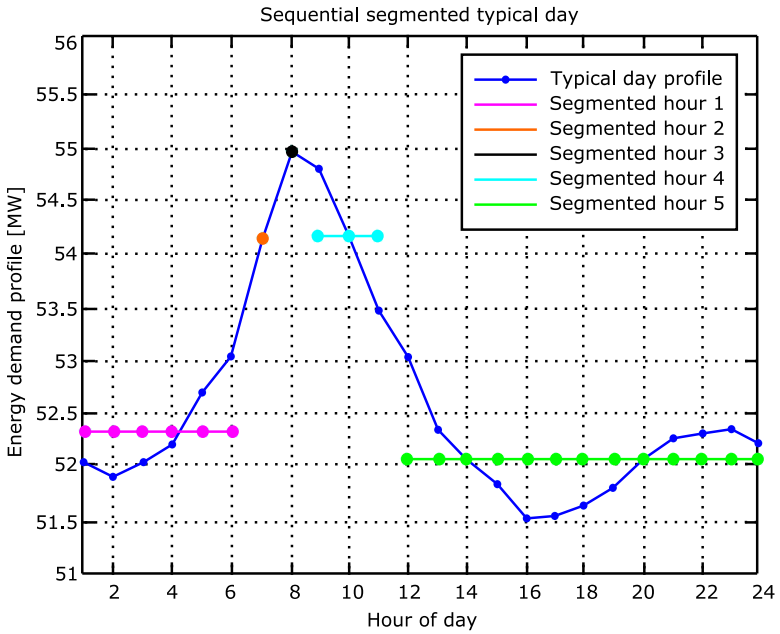

Figure 2.11: Example of segmentation in a typical day (Adapted from (Fazlollahi *et al.*, 2014b))

ported in the literature. In one of the methodologies, typical days were selected by applying a partitioning clustering algorithm to the whole year demand data (Domínguez-Muñoz *et al.*, 2011). The results were then evaluated by calculating their quality indexes and calendar visual inspection. In a further improvement of this method, an optimisation step based on ϵ-constraints technique was performed after the partitioning clustering algorithm (Fazlollahi *et al.*, 2014b). Once the typical days were defined, they were simplified further by segmenting within the day (Fig. 2.11). The method has been applied to test cases and results were compared with reference values which were calculated with complete demand data sets. Savings in computational time were significant, while differences in optimisation results were relatively small apart from peak-covering equipment.

Another approach in generating typical periods employs non-uniform time discretisation rather than the typically used uniform time step. For instance, one year can be divided into four seasons and each season consists of repeated sets of selected weekday and weekend (Fig. 2.12) (Samsatli and Samsatli, 2015). This approach exploits case-specific pattern in the time domain, i.e. the seasonal variation of wind speed and weekday/weekend demand profiles. For example, instead of solving for 8760 hourly time steps in a year, the proposed method can reduce the time steps to 192 by assuming four season types, two day types and 24 hours in a day.

The hierarchical structure of typical periods was also implemented in the optimisation of an air separation plant (Mitra *et al.*, 2014). The multi-scale nature of the developed

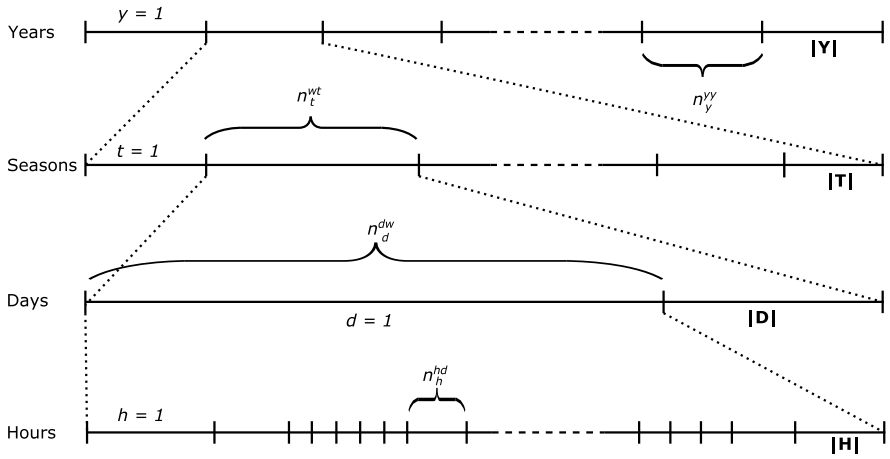

Figure 2.12: Non-uniform hierarchical time discretisation (Adapted from (Samsatli and Samsatli, 2015))

model was achieved by selecting a representative week for each season and assuming a cyclic weekly schedule for each season. A two-stage stochastic approach was utilised with two types of variables: investment and operational decisions variables. The first type of variables corresponds to design-related decisions, e.g. upgrading or installing new equipment, while the latter includes equipment mode of operation and inventory levels.

The use of typical periods has its particular challenge when it is implemented on systems with energy storage. As mentioned earlier, the presence of storage means that the decisions between time steps are now coupled, i.e. information on the storage state-of-charge needs to be passed on to the next time step in order to: (i) calculate the static energy loss; (ii) decide whether to charge, discharge or store the energy, and (iii) calculate the latest state-of-charge. One way to overcome this peculiarity is by enforcing a cyclic constraint within a typical period. That is to assume the same state-of-charge value at the beginning and end of a typical period (Fazlollahi *et al.*, 2014a; Stadler *et al.*, 2016). The cyclic constraint is a reasonable assumption in the case of daily storage, such as domestic hot water tank. It should be noted that this assumption excludes the possibility of using the storage for non-daily peak shaving and balancing between days.

The implementation of cyclic constraint has also been reported for cases of larger storage size in district heating systems. Soderman and Pettersson used the daily cyclic constraint in combination with the typical period approach, where a year is represented with four days, one for each season, and two sub-periods (day and night) (Söderman and Pettersson, 2006). However, the impact of these assumptions on the resulting operational profile is not discussed further in the study.

A formulation with typical periods but without cyclic constraint was proposed by Tveit et al. for the case of district heating system with long-term storage (Tveit *et al.*, 2009). The study used 13 periods per year as the time step discretisation and assumed a constant temperature during a given period. Furthermore, due to the non-linear formulation, a MINLP method was used to solve the problem. In order to reduce the chance of obtaining a local optimum solution, the model has to be solved several times, and the best solution is then reported. Therefore, although the computational cost will increase, the global optimality is still not guaranteed.

In district heating systems which attempt to cover most demand from renewable energy, it is increasingly common to install both short- and long-term storage. As expected, the combination of two temporally different storage technologies will increase the optimisation complexity. An optimisation framework capable of modelling short- and long-term thermal energy storage has been proposed in the literature (Rager, 2015). The two types of storage are modelled in two timescales, of which one is the smaller parts of the other. However, the framework is focused on the design optimisation, with little attention given to the influence of different assumptions on the operational profile. Furthermore, it is concluded that the typical days approach followed in the study still produces a relatively large problem due to the usage of two detailed time scales. A further complication might arise if these storages are connected to each other, as it is normally the case in solar district heating systems.

Based on the aforementioned overview, the identified knowledge gap in time decomposition is ***an alternative time series representation in energy systems optimisation*** which can reduce the computational cost without significantly damaging the results accuracy. This is particularly relevant for systems with equipment of different temporal characteristics, such as solar district heating with short- and long-term thermal energy storage.

2.3.5 Optimisation and dynamic simulation

Optimisation and simulation are both essential in designing energy systems. Their impacts can even be more significant in low-carbon systems which typically include costlier equipment than traditional systems and can involve multiple energy vectors in an integrated manner. Both can be implemented on any level of energy systems, from component up to national level.

A theoretical comparison between the two has been discussed in a recent study (Lund *et al.*, 2017). The focus was more on a national level of energy systems, with planning and policy-making aspects directly included in the models. Nevertheless, the identified differences between optimisation and simulation models are sufficiently generic to be

Table 2.5: Difference in characteristics between optimisation and simulation models (Adapted from (Lund *et al.*, 2017)).

	Optimisation	Simulation
Definition	A model that internally establishes an optimal energy system design; typically through optimising decision variables for objective function(s) subject to constraints.	A model that simulates the behaviour of a user-defined energy system design through the same mathematical principles as the optimisation models or other principles.
Purpose	To identify the optimal solution.	To calculate the performance of the system.
Modeller/Computer relation	Crucial design decisions are made inside the computer by in-built rules, restrictions, and presumptions.	Design decisions are made outside the computer by the modeller.
Typical technical characteristics	Simplified physical modelling.*	Detailed physical modelling.*
	Long computational time and/or low temporal resolution.	Short computational time and high temporal resolution.
	Well-suited for forecasting.	Well-suited for backcasting.

*) Added by the author

considered for other levels, such as building and district energy system. Table 2.5 shows the key points relevant to building and district energy systems.

In addition to the points argued by Lund et al., another major difference between optimisation and simulation is on the implemented modelling approach. Optimisation typically employs reduced-order models to avoid an overly complex problem which can lead to excessive computational time. In contrast, simulation usually implements higher order model that better represent the real system. These differences also illustrate the strengths and weaknesses of both design tools. Furthermore, their results should be analysed with these characteristics in mind.

As one of the tools in designing and operating energy systems, it is important to highlight the role and position of optimisation models of energy systems in the overall design process. Fig. 2.13 illustrates a typical process flowchart in energy system design and implementation. Optimisation study can be positioned between a preliminary design study and a detailed system simulation study. The results of optimisation can then be used to inform the designers and engineers on which configurations need to be studied in detail using simulation software.

Energy systems are typically designed with the help of simulation tools. On the spatial scale of building and district system, some of the widely used simulation software include

TRNSYS, EnergyPlus, esp-r, HOMER, and Modelica. Although optimisation can be performed within these tools, they often have limited design space exploration capability and relatively high computational cost. Simulation models are descriptive in nature and developed to help to understand the system, while optimisation models are more prescriptive and typically developed to help in decision making.

Due to the wide range of energy systems and available simulation tools, a plethora of studies on energy systems simulation can be found in the literature. Recent reviews on various tools and modelling approaches in energy systems are available, for example in Ref. (Keirstead *et al.*, 2012; Allegrini *et al.*, 2015; Olsthoorn *et al.*, 2016). In the following paragraphs, the focus is on the combined approach of simulation and optimisation on thermal energy systems.

As one of the most widely used engineering tools, Simulink and Matlab have been employed in the simulation and optimisation of energy systems. A framework based on these tools which can simulate and optimise a greenhouse solar heating system equipped with seasonal storage has been developed in Ref. (Durão *et al.*, 2014). Genetic Algorithm was employed as the optimisation algorithm in the study. An iterative procedure was implemented to connect the optimisation and simulation routine. Simulink/Matlab modelling has also been used in conjunction with a hybrid GA-MILP optimisation algorithm to optimise a district heating system (Vesterlund *et al.*, 2017). In the study, a simulation routine was embedded in the evaluation step of the GA optimisation.

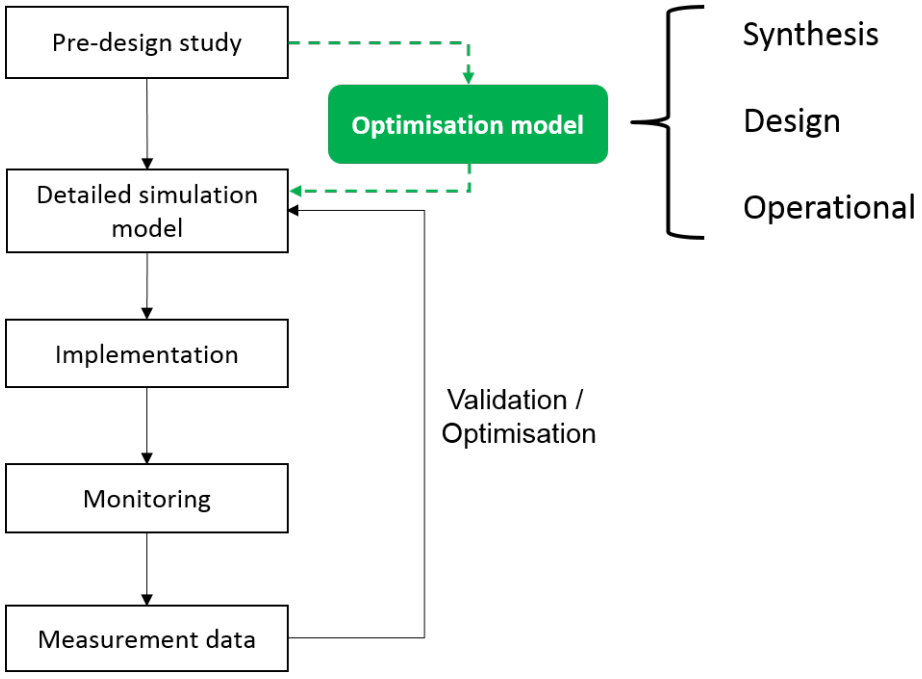

Figure 2.13: Typical steps involved in the design and implementation of energy systems.

The combination of TRNSYS and GenOpt to simulate and optimise a residential solar combisystem has also been reported (Cheng Hin and Zmeureanu, 2014). A hybrid PSO and Hooke-Jeeves pattern search algorithm were used in the study. The generic optimisation software, GenOpt, provides various algorithms as standard options and can be connected to simulation software, such as TRNSYS and EnergyPlus. It works by calling the simulation program in every iteration of the optimisation routine, i.e. iterative in nature. The same combination of tools has also been used to study a solar district heating system with seasonal storage (Tulus *et al.*, 2016).

Simulation and optimisation routines can also be implemented on different optimisation levels. For example, Evins developed an optimisation framework which combined GA, MILP, and EnergyPlus simulation to address the design and operation of a building and its energy system (Evins, 2015). The GA optimised building and plant variables, while the MILP optimised the operational variables. Building design performance was simulated in EnergyPlus. The interaction between simulation and MILP optimisation in this work was sequential, i.e. simulation results are inputs to the optimisation, while the iterative routine occurred within the GA's evaluation, selection and mutation steps.

The benefits of both approaches can also be used to assess each other in a non-iterative way. The most straightforward example is to compare the results of optimisation with those of simulation. For instance, Omu et al. compared the results of MILP optimisation and EnergyPlus simulation in the design of solar thermal systems with short-term TES (Omu *et al.*, 2016). They developed an iterative two-level MILP optimisation framework that can accurately represent the dynamic behaviour of the system.

It is also possible to have a combined interaction, i.e. comparative and iterative, between simulation and optimisation routines. This has been proposed by Wallerand et al. for the optimisation of a solar-integrated process system using a combination of MILP and TRNSYS simulations (Wallerand *et al.*, 2016). In the study, the TRNSYS model of the problem was used for tuning of parameters in the MILP (iterative) and for testing the optimal set of decision variables (comparative). In the latter role, the results of MILP optimisation were fed as inputs to the TRNSYS model. This was done by implementing a control assumption which mimicked the MILP operational profile. This is feasible given the complexity of the investigated system; however, such an approach could become highly cumbersome for more complex systems involving more production technologies and heating demands.

From the overview of the literature, it can be concluded that there are three ways in which optimisation and simulation interact during the design process: embedded, iterative and comparative (Fig. 2.14). In the first form, the simulation part is usually embedded in a bi-/multi-level optimisation framework; while in the second, the simulation routine is typically called from the outset of the optimisation. In the third form,

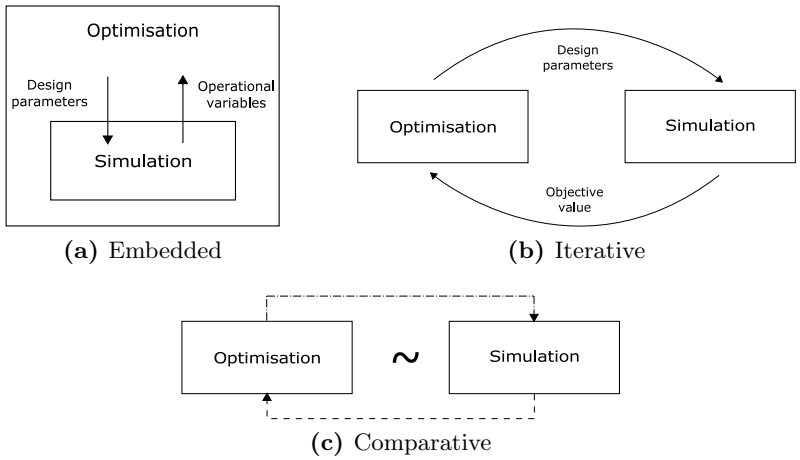

(a) Embedded **(b)** Iterative

(c) Comparative

Figure 2.14: Interactions between optimisation and simulation routine: (a) embedded, (b) iterative, and (c) comparative.

the relation is more independent, with the simulation generally acts as a reference to improve the accuracy of equipment models in the optimisation.

The embedded approach allows the user to perform multi-level optimisation (see Fig. 2.9), for example by using different methods at each level as shown in Ref. (Evins, 2015). However, computational time of such an approach can be quite long due to the integrated simulation routine. Furthermore, its applicability could be constrained by how the simulation model can be connected to other software.

The iterative approach is relatively more straightforward to implement than the embedded one. Similar to the embedded approach, the simulation routine could become a computational bottleneck, especially if the considered system is highly complex.

In the comparative approach, the general idea is to evaluate the accuracy of the optimisation by comparing its results or equipment models with dynamic simulations. This method preserves the main benefit of each routine: fast optimisation and accurate simulation. As illustrated in Fig. 2.14c, iterative loops may be present in this approach. However, unlike in the previous approach, the iteration is more towards tuning the optimisation model, rather than working towards convergence in the optimisation process.

Among these three types of interaction, the comparative approach is the least well studied relative to the others. From the available studies employing this approach, e.g. Ref. (Omu *et al.*, 2016; Wallerand *et al.*, 2016), it is clear that the advantages are becoming more relevant as the complexity of energy systems increases. In other words, an optimisation model with the accuracy close to a simulation model would enhance the applicability of mathematical optimisation in designing energy systems.

Therefore, it is important to ***evaluate the relation and potential interactions between deterministic optimisation and dynamic simulation of energy systems***

in the comparative approach. One way to do this is by performing both deterministic optimisation and dynamic simulation for a given energy system and comparing the subsequent results.

2.4 Knowledge gaps

From the overview of energy systems optimisation and thermal energy storage presented in this Chapter, three knowledge gaps have been identified and are addressed in this thesis:

1. *Comparative evaluation of energy systems optimisation results (Chapter 4).*
   Most energy systems optimisation studies consider the optimisation step in isolation relative to other design processes, such as dynamic simulation of the system. Due to the reduced-order models used in typical optimisation problem formulation, it is important to know the relative accuracy of the optimisation results.
   In order to elucidate the advantages and limitations of an MILP optimisation model, a study on a residential heating system has been performed and reported in Chapter 4. The optimisation results are compared to dynamic simulation of the system.
2. *Time-series modelling in systems with temporally different storage technologies (Chapter 5).*
   Time series reduction is typically performed to reduce the size of optimisation problems. The most common method is the typical period approach where the entire time horizon of the problem is represented by several typical periods, e.g. days, weeks or months. However, such an approach becomes problematic if storage technology is present in the system, due to the coupling between time steps. Cyclic constraints can be introduced to overcome this problem, i.e. the state-of-charge of a storage is equal at the first and last time step within a typical period. Modelling seasonal storage with this approach has two main challenges: (i) its cyclic nature cannot be confined to days or weeks, and (ii) heat losses mechanism requires retaining information from the previous time step.
   In Chapter 5 of this thesis, a multiple time grids method is tested as a solution to the problem of reducing the time series in systems with seasonal storage. A solar district heating system is employed as a case study. The computational time and accuracy are then compared to the reference case which uses the typical hourly time series.
3. *Quantifying the performance of a UK-based solar district heating system with seasonal storage (Chapter 6).*
   The combination of district heating systems and seasonal storage has been well tested in different countries, such as Denmark, Germany, and Canada. The potentials of

such system in the UK has also been highlighted in different reports. Nevertheless, bottom-up studies to provide quantification to these potentials are very limited.

The quantification can be provided by simulating a solar district heating system using UK-specific inputs, such as heat demand and weather profiles. Using the outcome of investigating the previous two knowledge gaps, a validated simulation model of a solar district heating system is used to study the performance of the solar district heating system if it is deployed in the UK. This is part of the techno-economic study reported in Chapter 6.

These knowledge gaps are addressed using optimisation frameworks and dynamic simulation software which are implemented in case studies. The equipment models, objective functions, and general assumptions considered in this thesis are described in Chapter 3.

Chapter 3

Generic optimisation and simulation model

3.1 Overview

In this chapter, the general optimisation and dynamic simulation models used in this thesis are elaborated further. They form the methodological foundation for Chapter 4 - 6. The overall methodological framework is illustrated in Fig. 3.1. The core components of the framework are the heat demand model, design and operational optimisation, and dynamic simulation. The remaining parts are the most relevant inputs and outputs of the main components.

A heat demand model was developed to generate synthetic heat demand profiles, which in turn acts as one of the main inputs to both optimisation and simulation models.

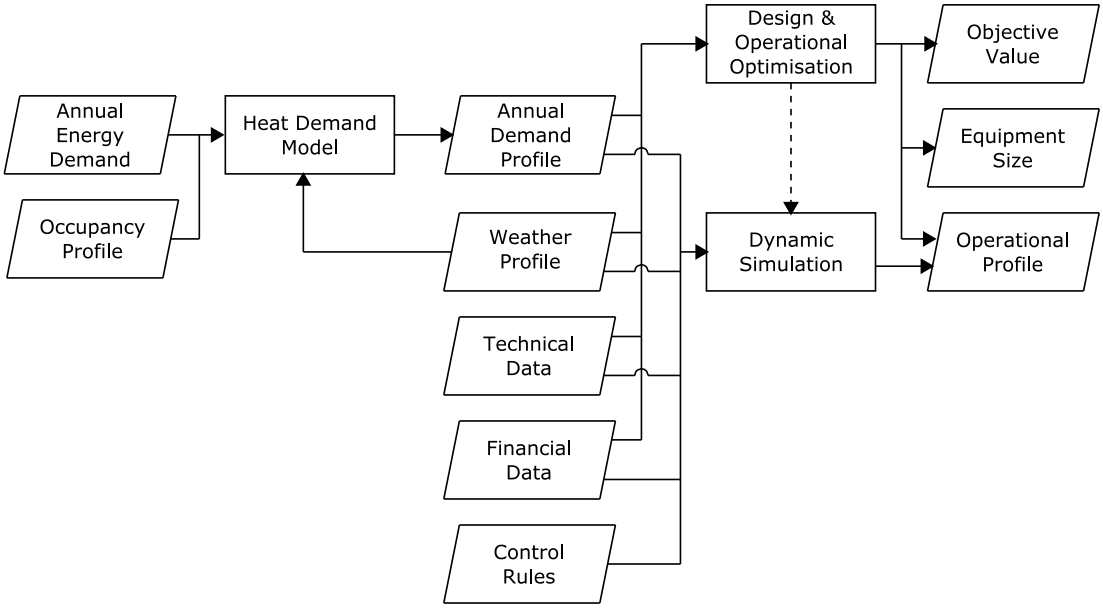

Figure 3.1: Overall framework of the optimisation and simulation models developed and used in this thesis.

The heat demand model uses a total annual demand value, occupancy profiles of the considered building, and a weather profile (i.e. external temperature) as inputs. It then produces an hourly demand profile over the entire year. Details on the heat demand model are given in Section 3.5.

The design and operational optimisation were performed on the problem which is defined by the parameters, variables, objective function, and constraints. In addition to the synthetic heat demand profile, the optimisation also used weather profile, technical data, and financial data as inputs. The outcomes, or solutions, of the optimisation include the objective value, equipment sizes, and optimal operational profiles. As discussed in Subsection 2.3.5, there are possible interactions between optimisation and simulation, which are illustrated as a dotted arrow in Fig. 3.1. Section 3.3 will describe the generic design and operational optimisation model in a more detailed manner.

The dynamic simulation models in this thesis were developed in TRNSYS (Klein *et al.*, 2017). Similar to the optimisation models, the simulation models also used weather profile, technical data, and financial data as inputs. However, unlike in the optimisation models, control rules were also taken as input in the simulation models. The main output of the simulation models is the operational profile of the whole system. Performance metrics can be further derived form this operational profile, for example the system efficiency and operational costs. Further description on the generic simulation model can be found in Section 3.4.

Before the main components in the framework are discussed further, it is useful to have a reference energy system for describing the optimisation and simulation models. For this purpose, a generic energy system is firstly defined in the following section.

3.2 Generic energy system with thermal energy storage

In general, the energy systems considered in this thesis consist of three main components: energy conversion equipment (CON), energy storage (TES), and energy demand (DEM), as illustrated in Fig. 3.2. The number of components and their connections in a real system are typically higher than shown in the figure. Nevertheless, this generic and simplified system is sufficient to serve as a foundation for the formulation of the optimisation and simulation models employed in this thesis. Furthermore, all systems considered in this thesis are assumed to be in quasi-steady state in each time step.

The energy conversion equipment receives input, $\dot{Q}_{in,t}^{CON}$, in the form of electricity, fuels, or renewable sources, such as solar energy. It then converts the input energy into the corresponding output energy vector, $\dot{Q}_{out,t}^{CON}$. In this thesis, the primary output vector

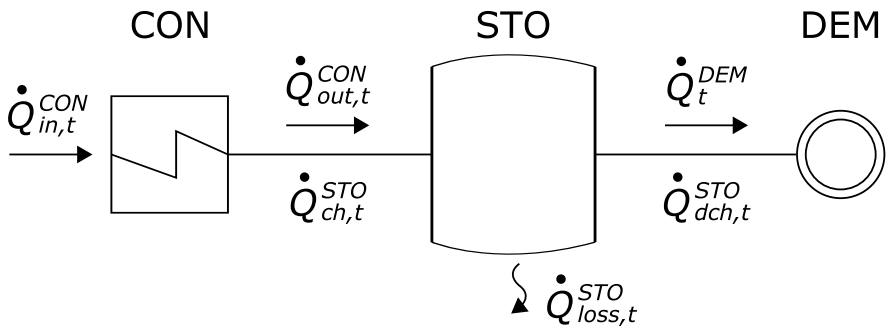

Figure 3.2: Generic energy systems: energy conversion equipment (CON), energy storage (TES), and energy demand (DEM).

considered is thermal energy in the form of hot water. Thus, relevant energy conversion equipment includes boilers, heat pumps, and solar thermal collectors.

The energy storage equipment has three energy flows: charge ($\dot{Q}^{STO}_{ch,t}$), discharge ($\dot{Q}^{STO}_{dch,t}$), and static loss ($\dot{Q}^{STO}_{loss,t}$). In Fig. 3.2, charging is performed by the output of the conversion equipment, while discharging is fulfilling the energy demand. The stored energy can be calculated by performing energy balance calculation on the storage equipment.

The heat demand node represents the energy required for every time step in a given time horizon. An hourly time step is taken as the generic time step size in this thesis, while the time horizon varies from daily up to multi-year depending on the problem at hand.

3.3 Optimisation model

The general optimisation framework employed in this thesis prescribes the objective function and the constraints as linear functions. As discussed in Subsection 2.3.2, linear formulations can produce sufficiently accurate results with significantly faster computational time compared to non-linear ones. In addition to continuous variables, such as energy flow, the problems considered in this thesis also include integer variables, for example, the decision variables related to discrete equipment sizes in design optimisation and equipment operation (ON/OFF) in operational optimisation. Therefore, the optimisation problems are formulated as mixed-integer linear programming (MILP) problems.

The general formulation of the MILP model is shown in Eq. 3.1, where $f(\boldsymbol{x}, \boldsymbol{y})$ is the objective function to be minimised, $\boldsymbol{x}$ is the vector of continuous decision variables, $\boldsymbol{y}$ is the vector of integer decision variables, $c1$ and $c2$ are the coefficient matrices, b is the vector of parameters, and l and u are the lower and upper bound of the continuous variables, respectively.

$$\begin{aligned} \min_{x,y} \quad & f(\boldsymbol{x}, \boldsymbol{y}), \\ \text{s.t.} \quad & c_1\boldsymbol{x} + c_2\boldsymbol{y} \leq b, \\ & l \leq \boldsymbol{x} \leq u, \quad \boldsymbol{y} \in 0, 1 \end{aligned} \tag{3.1}$$

To guarantee the optimality of solutions, deterministic algorithms are employed to solve the optimisation problems in this thesis. The algorithms are part of Mixed Integer Programming solvers inside CPLEX, which is used as the solver software package for the optimisation work in this thesis (IBM, 2017).

Furthermore, the optimisation problems considered in this thesis are limited to design and operational optimisation. Chapter 4 includes a study on design and operational optimisation, while Chapter 5 focuses solely on an operational optimisation. In both cases, the superstructure of the system is assumed to be given.

3.3.1 Objective function

In this thesis, only a single objective optimisation is considered. This limitation is taken to focus on the interactions between optimisation and simulation model, as well as on the impact of complexity reduction techniques on the results accuracy.

The objective function is financial and depending on the optimisation level, can take form as either the total cost or operational cost. The total cost formulation is shown in Eq. 3.2 and based on the concept of Net Present Value (NPV). It includes investment cost C_{inv}, operational cost C_{opr}, revenue from subsidy R, discount rate, r, and time of the cash flow, τ.

$$\min \quad C_{tot} = \min \left\{ C_{inv} + \sum_{\tau=1}^{N} \frac{C_{opr} - R}{(1+r)^{\tau}} \right\} \tag{3.2}$$

In the illustrative system, the investment cost is the sum of capital and installation cost of both conversion and storage equipment (Eq. 3.3).

$$C_{inv} = C_{inv}^{CON} + C_{inv}^{TES} \tag{3.3}$$

The operational cost is considered as the objective function in the operational optimisation of energy systems, where equipment sizes are predetermined (as in Chapter 5). An example of operational cost formula for the system in Fig. 3.2 is shown in Eq. 3.4.

The operational cost is calculated by multiplying the input energy to the conversion equipment, $\dot{Q}_{in,t}^{CON}$, with the cost of the input energy, C_{in}^{CON}, and the corresponding time step size, Δt.

$$\min \quad C_{opr} = \min \sum_{t_{start}}^{t_{end}} \left(\dot{Q}_{in,t}^{CON} \cdot \Delta t \cdot C_{in}^{CON} \right) \tag{3.4}$$

As for the revenue streams, there are several possible sources depending on the considered system. These include selling the output energy to the grid (e.g. electricity), and policy-based subsidies, such as the Renewable Heat Incentive in the UK (Ofgem, 2017).

3.3.2 Equipment constraints

In modelling the equipment in the optimisation models, an energy flow approach is adopted in this thesis. It is based on the first law of thermodynamics, i.e. energy balance, and does not dynamically model the temperature of the flow. The temperature of the flow is instead assumed in the calculation of the energy flow. For instance, in the optimisation model of Chapter 4, the heating flow temperature of 50 °C is considered, while a temperature difference of 10 °C is assumed for the storage tank. The benefits and limitations of this particular approach will be discussed further in Chapter 4.

Discrete equipment size

The available size of standard equipment is typically discrete; thus it is represented by an integer in the problem formulation. As an illustration, if the conversion and storage equipment shown in Fig. 3.2 have a discrete set of sizes from which one can be selected; this can be ensured by implementing Eq. 3.5 and 3.6. Binary variable y_i corresponds to whether equipment of size i is selected or not, while continuous variable $\dot{Q}_{i,nom}^{CON/STO}$ is the nominal capacity of the equipment of size i. Similar constraints can also be applied to describe the decision if a specific equipment type is installed or not.

$$\sum_{i=1}^{n} y_i = 1, \qquad y_i \in \{0, 1\} \tag{3.5}$$

$$\dot{Q}_{nom}^{CON/STO} = \sum_{i=1}^{n} y_i \cdot \dot{Q}_{i,nom}^{CON/STO} \tag{3.6}$$

Conversion equipment

The output of a conversion equipment can be modelled as the product of energy input and equipment efficiency, η^{CON} (Eq. 3.7). Furthermore, it is limited by the nominal capacity at the upper side and by the minimum load factor at the lower side (Eq. 3.8). LF_{min} is the minimum load factor, while δ_t^{CON} is the ON (1)/OFF (0) status of the equipment at time t. If the equipment model does not include a minimum load factor, the left-hand side of Eq. 3.8 is zero.

Eq. 3.8 includes nonlinearity in the form of a bilinear term $\delta_t^{CON} \cdot \dot{Q}_{nom}^{CON}$. This nonlinearity is reformulated into linear equations (Glover, 1975). Further information on the reformulation can be found in Appendix A. The reformulation also allows for continuous equipment sizes to be used in the problem formulation.

$$\dot{Q}_{out,t}^{CON} = \eta^{CON} \cdot \dot{Q}_{in,t}^{CON} \tag{3.7}$$

$$LF_{min} \cdot \delta_t^{CON} \cdot \dot{Q}_{nom}^{CON} \leq \dot{Q}_{out,t}^{CON} \leq \delta_t^{CON} \cdot \dot{Q}_{nom}^{CON} \tag{3.8}$$

Storage equipment

The stored energy at every time step is calculated according to Eq. 3.9.

$$Q_{sto,t}^{TES} = \left(1 - \phi^{TES}\right) \cdot Q_{sto,t-1}^{TES} + \left(\dot{Q}_{ch,t}^{TES} - \dot{Q}_{dch,t}^{TES}\right) \cdot \Delta t \tag{3.9}$$

where

$Q_{sto,t}^{TES}$	is the energy content of storage TES at time step t.
$\dot{Q}_{ch,t}^{TES}$	is the rate of energy charged to storage TES at time step t.
$\dot{Q}_{dch,t}^{TES}$	is the rate of energy discharged from storage TES at time step t.
ϕ^{TES}	is the loss fraction of storage TES.
Δt	is the time step size.

In this thesis, the charge and discharge process of a TES are assumed to occur without losses. Furthermore, the storage variables are also constrained by their respective maximum value, as shown for the case of maximum storage capacity, Q_{max}^{TES} (Eq. 3.10), maximum charge rate, $\dot{Q}_{ch,max}^{TES}$ (Eq. 3.11), and maximum discharge rate $\dot{Q}_{dch,max}^{TES}$ (Eq. 3.12).

$$0 \leq Q_{sto,t}^{TES} \leq Q_{max}^{TES} \tag{3.10}$$

$$0 \leq \dot{Q}_{ch,t}^{TES} \leq \dot{Q}_{ch,max}^{TES} \tag{3.11}$$

$$0 \leq \dot{Q}_{dch,t}^{TES} \leq \dot{Q}_{dch,max}^{TES} \tag{3.12}$$

The state-of-charge of the storage equipment, SOC_t^{TES}, is calculated as the ratio between the stored energy at time step t and the storage maximum capacity (Eq. 3.13). The storage operation can be further constrained by prescribing a cyclic behaviour for a given time horizon (Eq. 3.14), for example, daily cycle for a domestic hot water tank. In most cases, this is performed to limit the problem complexity caused by the flexibility of the storage equipment.

$$SOC_t^{TES} = Q_{sto,t}^{TES} / Q_{max}^{TES} \tag{3.13}$$

$$SOC_{t=0}^{TES} = SOC_{t=t_{end}}^{TES} \tag{3.14}$$

Heat exchange

The interactions between conversion equipment, storage, and demand are defined by energy balance constraints which represent the energy flows between them. For the illustrative case of Fig. 3.2, two constraints can be defined as in Eq. 3.15 and 3.16. It should be noted that building inertia is not considered in the model; thus, the equality is prescribed between the TES discharge and the heat demand in Eq. 3.16.

$$\dot{Q}_{out,t}^{CON} = \dot{Q}_{ch,t}^{TES} \tag{3.15}$$

$$\dot{Q}_t^{DEM} = \dot{Q}_{dch,t}^{TES} \tag{3.16}$$

Modelling tools

The optimisation models are developed in Pyomo 4.0, a Python-based, open source optimisation modelling language (Hart *et al.*, 2012). After all the data sets, parameters, variables, objective function, and constraints are formulated in Pyomo, it constructs the corresponding problem matrices to be solved by the selected solver software. In this thesis, the optimisation problems are solved by invoking CPLEX 12.6.2 solver from within the Python source code. The CPLEX mixed integer solver algorithm is based on branch & cut algorithm (IBM, 2017). A relative optimality gap of 1% is implemented

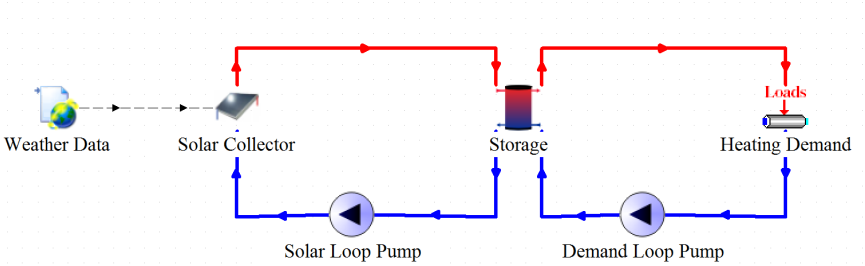

Figure 3.3: An example of TRNSYS model.

in the optimisation reported in this thesis unless stated otherwise. Apart from the optimality gap, the default configuration of CPLEX is used to solve the optimisation problems. All optimisation runs were performed on a Windows computer with 3.4GHz i7 Intel processor and 16 GB of RAM.

3.4 Dynamic simulation model

The dynamic simulation software used in this thesis is Transient System Simulation Tool (TRNSYS) (Klein *et al.*, 2017). The software has been developed since 1975 by the Solar Energy Laboratory at the University of Wisconsin, Madison, and used extensively in the industry. It consists of two main programs: the simulation engine (kernel) and the visual interface. The simulation engine performs the core computation and input/output preparations, while the visual interface uses drag-and-drop mechanism to assist the user in creating the modelled energy system. The simulation engine numerically solves the coupled system of algebraic and differential equations that model the energy system.

As an example, Fig. 3.3 shows the TRNSYS model of the generic energy systems (Fig. 3.2) with a solar collector as the energy conversion equipment and a hot water tank as the storage equipment. Typical outputs of such simulation include the temperature profiles of the flows, total solar energy collected, energy loss from the storage, total energy from auxiliary heater within the storage, and electricity consumption of the pumps. Furthermore, a parametric study can be performed to assess the influence of system's parameters on the outputs. It should be noted that for the same case study, identical equipment parameters are implemented in both optimisation and simulation models. This is important in order to maintain comparability between results of the two approaches.

The equipment model in a TRNSYS simulation depends on the "Type" employed to represent the equipment. Essentially, a Type in TRNSYS is a black box which receives inputs from the kernel and produces outputs according to its own modelling equations. These can range from a simple summation calculation up to differential equations.

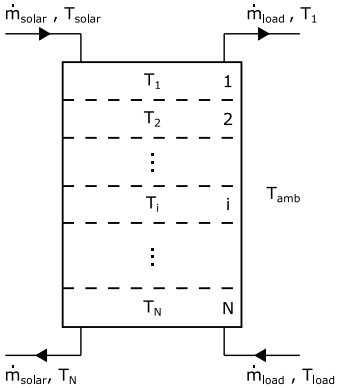

Figure 3.4: Storage tank stratification in Type 4a model.

In the example, the solar collector is represented by Type 1a, which implements quadratic efficiency and no incidence angle modification. The corresponding efficiency formulation is shown in Eq. 3.17. The user then has to provide the value of parameters η_0, a_0 and a_1, which are typically available from manufacturer's data sheets or standardised tests. Solar irradiance at the surface, G_T, is given as an input from the weather data component, while the specific heat of the fluid, c_p, and the collector area, A are given as parameters. The solver will calculate the useful energy gain, $\dot{Q}_u$ by considering the mass flow rate, $\dot{m}$, the inlet T_{in} and outlet temperature, T_{out}, which are coupled with other components in the system, in this case, the solar loop pump and storage tank. In Eq. 3.17, ΔT corresponds to the difference between the inlet temperature, T_{in}, and the external air temperature, T_{ext}. The equation is the basis of the standard test methods for solar collectors (Duffie and Beckman, 2013), and typically valid along the $\frac{T_{in}-T_{ext}}{G_T}$ value of 0 up to 0.2 $m^2°C/W$.

$$\eta = \frac{\dot{Q}_u}{AG_T} = \frac{\dot{m}c_p(T_{out} - T_{in})}{AG_T} = \eta_0 - a_0\frac{\Delta T}{G_T} - a_1\frac{\Delta T^2}{G_T} \tag{3.17}$$

There are several models available to represent a hot water tank storage in TRNSYS. Type 4a Stratified Storage Tank with Fixed Inlets and Uniform Losses is implemented in the example. It models a fluid-filled sensible TES tank with N thermally stratified layers, as shown in Fig. 3.4. Energy balance equations for each layer are solved by TRNSYS to determine the temperature profile of the tank at time step t. In addition to the storage volume and fluid properties, other important parameters to be defined by the user include the number of layers, the location and maximum power of auxiliary heaters, and the tank loss coefficient.

In addition to physical equipment and input/output types, it is also possible to model the control of the system in TRNSYS. For example, the flow rate of the solar loop

pump in Fig. 3.3 can be controlled proportionally to maintain a certain temperature level at the outlet of the solar collector.

The connection between two components in the model determines which output variables of the first one become the input of the second. Among physical equipment, these are typically the temperature and rate of the flow. For instance, the outlet temperature and flow rate of the solar collector in Fig. 3.3 act as inputs for the storage equipment.

In performing the simulation, TRNSYS arranges the components in an order and tries to numerically solve the corresponding equation of each component for every time step. Due to the coupled nature of the components, the computation for every time step is performed iteratively until a level of convergence is reached before moving on to the next time step. At each iteration and at each time step, a component transforms the current values of inputs and parameters into outputs.

3.5 Synthetic heat demand

One important input to a heating system optimisation and simulation is heat demand data. A real measurement-based demand profile with complete supporting information is difficult to obtain and rarely available in the literature. For example, hourly gas and electricity consumptions for several houses in the Milton Keynes Energy Park (MKEP) project are available, but details on housing characteristics and social information are missing (UK Energy Research Centre, 2015). Thus, a heat demand model is used in this thesis to generate synthetic heat demand profiles.

Heat demand depends on numerous factors, such as weather conditions, building characteristics, occupancy profile, the installed heating system and occupant's behaviour. A heat demand model typically reduces this complexity by various simplifications depending on the modelling approach. Residential energy demand can be modelled by two modelling approaches: top-down and bottom-up (Swan and Ugursal, 2009). The top-down approaches rely on highly aggregated historical energy consumption data and are relatively straightforward to develop. On the other hand, the bottom-up approaches, which can be further categorised into bottom-up statistical and bottom-up engineering approaches, require more detailed input information (e.g. building characteristics and billing data) and can be computationally intensive.

The synthetic heat demand model developed in this thesis combines different aspects of the aforementioned modelling approaches: aggregated consumption data from the top-down approach and occupancy data from the bottom-up approach. The model requires the total annual heat demand, external temperature data and occupancy profile as inputs. The latter two are selected over other influencing factors, e.g. solar gain, due

to their relative importance as reported by various studies (e.g. (Kelly *et al.*, 2013; Kane *et al.*, 2014)). The model is based on the energy signature method, where the heat demand is assumed to be a linear function of external temperature (Heller, 2002; Girardin *et al.*, 2010), with the extension of occupancy profiles consideration.

The fundamental concept behind the model is to distribute the total annual heat demand (Q^{DEM}_{annual}) into smaller time steps, e.g. hourly, assuming that the demand for a given time step is available only if the external temperature (T_{ext}) drops below a certain threshold temperature (T_{thld}). Clearly, the integration of the demand at smaller time steps should be equal to the total annual heat demand (Eq. 3.18).

$$Q^{DEM}_{annual} = \int_{year} \dot{Q}(t)\mathrm{d}t \tag{3.18}$$

The external temperature is used as a reference, instead of the internal comfort temperature, because the heat demand is modelled as a simple load flow rather than as a thermal model of the house. Thus, building inertia is not considered in the model. This simplification is implemented to minimise the complexity of the model by focusing more on the supply equipment. The benefits of such approach will become more apparent when larger energy systems with various demand points are examined.

The distribution of annual heat demand is then performed using Eq. 3.19 - 3.22. Two threshold temperatures are defined in the model to better emulate the occupancy profile of a building: active (T^{ac}_{thld}) and inactive threshold temperatures (T^{ic}_{thld}). This feature was not available in the energy signature model in the literature and added during the development of the heat demand model used in this thesis. In Eq. 3.19 - 3.22, the subscript *ac* and *ic* correspond to the active and inactive period, respectively. In a typical residential building, inactive period includes night time sleeping and day time working hours. Furthermore, the heat demand, $\dot{Q}(t)$, is strictly positive in Eq. 3.19.

$$\dot{Q}(t) = \begin{cases} k_1 \cdot T_{ext}(t) + k_2^{ac} & \text{if } T_{ext} < T^{ac}_{thld} \wedge t \in t^{ac} \\ k_1 \cdot T_{ext}(t) + k_2^{ic} & \text{if } T_{ext} < T^{ic}_{thld} \wedge t \in t^{ic} \\ 0 & \text{otherwise} \end{cases} \tag{3.19}$$

$$k_1 = \frac{Q^{DEM}_{annual}}{HH^{ac} + HH^{ic}} \tag{3.20}$$

$$
\begin{aligned}
HH^{ac} &= \int_{t \in t^{ac}: T_{ext} < T^{ac}_{thld}} T_{ext}(t)\,\mathrm{d}t - \int_{t \in t^{ac}: T_{ext} < T^{ac}_{thld}} T^{ac}_{thld}(t)\,\mathrm{d}t \\
HH^{ic} &= \int_{t \in t^{ic}: T_{ext} < T^{ic}_{thld}} T_{ext}(t)\,\mathrm{d}t - \int_{t \in t^{ic}: T_{ext} < T^{ic}_{thld}} T^{ic}_{thld}(t)\,\mathrm{d}t
\end{aligned}
\tag{3.21}
$$

$$
\begin{aligned}
k_2^{ac} &= -k_1 \cdot T^{ac}_{thld} \\
k_2^{ic} &= -k_1 \cdot T^{ic}_{thld}
\end{aligned}
\tag{3.22}
$$

In Eq. 3.19, the assumed linear relation between heat demand and external temperature is constructed using two signature variables k_1 and k_2. The first signature variable is calculated by dividing the total annual heat demand with the heating degree hours, HH (Eq. 3.20). The latter corresponds to the number of hours in a year when heating is required and is calculated according to Eq. 3.21. The second signature variable is calculated according to Eq. 3.22.

The synthetic heat demand profiles generated in this thesis were based on the occupancy profile of 2 working adults working full-time. This corresponds to a scenario which has an unoccupied period, i.e. inactive, from 09.00 to 18.00 (Yao and Steemers, 2005). During the occupied period the heating system is operational if the external temperature is below the threshold temperature. Here, the night-time (23.00 - 07.00) counts as the inactive period with the inactive threshold temperature $T^{ic}_{thld} = 0$ °C while the rest of the day uses the active threshold temperature $T^{ac}_{thld} = 14$ °C. The decision to not differentiate between weekday and weekend profile was based on a city-scale study of indoor temperature measurements in the UK, which found that there was no noticeable difference in the heating pattern between weekdays and weekends (Kane *et al.*, 2014). The same study also reported that the average threshold heating temperature for monitored UK homes is 13.3 °C with 1.4 °C standard deviation. This value is the basis for the $T^{ac}_{thld} = 14$ °C assumption used in this thesis. Furthermore, the inactive threshold temperature assumption was taken to consider that the heating system is typically switched off during inactive period, apart from the unusually cold days when it is switched on even during inactive night time period. The $T^{ic}_{thld} = 0$ °C was assumed to consider these unusually cold days. Moreover, different values of occupied periods and threshold temperatures can be set relatively easily in this synthetic heat demand generation methodology.

Fig. 3.5 illustrates example of synthetic heat demand profiles generated by the model. The annual energy consumption of the modelled dwelling is calculated by multiplying the average natural gas consumption for space and water heating in a Scottish dwelling (i.e. approximately 15000 kWh/year (Walker, 2012)) with assumed boiler efficiency of

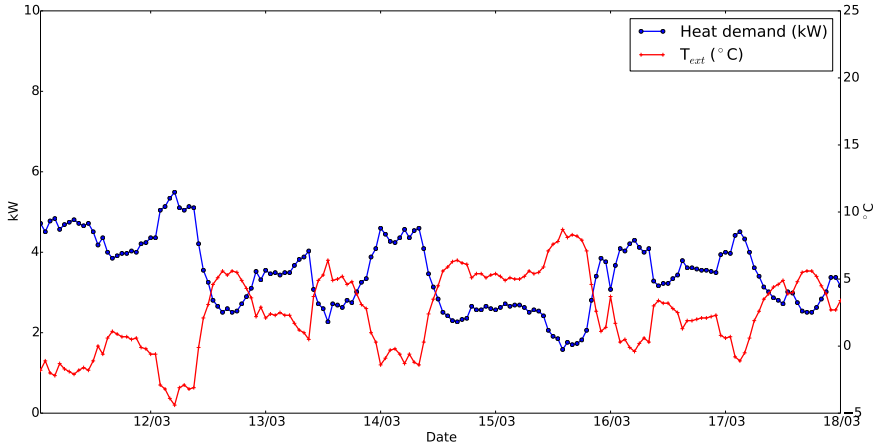

(a) Synthetic demand without occupancy factor

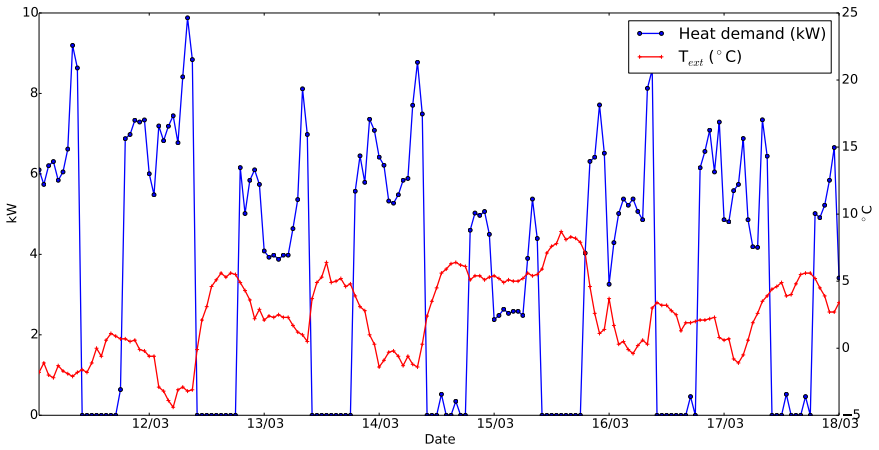

(b) Synthetic demand with occupancy factor

Figure 3.5: The influence of occupancy profile on the generated synthetic heat demand profile.

90%. The efficiency value is assumed to be constant due to the relatively small range of efficiency fluctuation in a typical condensing boiler (85% - 95%) (Baldi *et al.*, 2017). The external temperature data are gathered from Met Office data for an Edinburgh weather station in 2013 (Met Office, 2006). This demand profile is a part of an annual profile used in the design and operational optimisation in Chapter 4.

The inclusion of occupancy profile has a profound impact on the synthetic demand profile, as can be seen in the comparison between Fig. 3.5a and 3.5b. Without occupancy profile, the resulting demand profile does not show sharp peaks and no demand period, which is not realistic in a domestic house case. These demand peaks are crucial for a proper sizing of the energy conversion and storage equipment.

In order to evaluate the resulting synthetic demand profile against real heat demand data, the heat demand and external temperature data of a house in Milton Keynes

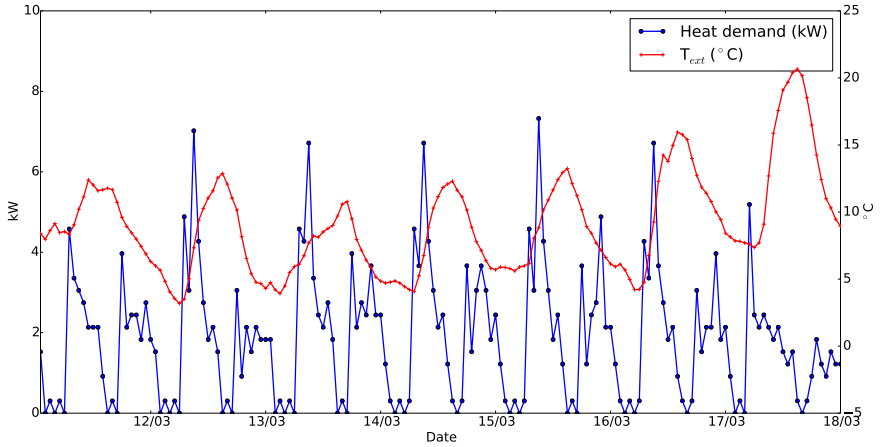

(a) MKEP real heat demand

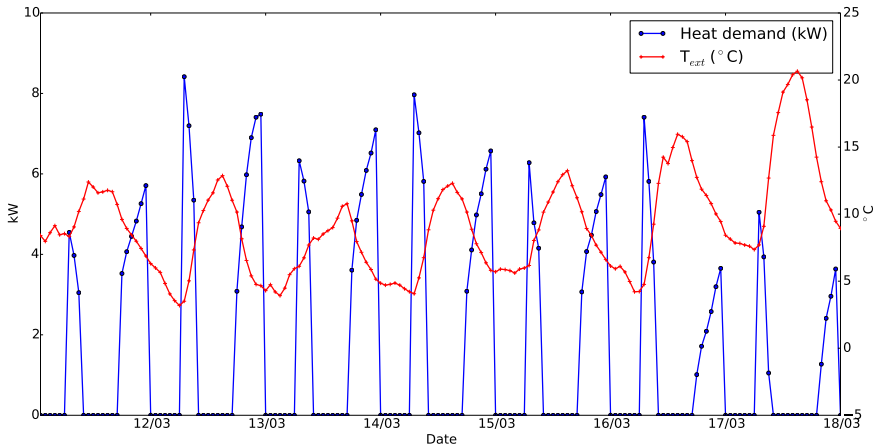

(b) MKEP synthetic heat demand

Figure 3.6: Comparison between the real and synthetic heat demand profile of an MKEP house.

Energy Park are shown in Fig. 3.6. In this case, the heat demand is derived from the gas consumption, which is available as hourly measured data in the MKEP datasets. Annual gas consumption of the MKEP house is 13456 kWh. The general trend of the synthetic heat demand profile is comparable to the real demand profile of the selected house. The difference in detailed peaking pattern between the two profiles can be attributed to the domestic hot water (DHW) demand, which is not modelled in the synthetically generated profile shown in Fig. 3.6b. Nevertheless, the synthetic demand is able to capture the important demand peaks, both in magnitude and time of occurrence. This shows that the synthetic demand profile is sufficiently accurate for sizing purposes.

3.6 Summary

The general optimisation and simulation models used in this thesis have been presented in this chapter. Optimisation of energy systems is formulated as a mixed integer linear programming problem, while their simulation is performed using a dynamic simulation software, TRNSYS. The general information in this chapter serves as foundations for answering the research questions, which will be elaborated in the following chapters.

Chapter 4

Optimisation and simulation of a residential heat pump system

Part of the work presented in this chapter is based on a published article (Renaldi *et al.*, 2017).

4.1 Introduction

Among the three types of interaction between optimisation and simulation discussed in Chapter 2, the comparative approach has several advantages over the other methods. First, it preserves the strengths of both models, while minimising their weaknesses. For instance, a simulation model can be used to validate or improve the equipment models implemented within an optimisation model. On the other hand, an optimisation model is capable of covering a wider design space than the expert knowledge of a modeller, which is typically relied upon in building a simulation model. Second, by keeping the models relatively independent to each other, the general applicability of this approach is arguably higher than the other interactions. For example, the design team does not have to use or build a specific framework which is tailor-made to exploit particular connections between the two models.

However, it is important to examine how this interaction can be implemented in a design workflow. In the literature, studies that apply the comparative approach are typically performed at a component and systems level. For example, Omu et al. compared equipment models of short-term storage to be used in an optimisation model with the EnergyPlus model of the same equipment (Omu *et al.*, 2016). This component-based comparison is useful to overcome the potential of over-simplification in modelling physical equipment in optimisation models. Such a comparison was also employed by Wallerand et al. to find the loss coefficient of three different storage models (Wallerand *et al.*, 2016). In addition to this, they also performed a system level comparative interaction by implementing the resulting optimal operating strategy from MILP optimisation into the TRNSYS model. Nevertheless, the system level interaction was performed

empirically by modifying the flow diverters in the systems in such a way that the resulting operational profile would mimic the MILP results. As the systems complexity increases, this empirical approach would not be sufficient or practical to model the operational profile.

One option to overcome this issue is to directly use the MILP operational profile as an input to the TRNSYS model. Despite its more systematic nature, there are inherent challenges that need to be addressed since it attempts to bridge two different models and uses the time series output of one as the input of another. This particular approach of comparative interactions between optimisation and simulation model is one of the main points in this chapter.

In order to illustrate it, a case study based on a residential heating system is considered. Although a more complex system, e.g. urban energy systems, could be used as a case study, it is more important to focus on the comparative interaction and maintain the tractability of the model in this study. The chapter also highlights the ability of the optimisation model to examine the design space and provide insight towards the best system configuration. A low-carbon residential heating system based on a heat pump and TES is selected for these purposes.

4.2 Heat pump and thermal energy storage

The utilisation of heat pumps (HP) to fulfil heat demand is one of the potential solutions towards low carbon heating systems, given the prerequisite that the electricity is generated mainly by renewable energy sources. Fig. 4.1 illustrates how heat pumps can reduce primary energy consumption in a domestic setting (Staffell *et al.*, 2012). A heat pump system has a primary energy utilisation of greater than one since heat is recovered from the environment (Fig. 4.1a), as opposed to the completely wasted heat in the case of condensing boiler (Fig. 4.1b).

Heat pumps, along with refrigerators, can be considered as reversed heat engines. As illustrated in Fig. 4.2, a heat pump system moves thermal energy from a low temperature, $\dot{Q}_{HP,in}$, to a high temperature region, $\dot{Q}_{HP,out}$, using mechanical work as an input. The mechanical work input is provided by the compressor, which uses electricity as its input ($P_{HP,in}$). Most heat pump systems in common use at present are of the vapour-compression type. The basic components of this type are a compressor, condenser, expansion valve, and evaporator, as shown in Fig. 4.2.

Further integration of heating and electricity networks also expands the opportunities for demand side management. One of these is the combination of HP with thermal energy storage (TES) to shift heating-related electrical load from on-peak to cheaper

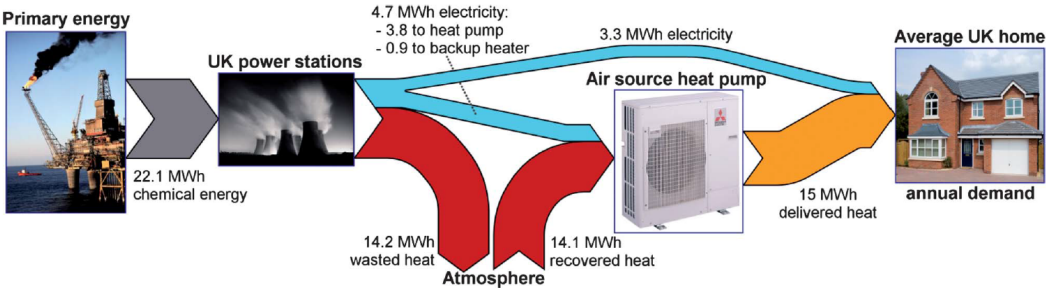

(a) Heat pump

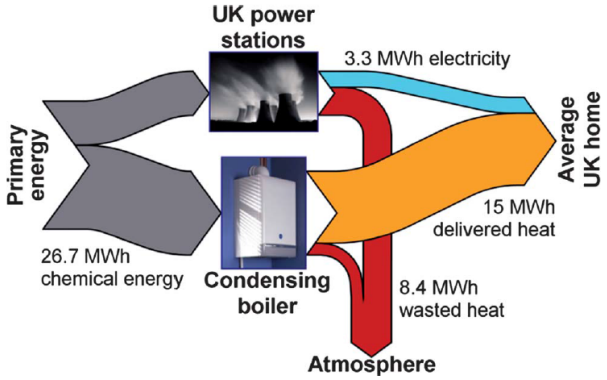

(b) Condensing gas boiler

Figure 4.1: Sankey diagram of a heat pump system (a), and condensing gas boiler (b) for a typical case in the UK (Staffell *et al.*, 2012).

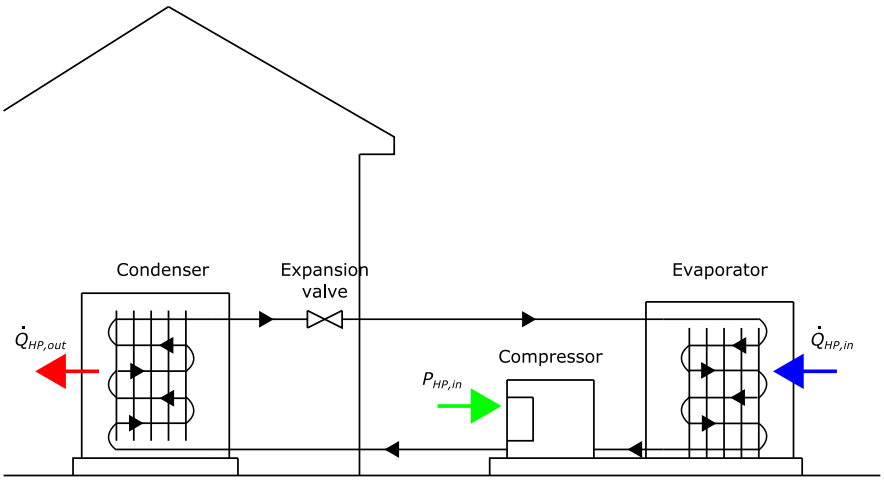

Figure 4.2: Schematic of a vapor-compression heat pump system.

off-peak hours (Arteconi *et al.*, 2013), and in the future to times with surplus renewable electricity. The aggregation of such system has been shown to have the potential benefits to reduce required investments in peak and reserve capacity through peak load shaving with intelligent operational control (Hedegaard and Balyk, 2013).

An early study on the implementation of this system in the UK was done by Tassou et al. which explored the installation of heat pumps in the UK and compared its economic performance with typical heating systems in the late 1980s (Tassou *et al.*, 1986). It was concluded that for the heat pump system to be competitive with a gas central heating system, its capital cost has to be substantially reduced and its technical performance to be significantly improved. Since then, technological improvements and supporting policies have promoted heat pumps beyond the early stage limitations. However, despite the improvements, heat pumps are not the primary choice of the UK domestic consumer. This can be attributed to various factors, such as cost, technical familiarity, climate effect, and policies (Singh *et al.*, 2010; Pan and Cooper, 2011).

Results from a recent field trial in the UK illustrate the real performance of the technology (Dunbabin *et al.*, 2013). One of the main recommendations based on the field trial results was to properly define system boundaries in referring to performance metrics, such as seasonal performance factor, as well as providing a more realistic metric and clearer control options to the users. In another study, the actual performance measured in UK and German field trials were compared (Staffell *et al.*, 2012). It was concluded that the difference in results from the trials highlights the importance of design, installation, and operation in the energy and CO_2 saving that can be achieved by heat pump systems.

Simultaneous design and operational optimisation of HP-TES systems are essential to ensure that the installations of new energy systems lead to improvements, both financially and environmentally, compared to conventional heating systems. Furthermore, this optimisation has to be performed for every installation due to the vastly different local weather conditions, occupancy profiles, energy tariffs, government subsidies and building types. For example, the optimal sizing of the HP is crucial due to the large variations in heat demand throughout the year (Singh *et al.*, 2010; Staffell *et al.*, 2012). An undersized HP might worsen the overall economic and environmental performance by increased utilisation of electric resistive heating to cover the heat demand while an oversized HP would increase the capital costs. Additionally, the operational optimisation is particularly relevant when different energy vectors are intertwined in the future smart energy system, e.g. widespread installation of HP-TES systems. However, such an integration brings new challenges in the control and operation of the energy system. For example, it has been shown that synchronised load-shifting with HP-TES systems can lead to a significantly increased peak load in the electricity system (Kelly *et al.*, 2014). Thus it is essential to be able to assess the performance of an HP-TES system before the installation and also during the operation of the system. As Kelly et al. showed, the latter point is particularly important to enable a concerted operation of multiple HP-TES systems in either an integrated energy system or a district heating

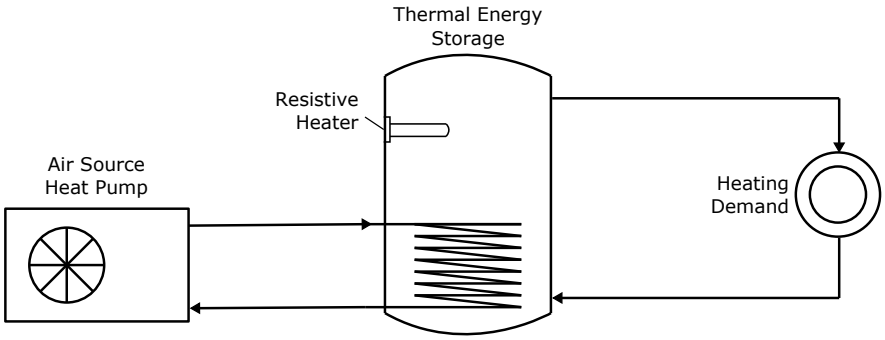

Figure 4.3: Case study: a residential heating system with air source heat pump and thermal energy storage.

network.

The design and operational optimisation of heat pump systems have been investigated in different studies using various tools. For example, Shiba et al. used a linear programming method to determine the optimal sizing of a commercial heat pump / thermal storage system (Shiba *et al.*, 1995). It was shown that the introduction of storage could shift the electricity consumption from on-peak to off-peak hours. The effects of off-peak tariff periods and building fabric characteristics on heat pump annual performance have also been investigated using a TRNSYS model (Cabrol and Rowley, 2012). In addition to design and operational optimisation, the control aspect of residential heat pump systems has also been subjected to various studies. Verhelst et al. investigated multi-objective optimal control of a residential heat pump (Verhelst *et al.*, 2012a).

Given the significant potentials of a heat pump-based residential heating system in the future UK energy system, it is chosen as a case study in this chapter. Furthermore, various tools have been employed to study such systems in both optimisation and simulation work. Nevertheless, there is less information in the literature regarding the interaction between the two approaches in designing the system.

4.2.1 Case study

The system consists of a monovalent air-source heat pump with hot water tank as thermal energy storage, as shown in Fig. 4.3. The heat pump provides energy to the storage through a coil heat exchanger at the bottom of the tank, and a resistive heating element acts as the backup heat source. Equipment sizes considered for optimisation are based on commercially available sizes for domestic application, i.e. 5 - 14 kW for heat pump, and 120-300 L for energy storage. In both the optimisation and simulation model, the heat demand is modelled as the energy flow to be satisfied with an hourly time step.

Table 4.1: DHW probability distribution

Time period	Ratio of daily DHW-volume
Weekdays / Weekends	
07.00 - 09.00 / 08.00 - 10.00	50 %
09.00 - 18.00 / 10.00 - 16.00	10 %
18.00 - 23.00 / 16.00 - 00.00	30 %
23.00 - 07.00 / 00.00 - 08.00	10 %

4.2.2 Optimisation and simulation framework

The overall framework shown in Fig. 3.1 was employed in developing the optimisation and simulation model of the case study. Three main components in the framework, namely the heat demand model, design and operational optimisation, and simulation, are explained further in the following paragraphs.

4.3 Heat demand model

The space heating demand is constructed using the synthetic heat demand method described in Section 3.5. The annual energy consumption of the modelled dwelling is calculated by multiplying the average natural gas consumption for space and water heating in a Scottish dwelling (i.e. approximately 15000 kWh/year (Walker, 2012)) with an assumed boiler efficiency of 90%. The external temperature data are gathered from Met Office data for an Edinburgh weather station in 2013 (Met Office, 2006).

Domestic hot water (DHW) demand is included by calculating the draw profile with the *DHWcalc* software (Jordan and Vajen, 2005). In estimating the DHW draw profile, *DHWcalc* requires some inputs, such as house type, mean daily draw-off volume and probability distributions of the draws. Table 4.1 shows the distribution used in this study. The 10% daily draw assumption during the unoccupied hours is chosen to consider the small irregularity in occupancy profiles and possible demand from appliances.

In producing the DHW profile, the software calculates the number of draw-off incidences by dividing the total annual draw-off volume by the mean flow rate for each category, e.g. bath, shower, etc. The draw-off incidences are then spread throughout the time period using the cumulated frequency method. More detailed descriptions of the methodology can be found in Ref. (Jordan and Vajen, 2005).

4.4 Design and operational optimisation

4.4.1 Objective function

The main optimisation problem of this study is to find the optimal sizing and operational profile which minimises the total cost over the time horizon, as defined in Eq. 3.2. The optimisation run was performed over an entire year in hourly time steps, i.e. 8760 h.

The investment cost includes equipment price and installation costs. The latter was assumed to be £1500 and £500 for HP and TES, respectively (Staffell *et al.*, 2012). The annual operational cost consists of the total amount of electricity input to the heat pump, P_{in}^{HP}, and resistive heater, P^{RH}, multiplied by the appropriate electricity tariff, C^{EL} (Eq. 4.2). The resulting annual operational cost was then repeated over the time horizon in calculating the total cost. In Eq. 3.2, the net present value is utilised to consider the future operating cost and revenue, with 5.5% interest rate, r and 20 years time horizon τ (Rogers *et al.*, 2015).

$$C_{inv} = C_{inv}^{HP} + C_{inv}^{TES} \tag{4.1}$$

$$C_{opr} = \sum_{t=0}^{8759} \left(P_{in,t}^{HP} + P_t^{RH}\right) \cdot \Delta t \cdot C_t^{EL} \tag{4.2}$$

The type of subsidy considered in this study is the Domestic Renewable Heat Incentive (RHI) (Ofgem, 2017). The UK government launched this policy to foster the implementation of non-fossil fuel domestic heating systems. It is a financial incentive policy which offers payments to the consumers for the amount of heat their system produces for seven years. Eligible heating systems are biomass boilers, heat pumps (both air and ground source), and solar thermal collectors. The RHI tariff, R_{RHI}, for air source heat pumps in 2015, i.e. £0.0742/kWh, is used in the calculation. The annual revenue, R, is calculated based on the annual heat demand, Q_{annual}^{DEM} (e.g. based on Energy Performance Certificate) and the average seasonal performance factor (SPF) of the heat pump (Eq. 4.3). The SPF is defined as a ratio between the total heat energy output per year and the total input electricity per year. For RHI revenue calculation, the value of SPF is taken from a Microgeneration Certification Scheme (MCS) certificate (Ofgem, 2017).

$$R = Q_{annual}^{DEM} \cdot \left(1 - \frac{1}{SPF}\right) \cdot R_{RHI} \tag{4.3}$$

4.4.2 Heat pump

The performance of a heat pump can be quantified by the coefficient of performance (COP), which is defined as the ratio between the thermal power output, $\dot{Q}^{HP}_{out,t}$, and the electrical power input, $P^{HP}_{in,t}$ (Eq. 4.4). The COP is affected by different variables, such as external temperature, supply water temperature, inlet water temperature and load factor. Simplifications can be made to reduce this complexity, but this should be done with care as it can affect the optimal control result. For example, it has been shown that a simplified model which neglects the dependency of the COP on the external temperature can produce higher electricity consumption, relative to the more complex model (Verhelst *et al.*, 2012b).

$$COP = \frac{\dot{Q}^{HP}_{out,t}}{P^{HP}_{in,t}} \tag{4.4}$$

The COP of the heat pump in this thesis is modelled as a function of temperature lift, T_{lift}, which is the difference between the heating flow temperature and the external air temperature (Eq. 4.5). The considered heating flow temperature is 50 °C, which is within the range of operational temperature of a wall radiator. Due to the energy flow modelling approach, the dynamics of the flow temperature is not modelled in the optimisation model. This simplification may influence the heat pump performance and, as will be shown later in this chapter, high heating flow temperature fluctuations. However, it has been shown that a more detailed heat pump model, e.g. including the influence of compressor frequency, the heating flow temperature, and the ambient temperature, is more relevant on a detailed control optimisation problem (Verhelst *et al.*, 2012b). In a design and operational optimisation problem that accounts for longer time period, a simplified model can be implemented in order to balance the trade-off between model complexity and tractability.

$$COP = a \cdot T_{lift} + b \tag{4.5}$$

Required data to produce the linear regression fits were derived from manufacturer's data (Mitsubishi Electric, 2013). The curve fitting to produce Eq. 4.5 was performed between temperature lift of 25 °C and 52 °C. Relevant heat pump data can be found in Table 4.2. Furthermore, SPF value of 2.9 is assumed in the calculation of RHI (Eq. 4.3) (Thomas and Charlick, 2013).

Equipment modelling in the MILP model is performed by prescribing constraints which reflect the characteristics of the equipment. The current study considers a discrete set of heat pumps, from which only one must be selected. This is ensured by Eq. 4.6 and

Table 4.2: Air source heat pump data

Type	Capacity (kW_{th})	C_{HP}^{inv} (£)	a (K^{-1})	b
1	5.0	2778	-0.066	5.7
2	8.5	3784	-0.087	6.8
3	11.2	4506	-0.072	5.6
4	14.0	5701	-0.077	6.1

4.7, where y_i^{HP} is a binary variable describing whether heat pump model i is installed or not.

$$\sum_{i=1}^{4} y_i^{HP} = 1 \tag{4.6}$$

$$\dot{Q}_{nom}^{HP} = \sum_{i=1}^{4} y_i \cdot \dot{Q}_{nom}^{i} \tag{4.7}$$

The thermal power output of the HP is limited by a minimum load factor and maximum capacity, as shown in Eq. 4.8. The binary variable ζ_t describes the operational status of the heat pump at time step t. Eq. 4.8 includes nonlinearity in the form of a bilinear term $\zeta_t^{HP} \cdot \dot{Q}_{nom}^{HP}$. This non-linearity is reformulated into linear equations (Glover, 1975). Further information on the reformulation can be found in Appendix A. The minimum load factor LF_{min}^{HP} is set at 35%.

$$LF_{min}^{HP} \cdot \zeta_t^{HP} \cdot \dot{Q}_{nom}^{HP} \leq \dot{Q}_{out}^{HP} \leq \zeta_t^{HP} \cdot \dot{Q}_{nom}^{HP} \tag{4.8}$$

4.4.3 Thermal energy storage

The thermal energy storage included in this study is a typical domestic hot water tank with 120 - 300 L volume range, as summarised in Table 4.3. The energy content of the TES is calculated by Eq. 4.9. For a heat pump heating system, the temperature increase in the storage tank, ΔT^{TES} is set to 10 K (Harb *et al.*, 2016).

$$Q_{i,max}^{TES} = \frac{V_i^{TES} \cdot \rho_w \cdot c_p \cdot \Delta T^{TES}}{3600} \tag{4.9}$$

The interaction between the heat pump and the thermal energy storage is strictly based energy flow due to the energy-based optimisation modelling approach discussed in Chapter 3. Therefore, similar with the heat pump model, the temperature dynamics in the storage are not tracked by the model. This simplification is also known as

Table 4.3: Thermal energy storage data

Type	Capacity (L)	C_{HP}^{inv} (£)	ϕ^{TES} (%)
1	150	1375	0.95
2	180	1425	0.93
3	210	1453	0.93
4	250	1575	0.91
5	300	1700	0.83

the capacity model in modelling hot water tank TES (Schütz *et al.*, 2015). As will be discussed later in this chapter, the modelling approach may produce less realistic temperature profile if the resulting operational profile is used in a simulation. This is also related to the influence of the heating flow temperature on the heat pump performance.

Nevertheless, the capacity model used in this thesis is another example of trade-off consideration between complexity and tractability in the optimisation model. The optimisation study in this chapter has a yearly time horizon with hourly time step. Therefore, a simplified model based on energy flow is considered to limit the problem size. Furthermore, the continuous nature of the selected temporal representation means that a cyclic constraint for the TES is only performed once at the end of the year instead of on a daily basis, for example, if typical days were used.

Similar to the heat pump sizing, the TES size has to be selected from the available discrete volumes. It is reflected in the implementation of constraints in Eq. 4.10 and 4.11.

$$\sum_{i=1}^{5} y_i^{TES} = 1 \tag{4.10}$$

$$Q_{max}^{TES} = \sum_{i=1}^{5} y_i^{TES} \cdot Q_{i,max}^{TES} \tag{4.11}$$

Other TES related constraints in the MILP formulation are shown in Eq. 4.12 - 4.15. The energy stored in the TES at time t, $Q_{sto,t}^{TES}$ is calculated according to Eq. 4.12, and limited by the maximum energy content (Eq. 4.13). The standing losses fraction, ϕ^{TES}, was derived from standard losses reported in the manufacturer's datasheet (Kingspan Environmental, 2017). The values of ϕ^{TES} range between 0.83% to 0.95% depending on the tank size. Furthermore, the TES charging rate is equal to the heat pump thermal power output (Eq. 4.14). The charge and discharge of the storage are assumed to occur without energy losses.

$$Q_{sto,t}^{TES} = \left(1 - \phi^{TES}\right) \cdot Q_{sto,t-1}^{TES} + \left(\dot{Q}_{ch,t}^{TES} - \dot{Q}_{dch,t}^{TES}\right) \cdot \Delta t \tag{4.12}$$

$$Q_{sto,t}^{TES} \leq Q_{max}^{TES} \tag{4.13}$$

$$\dot{Q}_{ch,t}^{TES} = \dot{Q}_{out,t}^{HP} \tag{4.14}$$

The house heat demand is fulfilled by discharging energy from the TES, along with the additional backup resistive heater, as stated in Eq. 4.15. The ON/OFF status of the resistive heater is represented by the binary variable $\zeta_{rh,t}$, while its thermal power output, $\dot{Q}^{RH}$, is fixed at 3 kW. A fixed resistive heater power is assumed in order to better represent the commercially available storage tanks (Kingspan Environmental, 2017). Moreover, P_t^{RH} is equal to $\dot{Q}_t^{RH}$, assuming a 100% efficiency of the resistive heater.

$$\dot{Q}_{dch,t}^{TES} + \zeta_t^{RH} \cdot \dot{Q}_t^{RH} \geq \dot{Q}_t^{DEM} \tag{4.15}$$

4.4.4 Electricity tariff

Three types of electricity tariffs are considered: Standard, Economy 7 (E7), and Economy 10 (E10). Both E7 and E10 are two rate tariffs with off-peak duration of 7 and 10 hours, respectively. The off-peak hours for E7 are from 00.00 to 07.00, while E10 off-peak hours are between $00.00 - 05.00$, $13.00 - 16.00$, and $20.00 - 22.00$. Table 4.4 shows the summary of the electricity tariffs (EDF Energy, 2013).

Table 4.4: Electricity tariffs

Tariff	On-peak (£/kWh)	Off-peak (£/kWh)
Standard	0.144	0.144
Economy 7	0.1747	0.0765
Economy 10	0.1744	0.071

4.5 Simulation model

A TRNSYS model of the residential heating system was developed to examine the potential interactions between optimisation and simulation model. In the TRNSYS model, the operational profile from MILP optimisation is directly used as an input to the simulation. Fig. 4.4 shows the main components of the developed model. A brief overview of the TRNSYS model is given in the following paragraphs, while further details can be found in Appendix B.

4.5.1 Heat pump

The heat pump is modelled with Type 581 Multi Dimensional Data Interpolation (HP_PartLoad_Table in Fig. 4.4) and Type 682 Flowstream Loads (HP_Load in Fig. 4.4), rather than using available heat pump models in TRNSYS. This is because none of the heat pump types in TRNSYS is capable of modelling a variable speed compressor heat pump. Therefore, the part load performance of the heat pump was modelled using Type 581 with data from the manufacturer's data sheet (Mitsubishi Electric, 2013). Furthermore, the heat pump is linked to the storage tank through a circulation pump modelled with a Type 977 Variable Speed Pump - Volumetric (Pump_1).

In order to evaluate the results of the MILP optimisation, the equipment size and heat pump operational profile of the optimal cases (Section 4.6.1) were used as an input to the TRNSYS model. The operational profile input is shown as MILP_HP_Profile in Fig. 4.4. It supplies the heat pump thermal power output to: (i) the part load table (HP_PartLoad_Table) to calculate the corresponding COP, and (ii) the flowstream loads (HP_Load) to increase the heating flow temperature. The part load table also receives the external temperature data from the supplied weather data (Weather_Profile). The latter is the same weather profile as the one used in the optimisation model (Section 4.3).

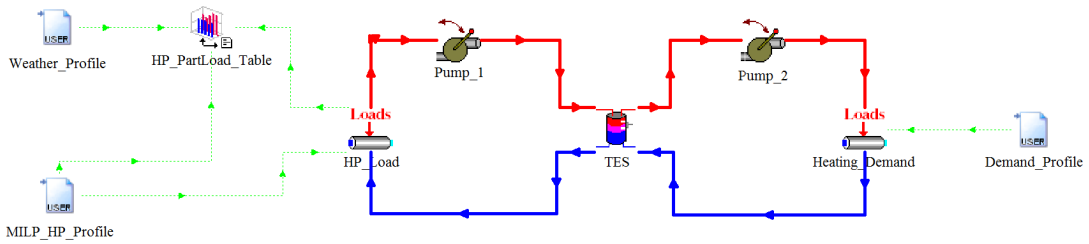

Figure 4.4: TRNSYS model of the residential heating system.

4.5.2 Thermal energy storage

The storage tank is modelled using Type 60d with one inlet-outlet pair for the demand loop and an internal heat exchanger for the heat pump loop. The Type was selected among other storage tank types by considering a balance between a model which is as close as the real tank and data availability for the type's input. Type 60d employs a thermocline approach similar to Type 4a shown in Chapter 3, with additional internal heat exchanger modelled in the type.

The storage tank parameters were gathered from the same manufacturer's data sheet as used in the optimisation model (Kingspan Environmental, 2017). Similar with the heat pump connection, the storage tank is connected to the demand by a Type 977 Variable Speed Pump - Volumetric (Pump_2).

4.5.3 Heat demand

The heating demand is modelled with Type 682 Heating Loads Imposed on a Flow Stream (Heating_Demand in Fig. 4.4), which reads the heat demand values from an input file (Demand_Profile) and applied them to the working fluid. In the case of heating, this will result in increasing working fluid temperature at the outlet of Type 682.

4.6 Results and discussion

4.6.1 Optimisation results

In the optimisation runs, the solver tries to find the combination of HP, TES, and their operational profiles able to produce the minimum total cost. The equipment sizes were defined as discrete variables with available sizes shown in Table 4.2 and 4.3 for HP and TES, respectively.

Effect of electricity tariff

The result of design and operational optimisation runs with different electricity tariffs are shown in Table 4.5. The optimised heat pump size of 8.5 kW is identical for all tariffs, while the TES size varies with 210, 250, and 300 L for Standard, E7, and E10 tariff, respectively. The E10 case has the lowest annual operational cost and total cost. From these results, it is clear that the use of a differential tariff can produce lower operational cost than the standard tariff, with up to 20% lower operational cost in the case of the E10 tariff.

Table 4.5: Results of design and operational optimisation for different electricity tariffs.

Variables	E7	E10	Standard
HP size (kW)	8.5	8.5	8.5
TES size (L)	250	300	210
HP electricity input (kWh/year)	5045	5037	5047
Annual operational cost (£/year)	647	579	727
Total cost without RHI (£)	15095	14405	15923
Total cost with RHI (£)	11412	10722	12241

It is interesting to note that the operational cost of HP-TES on E7 and E10 tariff is already lower than the operational cost of a gas boiler to satisfy the same heat demand. Assuming a gas price of £0.045/kWh, a gas boiler case will have an operational cost of approximately £675/year. Therefore, an operational cost reduction up to 14% can be achieved by the HP-TES system on E10 tariff.

Nevertheless, due to the different TES size in the optimal results, it is less straightforward to assess the influence of storage size on the total cost. In order to evaluate this, the total cost comparison between HP-TES cases and a gas boiler case will be discussed further in the next sub-section.

The equivalent CO_2 emission can be calculated using the average carbon dioxide intensity of the electricity grid of 0.41205 $kgCO_2e/kWh$ (Department for Business, Energy & Industrial Strategy, 2016). This corresponds to approximately 2075 $kgCO_2e$ for all cases since the HP electricity inputs are almost the same. However, this neglects the generally lower CO_2 intensity during off-peak hours. Furthermore, using a CO_2 factor of 0.184 $kgCO_2e/kWh$ for natural gas, a gas boiler case will have an equivalent emission of around 2830 $kgCO_2$. Thus, the HP-TES systems can reduce approximately 26% of CO_2e emission. An even larger reduction can be achieved if the share of renewable-based electricity increases, reducing the carbon intensity of the electricity grid.

Fig. 4.5 and 4.6 illustrate operational profiles of the optimised system over two winter and summer days, respectively. The legends of both figures correspond to the defined variables as follows: TES discharge ($\dot{Q}^{TES}_{dch,t}$), resistive heater ($\dot{Q}^{RH}_{t}$), heat demand, ($\dot{Q}^{DEM}_{t}$), TES charge ($\dot{Q}^{TES}_{ch,t}$), and TES state-of-charge (SOC^{TES}_{t}). Furthermore, it should be noted that the operational profiles were generated by the solver, and there was no load shifting prescribed in the optimisation model.

During the two winter days shown in Fig. 4.5, all of the heat demand were fulfilled by the TES discharge in all cases. Thus there are no differences between the left figures.

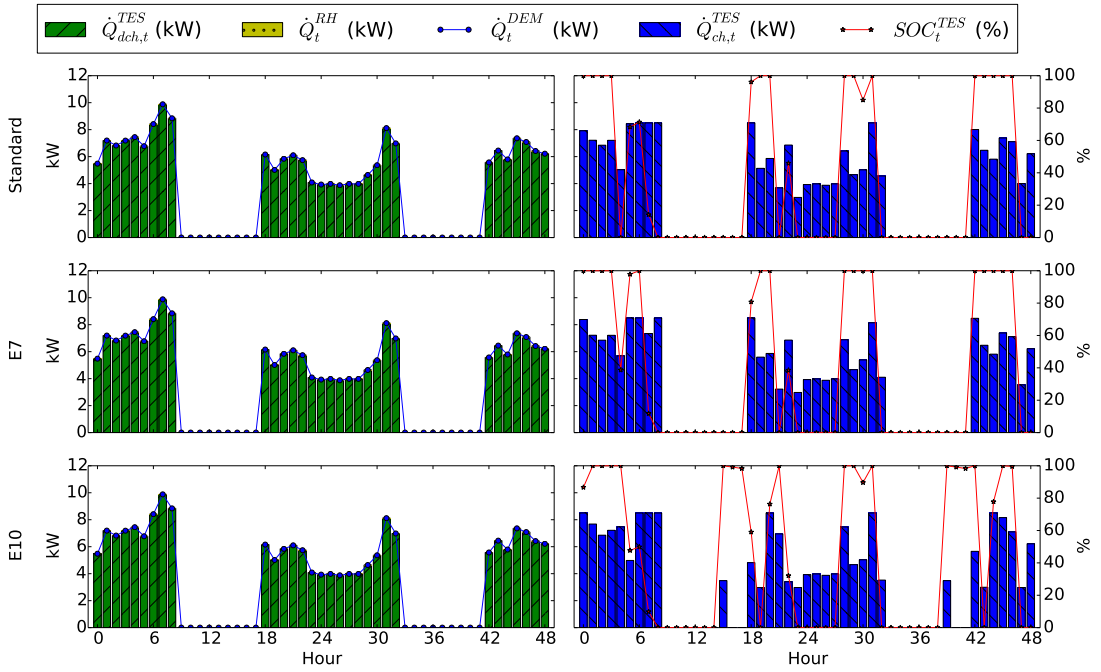

Figure 4.5: Example of operational profiles over two winter days of the optimal system size for different tariffs. Figures on the left show the fulfilment of heat demand by TES discharge and resistive heater, while figures on the right display the TES charging profiles and state-of-charge.

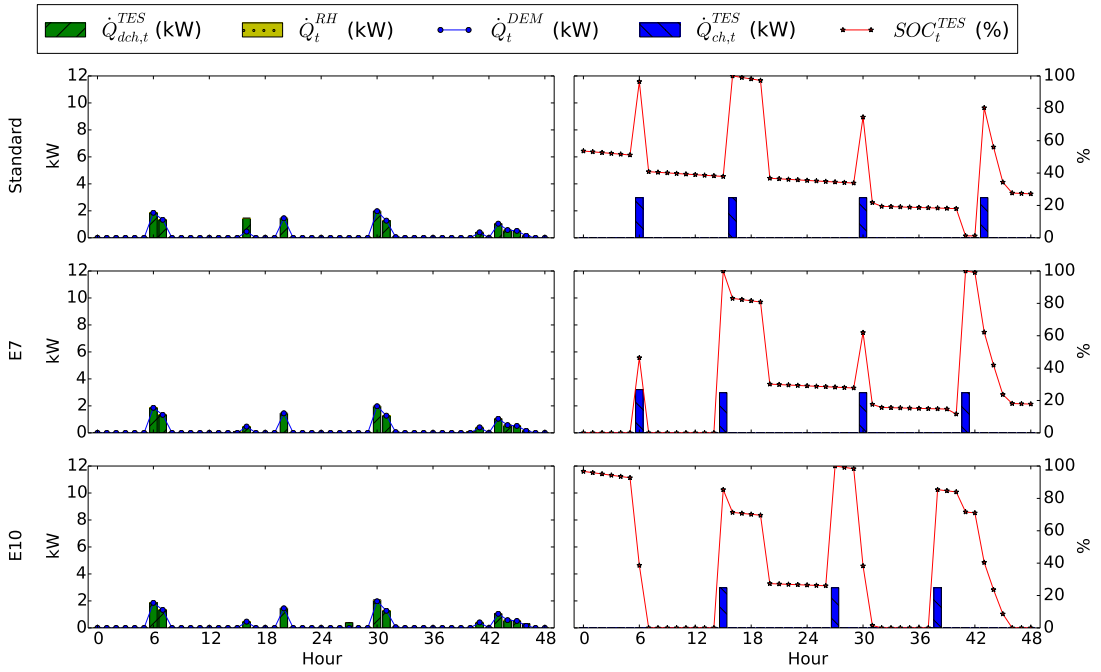

Figure 4.6: Example of operational profiles over two summer days of the optimal system size for different tariffs. Figures on the left show the fulfilment of heat demand by TES discharge and resistive heater, while figures on the right display the TES charging profiles and state-of-charge.

The influence of electricity tariff can be observed in the TES charging pattern in the right figures. There are little differences on the charging patterns of the Standard and E7 during night inactive time (00.00 - 07.00) because the TES has to discharge to fulfil the demand regardless of electricity price. However, the TES in E10 case has different overall charging pattern than the other two. For instance, it started to charge at 15.00, while the other two cases were not charging until the start of heat demand at 18.00. This happened because E10 has an off-peak window between 13.00-16.00, which can contribute to a lower operational cost. Similarly, the TES in E10 is always charged with more energy between 20.00-22.00 than the one in Standard and E7 case.

In contrast with Fig. 4.5, the two summer days shown in Fig. 4.6 contain the hottest day of the year. Thus, there is minimal heat demand in this period. Nevertheless, the influence of electricity tariff on the TES charging profile is even more visible because of the low demand. For the standard case, it appears that the charging occurs whenever the heat demand cannot be satisfied by the available stored energy. On the other hand, the TES in E10 is charged exclusively during off-peak period, while the TES in E7 is charged during both off- and on-peak periods.

On the left figures of the Standard and E10 profiles in Fig. 4.6, there are points where the TES discharge is larger than the heat demand. This can be explained by examining the heat demand satisfaction constraint (Eq. 4.15), which uses greater-than rather than equality. This was considered because the heat pump output was modelled with a lower limit (Eq. 4.8); thus, there is a possible situation where the TES needs to be charged, but there was not enough TES capacity to contain the heat pump minimum output energy. In this situation, the system 'dumps' the extra energy to the demand circuit. Although it was not modelled in this thesis, the presence of a dump radiator is common in a residential heating system, which typically used to ensure the water can circulate during start up and whenever all controlled radiators shut off.

In addition to the electricity tariff, the solver also takes into account other aspects that can influence the objective function, such as a more favourable external temperature for operating the heat pump to produce a better COP. Furthermore, it should be noted that the solver tries to determine the operational profile of the system simultaneously for all time steps, in this case 8760 time steps. Thus, the decisions on each time step are influenced by the previous and next one. As an example, the starting state-of-charge values in the two days operational profiles shown in Fig. 4.5 and 4.6 were related to the profiles of the day before.

The limitations of the energy based modelling in the heat pump and TES model should also be considered in interpreting the results. For instance, the COP is calculated as a function of the temperature lift with a fixed heating flow, while the TES is modelled with a fixed temperature difference. This may lead to less accurate operational profile,

especially on the temperature profiles of the system. Sub-section 4.6.2 on the simulation results will further discuss this particular issue.

Lower operational cost and emission of a heat pump system relative to a gas boiler system were also observed in a simulation study of a similar heat pump-based residential heating system (Cabrol and Rowley, 2012). For example, it was concluded that 45% operational cost reduction and CO_2 reduction of up to 26% are achievable for the case with E10 tariff in a similar location and number of degree days as the modelled demand in this chapter. The discrepancy in the percentage of reduction with those reported in this chapter, particularly on the operational cost, can be attributed to the difference in the modelled heating system. The previous study implemented an underfloor heating system, which requires lower flow temperature than regular radiators. The current study assumes 50 °C heating flow temperature, which is within the required range for systems with regular wall radiators. This difference can have a large influence on the COP since the temperature lift is higher in this study, thus reducing the COP.

In order to investigate the effect of heating flow temperature on operational cost and emission, an optimisation problem with heating flow temperature of 35 °C was solved. The chosen temperature is typical for an underfloor heating system. The value of linear regression coefficients in Eq. 4.5 were modified accordingly, taking into account the lower heating flow temperature. The resulting values for the two heating flow temperatures for the E10 tariff are given in Table 4.6.

As expected, the system with 35 °C heating flow temperature has lower operational cost and lower emission than the one with 50 °C. Relative to a gas boiler case, the HP-TES with lower heating flow temperature achieves approximately 47% and 50% reduction in operational cost and CO_2 equivalent emission, respectively. The larger reduction in CO_2 equivalent emission relative to the one reported in Ref. (Cabrol and Rowley, 2012) can be attributed to the difference in the carbon intensity value of the electricity grid in 2011 and 2016. This illustrates that the combination of HP with regular radiators can limit the overall benefits of HP based systems and that a careful design of these systems is required.

Total cost

As briefly indicated in the previous section, the influence of storage size on the total cost is difficult to assess from the optimal solutions reported in Table 4.5 due to differing storage size for each tariff. Thus, here the total cost of different HP-TES combinations are assessed further by using the results of operational optimisation with fixed equipment size.

The results of total cost calculation for an 8.5 kW HP with different TES sizes on all

Table 4.6: Influence of heating flow temperature on operational cost and emission

Variables	T_{out} = 50 °C	T_{out} = 35 °C
HP size (kW)	8.5	8.5
TES size (L)	300	300
HP electricity input (kWh/year)	5037	3380
CO_2 equivalent emission ($kgCO_2e$/year)	2075	1392
Annual operational cost (£/year)	579	388
Total cost without RHI (£)	14405	12126
Total cost with RHI (£)	10722	8443

tariffs are illustrated in Fig. 4.7, along with the total cost of a 5 kW HP with 300 L TES, an 8.5 kW HP-only, and a gas boiler scenario. A scenario with 5 kW HP is included in the total cost comparison in order to evaluate the cost of a system with lower HP size. Operational optimisation runs of 5 kW HP with different TES sizes were performed, and it was found that only the one with 300 L TES was able to cover the heat demand. Furthermore, an HP scenario without TES is considered to illustrate the magnitude of financial benefit from using a TES, while a gas boiler scenario is included as an incumbent technology.

Overall, it can be seen in Fig. 4.7 that the differences in total cost between the HP-TES scenarios are relatively small. There is around 1% difference between the highest and lowest total cost among the systems with the same HP size and different TES sizes in the Standard tariff. This value is 1.7% and 6% for E7 and E10, respectively. These small differences show that the savings achieved by using larger TES are within the same magnitude as the difference in TES investment cost.

Nevertheless, despite the minimal differences, a slight variation exists in the relationship between the TES size and total cost. For E10 scenarios with TES (Fig. 4.7c), a higher storage volume produces lower total cost, albeit relatively small. It is interesting to note that a similar trend of total cost reduction with increasing storage volume is not found for E7 (Fig. 4.7b). Increasing the TES size beyond 250 L on the E7 tariff will increase the total cost. This is also observed in scenarios with the Standard tariff. One possible explanation for this is that the increase in the investment cost due to larger TES can only be compensated by lower operational cost in all TES size in E10 scenarios.

Furthermore, the total cost is lower for all heat pump with TES scenarios than the heat pump only scenario for all electricity tariffs. This is because the operational cost savings from TES compensate for its capital cost. It is also interesting to note that

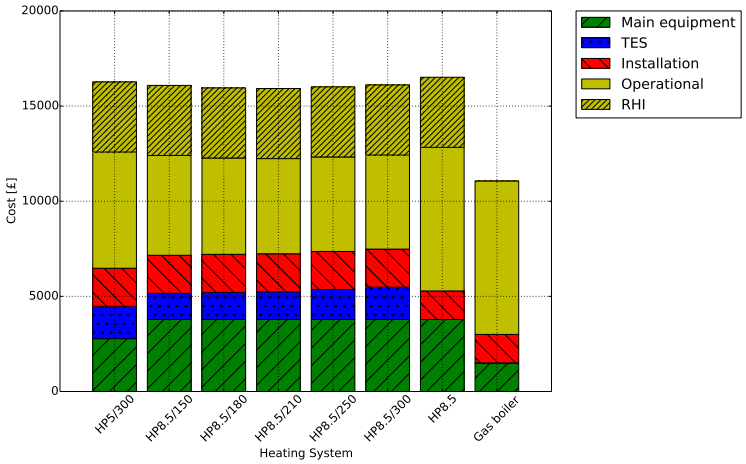

(a) Total cost (Standard)

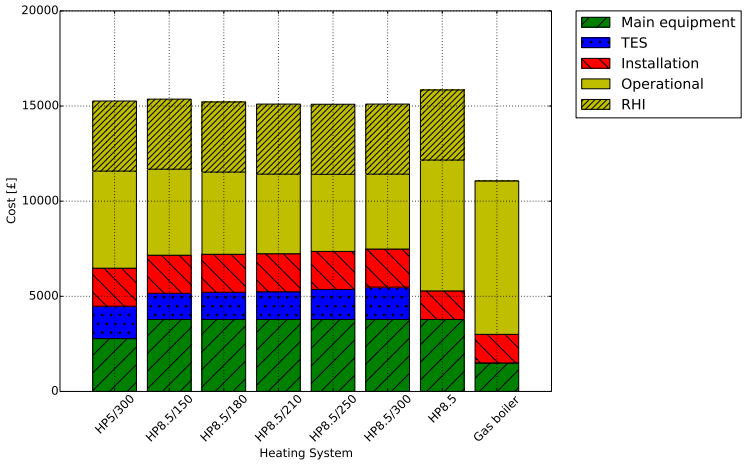

(b) Total cost (E7)

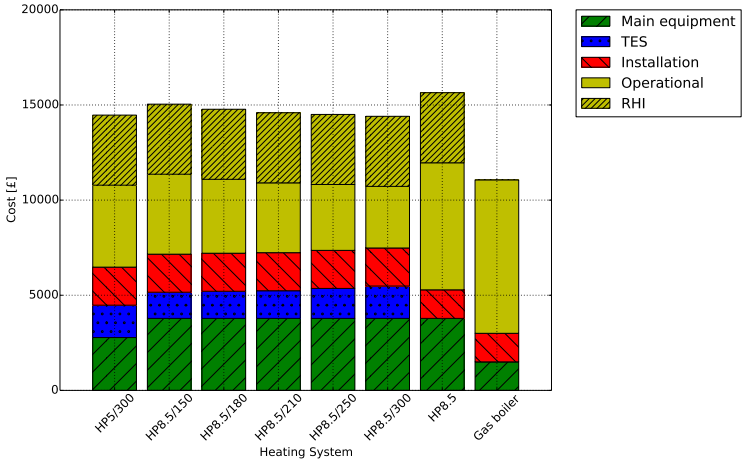

(c) Total cost (E10)

Figure 4.7: Total cost of different heating systems on the 2015 RHI and Standard (a), E7 (b) and E10 electricity tariff (c).

the system with lower HP capacity (HP5/300) has a relatively similar total cost with the 8.5 kW cases. As can be seen from Fig. 4.7c, the lower investment cost of a 5 kW heat pump is offset by a larger operational cost. This includes a contribution from the resistive heater which has to compensate the lack of heat pump capacity to charge the storage. The assumed fixed resistive heater power also has a role in the resulting heat pump sizing. The optimal HP and TES size might differ if the resistive heater size was considered as a design variable. However, this possibility is not examined further in this thesis since most domestic storage tanks in the market have a fixed resistive heater rating.

The inclusion of RHI has a significant impact on reducing the total cost of HP-based systems, as shown in Fig. 4.7. It is clear that RHI reduces the operational cost by a large margin, and can make the heat pump scenarios cost competitive with the gas boiler option. The RHI included in Fig. 4.7 is based on 2015 value (£0.0742/kWh). By the time of this thesis being written, the RHI tariff has been increased to £0.1018/kWh. In order to evaluate this updated value, the total cost of different configurations has been recalculated using the increased tariff. The results are shown in Fig. 4.8. It is clear that the increased RHI can further improve the economic competitiveness of heat pump systems by lowering the total cost even below the gas boiler system.

4.6.2 Simulation results

The TRNSYS simulation models used the equipment sizing and heat pump operational profiles from the MILP optimisation as inputs. Annual simulation runs were performed, and the corresponding results are reported in the following paragraphs.

Annual performance

The results of the TRNSYS simulations are shown in Table 4.7. The overall trend in the annual operational cost trend is similar between the MILP and TRNSYS results, with the E10 case as the lowest and the Standard tariff case as the highest. One of the main differences between MILP and TRNSYS results is the heat pump electricity input and, consequently, the operational cost value. The heat pump input in the TRNSYS simulations is 3-9% higher than those of MILP, while the increase in operational cost ranges from 3-18%.

The difference in electricity input can be attributed to the more detailed part-load COP data in the TRNSYS model, while the MILP model employed a simplified linear relation (Eq. 4.5). In order to examine the extent of this discrepancy, parity plots of the heat pump electricity input from both models are illustrated in Fig. 4.9 for all three tariffs. It can be observed that in all cases, the discrepancy is relatively small in

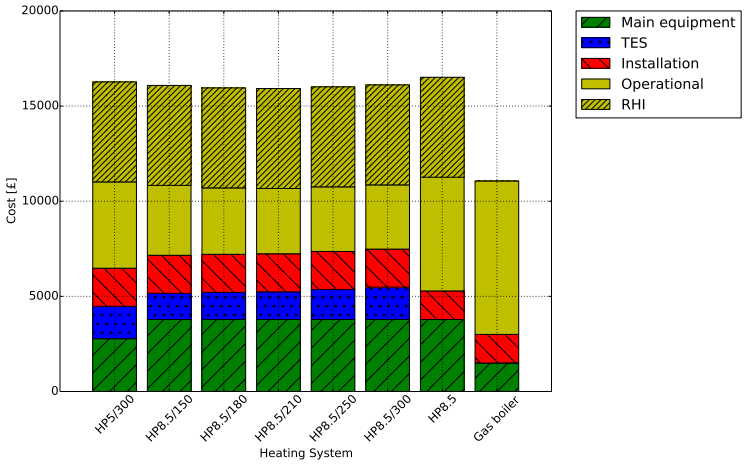

(a) Total cost (Standard)

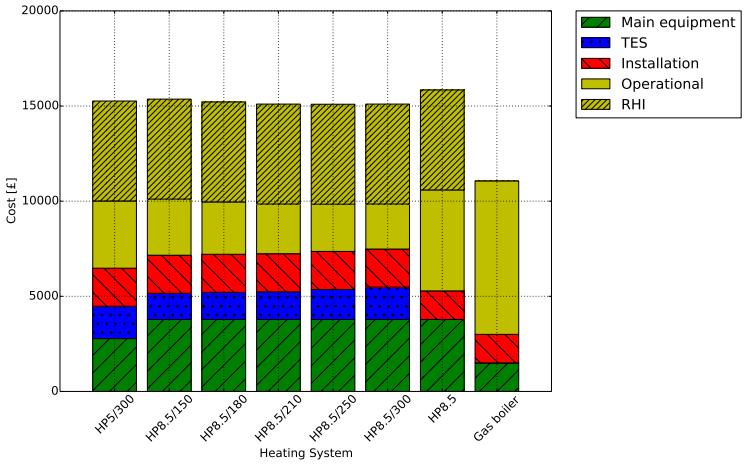

(b) Total cost (E7)

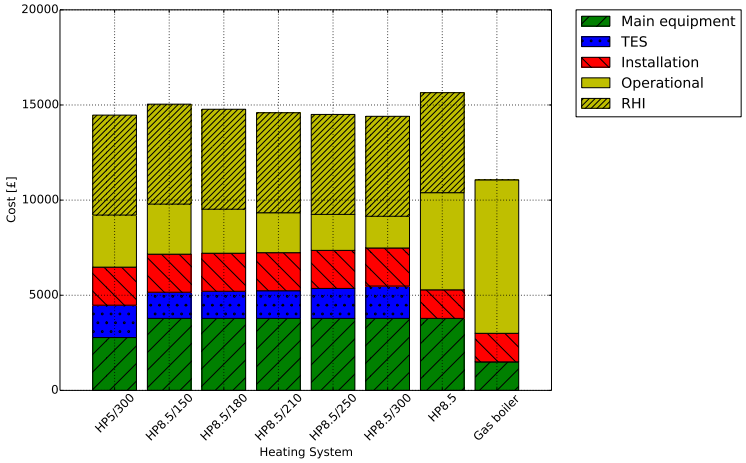

(c) Total cost (E10)

Figure 4.8: Total cost of different heating systems on the 2017 RHI and Standard (a), E7 (b) and E10 electricity tariff (c).

Table 4.7: TRNSYS and MILP results of the optimum cases

Model	E7		E10		Standard	
	MILP	TRNSYS	MILP	TRNSYS	MILP	TRNSYS
HP size (kW)	8.5	8.5	8.5	8.5	8.5	8.5
TES size (l)	250	250	300	300	210	210
Electricity input (kWh/year)	5045	5259	5037	5502	5047	5237
Annual operational cost (£/year)	647	712	579	686	727	754

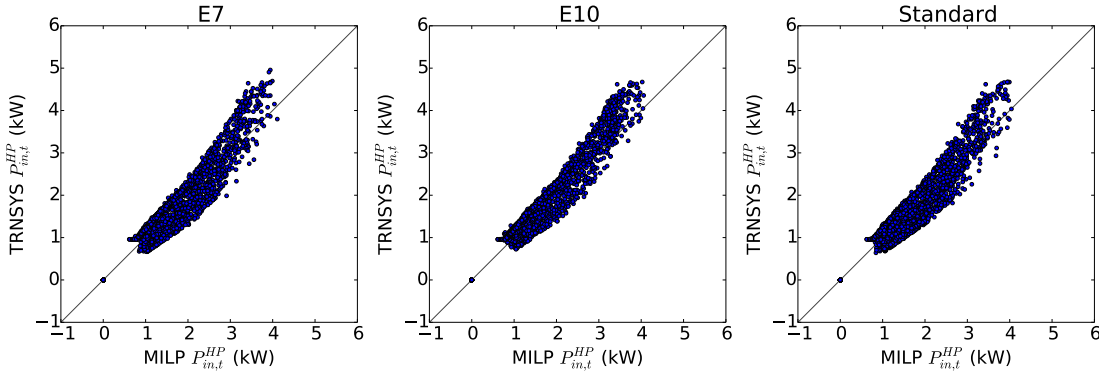

Figure 4.9: Parity plot of the heat pump electricity input (kW) from the MILP and TRNSYS results of the optimum cases.

lower electricity input value and slightly increasing as the heat pump load increases. It shows that as the heat pump operates toward full load, the COP calculated by the MILP model becomes more optimistic in comparison with the TRNSYS model. From Table 4.7 and Fig. 4.9, it can be concluded that the linearised model implemented in the MILP optimisation is sufficiently accurate for yearly simulation of the system.

Representative operational profiles

In order to assess the operational profile validity of the TRNSYS model, it is necessary to see the resulting temperature profiles from the simulations. Fig. 4.10 and 4.11 show the charge/discharge profiles and average tank temperature from the TRNSYS simulations for the same periods as in Fig. 4.5 and 4.6.

Clearly, the energy demand, TES charge, and TES discharge are the same as in the MILP profiles since they were part of the inputs to the TRNSYS simulations. It is interesting to note how the average TES temperature shown in Fig. 4.10 and 4.11

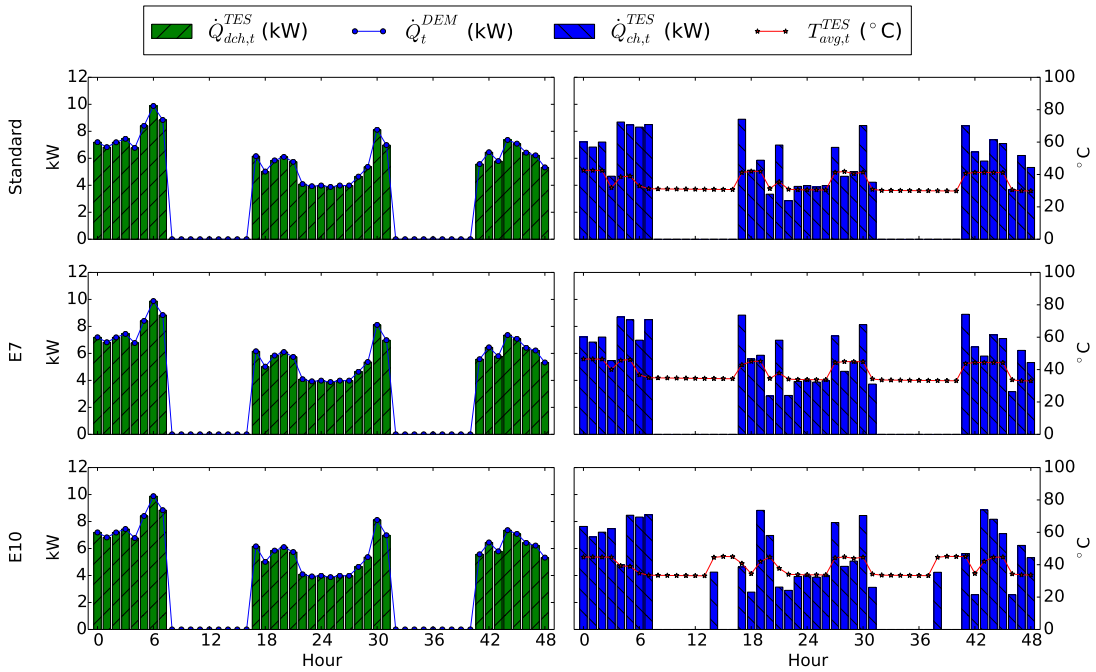

Figure 4.10: Example of operational profiles over two winter days from the TRNSYS simulations.

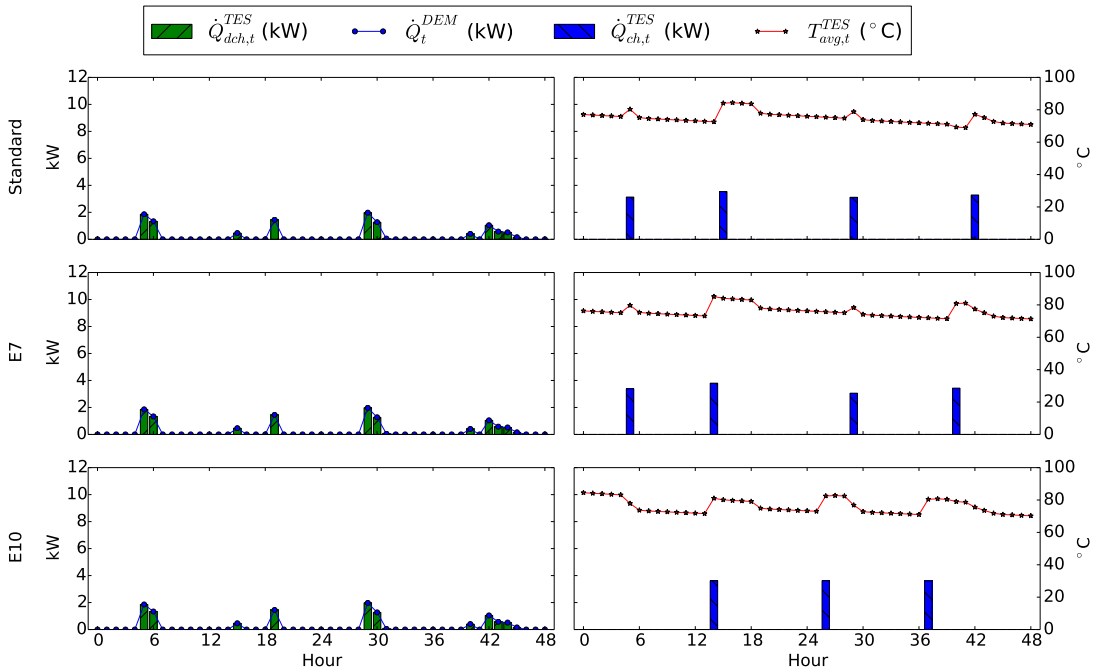

Figure 4.11: Example of operational profiles over two summer days from the TRNSYS simulations.

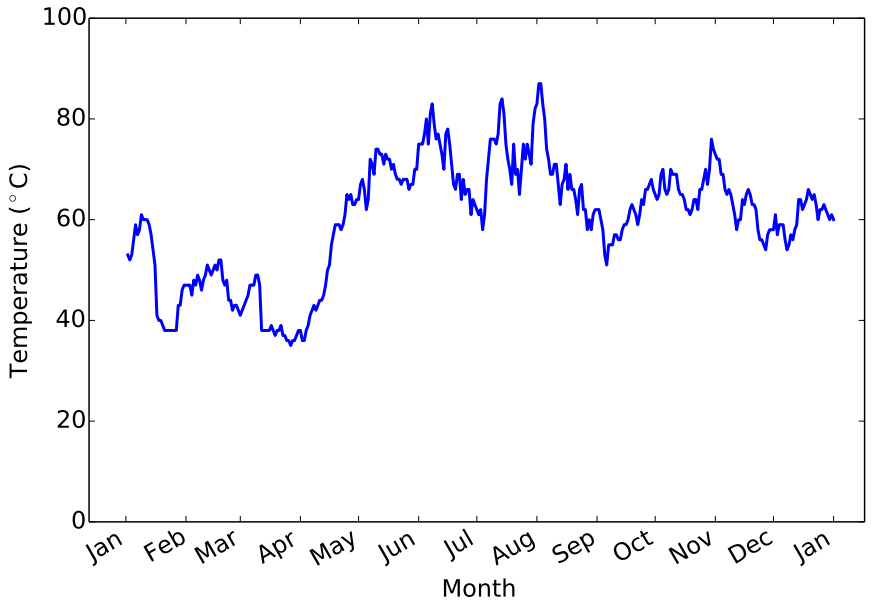

Figure 4.12: Annual profile of the daily average TES temperature from the TRNSYS model of E10 case.

correspond with the TES state-of-charge shown in Fig. 4.5 and 4.6. In the winter, the average temperature of 40 °C correlates with 100% state-of-charge, while in the summer, the value is 80 °C. As can be seen in Fig. 4.12, the daily average TES temperature in the E10 case ranges between 35 °C in the winter and 80 °C in the summer. During the winter period, the TES is charged and discharged quite often; thus, the overall average TES temperature is relatively low. During the summer period, the TES is not discharged as often as in winter, but whenever it is charged, the input energy corresponds to the lower load factor limit of the heat pump. Thus, the average TES temperature rises simply because the TES is charged with more energy than is discharged.

These fluctuations in average TES temperature is rather unrealistic in a residential heating system. During several periods between January and May in Fig. 4.12, the average TES temperature even dropped lower than the prescribed 50 °C heating temperature. Typically, a system with heat pump and TES is controlled based on the TES temperature and room temperature. For example, the heat pump can be operated to maintain the TES temperature around 50 °C, and the demand loop pump can be controlled to maintain the space temperature in the living area between 19 and 22 °C (Kelly *et al.*, 2014). The lack of such control rules in the developed TRNSYS model caused the fluctuations in the average TES temperature, which can also lead to higher costs. This can be seen as one of the limitations in using the operational profiles of the MILP optimisation.

As described in Chapter 3, an energy flow approach is followed in the optimisation

models developed in this thesis. Thus, the resulting operational profiles are accurate from an energy viewpoint but may result in unrealistic values from a temperature viewpoint. The accuracy of the energy flow approach is also illustrated by the energy content of the TES. Despite the unrealistic TES temperature values, the difference in temperature (ΔT^{TES}) between an empty and fully-charged TES is relatively constant at 10 °C, as illustrated in Fig. 4.10 and 4.11. This is consistent with the prescribed limitation given in Eq. 4.9.

Furthermore, operational optimisation results have the potential to be implemented in a closer to real-time setting, for example using Model Predictive Control (MPC) in the operation of energy systems. By minimising the time horizon of the optimisation, a more detailed model can be used to better capture the systems behaviour. The resulting MPC profile over the defined control time horizon can also be used as an input to the simulation model, which in turn inform the decision-making in operating the energy systems. These can be considered as potential extensions from the work described in this chapter.

4.7 Conclusions

A MILP optimisation model of a heat pump-based residential heating system has been developed to investigate the influence of electricity tariff on the optimal sizing and operation of the system. A TRNSYS simulation model of the same system has also been implemented to study the possibility of using the MILP output as an input to the simulation model.

The MILP optimisation shows that the heating system with 8.5 kW HP and 300 L TES operating on E10 has the lowest operational and total cost. It also has slightly lower operational cost and equivalent CO_2 emission than the gas boiler system. These are achieved by a heating system with conventional radiators and the current high CO_2 grid intensity. By moving to underfloor heating which requires lower heating flow temperatures, the cost and emission savings of the HP system are 47% and 50%, relative to a conventional gas boiler system. The emission savings will increase with the continuing reduction in CO_2 grid intensity.

The total cost of the studied heating systems has dissimilar trends for different tariffs. The total cost of HP-TES systems on E10 decreases with increasing storage capacity, while systems for other tariffs show an increasing trend as the storage goes beyond 250 and 210 L for E7 and Standard tariff, respectively. Nevertheless, for the same HP size, the influence of TES size over the total cost is minimal because the difference in investment cost is only slightly offset by the reduced operational cost.

In general, it can be concluded that HP-based heating systems, with or without TES, have significantly higher cost than natural gas boiler heating system. However, for cases with TES, the operational cost are lower than the HP-only scenario. This justifies the investment cost of TES because it leads to a lower operational cost. Moreover, it has been shown that the new increased RHI-tariff can significantly reduce the total cost and make heat pumps a more attractive option for end users in the UK.

The resulting annual performance and operational profiles of the TRNSYS simulations illustrate how the optimisation and simulation can be implemented in the comparative approach as defined in Chapter 2. By directly using the heat pump operational profile from the MILP optimisation in the TRNSYS simulation, it has been shown that the annual electricity inputs are relatively similar between MILP and TRNSYS. Therefore, the simplified linear COP model in the optimisation is sufficiently accurate relative to the more detailed model employed in the TRNSYS simulations. However, the direct use of the MILP operational profiles can lead to unrealistic simulation profiles due to the energy flow approach followed in the optimisation model.

This also shows the limitation of the energy flow approach in modelling the HP and TES. For example, the HP model assumed a constant supply water temperature while a dynamic supply water temperature can increase the COP, while the TES model used a capacity model without considering the temperature stratification. On the other hand, the reduced computational complexity of the presented framework makes it possible to solve the optimisation problem with hourly time step for the whole year. Although it is less crucial in smaller systems such as a single residential heating system, its significance increases as the system becomes larger, as will be exemplified in the next chapter.

Overall, the results of the TRNSYS simulations indicate that the MILP optimisation model is sufficiently accurate for design optimisation (i.e. equipment sizing) and deriving annual performance values. Moreover, operational control algorithms derived directly from the optimisation model have the potential to be implemented, for instance using the Model Predictive Control concept with limited control time horizon.

It is evident from this chapter that an optimised operating profile is necessary to lower the total costs of HP and TES installation. The significance of operational optimisation is increasing as we move to larger energy systems, such as on neighbourhood, district, or city-level. This also comes with growing complexity due to larger number of equipment, demand nodes, and energy vectors, among others. In Chapter 5, a method to limit this increasing complexity in operational optimisation is analysed further.

Chapter 5

Multiple time grids in operational optimisation of a solar district heating system

The work presented in this chapter is based on a published article (Renaldi and Friedrich, 2017).

5.1 Introduction

Operational optimisation of energy systems is typically performed to determine the operational profiles of the given equipment over the specified time horizon which produces the best objective value(s). As illustrated in Fig. 2.9, operational optimisation is on the lowest level of overall optimisation, where the superstructure and size of equipment are considered as given in the problem formulation. At this level, the modelling of time has a significant role in the model formulation, as well as in interpreting the optimisation results since it can influence the problem size, computational cost, and quality of the solution.

For instance, it has been reported that using 1-h instead of 5-min time steps in the optimisation of a domestic micro-CHP system can produce an overestimation up to a doubling of the capacity of the optimal CHP size and up to 40% in CO_2 emissions reduction (Hawkes and Leach, 2005). Further analysis of the operational optimisation of a fixed size system also produced different outcomes, with differences up to 8% in the economic objective and 40% in the environmental objective. The study concludes that it is important to use a fine time step size when the effect of averaging will significantly influence how the model behaves as determined by the constraints and objective function sensitivity. In the investigated case of a domestic micro-CHP, the time step size in minutes is preferable due to the temporal nature of electricity demand.

Similar conclusions have also been reached in another study on the operational optimisation of a residential cogeneration system without electric power export (Wakui and

Yokoyama, 2015). The study highlights the influence of storage equipment, both battery and hot water tank, on the computational complexity of the problem. For example, the charge and discharge planning of the battery, with the aim of saving energy, can increase the computational time.

In addition to domestic or building-level energy systems, the influence of temporal resolution has also been investigated in the case of a complete hybrid energy system (Hoevenaars and Crawford, 2012). It is concluded that the impact of the time step was dependent on the system configuration, with different equipment having different sensitivity towards the change of time step size. The wind energy output and fuel consumption of the generator were found to be increasing with the temporal resolution, while the photovoltaic and battery were not affected by it. The study also shows that the system with a storage equipment, i.e. battery, has better agreement with results between different temporal resolution levels.

In most optimisation studies that include storage equipment, the time series modelling simplification is generally performed using typical period assumption with single time grid, e.g. one typical day with hourly time step as a representative of a whole season. Despite its usefulness in systems with one type of storage technology, this approach is not able to fully capture the behaviour of systems with different storage temporal characteristics. One prominent example of such systems is a solar district heating system with short- and long-term thermal energy storage. The short-term storage operates on a daily or weekly cycle, while the long-term storage works on a monthly or even seasonal cycle.

Studies on such systems have been reported in the literature and mostly use single time grid in simulating and optimising the system. For example, Tveit et al. implemented 13 periods per year in their Mixed Integer Non-Linear Programming (MINLP) operational optimisation of a district heating system with long-term storage (Tveit *et al.*, 2009). The relatively coarse time step was deemed to be sufficient in the study due to the focus on long-term investment analysis, instead of detailed operational profile over a short time horizon. Furthermore, it should be noted that short-term storage was not considered in the optimisation.

In another example, Rager included the implementation of both short- and long-term storage in a district heating optimisation study (Rager, 2015). The temporal representation used was the typical days based on a clustering approach. It was stated that the long-term storage requires a sequence of typical days to pass energy from one period to another. A weighting factor was included in order to estimate the charging behaviour of the long-term storage in a given period. The method has been shown to work well in a case study. However, the focus of the study was more on design optimisation, with less detail on how the system behaves on the operational level.

The limitation of the typical days approach in dealing with long-term storage, i.e. coupled decisions between days, was addressed in a recent study (Robineau *et al.*, 2016). It used an assumption that the long-term storage can only be charged or discharged for a given typical day. Furthermore, it also prescribed the maximum charged/discharged energy for every typical day except one which was used to balance the storage over the year. The study also acknowledged the main limitation of using the typical days approach in modelling long-term storage: appropriate consideration of the heat losses and soil temperature (for the case of borehole storage). This is because sequencing typical days may not best represent the time horizon of the problem, for example in cases with stochastic heat sources. Given these limitations of the typical period approach in modelling long-term storage equipment, an alternative time representation for problems with such technology is required.

The multiple time grids method is an option to overcome the limitations of the typical period approach. In the multiple time grids method, every equipment can have its own time grid which corresponds to its characteristics. The concept of multiple time grids has been explored in the field of process systems engineering (e.g. (Floudas and Lin, 2004; Velez and Maravelias, 2013, 2014) and electric power system (e.g. (Winkelman *et al.*, 1980; Kargarian *et al.*, 2016)). Nevertheless, its implementation on energy systems with different types of storage is less well studied, particularly for systems with seasonal storage.

The work presented in this chapter aims to fill this gap by investigating the implementation of the multiple time grids formulations in the optimisation of energy systems with multiple storage technologies. The considered system is a solar district heating installation with short- and long-term thermal energy storage. Different time grids formulations were then implemented within the mixed-integer linear programming (MILP) optimisation. The results of optimisation runs were compared concerning their relative error and computational cost. The trade-off between these two aspects is central to the contributions of this work to the body of knowledge. If the use of multiple time grids approach in energy systems optimisation can lower the computational cost while maintaining an acceptable level of accuracy, the saved computational effort can be utilised to improve the overall performance of the optimisation model. For instance, finer time steps might be required during peak periods for a CHP equipment, or a more complex model might be needed to consider the degradation of a storage equipment.

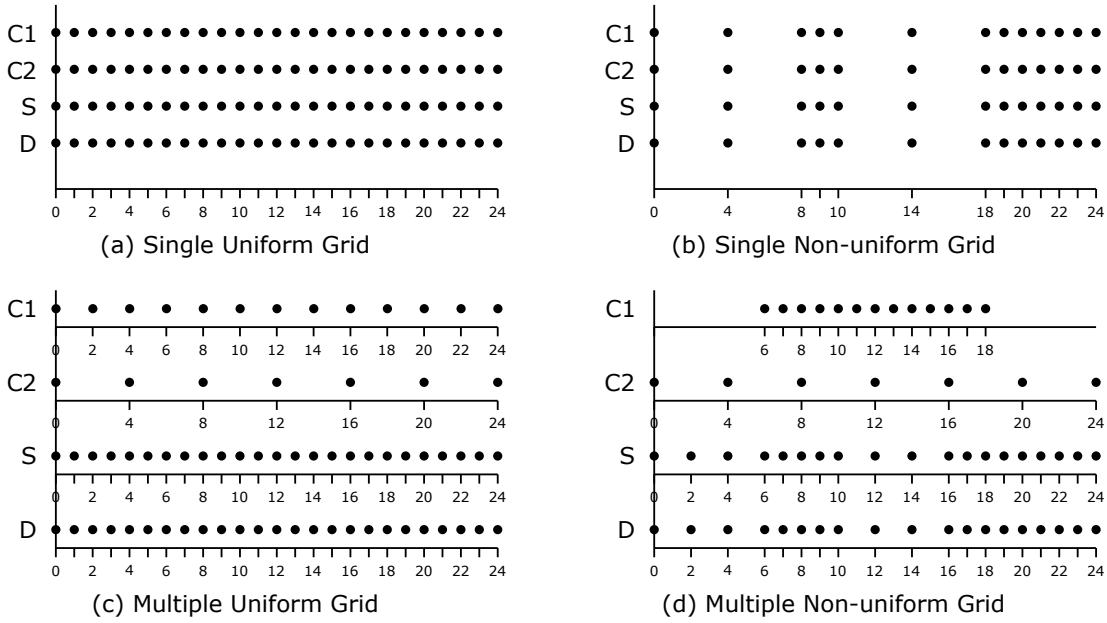

Figure 5.1: Types of time grids. Conversion equipment (C1, C2), storage equipment (S), and demand (D) time grids over 24 hours period are shown for illustrative purpose

5.2 Multiple time grids modelling

The main idea in the multiple time grids method is to formulate an optimisation model that uses different time grids for each equipment, resources, and materials (Ierapetritou and Floudas, 1998a,b; Castro and Grossmann, 2005). It has been proposed as a way to reduce the number of time steps in scheduling problems (Floudas and Lin, 2004). Although it is mainly developed in continuous-time representation, recent studies have shown that it is also applicable in discrete-time representation (Velez and Maravelias, 2013, 2014).

As illustrated in Fig. 5.1, time grids in discrete time optimisation can be categorised into four types: single-uniform (SU), single-non-uniform (SNU), multiple-uniform (MU), and multiple-non-uniform (MNU) time grids (Velez and Maravelias, 2013). Currently, an SU time grid is the one typically used in energy systems optimisation, with the grid size determined by the energy demand profile and operating characteristics of the considered equipment. Although an hourly time step is generally implemented, various step sizes have also been used in the literature. For example, Rieder et al. considered a 4-h time interval in their optimisation study due to a compromise between computational cost and the ability to capture the behaviour of the considered storage technology (Rieder *et al.*, 2014), while Tveit et al. captured the behaviour of seasonal storage with 13 periods per year (Tveit *et al.*, 2009).

In increasingly distributed and multi-vectors energy systems, equipment and demand

may have very different temporal characteristics which are suitable for the implementation of the multiple time grids method. For example, solar district heating systems usually use both short- and long-term thermal energy storage in order to increase the solar fraction (Bauer *et al.*, 2010). The short-term storage typically operates on a daily or weekly cycle, while the long-term one operates on a monthly or even seasonal cycle. This makes such a system an interesting case study for the implementation of the multiple time grids method.

5.3 Implementation of multiple time grids

In this thesis, the multiple time grids approach was implemented for the Drake Landing Solar Community (DLSC) energy system, a solar district heating installation in Okotoks, Canada (Sibbitt *et al.*, 2012). The system consists of solar thermal collectors, short-term storage, long-term storage and back-up boilers. It covers the space heating demand of 52 connected houses. Figure 5.2 illustrates the schematic of DLSC.

The solar collectors in DLSC are flat-plate glazed collectors with a total area of 2293 m^2. Two horizontal hot water tanks with a combined capacity of 240 m^3 act as the

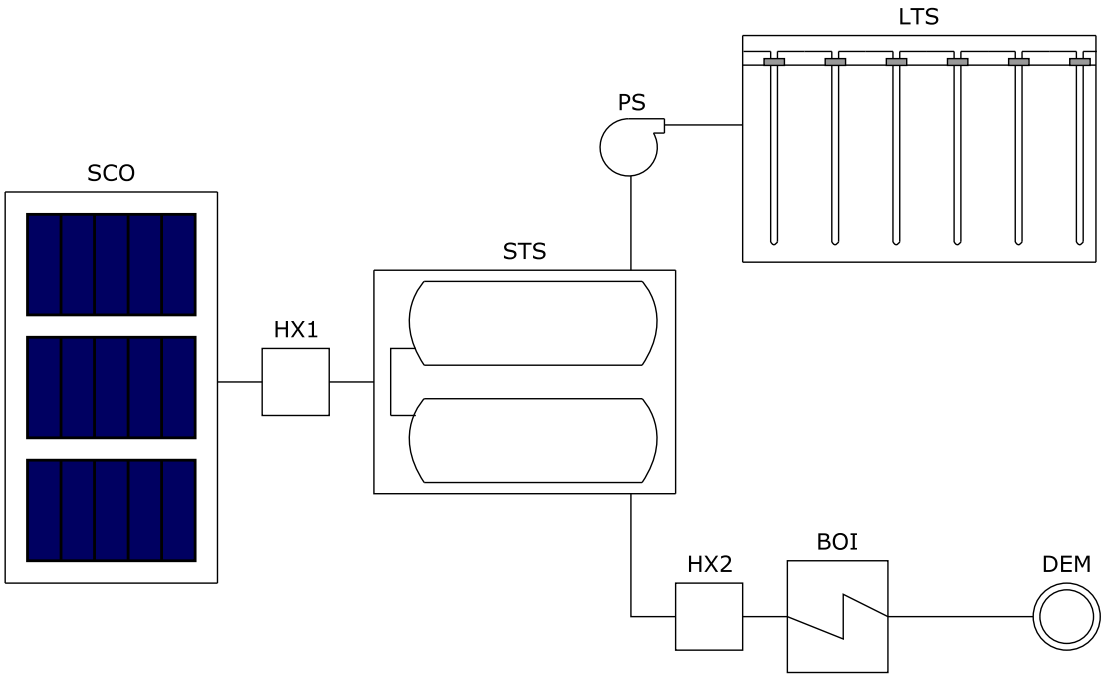

Figure 5.2: Schematic of the Drake Landing Solar Community. Main equipment is solar collectors (SCO), short-term thermal energy storage (STS), long-term thermal energy storage (LTS), and back-up gas boilers (BOI). They are operating to supply the heat demand (DEM) of the connected houses. Two heat exchangers (HX1, HX2) and one pump between the two storage (PS) were also modelled in the problem formulation

short-term thermal energy storage (STS) in DLSC. The STS can be charged by energy from the solar collectors and the long-term storage. The long-term thermal storage (LTS) in DLSC is a borehole thermal energy storage which consists of 144 boreholes of 35 m depth. In recent years, DLSC has been the subject of several studies related to its operational control (Quintana and Kummert, 2015), storage design (Shaarawy and Lightstone, 2016; Kandiah and Lightstone, 2016), and performance on different locations (Flynn and Sirén, 2015). A detailed description of DLSC can be found in Appendix C.

5.3.1 Problem statement

The operation optimisation problem can be stated as follows. The structure and design of an energy system with integrated short- and long-term TES are given. The objective is to determine the operational profile of the equipment over a given time horizon that minimises the total operational cost, as shown in Eq. 5.1.

$$\min C_{opr} = \min \sum_{t_{start}}^{t_{end}} \left(\dot{Q}_{in,t}^{BOI} \cdot \Delta t \cdot C_{in}^{BOI} + P_{in,t}^{PS} \cdot \Delta t \cdot C_{in}^{PS} \right) \tag{5.1}$$

The first term on the right-hand side of Eq. 5.1 represents the fuel cost of the back-up boilers calculated by multiplying the natural gas input, $\dot{Q}_{in,t}^{BOI}$, the cost of natural gas, C_{in}^{BOI}, and the time step size, Δt. The natural gas input is calculated by dividing the boiler thermal energy output, $\dot{Q}_{t}^{BOI}$, with a constant efficiency of 90%, as shown in Eq. 5.2.

$$\dot{Q}_{in,t}^{BOI} = \frac{\dot{Q}_{t}^{BOI}}{\eta^{BOI}} \tag{5.2}$$

The second term on the right-hand side of Eq. 5.1 corresponds to the electricity cost due to pump operations calculated by multiplying the input electricity, $P_{in,t}^{PS}$, the cost of electricity, C_{in}^{PS}, and the time step size, Δt. In reality, there are five pumps in DLSC, one for every loop and with four of them having a parallel back-up (Leidos Canada, 2014). Only one pump was modelled because the focus of the study is on the effect of the LTS time grids rather than finding the detailed optimised profile of all the pumps. Furthermore, it has been shown that managing the interaction between STS and LTS is very important in the effort to increase the share of renewable energy in the system (Quintana, 2013). Since the LTS has slower charge/discharge rate compared to the STS, the decision to charge/discharge the LTS has to be planned well in advance. As an example, a failure to anticipate a relatively higher demand during a period in winter, i.e. not discharging the LTS early enough, may result in the operation of the back-up boilers, which will reduce the solar fraction of the system.

5.3.2 Implemented time grids

Velez and Maravelias proposed a set of algorithms to generate non-uniform time grids for short-term scheduling of chemical processes (Velez and Maravelias, 2013, 2014). Essentially, the algorithms examined the temporal characteristics of the units, tasks, and materials involved in the scheduled processes, and formulated multiple grids according to a set of requirements which should not be violated. In energy systems, these correspond to the characteristics of the main equipment and the energy demand.

In this thesis, the multiple time grids were generated based on empirical examination of the energy system. Time point set and time step size of equipment i are denoted by ϵ^i and δ^i, respectively. These are illustrated in Fig. 5.3 - 5.5 for exemplary SU, MU, and MNU time grids of DLSC.

A single uniform (SU) time grid of DLSC has a constant time step size for all equipment, as shown in Fig. 5.3 for time step size (δ) of 2-h and 6-h. As stated in the previous section, an SU grid with a time step size of 1-h is the most common representation in energy systems optimisation studies. One of the reasons for this is due to the available demand and weather data, which are typically reported as the average value over 1-h time step.

In multiple uniform (MU) time grids, each equipment and demand can have its own time step size, and the size has to be uniform over the entire time horizon. For instance, in Fig. 5.4, the LTS has a time step size of 2-h or 6-h, while the time step of the remaining equipment and demand are fixed at 1-h.

The uniformity of time step size is not required in multiple non-uniform (MNU) time grids, as illustrated in Fig. 5.5. In the figure, the SCO has non-uniform time grid, where hourly time step is used during the day (e.g. 07.00 - 19.00) and 12-h time step size is used during the night (e.g. 19.00 - 07.00). The main concept behind the non-uniformity is to minimise the time points of equipment whenever it does not operate or a demand node if it can be averaged without significant departure from the original data. For the case of the solar collector SCO in Fig. 5.5 , its operational hours are limited by the solar energy resource.

Since the difference in temporal characteristics of STS and LTS is the focus in this chapter, different δ^{LTS} were tested in the optimisation runs, ranging from 1 up to 24-h. In SU, these sizes were also applied to other equipment, while they were only applied to LTS in MU. Furthermore, only the time grid of SCO was considered to be non-uniform in the MNU case. Table 5.1 summarises all the tested time grid step sizes.

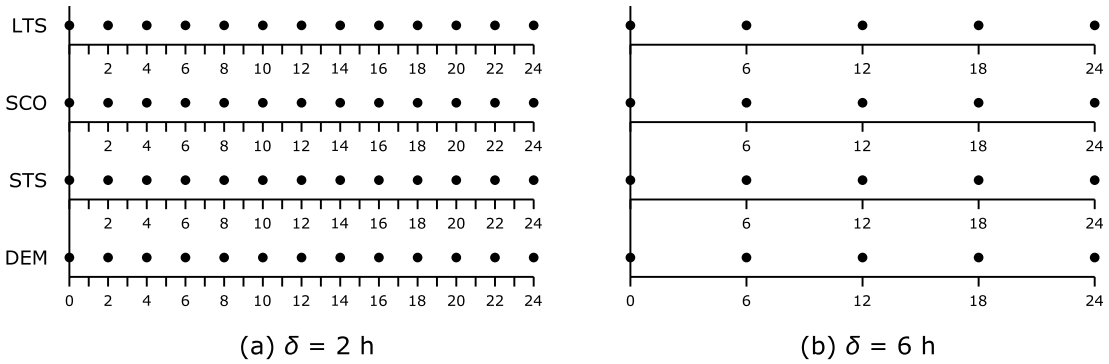

Figure 5.3: Examples of single uniform (SU) cases with (a) 2-h time step, and (b) 6-h time step.

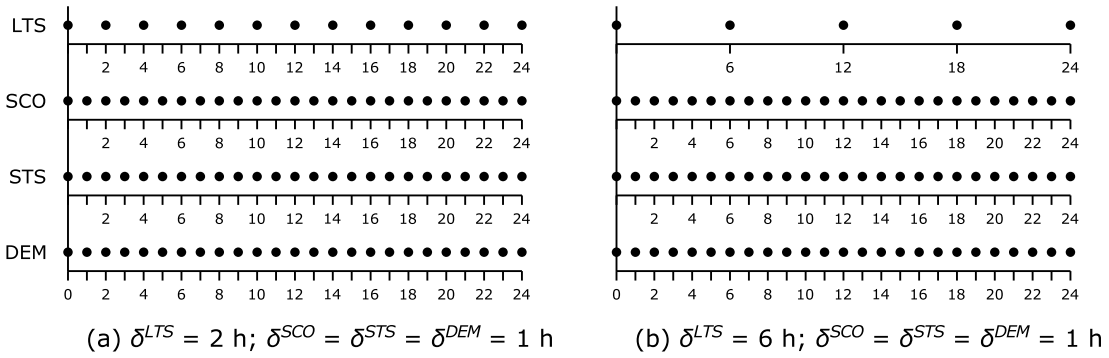

Figure 5.4: Examples of multiple uniform (MU) cases with different LTS time step size: (a) 2-h , and (b) 6-h.

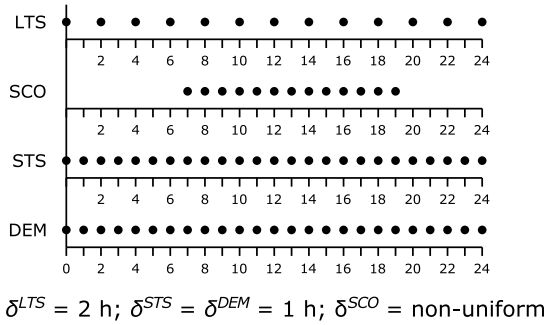

Figure 5.5: Example of the multiple non-uniform (MNU) case. Here only the solar collector (SCO) has non-uniform time grid, i.e. hourly during daytime.

Table 5.1: Tested time grid step sizes

Time grids	SU	MU	MNU
δ^{SCO}	$\{1, 2, 4, 6, 12, 24\}$	$\{1\}$	(non-uniform)
δ^{STS}	$\{1, 2, 4, 6, 12, 24\}$	$\{1\}$	$\{1\}$
δ^{LTS}	$\{1, 2, 4, 6, 12, 24\}$	$\{1, 2, 4, 6, 12, 24\}$	$\{1, 2, 4, 6, 12, 24\}$
δ^{DEM}	$\{1, 2, 4, 6, 12, 24\}$	$\{1\}$	$\{1\}$

5.3.3 Mathematical model

As stated in Section 3.3, the equipment modelling approach is based on the first law of thermodynamics; hence, it implements only the energy balance and does not include the dynamics of, for example, mass flow rate and temperature in the system. Although it has been shown that this type of formulation may lead to less accurate representation of real systems (e.g. in (Schütz *et al.*, 2015)), it is necessary to limit the equipment modelling complexity. This is because the main focus of this study is not about the absolute accuracy, but on the effects of different time grid formulations on the optimisation results. Parameters used in the optimisation run, along with their reference, are listed in Table 5.2.

Solar collector

The efficiency of the solar collector was assumed to be constant at $\eta^{SCO} = 50\%$. This value was taken from observation of the collector efficiency graph in (Sibbitt *et al.*, 2012). The constant efficiency approach in modelling the solar collector was followed because the flow inlet temperature was not modelled. Assuming this temperature as a constant would result in a very low efficiency figure at times when the ambient temperature is low, e.g. during the winter period. Thus, the absorbed incident solar irradiation Q_t^{SCO} was treated as a parameter and calculated with Eq. 5.3. The value of solar irradiance over the tilted angle, G_t, was taken from the input weather file, while the area of the solar collector, A^{SCO}, was given.

$$Q_t^{SCO} = \eta^{SCO} \cdot G_t \cdot A^{SCO} \tag{5.3}$$

Table 5.2: Parameter values in the operational optimisation of DLSC

	Parameter	Unit	Value	Reference
SCO	η^{SCO}		0.5	Assumption
	A^{SCO}	m^2	2293	(Sibbitt *et al.*, 2012)
STS	V^{STS}	m^3	240	(Sibbitt *et al.*, 2012)
	ρ_w	kg/m^3	1000	
	c_w	kJ/kg·K	4.2	
	ΔT^{STS}	K	50	(Shaarawy, 2014)
	ϕ_{STS}	%	0.02	Assumption
	Q^{STS}_{max}	MWh	14	Eq. (5.4)
	$\dot{Q}^{STS}_{ch,max}$	kW	2940	Charging flow rate = 14 l/s; Case 2 in (Shaarawy, 2014)
	$\dot{Q}^{STS}_{dch,max}$	kW	1260	Discharging flow rate = 6 l/s; Case 1 in (Shaarawy, 2014)
	$SOC^{STS}_{t=0}$	-	1.0	Assumption
LTS	V^{LTS}	m^3	33700	(Sibbitt *et al.*, 2012)
	$\rho_s \cdot c_s$	kJ/m^3·K	3203	(McDowell and Thornton, 2008)
	k_s	W/m·K	1.373	(McDowell and Thornton, 2008)
	ΔT^{LTS}	K	30	(Leidos Canada, 2014)
	ϕ_{LTS}	%	0.024	Assumption
	Q^{LTS}_{max}	MWh	900	Eq. (5.11)
	$\dot{Q}^{LTS}_{ch,max}$	kW	170	Avg. charging flow rate = 2.7 l/s (Leidos Canada, 2014)
	$\dot{Q}^{LTS}_{dch,max}$	kW	170	Avg. discharging flow rate = 2.7 l/s (Leidos Canada, 2014)
	$SOC^{LTS}_{t=0}$	-	0.2	Assumption
BOI	η^{BOI}		0.9	Assumption
	$\dot{Q}^{BOI}_{max}$	kW	1000	Assumption
Natural gas	C^{BOI}_{in}	\$/kWh	0.011	Average rate, July 2012 - June 2013 (Alberta Government, 2016).
Electricity	C^{PS}_{in}	\$/kWh	0.0866	Average rate, July 2012 - June 2013 (Alberta Government, 2016).

Short-term storage

The maximum stored energy, Q_{max}^{STS}, is calculated by Eq. 5.4 with the assumption of $\Delta T^{STS} = 50$ K. This yields a maximum stored energy of 50.4 GJ. The maximum operational STS temperature at the top of the tank is reported to be 70 °C, while the heat distribution temperature varies between 37 and 55 °C (Shaarawy, 2014; Quintana, 2013).

The stored energy for every time step, $Q_{sto,t}^{STS}$ is calculated with Eq. 5.5. Furthermore, Eq. 5.6 - 5.8 represent constraints for maximum stored energy, maximum charge rate ($\dot{Q}_{ch,max}^{STS}$) and maximum discharge rate ($\dot{Q}_{dch,max}^{STS}$), respectively. The STS state-of-charge, SOC_t^{STS}, is calculated by Eq. 5.9 and the cyclic behaviour of STS is defined by the constraint in Eq. 5.10.

The maximum charge rate is derived from a charging condition with maximum achievable flowrate of 14 L/s and 50 K temperature difference from the initial and final storage temperature (Shaarawy, 2014). For the maximum discharge rate, the considered flowrate is 6 L/s, with the same temperature difference. As stated in Table 5.2, the maximum charging rate of the STS is larger than its maximum discharging rate. This is because the energy from the solar loop has to be transferred as quickly as possible to the STS in order to increase the solar fraction of the system.

$$Q_{max}^{STS} = \frac{V^{STS} \cdot \rho_w \cdot c_w \cdot \Delta T^{STS}}{3600} \tag{5.4}$$

$$Q_{sto,t}^{STS} = (1 - \phi^{STS}) \cdot \delta^{STS} \cdot Q_{sto,t-1}^{STS} + \left(\dot{Q}_{ch,t}^{STS} - \dot{Q}_{dch,t}^{STS}\right) \cdot \delta^{STS} \tag{5.5}$$

$$0 \leq Q_{sto,t}^{STS} \leq Q_{max}^{STS} \tag{5.6}$$

$$0 \leq \dot{Q}_{ch,t}^{STS} \leq \dot{Q}_{ch,max}^{STS} \tag{5.7}$$

$$0 \leq \dot{Q}_{dch,t}^{STS} \leq \dot{Q}_{dch,max}^{STS} \tag{5.8}$$

$$SOC_t^{STS} = \frac{Q_{sto,t}^{STS}}{Q_{max}^{STS}} \tag{5.9}$$

$$SOC_{t=0}^{STS} = SOC_{t=t_{end}}^{STS} \tag{5.10}$$

Long-term storage

Similar to the STS, the LTS was modelled using the capacity model which assumes a fully distributed temperature inside the storage medium. However, unlike the STS, the LTS cannot be charged and discharged at the same time. This limitation is formulated as constraints in Eq. 5.14 - 5.16, in which the binary variable ψ corresponds to the charging ($\psi_{ch} = 1, \psi_{dch} = 0$), discharging ($\psi_{ch} = 0, \psi_{dch} = 1$), and store ($\psi_{ch} = \psi_{dch} = 0$) status of the LTS.

$$Q_{max}^{LTS} = \frac{V^{LTS} \cdot \rho_s \cdot c_s \cdot \Delta T^{LTS}}{3600} \tag{5.11}$$

$$Q_{sto,t}^{LTS} = (1 - \phi_{LTS}) \cdot \delta^{LTS} \cdot Q_{sto,t-1}^{LTS} + \left(\dot{Q}_{ch,t}^{LTS} - \dot{Q}_{dch,t}^{LTS}\right) \cdot \delta^{LTS} \tag{5.12}$$

$$0 \leq Q_{sto,t}^{LTS} \leq Q_{max}^{LTS} \tag{5.13}$$

$$0 \leq \dot{Q}_{ch,t}^{LTS} \leq \psi_{ch,t}^{LTS} \cdot \dot{Q}_{ch,max}^{LTS} \tag{5.14}$$

$$0 \leq \dot{Q}_{dch,t}^{LTS} \leq \psi_{dch,t}^{LTS} \cdot \dot{Q}_{dch,max}^{LTS} \tag{5.15}$$

$$\psi_{ch,t}^{LTS} + \psi_{dch,t}^{LTS} \leq 1 \tag{5.16}$$

$$SOC_{t}^{LTS} = Q_{sto,t}^{LTS} / Q_{max}^{LTS} \tag{5.17}$$

$$SOC_{t=0}^{LTS} = SOC_{t=t_{end}}^{LTS} \tag{5.18}$$

The implementation of the multiple time grids method in this thesis is particularly focused on the LTS time grid. It should be emphasised that the status of LTS is fixed for every time step, regardless of the time step size. For example, if $\psi_{ch,6}^{LTS} = 1$ in MU case with $\delta^{LTS} = 6$-h (see Fig. 5.4), it means that the LTS is constantly charging for 6- between $\epsilon_2^{LTS} = 6$ and $\epsilon_3^{LTS} = 12$.

Heat exchangers

The energy balance between supply and demand was formulated as the constraints describing the two main heat exchangers in the system. The first heat exchanger (HX1) transfers solar energy from the collector to the short-term storage (Eq. 5.19 - 5.20), while the second heat exchanger (HX2) satisfies the heat demand by the energy from STS discharge and the backup boilers (Eq. 5.21).

In Eq. 5.20 and 5.21, if the current time point is not in the time points of LTS, then the rate of energy charged to ($\dot{Q}^{LTS}_{ch,t}$) or discharged from the LTS ($\dot{Q}^{LTS}_{dch,t}$) equals the value at the last time point of LTS ($\dot{Q}^{LTS}_{ch,t=\epsilon^{LTS}_{n-1}}$ or $\dot{Q}^{LTS}_{dch,t=\epsilon^{LTS}_{n-1}}$). For example, if $\epsilon^{LTS} = \{0, 6, 12, 18, 24\}$ for one day time horizon, then the charge/discharge rate of the LTS at $t = 8$ is equal to its charge/discharge rate at $t = 6$.

$$\dot{Q}^{SCO-HX1}_{t} \leq \dot{Q}^{SCO}_{t} \tag{5.19}$$

$$\dot{Q}^{SCO-HX1}_{t} = \begin{cases} \dot{Q}^{STS}_{ch,t} - \dot{Q}^{LTS}_{dch,t} & \text{if } t \text{ in } \epsilon^{LTS} \\ \dot{Q}^{STS}_{ch,t} - \dot{Q}^{LTS}_{dch,t=\epsilon^{LTS}_{n-1}} & \text{otherwise} \end{cases} \tag{5.20}$$

$$\dot{Q}^{STS-HX2}_{t} = \begin{cases} \dot{Q}^{STS}_{dch,t} - \dot{Q}^{LTS}_{ch,t} & \text{if } t \text{ in } \epsilon^{LTS} \\ \dot{Q}^{STS}_{dch,t} - \dot{Q}^{LTS}_{ch,t=\epsilon^{LTS}_{n-1}} & \text{otherwise} \end{cases} \tag{5.21}$$

Heat demand and weather data

The heat demand in every time step, $\dot{Q}^{DEM}_{t}$ is fulfilled by the solar energy that is transferred from the STS to HX2, $\dot{Q}^{STS-HX2}_{t}$, and the additional energy from the back-up boiler, $\dot{Q}^{BOI}_{t}$, (Eq. 5.22).

$$\dot{Q}^{DEM}_{t} = \dot{Q}^{STS-HX2}_{t} + \dot{Q}^{BOI}_{t} \tag{5.22}$$

The heat demand (DEM) profile of the 52 houses was derived synthetically using the methodology explained in Section 3.5. Ambient temperature and solar irradiation data were gathered from publicly available data (Government of Canada, 2016; National Resources Canada, 2015). Two time horizons were considered: one year and multi-year horizon. The selected time horizon was from July 2012 to June 2013 for one-year optimisation and July 2007 to June 2013 for multi-year optimisation. The first time horizon corresponds to the sixth year of DLSC operation when the BTES had reached close to steady-state behaviour after five years of warming-up period. The second time

horizon starts from the period when DLSC became operational up to the latest available measurement report when the study was performed.

DLSC control implementation

An optimisation model with the DLSC control rules was also developed and solved accordingly. This particular model serves as a comparison to the regular optimisation model, in which the solver tries to find the optimal control rather than using a pre-determined rule.

The implemented rules correspond to the control of interaction between STS and LTS during the winter period, as explained in Ref. (Quintana, 2013). The control rules determine when the LTS should start charging and discharging during the winter by comparing the STS state-of-charge to a pre-determined required state-of-charge. The latter depends on the set-point temperature of the district loop. Further details on the control rule can be found in Ref. (Quintana, 2013).

The winter mode control rules were implemented in the optimisation model as one additional constraint (Eq. 5.23) which was only applied during the winter months (Jan-Apr and Sep-Dec, inclusive). $SOC^{STS}_{req,t}$ is the required state-of-charge at time t and its value is given as a parameter (Table C.1 in Appendix C). The combination of Eq. 5.23 and 5.16 ensured that the LTS is charged when $SOC^{STS}_{t} - SOC^{STS}_{req,t}$ is positive and it is discharged when is $SOC^{STS}_{t} - SOC^{STS}_{req,t}$ is negative. Thus, the whole system is actively working during the winter mode, with the LTS in either charging or discharging mode (Quintana, 2013).

$$-\psi^{LTS}_{dch,t} \leq SOC^{STS}_{t} - SOC^{STS}_{req,t} \leq \psi^{LTS}_{ch,t} \tag{5.23}$$

Two main parameters in the heuristic control rule are the set-point temperature of the district heating (DLSP) and the required STS state-of-charge ($SOC^{STS}_{req,t}$). DLSP is a function of the ambient temperature and calculated according to Eq. C.1 , which is based on Figure 2-4 in Ref. (Quintana, 2013). The values of $SOC^{STS}_{req,t}$ for three ranges of DLSP at a different time of the day were gathered from Figure 2-5 in Ref. (Quintana, 2013) and shown in Table C.1.

Table 5.3: Computational results for the reference case

Time grids	SU
Time step size ()	1
Binary variables	17522
Total variables	96372
Average computational time (s)	82.2
Relative gap	0.01
Objective value ($)	264.8
Solar energy collected (GJ)	5630.4
Solar energy to STS (GJ)	3676.7
LTS charge (GJ)	2089.4
LTS discharge (GJ)	908.9
Solar energy to district (GJ)	2473.4
Gas consumption (GJ)	15.5

5.4 Results and discussions

5.4.1 Reference case

In order to make a comparison between different time grid implementations, the single-uniform grid with 1h time step and 1% optimality gap was selected as the reference case. Its computational results are summarised in Table 5.3.

Furthermore, the resulting operational profiles of the LTS in the reference case are shown in Fig. 5.6. The charge and discharge profile are similar to the expected profile of a seasonal storage, i.e. charging in the summer and discharging in the winter. However, unlike the measured profile reported in (Leidos Canada, 2014), the optimised profile has a gap of only storing between mid-March and mid-May, i.e. no charging or discharging. This is because in the optimisation case, the solver looks over the prescribed time horizon in order to produce the optimal profile. It is necessary to solve the optimisation simultaneously over the whole time horizon since the presence of storage has coupled the decisions between different time steps. In other words, the solver has full knowledge of the future; thus, it knows exactly when the charging is sufficient for the period ahead, avoiding unnecessary charging which may worsen the objective value.

The resulting operational profiles of the short-term storage (STS) for the reference case are illustrated in Fig. 5.7 and 5.8. The yearly operational profile in Fig. 5.7 shows that over the course of a year, the STS is rarely in fully-charged condition. This can be attributed to the probable oversizing in the STS tank design and therefore the resulting

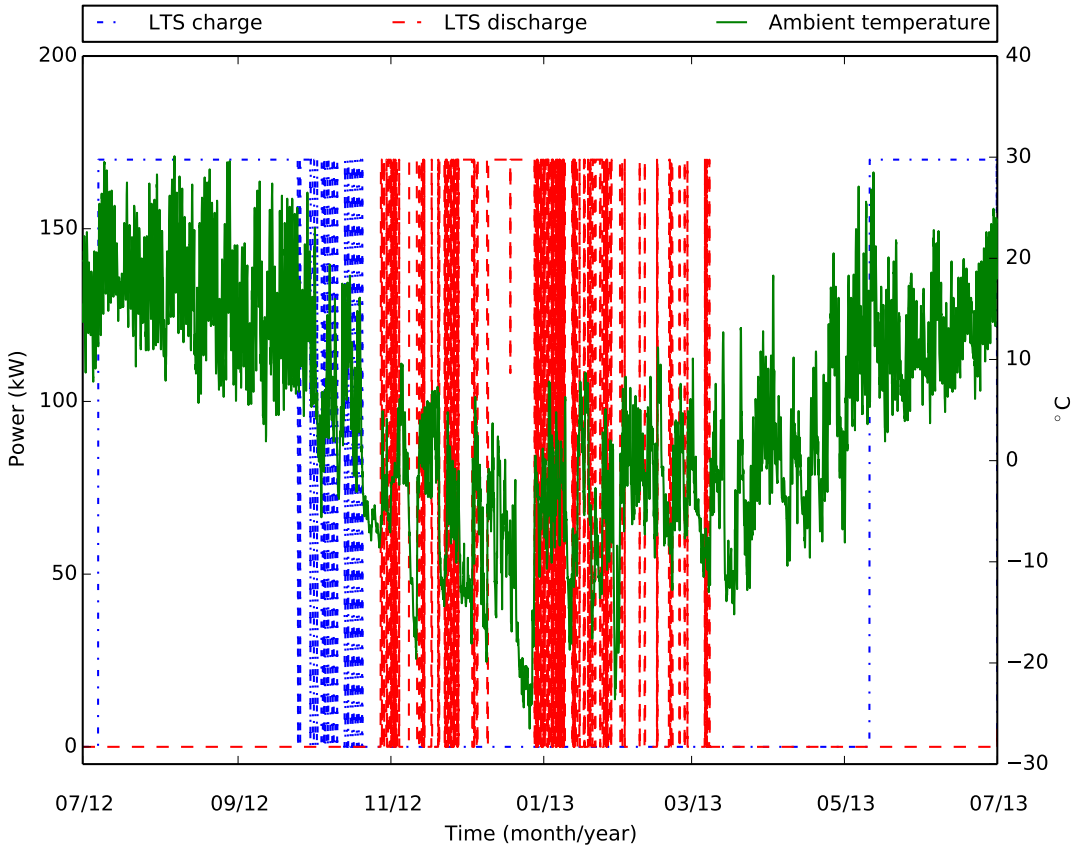

Figure 5.6: LTS charge/discharge profile for the reference case.

operational profile shows a general attempt to use the STS at its best to limit the losses.

For example, it can be seen in Fig. 5.8a that the charging pattern of STS is reasonable, i.e. matching the solar irradiation availability, while its state-of-charge remains relatively low due to the constant discharging to the LTS. In the real control of DLSC, the discharging from STS to LTS in the summer happens during the night or whenever the STS is fully charged (Quintana, 2013). It is clear that the LTS charging pattern from the optimisation is driven to minimise the STS static losses. These losses are more prevalent in the real control of DLSC since it waits until night time or a fully-charged STS to start charging the LTS. This highlights the potential improvement in performance that can be achieved by using optimisation results in the operation of DLSC.

As mentioned in Chapter 4, an operational optimisation can be implemented together with the Model Predictive Control (MPC) approach in a real-time operation of an energy system. For the case of DLSC, an MPC-based optimisation has been proposed in Ref. (Quintana, 2013). Therefore, the annual operational optimisation results reported in this chapter substantiate the important role of optimisation in improving the performance of energy systems in general, and the DLSC in particular. Furthermore,

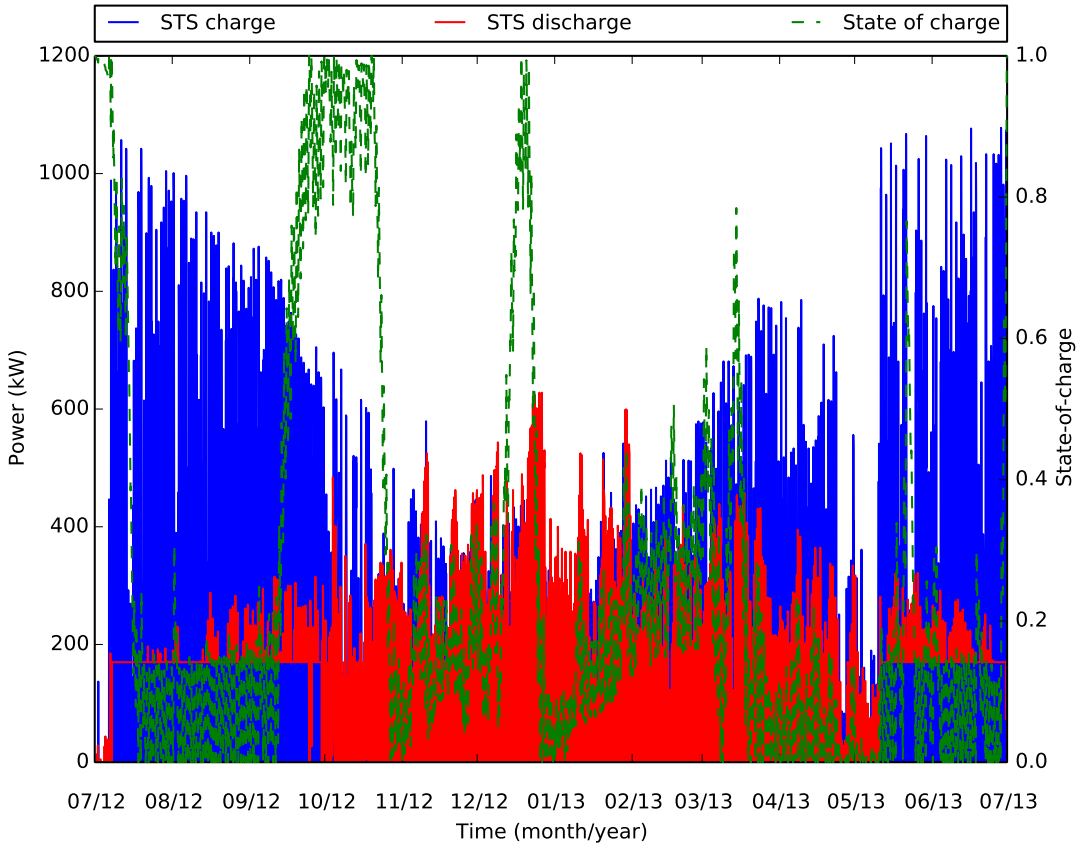

Figure 5.7: STS yearly operational profile for the reference case

the resulting operational profile form the deterministic yearly operational optimisation can be seen as the upper attainable by the system.

5.4.2 Comparison between time grids: computational times and relative accuracy

Annual operation optimisations of DLSC were performed using single-uniform and multiple-uniform time grids with 1% and 5% optimality gap. Results of single-uniform cases are shown in Fig. 5.9. As expected, the computational time follows a decreasing trend as the grid size increases. This corresponds to the lower number of optimisation variables as the time grid becomes coarser than the reference grid size. However, the decrease in computational time comes with the cost of increasing relative error of the objective value (Fig. 5.9b). The relative error of the objective value is calculated according to Eq. 5.24. This increasing relative error trend is caused by the averaging of the demand profile which eliminates inherent peaks. In addition to an increase in relative error, it will also affect the equipment sizing if design optimisation is performed, e.g. undersize equipment due to missing peak demand. This observation is in line with

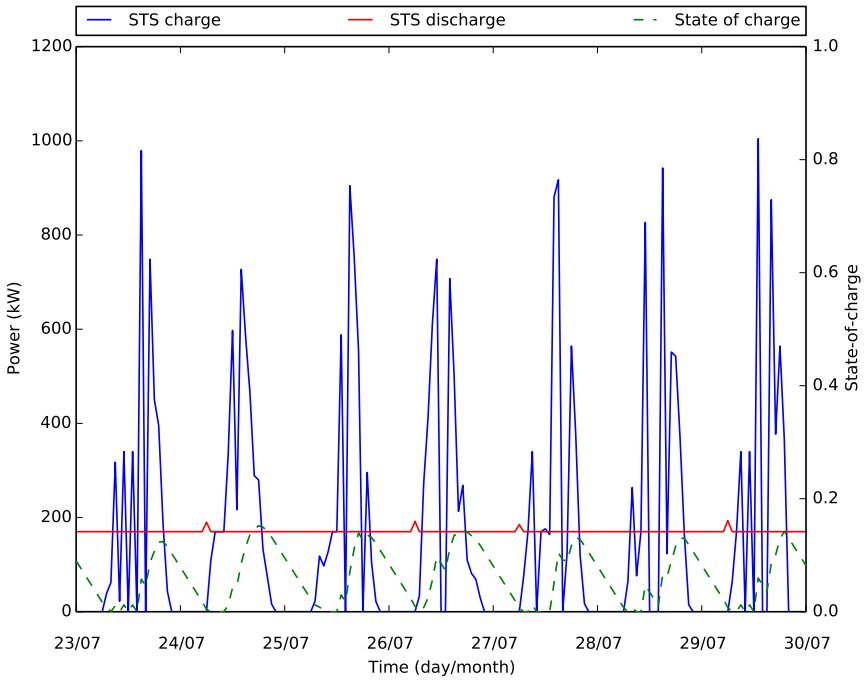

(a) Example of summer profile.

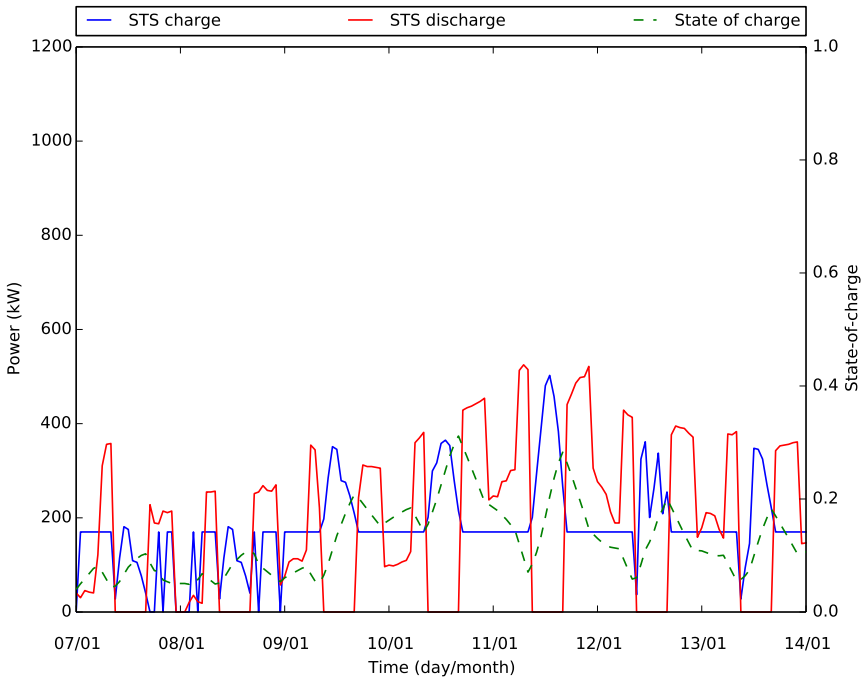

(b) Example of winter profile.

Figure 5.8: Example of STS weekly operational profile.

the study on the effects of temporal precision in optimisation of residential cogeneration systems (Hawkes and Leach, 2005; Wakui and Yokoyama, 2015)

$$Relative\ error(\delta^{lts} = n) = \left| 1 - \frac{C_{opr}(\delta^{lts} = n)}{C_{opr}(\delta^{lts} = 1)} \right| \tag{5.24}$$

In order to avoid the shortcomings of using a coarse single-uniform grid, the multiple-uniform grids approach was tested on the same optimisation problem. In measuring the computational time, the optimisation run with an LTS step size and optimality gap combination was repeated five times. The resulting average computational times and relative error are illustrated in Fig. 5.10. In this case, the computational time decreases by one order of magnitude as the LTS step size increases up to 2-h and 6-h for the 1% and 5% MIP gap case, respectively (Fig. 5.10a). Beyond these step sizes, the computational time has an increasing trend in both cases. This is significantly different than in single-uniform cases and can be explained by examining the operational characteristic of the LTS in the system.

The LTS serves as a large storage option to store excess solar energy during the summer and discharge them to the STS during the winter. Thus, as LTS charge/discharge behaviour is restricted to a larger number of hours with increasing time step δ^{LTS}, it becomes more difficult for the solver to find an optimal profile since it means that a larger amount of energy must be available/unavailable within the STS. This illustrates that although the number of variables is reduced due to the use of coarser δ^{LTS}, the problem can still become harder to solve. This observation is in line with a previous study which noted that the multiple grids model could have a worse solution time than the single uniform model (Velez and Maravelias, 2013).

Furthermore, despite the absence of a consistent decreasing trend in the computational time, the increasing LTS step size has a relatively small effect on the objective value, as shown in Fig. 5.10b. It is also interesting to note the similarity in relative error between cases with 1% and 5% optimality gap, as shown in Fig. 5.10b. Combined with the insights gathered from the results on computational time (Fig. 5.10a), it is clear that an optimality gap of 5% is preferable for this case. All in all, a multiple-uniform approach with δ^{LTS} = 6-h and 5% MIP gap is the best combination for this case study, with a computational time reduction of almost two orders of magnitude relative to the original single uniform 1-h time grid.

In an attempt to further lower the computational time, multiple-non-uniform (MNU) time grids were implemented in the case study. The non-uniformity of the grids stemmed from the SCO time grid which was prescribed to be only available during daytime; thus, reducing the number of variables even further. Nevertheless, the computational time and relative objective value for this case are practically the same with the multiple-uniform

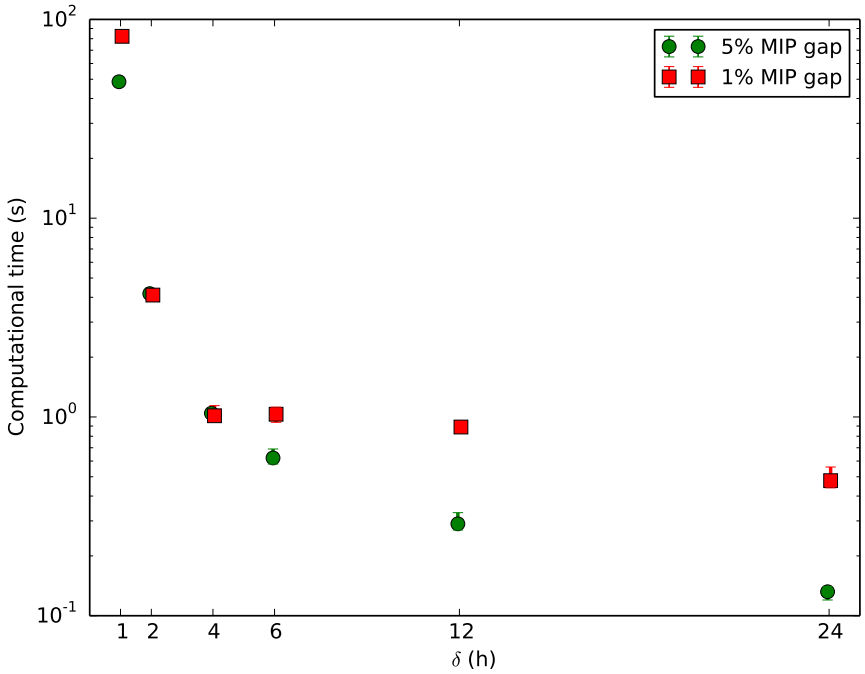

(a) Computational time

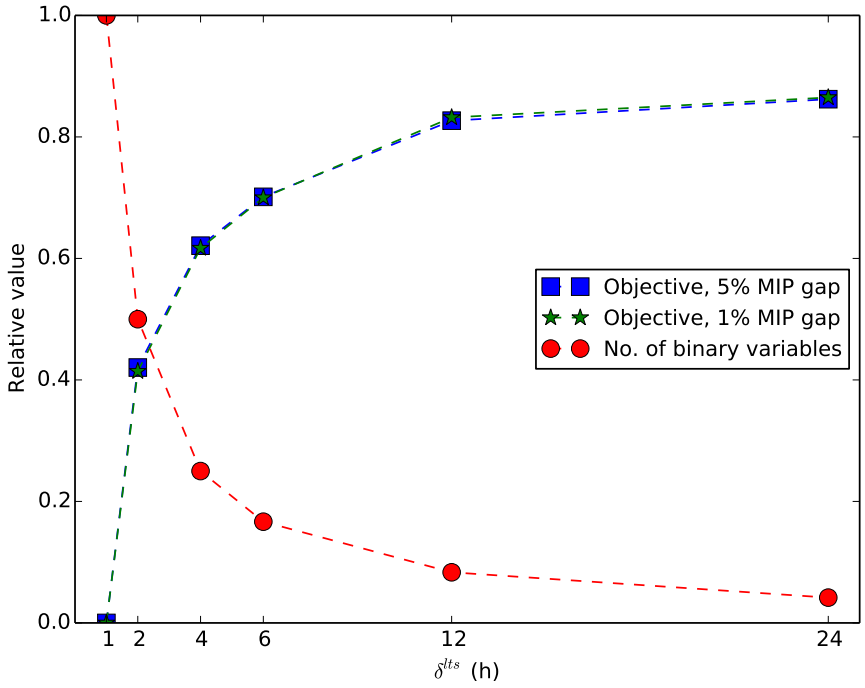

(b) Relative error of the objective function and number of binary variables.

Figure 5.9: Results for single-uniform cases: (a) Computational time, and (b) Relative error of the objective function and number of binary variables for different time step size. Note that there is a significant overlap between the two objective function relative error curves. The dashed lines are shown as a guide to illustrate the trend.

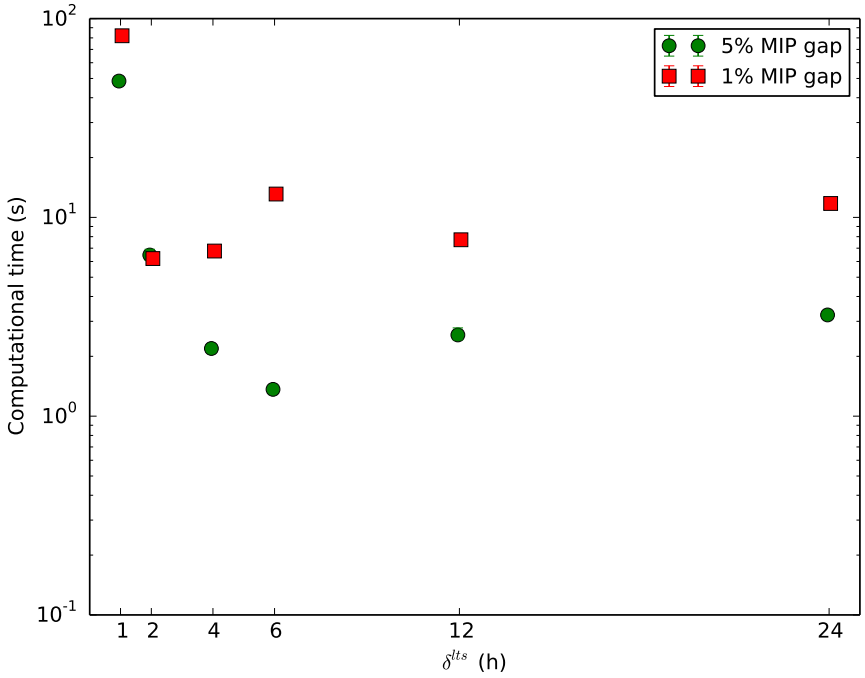

(a) Computational time

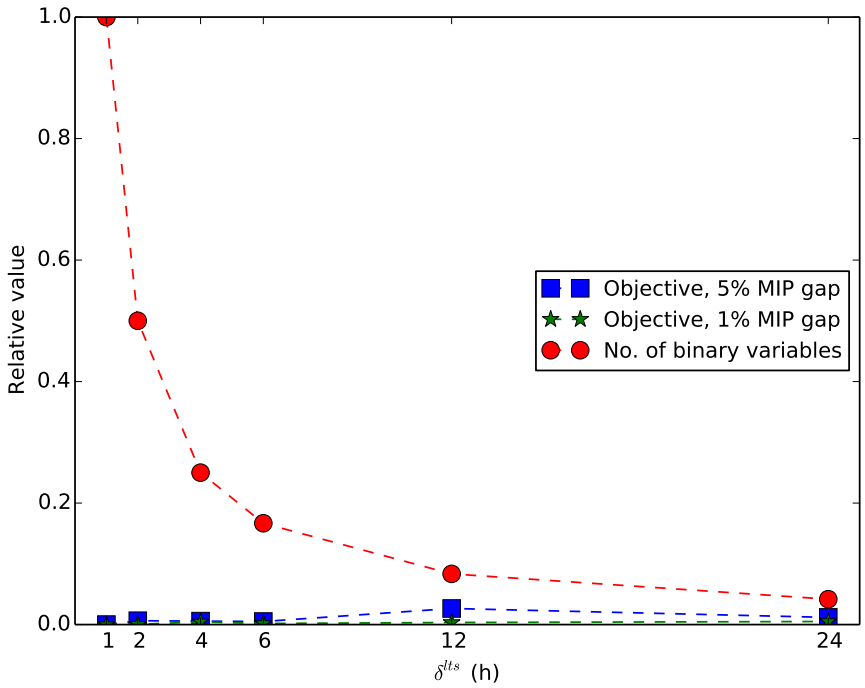

(b) Relative error of the objective function and number of binary variables.

Figure 5.10: Results for multiple-uniform cases: (a) Computational time, and (b) Relative error of the objective function and number of binary variables for different LTS time step size. Note that there is a significant overlap between the two objective function relative error curves. The dashed lines are shown as a guide to illustrate the trend.

one. This is because the solar irradiation acted as a parameter in the formulation and the collected solar energy variable (Q^{SCO}) was defined as a simple multiplication between irradiation and collector efficiency (Eq. 5.3). Therefore, a reduction in the number of this variable by removing the zero-valued due to unavailable solar irradiation has little impact on computational time. Furthermore, the pre-solve step employed by the solver may also contribute to the negligible impact of SCO time grid reduction. It should be noted that MNU time grids may have more impacts in more complex models, for example in multi-vector energy system with various demand profiles.

From the comparison between time grid implementations, it is clear that increasing the time step size in SU model can significantly affect the objective value, while this is not the case in the implemented MU model. However, the computational time reduction in the MU model is not always guaranteed by increasing the equipment time step size, in this case, the LTS (δ^{LTS}). For the modelled system, the computational time reaches a minimum before it starts an increasing trend with δ^{LTS}, indicating an optimal δ^{LTS} for a given system.

5.4.3 Grid size and equipment characteristics

In order to evaluate whether the optimal time grid size of a storage equipment depends on its characteristics, MU optimisation runs with varying storage parameters were performed. One relevant characteristic is the storage thermal power (maximum charge/discharge rate). The MU optimisation runs were conducted using different LTS powers which include halving (85 kW) and doubling (340 kW) the originally prescribed power (170 kW). The resulting computational time graphs are shown in Fig 5.11.

The overall trend shows that there is a significant decrease in computational time as δ^{LTS} was increased from 1 to 2-h. In the 340 kW (Gap=1%) case, the exception from this trend is relatively small compared to the drop of computational time in other cases.

However, as the LTS power grows, the use of large δ^{LTS} becomes less beneficial due to increasing computational time. The case of 340 kW (Gap=1%) even failed to reached optimality within the prescribed time limit when 12-h time step is used. Nevertheless, the case with the same LTS power but larger optimality gap (5%) managed to reached optimality in all time steps used. The same trend can also be observed in the 170 kW LTS power, where cases with 5% optimality gap have lower computational time than 1% gap for the same δ^{LTS}. An exception to this is the 85 kW LTS power, where both optimality gaps produce relatively similar computational time. These trends occur because as the LTS power grows, it becomes more difficult for the solver to ensure sufficient energy or available storage capacity within the STS, which is required to charge or discharge the LTS.

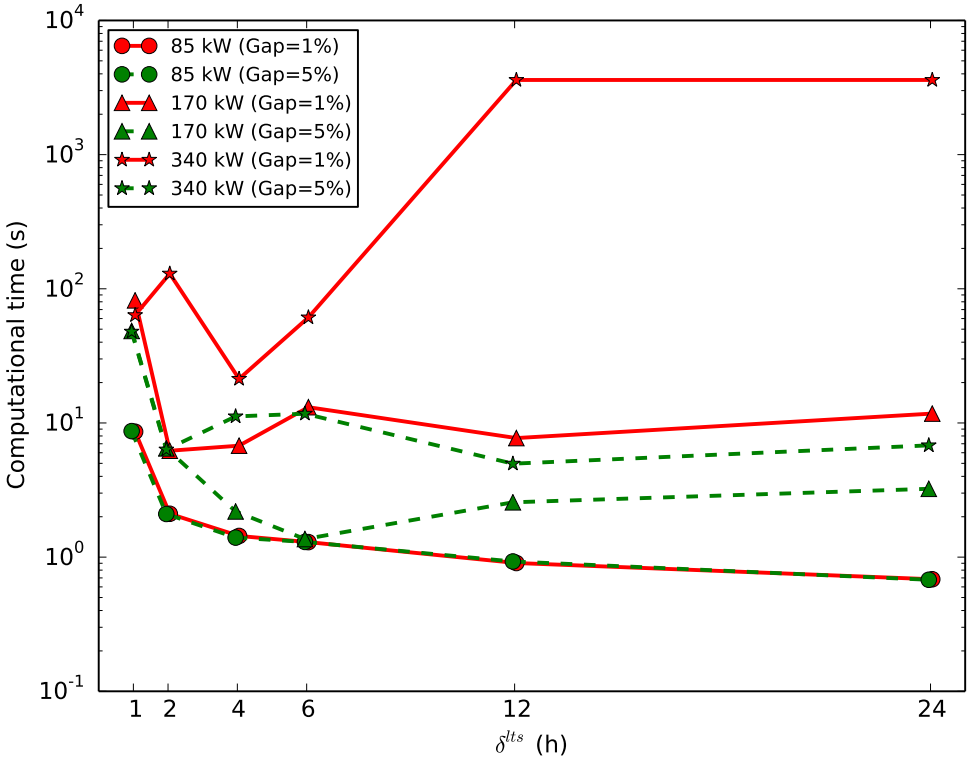

Figure 5.11: Computational time for optimisation run with different LTS charge/discharge power (kW) and MIP gap (%).

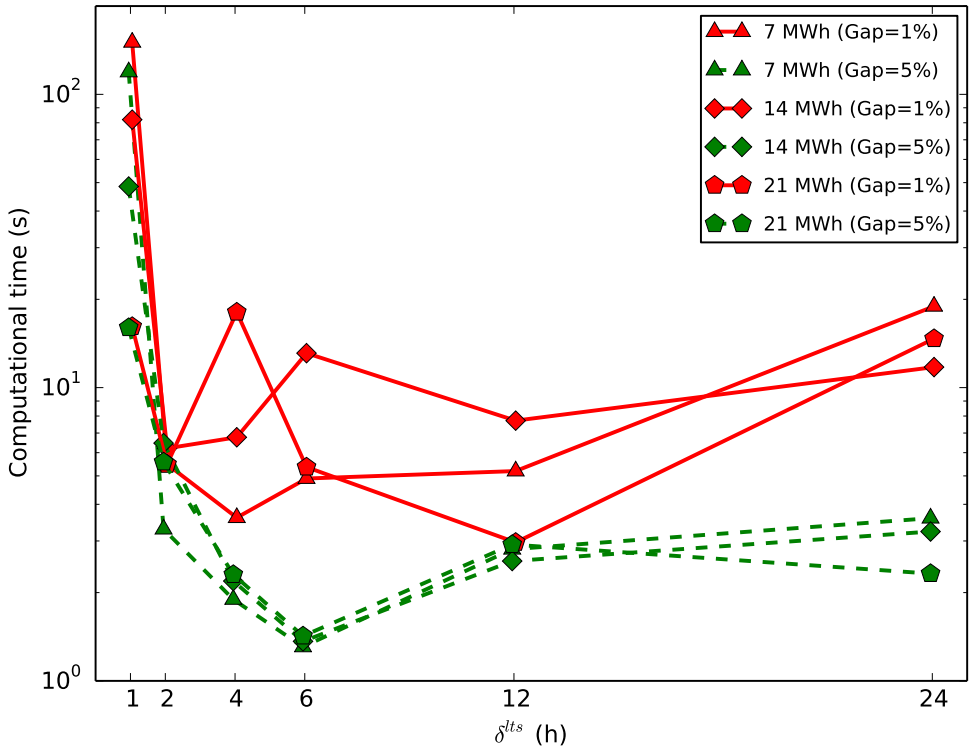

Figure 5.12: Computational time for optimisation run with different STS size (MWh) and MIP gap (%).

Since the LTS operation is highly coupled to the STS, MU optimisations with different STS sizes were also performed in order to evaluate the possible effects. The results are illustrated in Fig. 5.12. The STS size was selected to be 0.5 and 1.5 times of the original. All cases show a similar trend of steep decrease in computational time as δ^{LTS} goes from 1 to 2-h. The computational time tends to increase again when δ^{LTS} is larger than 4 and 6-h for 1% and 5% gap, respectively. It can also be observed that cases with 5% optimality gap have considerably lower computational time than those with 1% gap.

However, unlike the cases with different LTS power, there is no clear trend in computational time for cases with different STS size for the same δ^{LTS} value. For example, the computational time of 21 MWh (Gap=1%) gap has the lowest computational time among other 1% cases at δ^{LTS} = 1-h, but not at 4, 6, and 12-h. Similar inconsistent relative position in computational time can also be observed for the other two STS sizes. This behaviour can be partly caused by the unchanged STS power for different STS sizes. Thus, the changes in storage capacity have no direct influence on the rate of energy transferred between STS and LTS.

From the two varied parameters, i.e. LTS power and STS size, it can be concluded that the temporal characteristics of equipment will have more impact on determining the best time grid size. This should be considered in the future work of developing a systematic way to generate the multiple time grids.

Furthermore, the optimisation results from cases with different LTS power and STS size described above are compared with the reference case in Table 5.4. The reference case corresponds to the system with 170 kW LTS power and 14 MWh STS size.

It can be observed from Table 5.4 that an increase in LTS power can significantly improve the objective value by reducing the gas consumption to zero. This can be attributed to the better utilisation of LTS with more stored energy extracted compared to the reference case. The case with lower LTS power has a substantially worse objective value relative to the reference due to the low utilisation of the LTS. As for the cases with different STS size, the influence of STS size on the objective value is not as significant as in the LTS power cases. For instance, although the case with larger STS size is able to largely decrease the gas consumption, the total electricity consumption is unchanged due to the similar LTS charge-discharge profiles with the reference case.

The optimisation runs with different equipment characteristics illustrate that the LTS power has a more significant influence over the objective value relative to the STS size. The limited influence of STS size over different performance metrics will be revisited in Chapter 6 where a validated simulation model of DLSC is employed in a parametric study.

Table 5.4: Optimisation results of cases with different STS and LTS characteristics.

	Reference	LTS power		STS size	
		85 kW	340 kW	7 MWh	21 MWh
Solar energy collected (GJ)	5630.4	5630.4	5630.4	5630.4	5630.4
Solar energy to STS (GJ)	3676.7	3126.3	3611.7	3627.6	3703.1
LTS charge (GJ)	2089.4	1668.3	2007.3	2086.3	2084.8
LTS discharge (GJ)	908.9	648.4	921.5	920.9	900.7
Solar energy to district (GJ)	2473.4	2066.6	2488.8	2449.4	2488.4
Gas consumption (GJ)	15.5	422.2	0.0	39.5	0.5
Electricity (GJ)	8.8	13.6	4.3	8.9	8.8
Objective value ($)	264.8	1761.6	103.9	347.1	212.9

5.4.4 Optimisation with currently implemented control rules

One of the aims of performing the operational optimisation is to find the optimal operational profile of equipment in the system. Although it can be seen as too ideal for real application, the resulting profile can assist the engineers in designing the operational control of the system. It can also act as a benchmark to evaluate the real control options.

In order to assess the currently implemented control rules of the DLSC, an optimisation run with additional constraints describing the rules (Eq.5.23) was performed. In this optimisation run, the operational behaviour of LTS was only optimised during the summer period (May-Aug), while it was controlled by the implemented heuristic rules during the winter period (Sep-Apr). The implemented heuristic rules were limited to the winter period because only the winter period rules are publicly available in the literature (Quintana, 2013).

The resulting LTS profiles of the reference and heuristic case are shown in Fig. 5.13. It is interesting to note that during most of the winter period (Sep-Mar), the heuristic model produced a very similar profile as the reference one although the LTS is controlled by the heuristic rules in this time. However, unlike the reference case, the LTS in the heuristic model starts charging immediately after March. This does not occur until after May in the reference case since it only needs to start charging at this time in order to fulfil the cyclic storage constraint. Furthermore, it can be seen that starting from May, the heuristic profile starts to follow the reference profile since from this point, the LTS is again optimised by the solver and not controlled by the heuristic rules.

Results of the reference optimised model, the heuristic model and field measurement are summarised in Table 5.5. The heuristic model was run to approximately 7% optimality gap due to resource constraints. It can be seen that the heuristic model produces results which are closer to the measurement than the optimised one. As expected, the objective

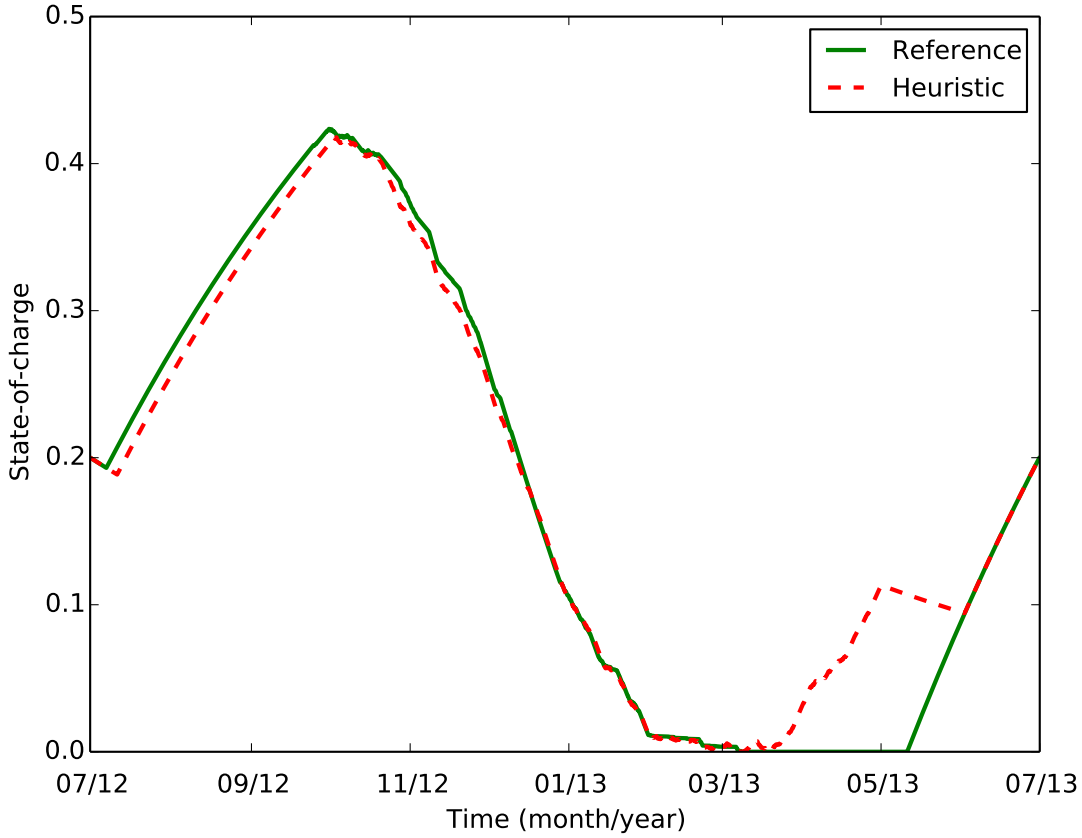

Figure 5.13: LTS state-of-charge profile for the optimised and heuristic case.

value of the heuristic model is worse than the optimised model due to the assumed LTS charge/discharge rules during the winter period. The charging of LTS between March and May which occurs in the heuristic LTS profile (Fig. 5.13) is also reflected by the higher electricity consumption relative to the optimised model. The relatively low value of the objective function in comparison to the size of the system is because only the natural gas for the boiler and the STS-LTS pump electricity consumption were included in the operational cost calculation. Additionally, the gas and electricity prices were the average prices over the time horizon.

In comparison with the measurement values, the optimised model clearly produces a better performance than the implemented control rules. For instance, a significantly lower gas consumption can be achieved by the optimised operation. This result reiterates the potential role of operational optimisation in a closer to real-time operation of the system, as highlighted earlier in this chapter and in Chapter 4.

Table 5.5: Results of the optimised model, heuristic model and measurement.

	Optimised model	Heuristic model	Measurement (Leidos Canada, 2014)
Solar energy collected (GJ)	5630.4	5630.4	4328.3
Solar energy to STS (GJ)	3676.7	3700.8	4590.3*
LTS charge (GJ)	2089.4	2360.8	2566.2
LTS discharge (GJ)	908.9	1132.4	1306.8
Solar energy to district (GJ)	2473.4	2442.2	2434*
Gas consumption (GJ)	15.5	47.0	42.4
Electricity (GJ)	9	13.7	-
Objective value ($)	264.8	475	-

*Measurements error due to sensors imperfect calibration (Leidos Canada, 2014).

5.4.5 Multi-year optimisation

All optimisation runs in the previous sections were performed on a one-year time horizon, with the assumed cyclic storage constraint. In order to evaluate the benefits of the multiple time grids approach in optimisation with longer time horizon, a multi-year optimisation run of the DLSC was performed. The resulting LTS operational profile of the multi-year SU optimisation is illustrated in Fig. 5.14. Similar to the annual optimisation result, the LTS is charging over the summer and discharging until depletion in the winter, with a rest period afterwards before it starts charging again. It is also interesting to note that the LTS state-of-charge never goes beyond 50% during the whole time horizon. This can be attributed to the overestimation of the LTS maximum capacity due to the implementation of the capacity model.

Table 5.6 compares the performance of SU and MU in the multi-year optimisation run. The MU was run with $\delta^{LTS} = 6$h, which corresponds to the lowest computational time for the case study (see Fig. 5.10a). It has significantly lower computational time than the reference case (-94%) while maintaining a good agreement in objective value (+0.9%). The multi-year optimisation run exemplifies the main benefit of using the multiple time grids method in the operational optimisation.

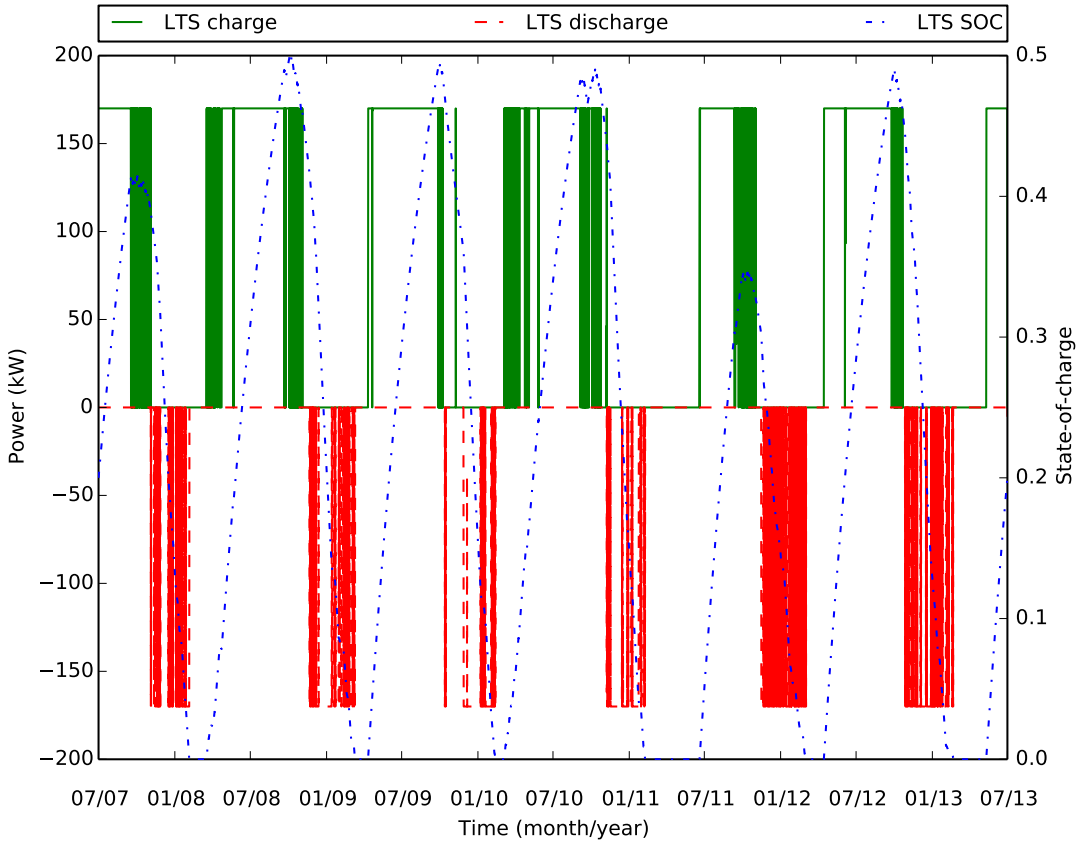

Figure 5.14: LTS operational profiles for multiple years optimisation (2007-2013).

Table 5.6: Details of single uniform and multiple uniform optimisation for the multiple years' case.

	SU	MU
Binary variable	105218	17538
Total variable	578700	359500
Computational time (s)	1985	121 (-94%)
MIP gap	5%	5%
Objective value ($)	4493	4534 (+0.9%)

5.5 Conclusions

This chapter evaluates the benefits and trade-offs of using the multiple time grids method in the optimisation of an energy system which has thermal energy storage equipment with different temporal characteristics. It has been shown through a case study that the multiple time grids method can reduce the computational cost of energy system optimisation without significantly decreasing the results accuracy.

The case study was modelled as a mixed-integer linear programming problem and im-

plemented with different time grids, i.e. single-uniform, multiple-uniform, and multiple-non-uniform. Although based on a specific case study, the presented key points are quite general in order to be considered when using multiple time grids in energy systems optimisation.

In the single-uniform case, the error in optimisation results grows as the time step increases. This will influence not only the operational optimisation but also the design optimisation where equipment sizing is performed. Therefore, despite the significant reduction in computational time, increasing the step size in the single-uniform case is not recommended.

In the multiple-uniform case, the computational time reduces significantly as the LTS time step size is increased from 1-h to 4-6 h, depending on the optimality gap. However, beyond this step size, the computational time has an increasing trend. Thus, increasing the time grid size of LTS does not guarantee an improvement in computational time. Unlike in the single-uniform case, the objective value does not suffer significantly when a larger LTS time step size is used. For the evaluated case study, the most significant computational time improvement occur in increasing the LTS time grid size from 1 to 2-h, with further improvement for larger grid size up to 6-h for the case with 5% MIP gap.

The LTS characteristics have significant influence over the benefits of using a larger time step size. For the case study, the advantage of using time step sizes greater than 4-h diminishes as the LTS thermal power increases. This should be taken into account if the multiple time grids method is to be used in design optimisation as different LTS characteristics may be considered in the optimisation. Moreover, it has been shown that the benefits of using multiple time grids become more apparent as longer time horizon is considered. In the case study, a 94% reduction in computational time relative to a single uniform hourly time grid has been achieved, with only 0.9% difference in the objective value.

In addition to the advantages of using the multiple time grids method, a careful selection of the time grids is necessary in order to avoid the unwanted computational time increase from using this method. On this aspect, one possible future research work is developing a systematic algorithm to generate the time grids which considers characteristics of different equipment (generation and storage) and demands (electricity, gas and heat).

It is also foreseen that the positive impacts of the multiple time grids method will be more significant on the design and synthesis-level of energy system optimisation. Further research work is needed to quantify the magnitude of these impacts. Moreover, the accuracy limit of the proposed method could be identified, for example, by comparing the objective function value with the results of a dynamic simulation, similar to the

comparison performed in Chapter 4 for the case of a residential heating system.

The results of an operational optimisation of an energy system can also be viewed as the upper limit of the real operation. Although direct application of the resulting operational profile may lead to less realistic simulation profile, as shown in Chapter 4, useful insights can still be derived from the optimisation results. These include the trend of optimal operational control and the performance of a control assumption relative to the optimal one. Further analysis can then be performed by using a dynamic simulation approach.

In Chapter 6, a study of DLSC with a simulation approach is reported. Specifically, a techno-economic analysis of DLSC is conducted to evaluate its applicability in the UK locations. The analysis is supported by a validated TRNSYS simulation model.

Chapter 6

Simulation for techno-economic analysis of solar district heating in the UK

6.1 Introduction

District heating has been acknowledged as one of the technological solutions towards decarbonising thermal energy provision in the UK, in addition to repurposing gas grids with hydrogen, electrification with heat pumps, and the implementation of other renewable-based heating technologies, such as biomass boilers and solar thermal (Chaudry *et al.*, 2015; MacLean *et al.*, 2016). Traditionally, the foundation of district heating was to use local fuel or heat sources that otherwise would be wasted, such as combined heat and power (CHP) plants, Waste-to-Energy plants, and industrial processes. Recent and future developments of district heating expand this idea by introducing renewable energy sources like solar thermal, biomass, and geothermal energy. This trend has amplified the benefits of district heating beyond financial value to include the environmental, and societal aspect of energy supply (Werner, 2017).

A report by the UK Department of Energy and Climate Change in 2013 identified 1765 district heating networks in the UK (Department of Energy and Climate Change, 2013). Most installations are small networks, i.e. an average of 35 residential dwellings and only 75 are classified as large ($>$ 500 homes or 10 non-domestic buildings). Furthermore, the majority of district heating systems are powered by natural gas boilers, with a smaller share of natural gas CHP systems.

In Scotland, district heating implementation is a part of the Heat Policy Statement published by The Scottish Government (The Scottish Government, 2015). The statement also highlights key policies in supporting the increase of renewable and other forms of low carbon heat. The currently installed district heating systems in Scotland are illustrated in Fig. 6.1. Similar to the condition in the UK, most of the supply technology used are based on gas boilers and CHP.

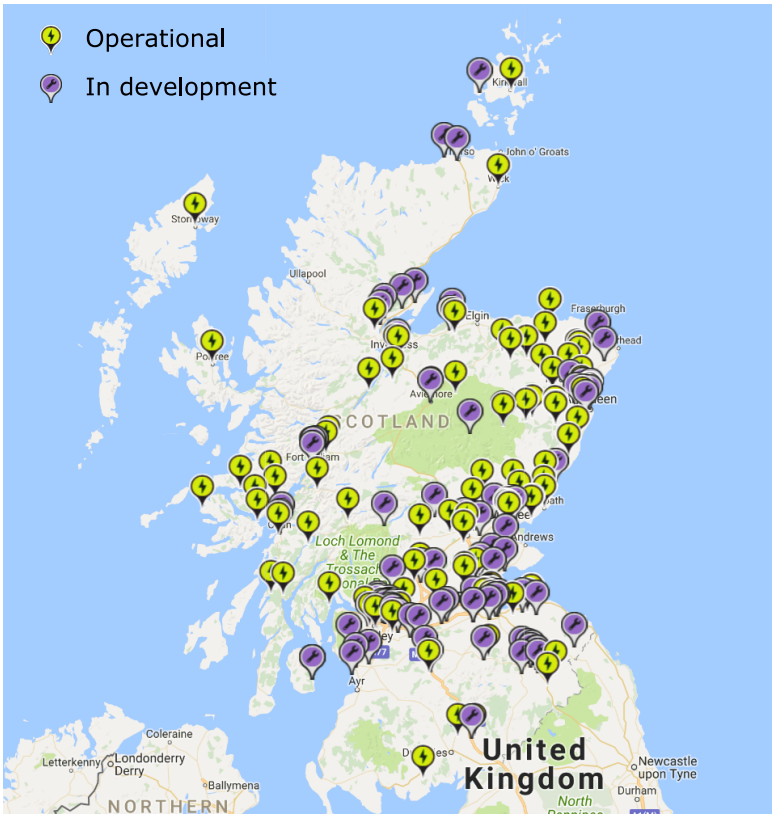

Figure 6.1: District heating installations in Scotland, both operational and in development (Heat Network Partnership, 2017).

Long-term thermal energy storage technology has been mostly installed in district heating applications, particularly solar district heating (Ochs *et al.*, 2009; Novo *et al.*, 2010; Xu *et al.*, 2014; Hesaraki *et al.*, 2015; Rad and Fung, 2016; Perez-Mora *et al.*, 2017). An example of these systems is the Drake Landing Solar Community in Canada, which is used as the case study in Chapter 5. Worldwide, Denmark has the highest number of solar district heating installations, followed by other European countries, as illustrated in Fig. 6.2. Solar district heating combines renewable heat sources with efficient delivery through a heat network. Therefore, it can be considered as a potential technology to contribute to the decarbonisation of heat in the UK. However, currently, there is no solar district heating or long-term thermal storage installation in the UK.

Most solar thermal installations in the UK are domestic applications with a hot water tank as the storage technology. Although there is no long-term thermal storage installation in the UK, its potential has been mentioned in recent reports on current situations and future development of energy storage technology in the UK (Taylor *et al.*, 2012; Institution of Mechanical Engineers, 2014; Eames *et al.*, 2014; Radcliffe and Li, 2015). Nevertheless, the discussions in the literature have been mainly qualitative in nature, while quantitative studies are required in order to determine the feasibility of

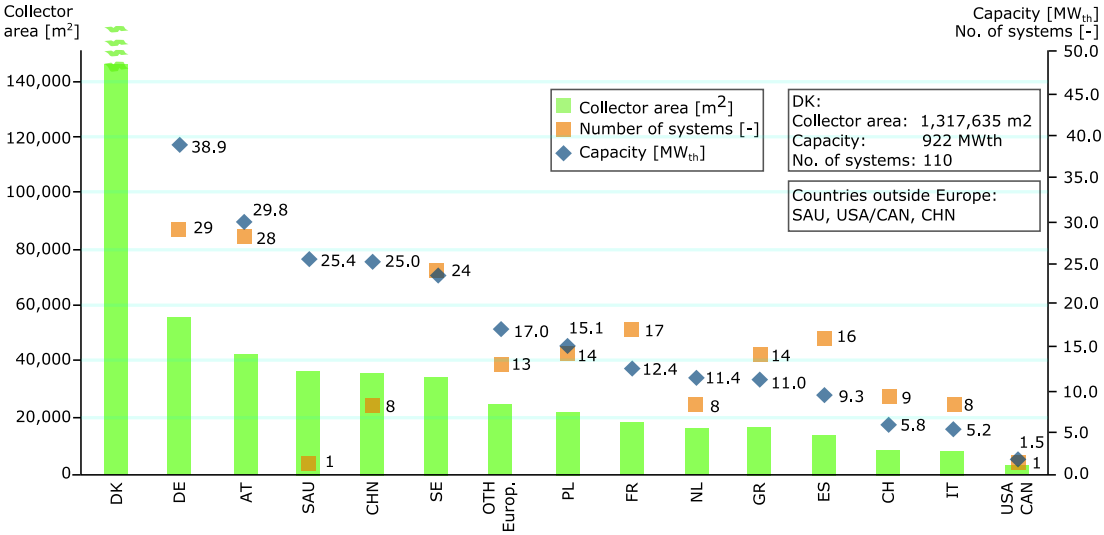

Figure 6.2: Solar district and cooling - worldwide capacities, collector area installed and number of systems in 2016 (Adapted from (Weiss *et al.*, 2017)).

a technology.

In order to address this lack of quantitative studies, a techno-economic study of a solar district heating system installed in UK locations is described in this chapter. The Drake Landing Solar Community is used once more as a case study. The influence of locations on DLSC has been reported in the literature (Flynn and Sirén, 2015). However, UK locations and financial aspects were not considered in the study. Furthermore, in addition to the techno-economic performance, the present study also investigates the potential of a policy-based subsidy to support the implementation of solar district heating in the UK.

6.2 Methodology

The techno-economic analysis performed in this chapter is illustrated in Fig. 6.3. It is an extension of the overall framework explained in Chapter 3. It starts with the development of a TRNSYS model of DLSC, which then is validated against monitoring results available in the literature. Once the model is validated, location-related input data are modified to represent the selected UK locations. These include weather data, soil properties, and synthetic heat demand input. The simulation results are then used to calculate the techno-economic performance metrics. Performance metrics of the system are then compared further with benchmark values available in the literature.

A parametric study is conducted to investigate the influence of different design parameters on the techno-economic performance of the system. In addition to technical

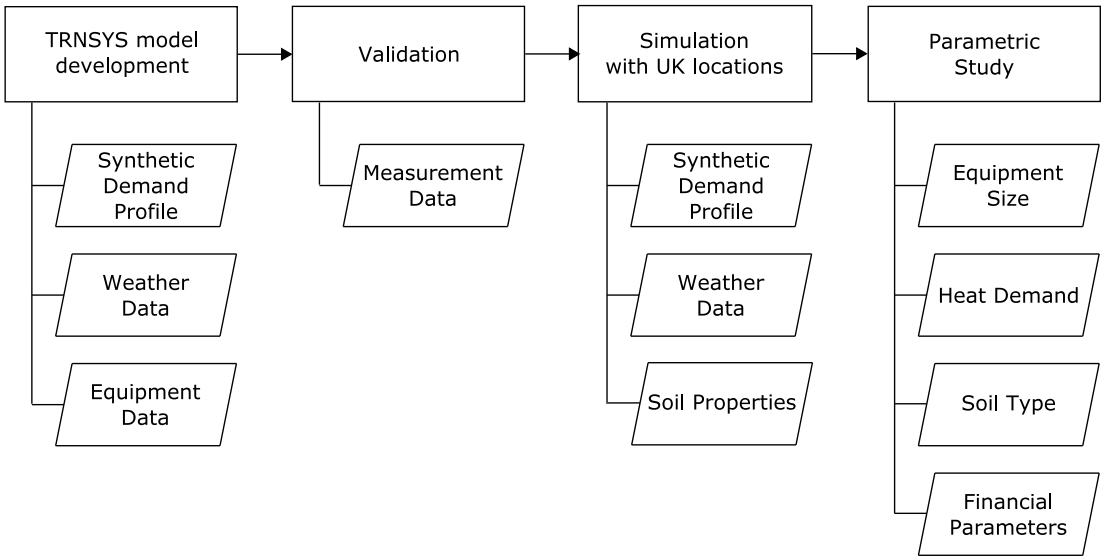

Figure 6.3: Techno-economic framework.

parameters, the influence of financial parameters, such as discount rate and subsidies, are also analysed. Currently available policy-based subsidies for renewable heat in the UK are considered, as well as the required tariff to improve the financial competitiveness of the system.

6.2.1 Case study: Drake Landing Solar Community

Since an overview of DLSC has been given in Chapter 5, only the metrics relevant to the techno-economic analysis are shown in Fig. 6.4. Furthermore, a more detailed description of DLSC can be found in Appendix C.

In Fig. 6.4, the variable $\dot{Q}_t^{SCO}$ represents the rate of solar energy collected by the collector, while $\dot{Q}_{ch,t}^{LTS}$ and $\dot{Q}_{dch,t}^{LTS}$ correspond to the charge and discharge rate of the long-term storage, respectively. The solar energy transferred to the district comes from the buffered energy in the short-term storage. This buffered energy is a combination of direct solar energy from the collector and the stored solar energy from the long-term storage. The rate of solar energy that goes to the district is represented by $\dot{Q}_t^{STS-HX2}$. Finally, the rate of energy to satisfy the heat demand is a combination of solar and boiler power, $\dot{Q}_t^{STS-HX2} + \dot{Q}_t^{BOI}$. In this chapter, the total energy flows are integrated over a yearly period.

6.2.2 Performance indicators

Thermodynamic performance

In the analysis, the thermodynamic performance of the solar district heating is described by its solar fraction, system efficiency and long-term storage efficiency. Solar fraction (SF) indicates the proportion of total energy supply that comes from solar thermal energy (Eq. 6.1). The system efficiency (η_{sys}) illustrates the performance of the system on utilising the collected solar energy (Eq. 6.2). It also represents the effectiveness of the solar energy collection and storage control in the system. The efficiency of long-term storage (η_{LTS}, Eq. 6.3) is included in the analysis because the component represents a significant investment cost; thus, its operational performance needs to be monitored and, if required, improved accordingly.

$$SF = \frac{Solar\ Energy\ to\ District}{Total\ Energy\ to\ District} = \frac{\sum_{t=0}^{8759} \dot{Q}_t^{STS-HX2}}{\sum_{t=0}^{8759} \left(\dot{Q}_t^{STS-HX2} + \dot{Q}_t^{BOI} \right)} \tag{6.1}$$

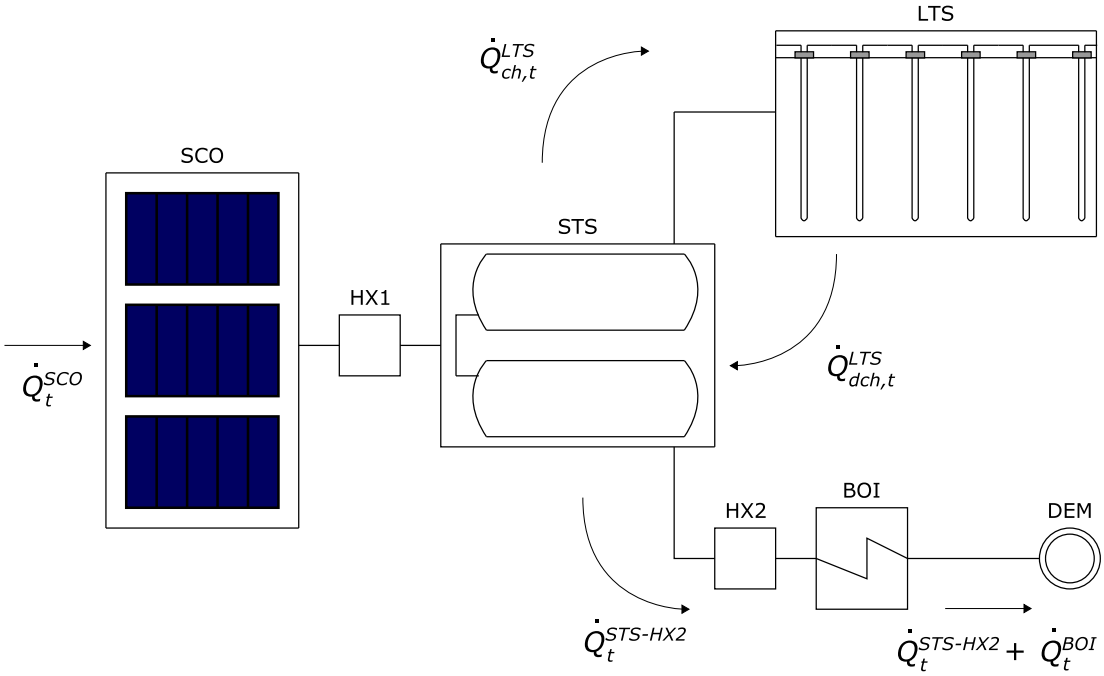

Figure 6.4: Schematic of Drake Landing Solar Community with the relevant metrics for the techno-economic analysis. Main equipment is solar collectors (SCO), short-term thermal energy storage (STS), long-term thermal energy storage (LTS), and back-up gas boilers (BOI). They are operating to supply the heat demand (DEM) of the connected houses.

$$\eta_{sys} = \frac{Solar\ Energy\ to\ District}{Solar\ Energy\ Collected} = \frac{\sum_{t=0}^{8759} \dot{Q}_t^{STS-HX2}}{\sum_{t=0}^{8759} \dot{Q}_t^{SCO}} \tag{6.2}$$

$$\eta_{LTS} = \frac{LTS\ total\ energy\ discharged}{LTS\ total\ energy\ charged} = \frac{\sum_{t=0}^{8759} \dot{Q}_{dch,t}^{LTS}}{\sum_{t=0}^{8759} \dot{Q}_{ch,t}^{LTS}} \tag{6.3}$$

Economic performance

In order to evaluate the economic performance of the systems, the following metrics are used in the analysis: Levelised Cost of Energy (LCOE), and Levelised Cost of Solar Thermal Energy ($LCOE_{ST}$). LCOE and $LCOE_{ST}$ are calculated according to Eq. 6.4 and 6.5, respectively. Both metrics use the total cost metric, as introduced in Chapter 3, as their numerator, while the denominator is the "present value" of total energy for LCOE, and total solar energy for $LCOE_{ST}$. For all economic metrics calculation, unless stated otherwise, the lifetime of the system is 25 years, while the discount rate is 3%. These values, along with the definition of $LCOE_{ST}$, were based on the report of Task 52 Solar Heat and Energy Economics in Urban Environments, IEA SHC Programme (Mauthner and Herkel, 2016).

$$LCOE = \frac{C_{inv} + \sum_{t=1}^{N} \frac{C_{opr,t} - R}{(1+r)^t}}{\sum_{t=1}^{N} \frac{Q^{STS-HX2} + Q^{BOI}}{(1+r)^t}} \tag{6.4}$$

$$LCOE_{ST} = \frac{C_{inv} + \sum_{t=1}^{N} \frac{C_{opr,t} - R}{(1+r)^t}}{\sum_{t=1}^{N} \frac{Q^{STS-HX2}}{(1+r)^t}} \tag{6.5}$$

The investment cost functions of the main equipment in the considered solar district heating are shown in Table 6.1. The operational cost consists of a fixed and variable operation and maintenance (O&M) cost. The fixed O&M cost is assumed to be 0.75% of the total investment cost per year (Mauthner and Herkel, 2016), while the variable cost is the total electricity and natural gas cost over the year. The pumps are responsible

Table 6.1: Investment costs for the solar district heating main equipment. €1 = £0.91.

Type	Costs function	Unit	Reference
Solar collectors	$200 \cdot A_{SCO} + (100 \cdot A_{SCO} - 666.7) + 2 \cdot (40 \cdot A_{SCO} - 10000)$	€	(Lizana *et al.*, 2017)
STS	$403.5 \cdot V_{STS}^{-0.4676} + 250$	€/m^3	(Mauthner and Herkel, 2016)
LTS	$20.57 \cdot V_{LTS} - 201841$	€/m^3	(Lizana *et al.*, 2017)
District piping	$L_{pipe} \cdot 345$	€	(Hsieh *et al.*, 2017)
Boiler	$24.83 \cdot \dot{Q}_{max} + 31859$	€	(Voll, 2013)

Table 6.2: Energy input and maintenance cost of the solar district heating.

Type	Costs	Unit	Reference
Natural gas	0.0379	£/kWh	(British Gas, 2017)
Electricity	0.1454	£/kwH	(British Gas, 2017)
Maintenance	0.75% $\cdot C^{inv}$	£/year	(Mauthner and Herkel, 2016)

for the electricity consumption, while the back-up boilers utilise the natural gas. The costs of energy inputs to the solar district heating system are given in Table 6.2.

6.3 TRNSYS model of Drake Landing Solar Community

The developed TRNSYS model of DLSC is depicted in Fig. 6.5. It consists of four main loops: solar, STS, LTS, and district loop. The solar loop circulates the collectors' working fluid which transfers the collected solar energy to the STS through a heat exchanger (HX1). The STS acts as a hub of the entire system by connecting the solar, LTS, and district loop. The LTS loop consists of the required equipment to model the charge/discharge of the long-term storage, namely the borehole storage itself, underground distribution pipe, a pump, a mixing valve and a diverter. Solar energy from the solar and LTS loop is then transferred to the district loop through another heat exchanger (HX2). When the solar energy is not sufficient to raise the flow temperature to the set-point temperature, the back-up boiler is switched on to cover the remaining energy.

An overview of equipment modelling, control, and input data are given in the following paragraphs, while more detailed descriptions can be found in Appendix D.

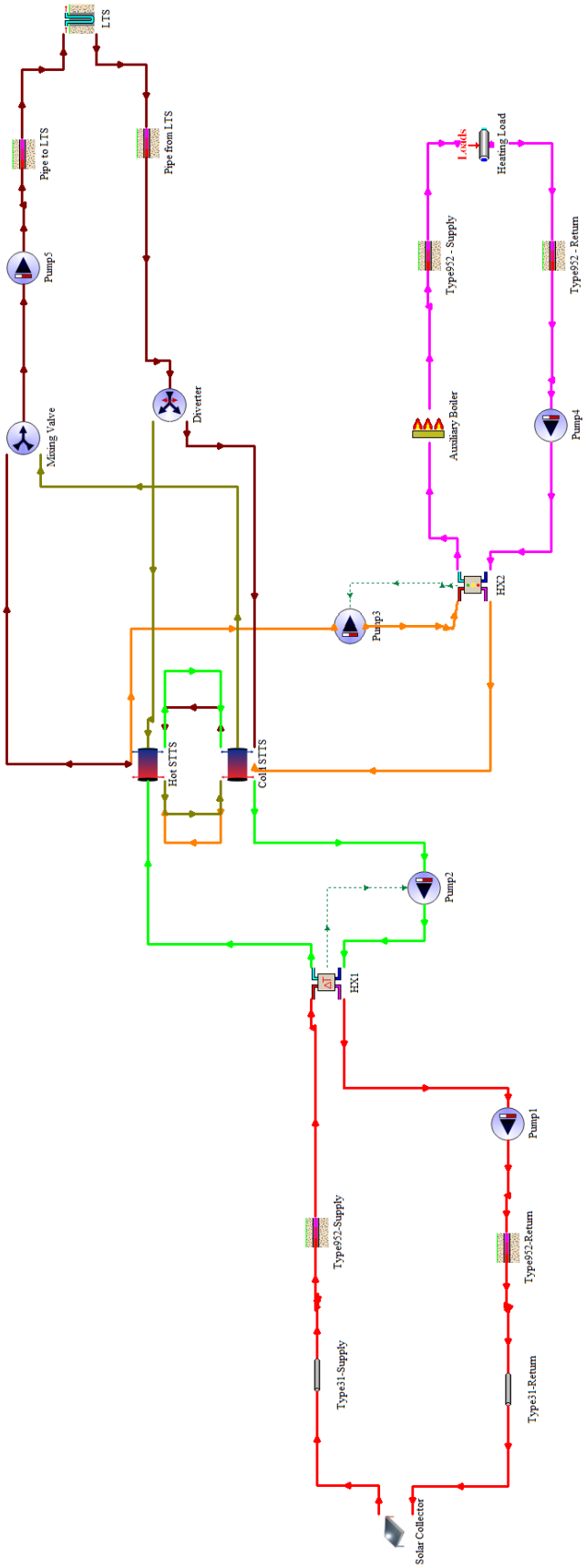

Figure 6.5: Overview of the developed TRNSYS model of DLSC. The four main loops are shown: solar loop (red), STS loop (light green & orange), LTS loop (brown & olive green), and district loop (magenta).

6.3.1 Equipment modelling

The solar collector array is modelled by Type 1a, a flat-plate solar collector model with quadratic efficiency curve and no Incidence Angle Modification. Its efficiency curve is defined by the performance characteristic equation as shown in Eq. 6.6 (Sibbitt *et al.*, 2012).

$$\eta_{sco} = 0.693 - 3.835\frac{(T_{in} - T_{ext})}{G} \tag{6.6}$$

η_{sco} is the collector efficiency, T_{in} [°C] is the collector inlet temperature, T_{ext} [°C] is the external air temperature, and G [W/m^2] is the total incident solar irradiation.

The short-term storage is modelled with two Type 534 cylindrical storage tanks, along with the connections to other loops. The horizontal storage tanks are modelled with three stratification nodes per tank. The hot STS tank is discharged to charge the LTS and satisfy the heat demand from the district loop; while it is charged by the solar collector loop and LTS discharge.

The long-term storage is modelled by a Type 557, Vertical U-Tube Ground Heat Exchanger, which was developed based on the duct storage model (DST) (Hellström, 1991). It allows the combined series-parallel configuration of the boreholes, as it is the case in DLSC storage with 24 parallel headers and six boreholes per header. The LTS can only be charged or discharged at any given time. This behaviour is modelled by using a mixer, diverter, and a controller.

In the district loop, heat demand is represented by a load flow type, Type 682, which imposes a specified load on a flow stream and calculates the outlet fluid temperature. The specified load is a synthetic heat demand calculated based on the methodology described in Chapter 3.

In addition to the main equipment, two heat exchangers and five pumps are also included in the model. The first heat exchanger (HX1) connects the solar loop with the STS and is modelled with Type 761, Heat Exchanger with Cold-Side Modulation to Maintain Temperature Difference. The second heat exchanger (HX2) connects the STS with the district loop and is modelled with Type 512, Heat Exchanger with Hot-Side Modulation to Keep Cold-Side Outlet Above its Setpoint. All the pumps in the model are modelled with Type 110, Variable Speed Pump. The heat exchangers and pumps are controlled according to control rules described in the next paragraphs.

6.3.2 Control assumptions

The key control assumption in DLSC is in the charging/discharging of LTS. As explained in Chapter 5, the LTS has lower charge/discharge rate relative to the STS. Thus its operation needs to be planned well in advance to ensure sufficient energy is available in the STS, minimising the need to operate the back-up boilers. In the original control, it was based on the prescribed value of the required state-of-charge for STS which depends on the time of day and supply set-point temperature, as explained in Appendix C. In the field, the control mechanisms have been modified along the operation of DLSC. Along with the non-public nature of the original control assumptions, these make control implementation in the TRNSYS model less straightforward than, for example, sizing the equipment.

In this thesis, the control mechanisms described by Yang et al. were implemented in the developed TRNSYS model (Yang *et al.*, 2017). Although it was not explicitly mentioned in the publication, the control rules were assumed to be the latest implementation in DLSC, taking into account that the authors were affiliated with the project leader in the design and monitoring of DLSC (CanmetENERGY-National Resource of Canada). The control rules are given in Table C.2 of Appendix C.

6.3.3 Weather data and heat demand

The weather data from Calgary Airport weather station were used in developing the validated model (Government of Canada, 2016), while the solar irradiation data at the DLSC location are gathered from satellite-based measurement (National Resources Canada, 2015). In both cases, the data from July 2007 up to June 2013 were considered as one of the inputs to the simulation and the heat demand model.

The heat demand profile was derived using the method described in Chapter 3. The annual demand values were calculated by subtracting the district loop loss from the total energy delivered to the loop (Sibbitt *et al.*, 2012).

6.4 Model validation

Representative energy flows and the solar fraction from the developed TRNSYS model are compared with the original simulation results and the measurement data, as illustrated in Fig. 6.6. The values of annual measurement data from 2007 to 2013 are given in Appendix C. It should be noted that the original simulation model was performed with January-December annual time horizon, while the measurement and the developed TRNSYS model in this thesis were performed with July-June horizon. This is because the DLSC system began operation in late June 2007 and its performance has been

monitored since then (Sibbitt *et al.*, 2012). Furthermore, the original simulation was developed to illustrate the performance of the system in the first five years; thus the missing values in the sixth year. In the following paragraphs, the term "TRNSYS model" corresponds to the TRNSYS model of DLSC developed in this thesis.

In general, the TRNSYS model is capable of reproducing the trend and magnitude of the measured energy flows. Prominent discrepancies in several points can be explained by examining the inputs used in developing the TRNSYS model and the operational improvements made in the field.

The differences between the measurement and TRNSYS model in annual solar energy collected range between 1% - 10%. This can be attributed to the solar irradiation data used in the simulation. The data were satellite-based data instead of ground-measured solar irradiation. Moreover, the surface tilt reported in the data was based on the latitude (50°). In reality, the solar collectors are installed at an inclination angle of 45°. Satellite-based data were used in the simulation because of the unavailability of ground measured solar irradiance data for the location and years of interest in the public domain. The ground solar data collection from the closest weather station was stopped in 2005 (Flynn and Sirén, 2015), while the satellite-based data are available from Ref. (National Resources Canada, 2015). Furthermore, it has been reported that the variability between ground- and satellite-based data is noticeably lower for the case of the Global Tilted Irradiance (GTI), which is the one used in this chapter, in comparison with the Direct Normal Irradiance (DNI) (Gueymard and Wilcox, 2011). Despite these constraints, the predicted solar energy collected from the developed TRNSYS model is closer to the measured values in comparison with the original DLSC simulation.

For the LTS performance, the TRNSYS model has lower annual charged energy and higher/equal discharged energy than the measurement. Thus, the LTS has higher efficiency in the TRNSYS model than in reality. These discrepancies can be explained by considering that the charge/discharge control of the LTS has been modified during the first five years of operation (Sibbitt *et al.*, 2012). The control algorithm implemented in the TRNSYS model is taken from the latest publication from NRCAN CanmetEnergy (Yang *et al.*, 2017); thus, it can be assumed to be the latest charge/discharge control of the LTS.

Similarly, the changes in operational control can contribute to the differing values of Solar Fraction. In the early years, the TRNSYS model has significantly higher solar fraction than measurement, while this trend diminishes from Year 4 onwards. In addition to LTS operational control, adjustments were also made on the set-point temperature in the district loop. These can also contribute to the deviation from the measurement data since higher set-point in the early years means that the boilers are operating more frequently, lowering the solar fraction. Overall, the predicted performance metrics by

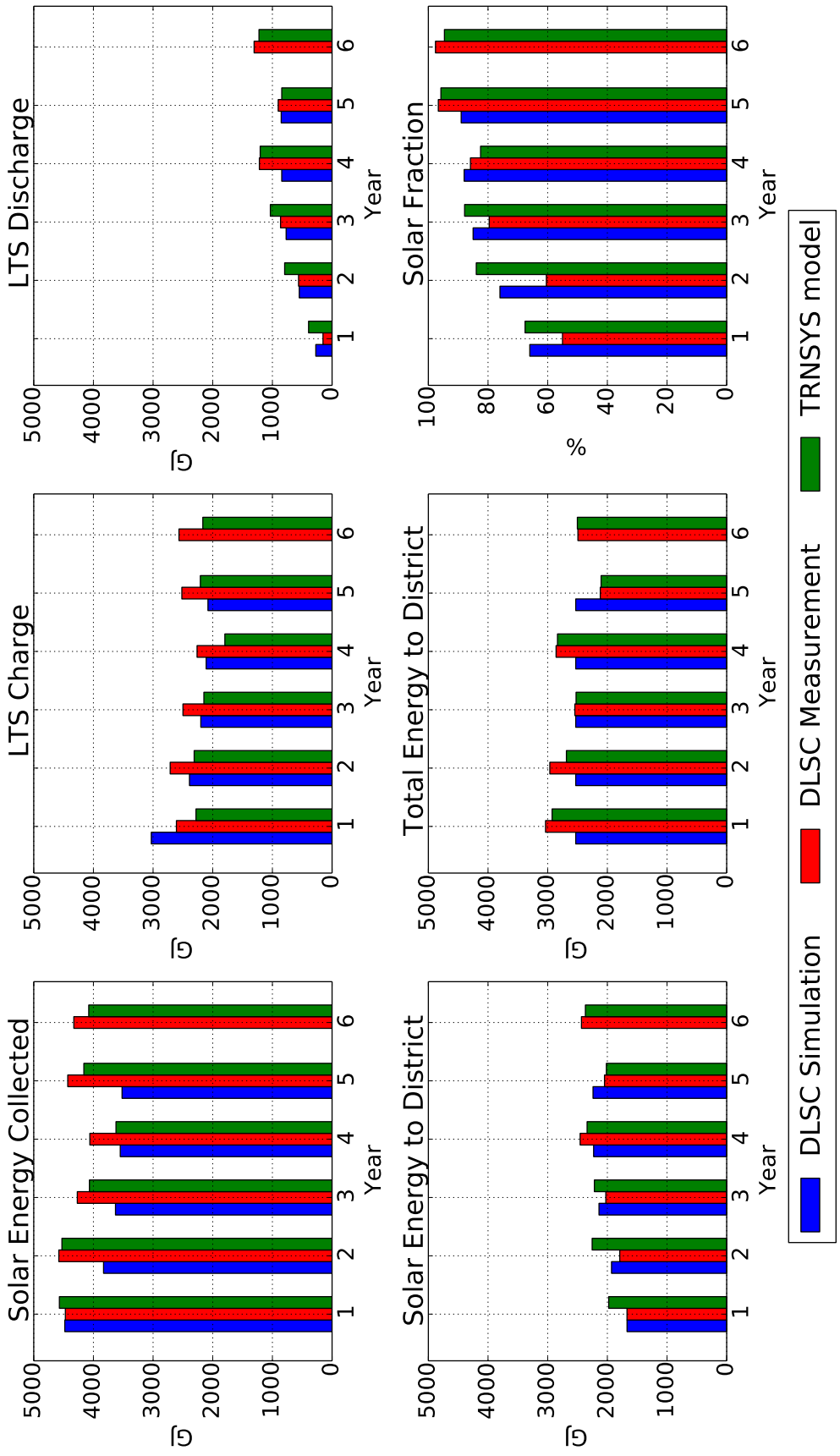

Figure 6.6: Representative DLSC energy flows and solar fraction in the first six years from the original simulation, measurement, and the developed TRNSYS model.

Figure 6.7: Selected UK locations for simulation of the DLSC.

the TRNSYS model are closer to the measured values in later years due to the control adjustments in the field.

With these factors considered, it is argued that the developed TRNSYS model is sufficiently accurate to investigate the techno-economic performance of a similar system if it is installed in the UK.

6.5 Simulation of the DLSC in UK locations

The two UK locations selected for the study are Aberdeen, Scotland, and Camborne, England (Fig. 6.7). They represent two regions with different supply-demand characteristics: lower solar resource and higher heat demand in Scotland, and higher solar resource and lower heat demand in the South of England.

6.5.1 Location specific inputs

Weather data for these locations were taken from Meteonorm data which are available in TRNSYS. They are typical meteorological year data which were generated using Meteonorm software (Meteotest, 2017). Therefore, the yearly data were repeated during the multi-year simulations.

The synthetic heat demand profiles were derived by using the methodology described in Chapter 3. In generating the synthetic heat demand profiles, the number of houses was increased to 52 from a single dwelling modelled in Chapter 4. This is the same number of houses as in the original DLSC system. For the Aberdeen case, the annual space heating demand of the house in Chapter 4, i.e. approximately 12000 kWh/y, was used in generating the heat demand profile. For the Camborne case, an annual space heating demand value of 8200 kWh/y was considered for a single house. The value was based on an approximation of a typical UK dwelling located in Plymouth, which has similar heating degree days as Camborne (The Green Age, 2015).

Although only one occupancy profile is considered in this thesis, the overall simulation results are not significantly affected by this assumption, as shown in the previous validation step. Furthermore, since the profiles were based on annual weather data, their implementation in TRNSYS simulations was also repeated accordingly.

In the district heating system, soil thermal properties are relevant not only for calculating losses in underground pipes but also in modelling the borehole thermal energy storage. The soil properties of the two locations are taken from Ref. (Busby, 2015, 2016) and shown in Table 6.3.

Table 6.3: Summary of the considered parameters of the two UK locations.

Properties	Unit	Aberdeen	Camborne
Global Horizontal Irradiation (Annual average)	kWh/m^2	900	1100
Heating Degree Days	degree-day	2417	1552
Annual space heating demand	kWh/year	12000	8200
Number of houses	-	52	52
Soil properties			
Thermal conductivity	W/mK	1.07	3.76
Specific heat capacity	J/kgK	1014	1169
Density	kg/m^3	1520	1380
Ground temperature	°C	9.3	12.1
Thermal diffusivity	x10^{-}6 m^2/s	0.6938	2.3343

6.5.2 Technical performance

The summary of simulation results of the DLSC system in UK locations is shown in Fig. 6.8 and 6.9. Overall, the energy flows for UK locations are lower than the original DLSC system. This is due to the lower solar irradiance and lower heat demand in the UK locations. The annual average Global Horizontal Irradiation values are approximately 900, 1100, and 1400 kWh/m^2 for Aberdeen, Camborne, and Okotoks, respectively (Solargis, 2017). The annual district heating demand values are approximately 2200, 1500, and 2500 GJ/y for Aberdeen, Camborne, and Okotoks, respectively.

In the Solar Energy Collected graph in Fig. 6.8, there is a downward trend in the collected solar energy in the first three years for both locations, despite the same solar irradiation data for every year. This is because the simulations started with empty storage, both STS and LTS. Therefore, more solar energy was collected in the first years to heat up the storage, particularly the LTS which has a large capacity and low charge rate. The collected solar energy started to stabilise beyond the third year as the system approaches steady state.

It can also be observed in Fig. 6.8 that due to its lower latitude, the system in Camborne has more incident solar irradiance, and solar energy collected than Aberdeen. This is also reflected in the amount of energy charged into the LTS. The overall lower trend of Total Energy to District in Camborne is because of its lower heat demand relative to the colder Aberdeen. Due to its higher solar irradiance and lower heat demand, the solar fraction (SF) in Camborne is always higher than Aberdeen (Fig. 6.9). In both cases, the SF curve has a sharp increase in the early years, and it starts to level off after approximately five years due to the borehole storage reaching its operational temperature. The SF curve of the original DLSC is less smooth than the SF curve of Aberdeen and Camborne case. The curves of the original DLSC shown in Fig. 6.9 are based on the measurement data. Thus, the weather profile and heat demand are not the same for every year. Furthermore, various improvements have been made during the operation of DLSC. These factors contribute to the resulting metrics profiles over the year.

It should be noted that the LTS was at the original ground temperature at the beginning of simulations, i.e. no pre-heating was prescribed. This is different than in historical operation of DLSC where the LTS was pre-heated up to 25 °C. The effect of pre-heating can be seen in the LTS efficiency curve in Fig. 6.9, where the original DLSC has a higher efficiency in the first year relative to the other two cases.

It is interesting to note that although the LTS in Camborne is charged more than Aberdeen, it is always discharged less (Fig. 6.8). This leads to lower LTS efficiency (η_{LTS}) for Camborne (Fig. 6.9). The lower efficiency can be attributed to the higher

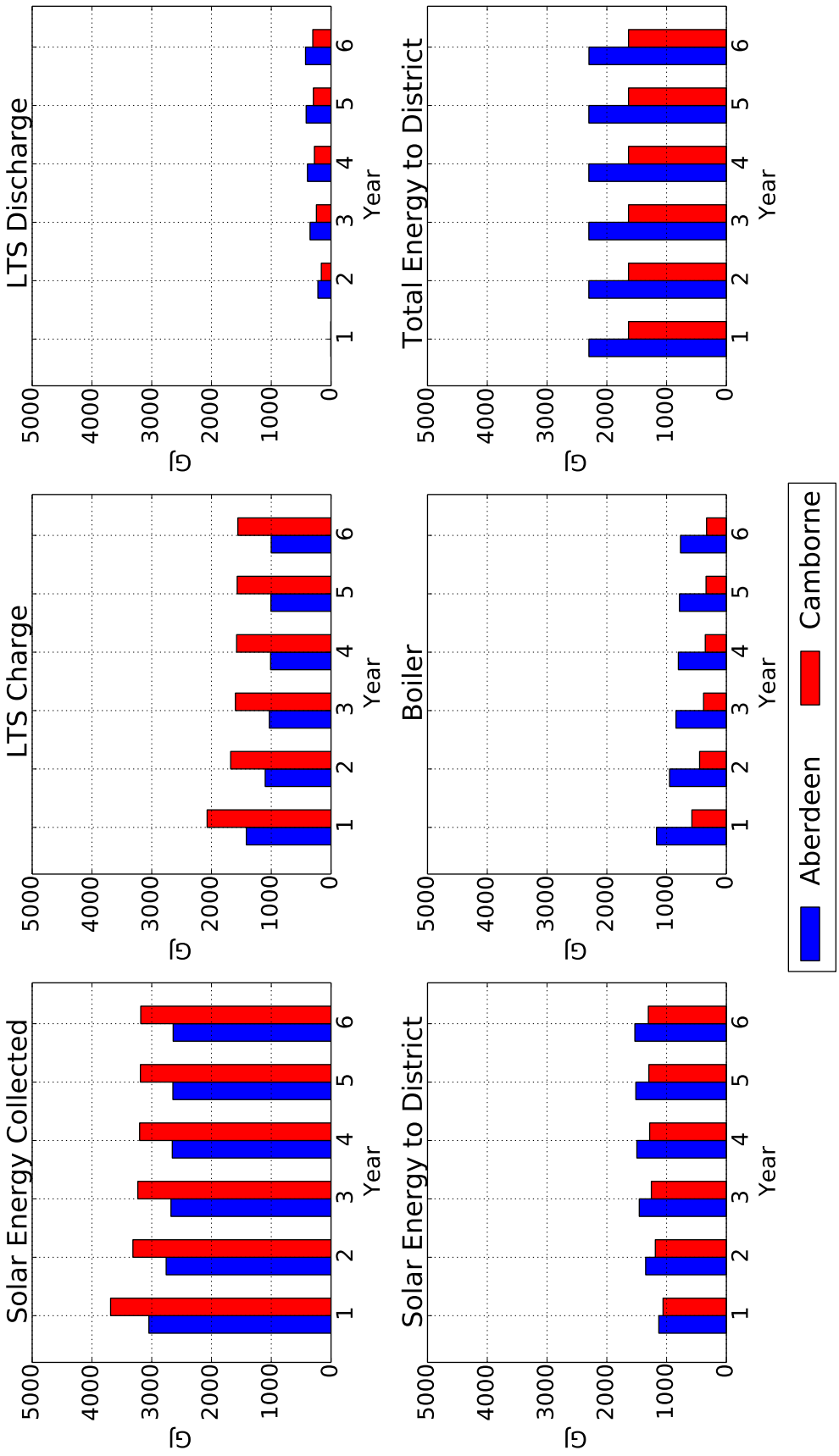

Figure 6.8: Energy flows of DLSC system in Aberdeen and Camborne, UK.

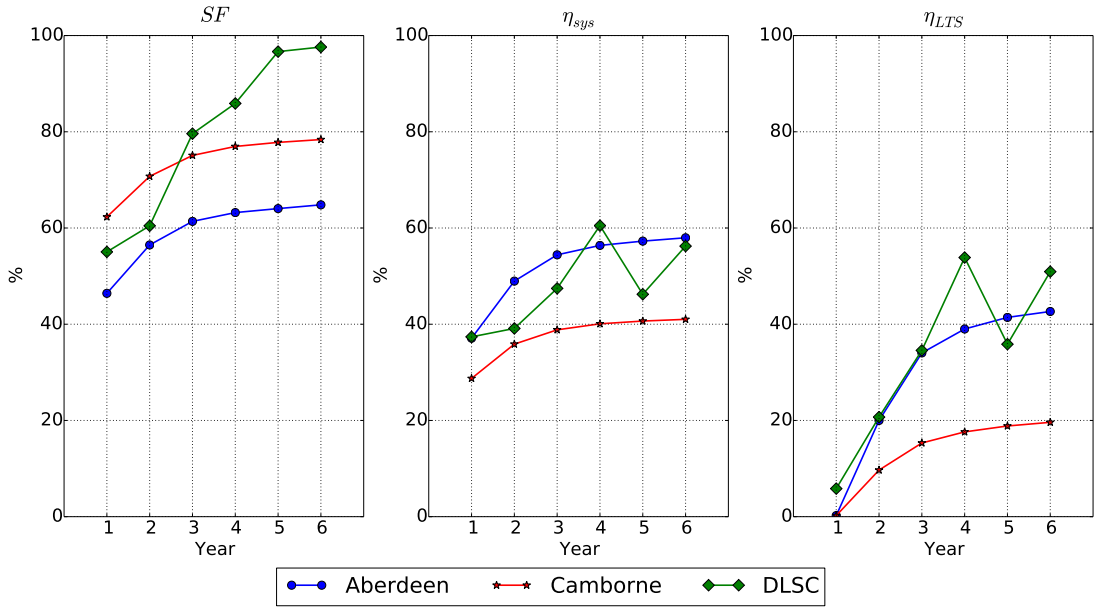

Figure 6.9: Technical performance metrics for the two UK locations and the original DLSC: Solar Fraction (SF), System Efficiency (η_{sys}), and Long Term Storage Efficiency (η_{LTS}).

thermal diffusivity of the ground in Camborne (see Table 6.3) which means higher LTS losses to the surrounding ground. Because of this, the system in Camborne has lower efficiency (η_{sys}) than Aberdeen, despite its higher solar fraction.

The system efficiency (η_{sys}) of the Aberdeen case is higher than the original DLSC for most of the time in the first six years of operation. This illustrates that with the latest control rules, a DLSC-like system installed in Aberdeen can have favourable performance in managing the collected solar energy, despite its lower solar fraction.

6.5.3 Economic analysis

Table 6.4 summarises the relevant costs and LCOE of the system at the two UK locations. The investment costs for both of them are the same, while the variable operational costs depend on the TRNSYS simulation results.

The slightly higher electricity cost in Camborne can be attributed to the higher availability of solar irradiation and more active charging and discharging operation of the LTS. These lead to higher electricity demand from the pumps. Furthermore, the significantly higher gas cost in Aberdeen is due to the lower solar fraction in this case.

Aberdeen has lower LCOE and LCOE_{ST} than Camborne, despite the latter having better solar resource. This can be related to two aspects: lower heat demand and higher LTS loss in Camborne. The lower heat demand means that the system is highly likely

Table 6.4: LCOE calculations for UK locations. €1 = £0.91

	Unit	Aberdeen	Camborne
Investment cost			
Solar collector	€	860933	
STS	€	70323	
LTS	€	491267	
Boiler	€	44274	
Distribution	€	690000	
Operational cost			
Maintenance (Fixed)	€/year	20039	
Electricity	£/year	5444	5639
Gas	£/year	8980 - 13676	3875 - 6754
Financial parameters			
Discount rate	%	3	
Technical lifetime	year	25	
Economic metrics			
LCOE	£/kWh	0.22	0.30
$LCOE_{ST}$	£/kWh_{solar}	0.34	0.39

to be oversized, which leads to higher investment cost than necessary. The higher loss means that there are wasteful operational costs in storing the solar energy to the LTS.

6.5.4 Comparison with similar systems

In order to evaluate the relative techno-economic performance of the system, a comparison with benchmark values has been made and summarised in Table 6.5. The benchmark values are based on roof-mounted solar thermal systems connected to block heating grids in Central European climate (Mauthner and Herkel, 2016).

It is clear that the installation of a DLSC-like system in Aberdeen will result in a more expensive system, albeit with a better solar fraction, compared to typical systems in continental Europe. This can be attributed to several reasons. For example, Aberdeen has lower solar resource than locations in Central Europe, as can be seen from the solar irradiation map shown in Fig. 6.10. This significantly influences the solar energy yield and therefore, the $LCOE_{ST}$. Another reason is related to the design of the system. The original DLSC was designed with technical performance in mind, i.e. achieving solar fraction beyond 95%. Thus, the equipment tends to be oversized in order to achieve the target solar fraction, which leads to a more expensive system. Finally, from heat demand viewpoint, it should be noted that the DLSC and the reported solar block heating systems in Ref. (Mauthner and Herkel, 2016) are designed to supply new and renovated low-energy neighbourhoods. On the other hand, the heat demand for the

Table 6.5: Comparison of techno-economic metrics between the benchmark case and DLSC-Aberdeen. The benchmark case values are taken from Ref. (Mauthner and Herkel, 2016), with an assumed currency exchange value of €1 = £0.91.

	Solar block heating	DLSC-Aberdeen
Technical metrics		
Typical size per unit (m^2-gross)	5000	2320
- range	(1000 - 10000)	
Typical storage volume per unit (m^3 water-equivalent)	12000	15800
Typical annual production per unit (MWh/a)	1500	638
Typical solar energy yield (kWh/m^2/a)	300	183
- range	(260 - 340)	
Typical solar fraction	50%	46-65 %
- range	(40-75%)	
Technical life time (years)	25	25
Economic metrics		
Specific investment cost, material only (£/m^2)	490	845
- range	(365-610)	
Fixed O&M per unit (£/m^2/a)	3.6	6.6
Variable O&M per unit (£/m^2/a)	1	6.5-8.5
$LCOE_{ST}$(£/kWh_{solar})	0.12	0.34
- range	(0.09 - 0.15)	

DLSC-Aberdeen is derived from the typical heat demand of a semi-detached dwelling in Scotland, which is mostly part of older, less energy-efficient building stock.

From the analysis in this section, it is apparent that several key design parameters could have a significant influence on the techno-economic performance of the system. For instance, the size of relatively expensive equipment (i.e. solar collectors and LTS) and the soil type may have a larger influence on the LCOE values than other parameters. As stated earlier, the heat demand may play a role in determining the feasibility of a solar district heating system. In the following paragraphs, this hypothesis is explored further by performing a parametric study using the validated TRNSYS model.

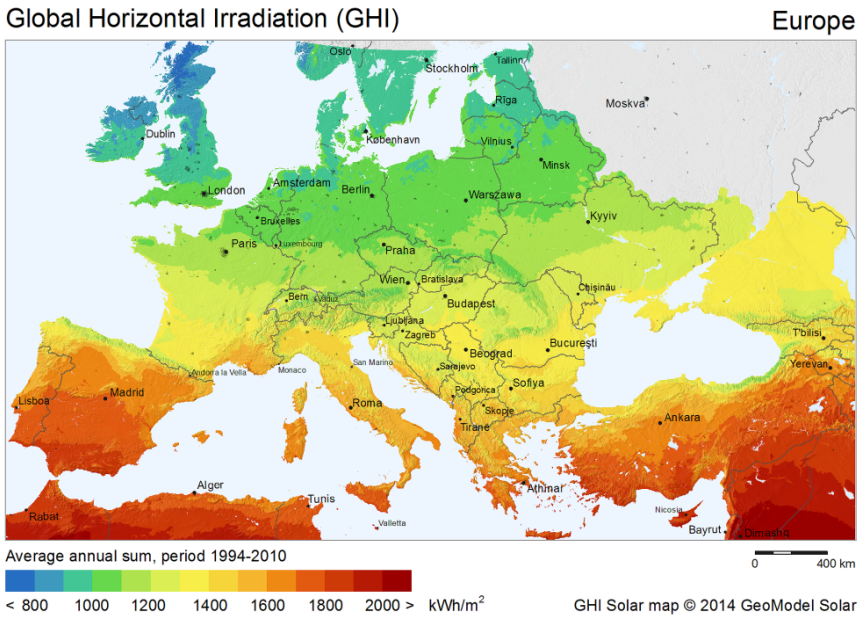

Figure 6.10: Global Horizontal Irradiation Solar map for Europe (Solargis, 2017).

6.6 Parametric study

The Aberdeen case is investigated further by examining the influence of different parameters on the techno-economic performance. Four parameter categories are considered in the study, namely equipment size, heat demand, soil properties, and financial parameters.

6.6.1 Equipment sizing

The three main equipment types included in the parametric study are the solar collector, short-term storage, and long-term storage. The original DLSC equipment sizes can be found in Table 5.2, Appendix C, and Appendix D.

Solar collector

The influence of collector area on the techno-economic metrics is illustrated in Fig. 6.11 and 6.12, for the efficiencies and LCOEs, respectively. The value of collector area was varied from 1000 to 3000 m^2, with the original value included in both figures.

In all cases, the trend in the technical performance metrics is similar to the original: a rapid increase in the first three years before starting to taper off. A slight exception can be observed in the case of 1000 m^2 collector area. Among the tested collector areas, the 1000 m^2 case has the worst performance in all metrics. This can be seen as a case of under-sizing of the solar collector, which results in lower solar fraction and efficiencies, as well as higher $LCOE_{ST}$.

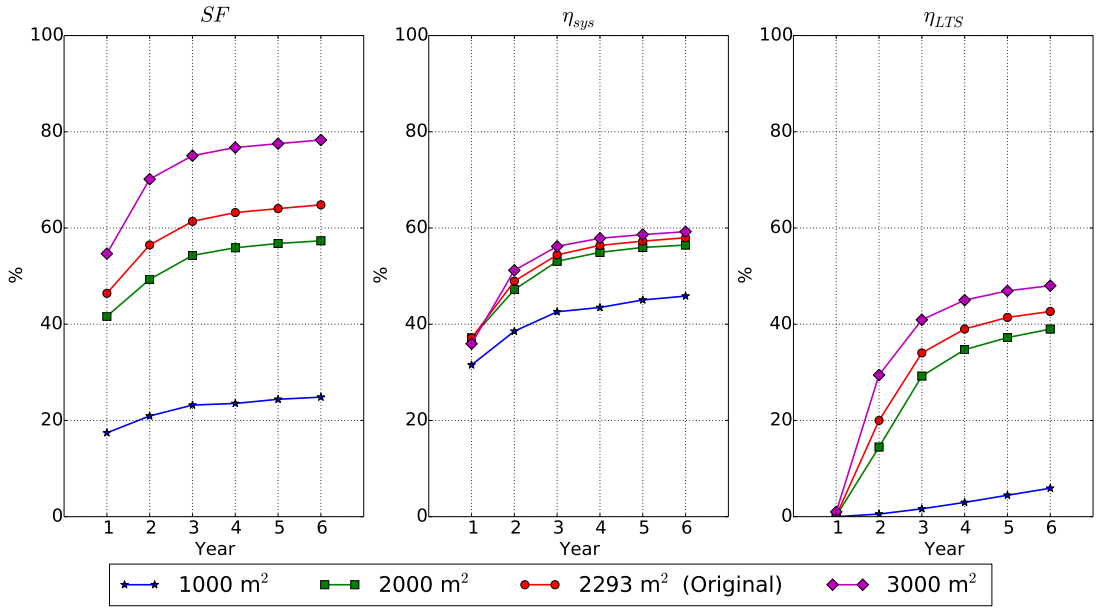

Figure 6.11: Technical performance metrics for system with various collector sizes: Solar Fraction (SF), System Efficiency (η_{sys}), and Long Term Storage Efficiency (η_{LTS}).

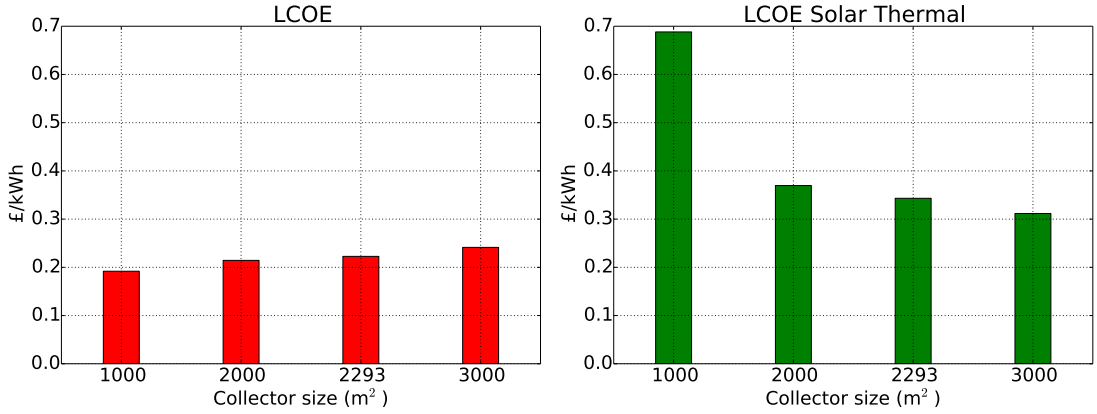

Figure 6.12: LCOE values for system with various collector sizes.

As for the other cases, systems with a larger collector area have a higher solar fraction, with SF close to 80% for the system with 3000 m^2 collector area. Nevertheless, the influence of collector size on system and LTS efficiency appears to be minimal. The system efficiency is relatively constant as the collector size increases, while although there is an increase in LTS efficiency, it is not as large as in the solar fraction.

From a financial perspective, an increase in collector area is followed by the LCOE value, while the LCOE$_{ST}$ has the opposite trend. This can be explained by the fast growth in solar energy to the district as the collector size increases. In the case of 1000 m^2, the solar energy to the district is too low, and the LCOE$_{ST}$ becomes relatively high. Furthermore, the investment cost also grew with the collector size, as illustrated

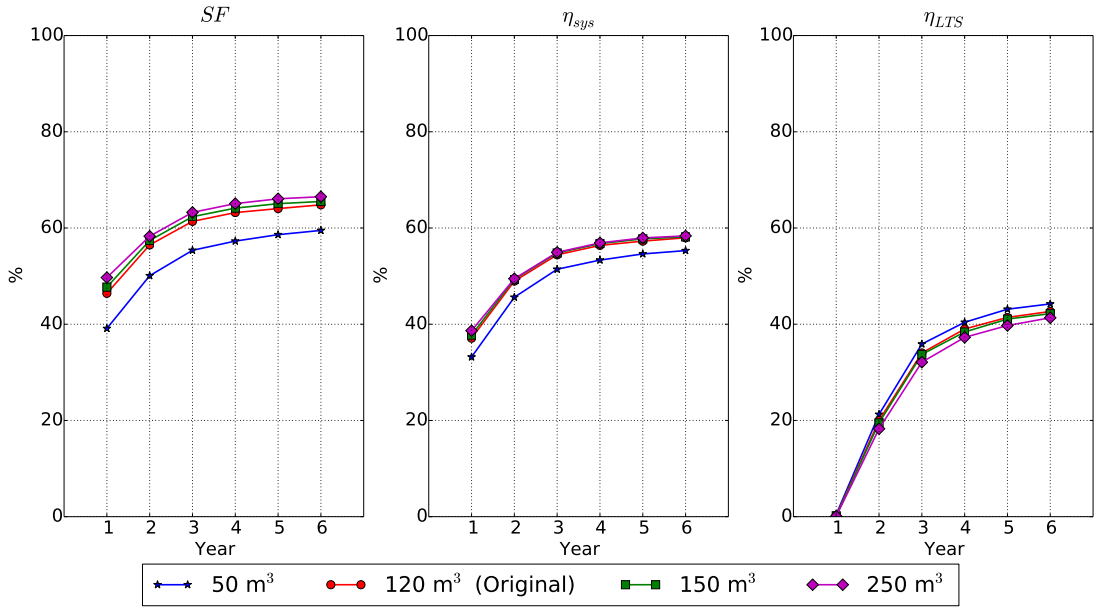

Figure 6.13: Technical performance metrics for system with various STS sizes: Solar Fraction (SF), System Efficiency (η_{sys}), and Long Term Storage Efficiency (η_{LTS}).

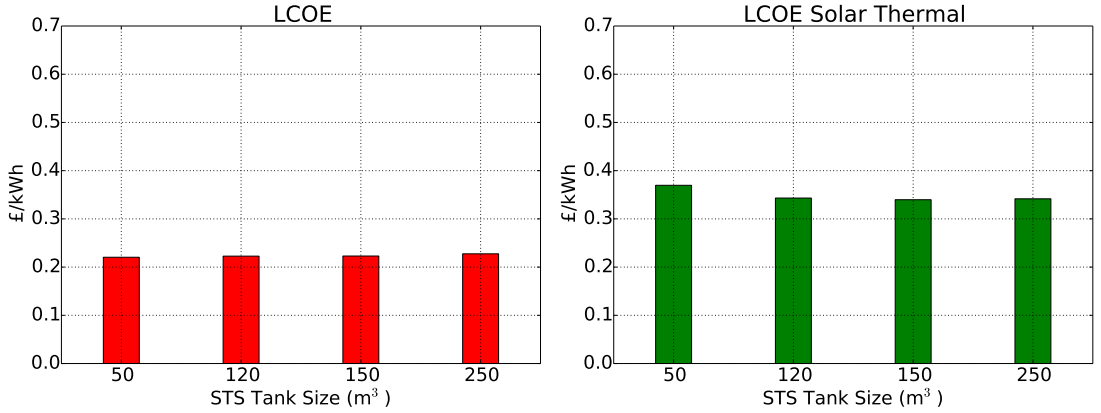

Figure 6.14: LCOE values for system with various STS sizes.

by the trend in LCOE. However, it is clear that the produced solar energy increases at a higher rate than the investment cost.

Short-term storage

Three storage sizes were tested in the parametric study: 50, 150, and 250 m^3. These are the sizes of one tank, so the total STS volume is double these values. The technical and financial performance metrics are shown in Fig. 6.13 and 6.14, respectively.

Apart from the 50 m^3 case, the increase in STS size has little influence on the solar fraction and system efficiency. It also does not have a large effect on the LTS efficiency. The slight decrease in LTS efficiency as the STS size increases is due to larger volume needs

to be heated/cooled in the STS to reach the temperature required to charge/discharge the LTS, as can be seen in the control assumptions (Table C.2).

The STS size is less influential towards the performance and financial metrics because it acts as a short-term buffer in the system and its investment cost is relatively low compared to other equipment. Thus, the size range in which the STS can fulfil its role without significantly affecting the performance is relatively wide.

Despite its low influence on the metrics, the STS size might affect the optimal system control strategy. This can be asserted from the central role of STS in the current and past control rules implemented in DLSC, which have been discussed in Chapter 5 and Appendix C. For instance, a larger STS size could reduce the system inertia, making it more responsive to changing heat demand.

Long-term storage

The modification of the LTS volume in the TRNSYS simulation is performed by changing the borehole number or the borehole depth. The borehole number considered was 90, 180, and 300, while its depth was changed to 15, 70, and 100 m. Both the energy storage capacity and power are directly affected by the change in LTS volume.

The influence of borehole number on the techno-economic metrics is shown in Fig. 6.15 and 6.16. It is clear that the increase in borehole number has a positive correlation with all metrics, both technical and financial. The increase in solar fraction and efficiency metrics can be explained by considering that a larger borehole storage with more boreholes in the central area will have improved performance due to reduced losses and better thermal stratification.

In the case of increasing borehole depth, it appears that the overall trend is not as obvious as in the borehole number, as can be seen in Fig. 6.17 and 6.18. The system with the shallowest borehole, i.e. 15 m, suffers from insufficient storage capacity and larger losses to the surrounding due to an unfavourable shape factor. These contribute to the relatively low values of solar fraction and efficiencies, as well as a slightly higher LCOE solar thermal from the original. Furthermore, as the depth increases beyond 35 m, the technical performance and LCOE solar thermal are also growing. It is interesting to note that the solar fraction and system efficiency are relatively constant in the case of 70 and 100 m depth, while the LCOE values are increasing. Thus, it can be concluded that there is an optimal value of borehole depth beyond which the performance does not improve further, or even possibly deteriorate due to larger surface to volume ratio.

From the comparison between the results of increasing borehole number and depth, it can be concluded that the best way to improve the techno-economic performance

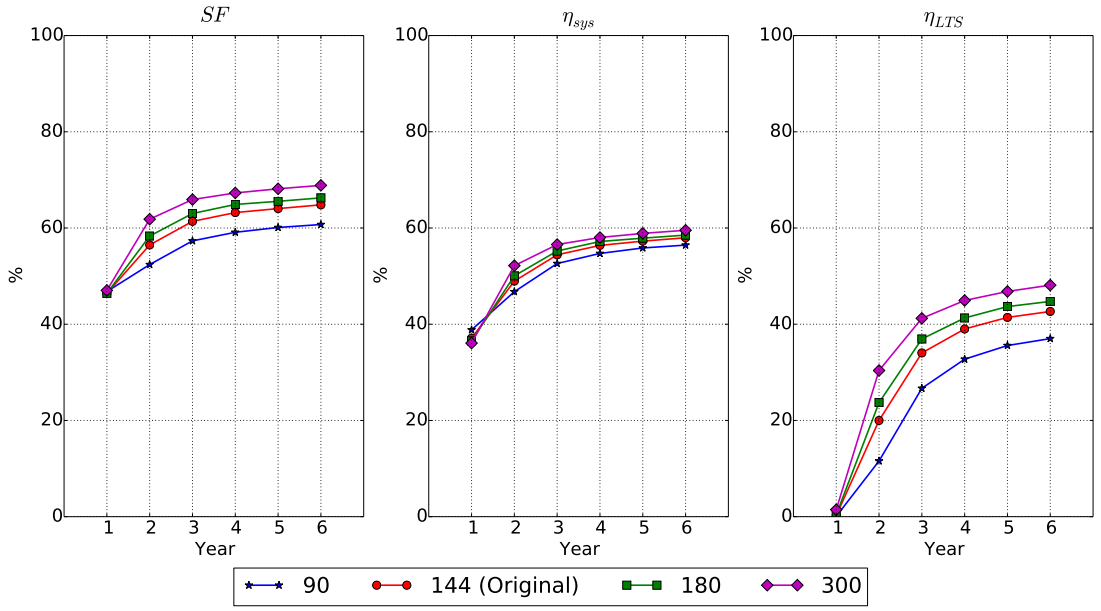

Figure 6.15: Technical performance metrics for system with various LTS number of boreholes: Solar Fraction (SF), System Efficiency (η_{sys}), and Long Term Storage Efficiency (η_{LTS}).

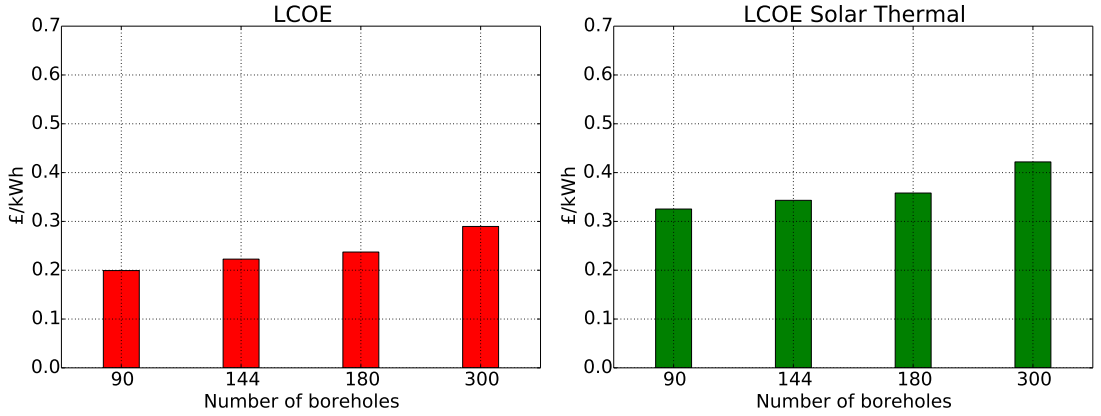

Figure 6.16: LCOE values for system with various number of boreholes.

through LTS modification is by increasing the borehole number rather than its depth. Indeed, this is also the most practical way to expand a borehole storage installation.

Another option in LTS modification is to remove it altogether from the simulation, thus modelling a system which only has a short-term storage. This was performed by excluding the borehole storage and its corresponding connections in the TRNSYS model. The resulting technical performance metrics are given in Fig. 6.19, while the LCOE calculations produced the value of £0.179/kWh and £0.342/kWh for LCOE and LCOE_{ST}, respectively. These values are similar to the original system (Fig. 6.20); thus, LTS can increase the solar fraction of the system without significantly degrading the

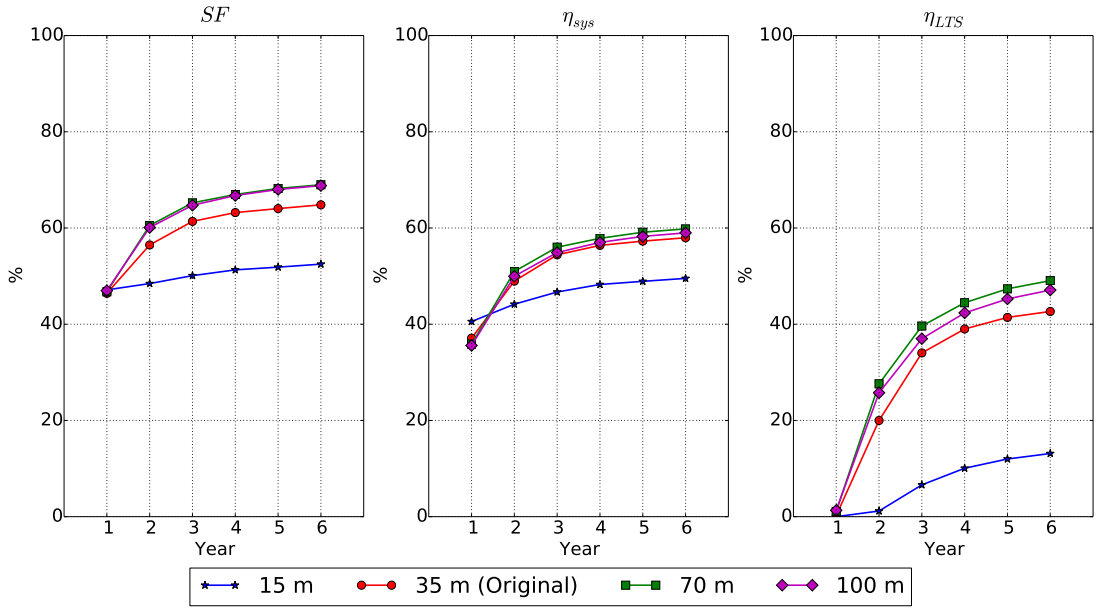

Figure 6.17: Technical performance metrics for system with various LTS depth of boreholes: Solar Fraction (SF), System Efficiency (η_{sys}), and Long Term Storage Efficiency (η_{LTS}).

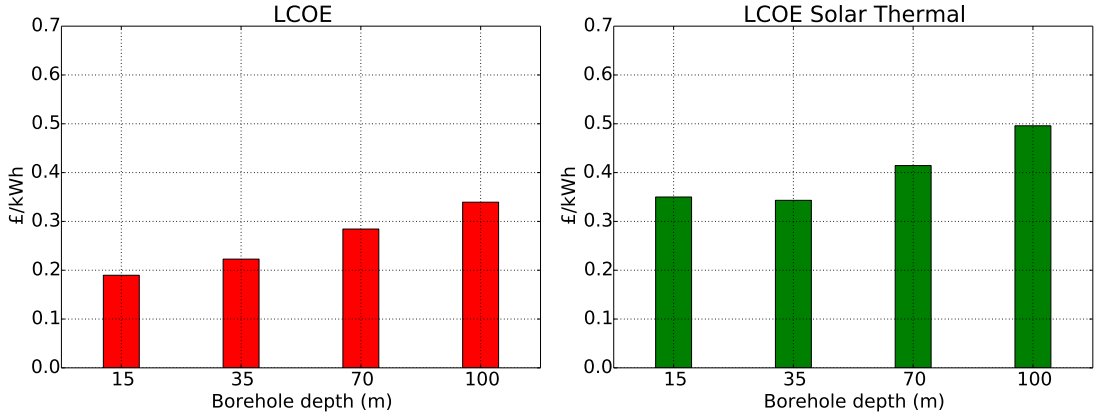

Figure 6.18: LCOE values for system with various depth of boreholes.

economic metrics.

6.6.2 Heat demand

The original DLSC system in Canada supplies space heating demand to 52 houses with Natural Resources Canada's R-2000 Standard energy efficiency certification. The average annual space heating energy consumption per house is approximately 115 kWh/m^2/year. This was calculated with the average total energy delivered to district loop of 3000 GJ/year, and floor area of 140 m^2.

In the case of UK locations, assuming a floor area of 96 m^2, the space heating con-

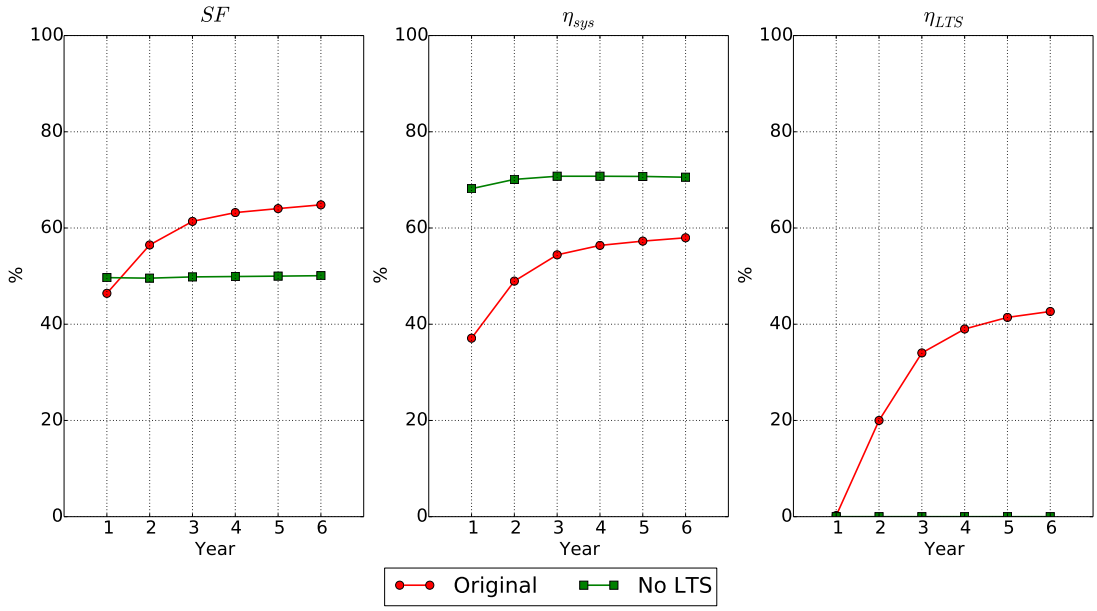

Figure 6.19: Technical performance metrics for system with and without LTS: Solar Fraction (SF), System Efficiency (η_{sys}), and Long Term Storage Efficiency (η_{LTS}).

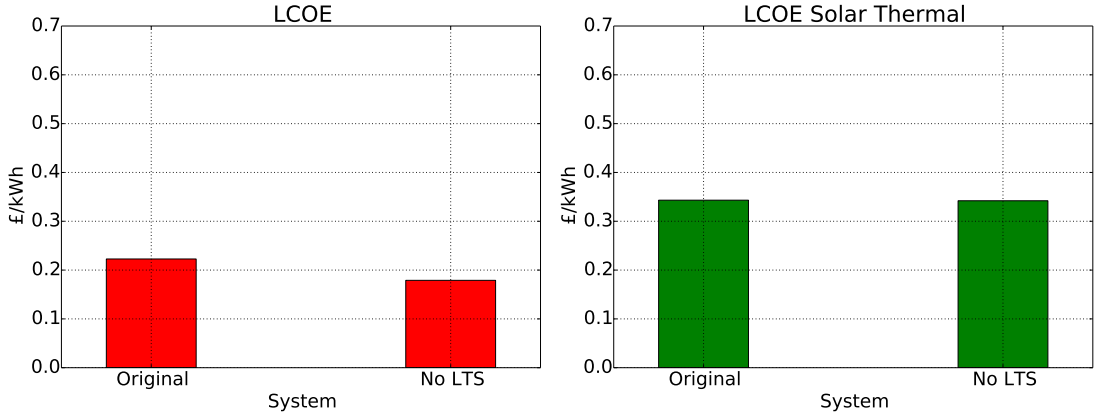

Figure 6.20: LCOE values for system with and without LTS.

sumption is approximately 120 and 85 kWh/m^2/year for Aberdeen and Camborne, respectively. These values correspond to the available building stock, which is mostly older buildings with relatively poor energy performance. For instance, a design calculation for a new built which complies with 2010 Scottish Building Standard (SBS) produces the value of 33.7 kWh/m^2/year for the annual space heating (Bros-Williamson *et al.*, 2016).

The influence of heat demand on the techno-economic performance of the system is investigated by modifying the heat demand input. Two annual space heating demand values are considered: 33.7 and 16 kWh/m^2/year, which corresponds to the SBS 2010 and Passive House specification, respectively. These were taken from the study of Bros-

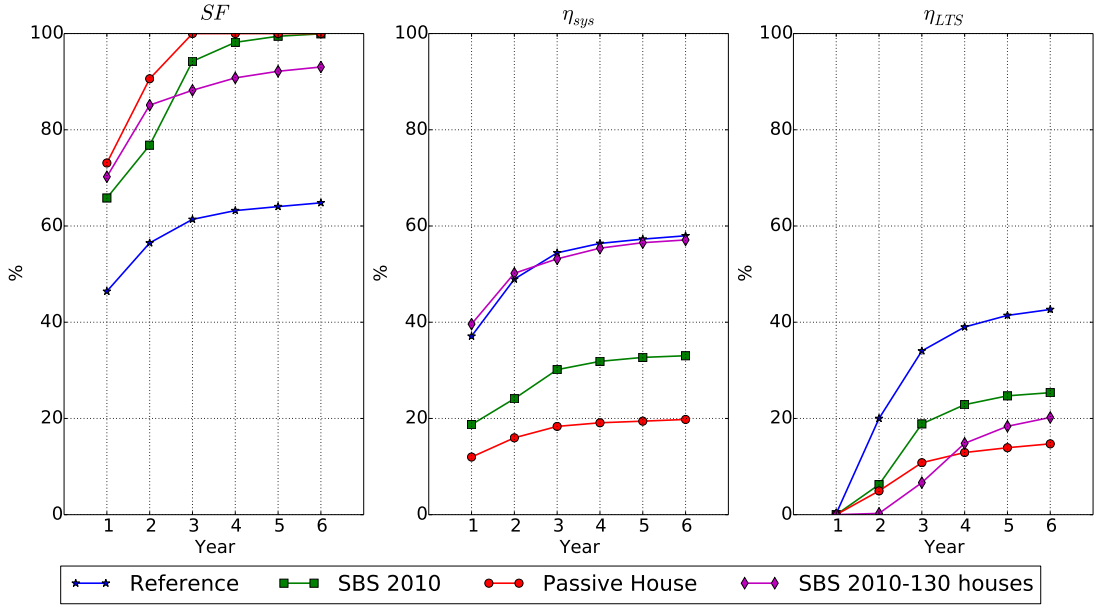

Figure 6.21: Technical performance metrics for system with different heat demand: Solar Fraction (SF), System Efficiency (η_{sys}), and Long Term Storage Efficiency (η_{LTS}).

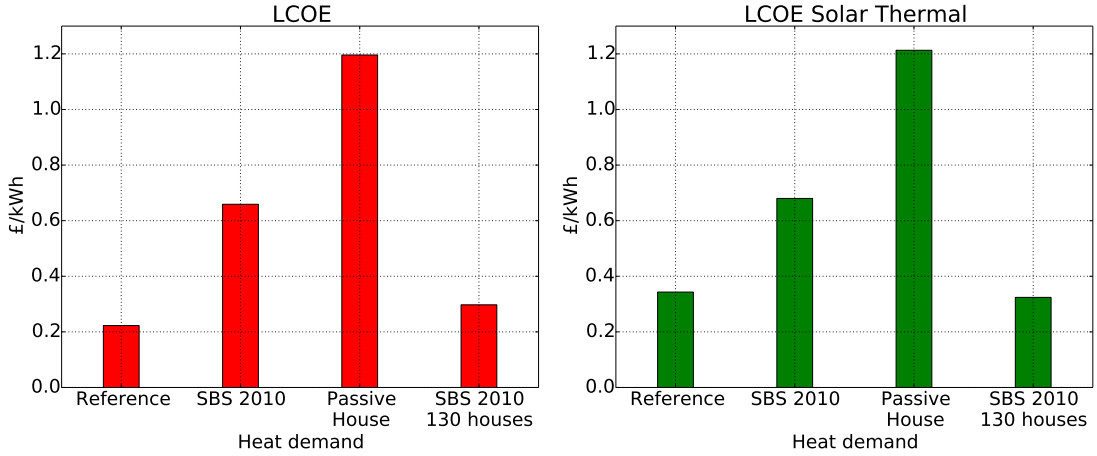

Figure 6.22: LCOE values for system with different heat demand.

Williamson et al., which compared the energy performance of two Scottish homes built according to SBS 2010 and Passive House (Bros-Williamson *et al.*, 2016).

Figure 6.21 and 6.22 summarise the influence of heat demand to the performance of the system. Both SBS 2010 and Passive House case can reach 100% solar fraction, but this is mainly due to equipment oversizing. As can be seen from the system efficiency and LTS efficiency, the reference case performs better because it simply utilises a larger share of the collected solar energy.

In order to evaluate the reduced heat demand while minimising the oversizing effect, a simulation run with 130 SBS 2010 houses was performed. The results are shown in

Fig. 6.21 and 6.22 with SBS 2010-130 houses legend. From a performance viewpoint, although the solar fraction in later years is now lower than the case of 52 houses SBS, they are still relatively high for a solar district heating system, even comparable to the solar fraction of the original DLSC (SF > 90%). The system efficiency in this case is also similar to the reference case, indicating a better utilisation of the solar energy collected. The relatively low LTS efficiency can be explained by the smaller amount of energy charged to the LTS as more solar energy is directly used to satisfy the demand. Since the LTS characteristics remain constant, a significant proportion of this charged energy is lost to the surrounding.

Both the LCOE and $LCOE_{ST}$ of the SBS 2010-130 case are significantly lower than the SBS 2010 and Passive House. This illustrates the influence of heat demand and equipment sizing on the financial metrics. The increased total heat demand in SBS 2010-130 improves the metrics because more energy is produced for the same equipment size, driving the LCOE down.

6.6.3 Soil properties

From the results of Camborne, it is clear that the soil properties can have a significant influence on the performance of the system. Three types of soil typically found in the UK are considered in this parametric study: sand, loam, and clay. The thermal properties of each type can be found in Table 6.6.

The influence of soil types on the techno-economic metrics is illustrated in Fig. 6.23 and 6.24. Despite having little influence on the LCOE values, the soil type can affect the technical performance of the system, particularly on the storage and system efficiency. Among the three soil types, loam has the best technical performance for the investigated system, with higher LTS efficiency the other two soil types as time progress.

It should be noted that the thermal properties considered are median values. In the case of Camborne, the unfavourable properties are outliers within the Clay soil type. This illustrates the importance of using the thermal properties of the particular soil type where the system will be installed, rather than the median or average values.

Table 6.6: Thermal properties of typical soil types in the UK. These are median values from the data in Ref. (Busby, 2016)

Properties	Unit	Sand	Loam	Clay
Thermal conductivity	W/mK	1.56	1.15	1.81
Specific heat capacity	kJ/kgK	1.014	1.267	1.398
Density	kg/m^3	1520	1280	1250
Thermal diffusivity	$x10^{-}6\ m^2/s$	0.9961	0.7173	1.0295

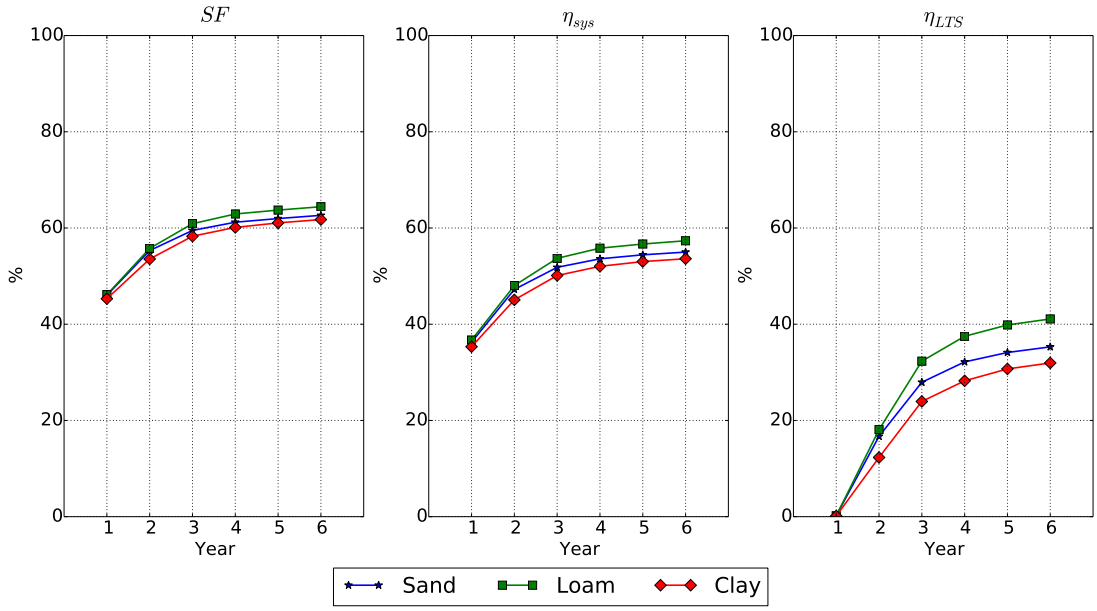

Figure 6.23: Technical performance metrics for systems with different soil type: Solar Fraction (SF), System Efficiency (η_{sys}), and Long Term Storage Efficiency (η_{LTS}).

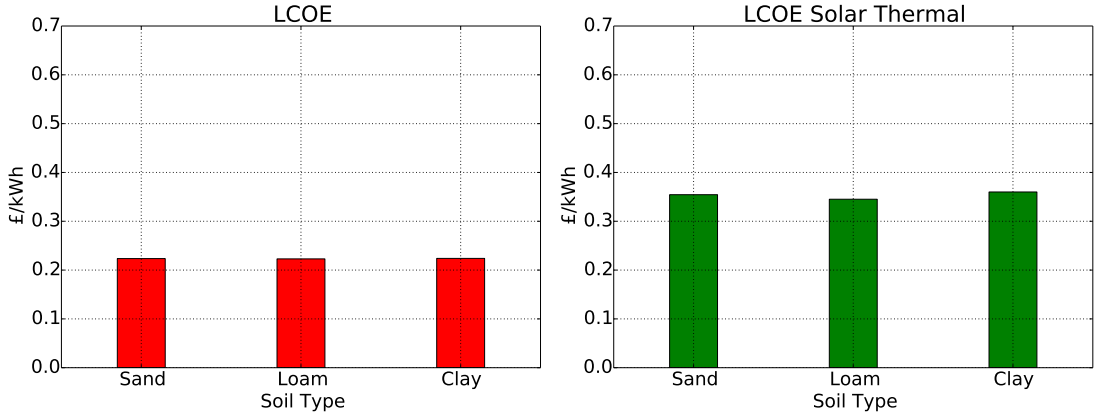

Figure 6.24: LCOE values for systems with different soil type.

Furthermore, soil thermal properties are only highly relevant if borehole TES was used as the long-term storage technology. Their importance is foreseen to be lower when a pit or tank TES is implemented, for example.

Because of the outlier thermal properties used in the Camborne case, it is interesting to evaluate the system performance if more average thermal properties were used. In order to illustrate this case, a simulation run of the Camborne case but with the soil characteristics of the Aberdeen case was performed. The resulting performance metrics for the sixth year are as follows: solar fraction (90%), system efficiency (52%), and LTS efficiency (43%). However, the financial metrics are only slightly improving at 0.29 and 0.33 £/kWh for LCOE and LCOE_{ST}, respectively. The results illustrate that

given a suitable soil condition for BTES, a relatively high technical performance can be achieved for a solar district heating system located in the southern UK.

6.6.4 Financial parameters

Both discount rate and time horizon can have a significant impact on the resulting LCOE values. The discount rate is typically selected according to the financing nature of the project, with values ranging from 3 up to 10%. Fig. 6.25 shows the resulting LCOE values for different discount rate. A 0% discount rate is included to consider a case with fully subsidised investment cost.

Currently, domestic RHI for solar thermal only applies to domestic hot water application and excludes space heating application. The annual payment is calculated based on the estimated annual generation on Microgeneration Certification Scheme (MCS) certificate. On the other hand, non-domestic RHI includes all applications of solar thermal systems and prescribes an upper capacity limit of 200 kW_{th}. The subsidy tariffs are 0.2006 and 0.1044 £/kWh of thermal energy for domestic and non-domestic RHI, respectively. Domestic RHI is tenable for seven years, while non-domestic RHI can be claimed for 20 years.

A system like DLSC is currently ineligible for both domestic and non-domestic RHI due to the space heating application and large thermal capacity. Nevertheless, it is interesting to see the influence of such subsidies on the LCOE values and whether a modified policy-based subsidy can be used to improve the financial attractiveness of the system.

The results of implementing both RHI schemes can be seen in Fig. 6.26. The solar energy generated was used to calculate the paid subsidy in this figure, as opposed to a fixed value based on certificates. Between the domestic and non-domestic RHI, the latter has slightly larger influence in reducing the LCOE values due to the significantly longer payment period.

It is interesting to identify the required non-domestic RHI tariff for solar thermal in order to make it more competitive with the incumbent technology. For instance, it has been reported that the range of LCOE values for biomass-based district heating in 2020 is in the range of £58-111/MWh, depending on the heat density of the location (Element Energy, 2015). If the top end of this range is used as a reference, then the required non-domestic RHI tariffs are approximately 0.2 and 0.28 £/kWh to achieve 0.11 £/kWh LCOE and $LCOE_{ST}$, respectively. Thus, it requires the implementation of the current domestic RHI tariff with the time horizon of the non-domestic one in order to significantly improve the financial competitiveness of DLSC-like solar district heating systems if it is located in Scotland. It should also be noted that the payment calcula-

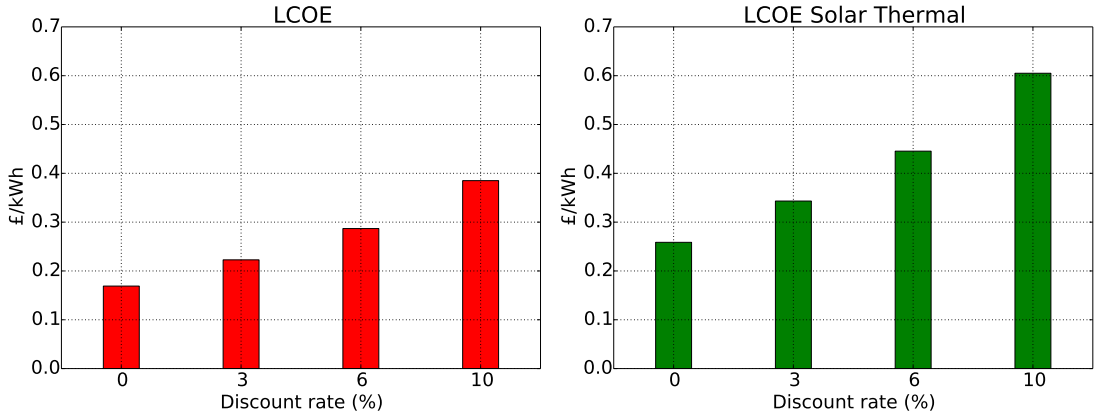

Figure 6.25: LCOE values for different discount rates.

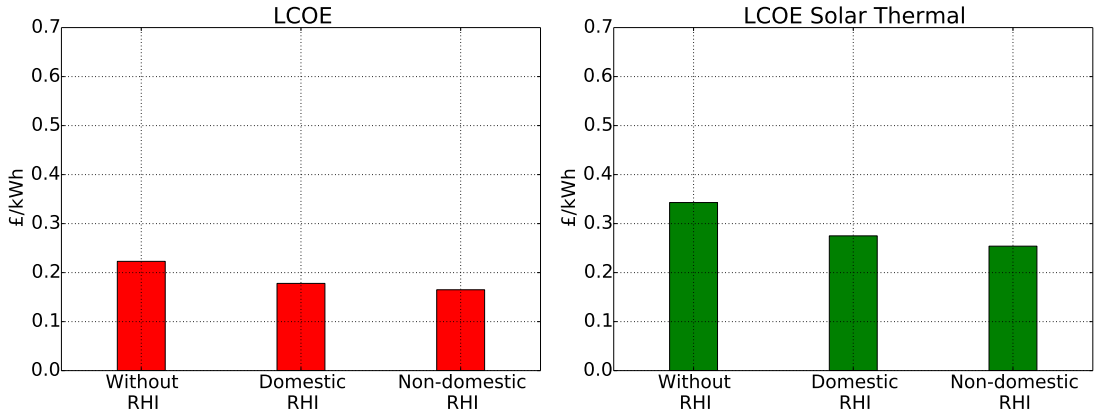

Figure 6.26: LCOE values for different subsidy types.

tion was based on measured energy production and without maximum capacity limit. Clearly, this needs to be re-evaluated from a policy perspective, but such treatment is outside the scope of this thesis.

6.7 Conclusions

The techno-economic performance of a solar district heating system installed in two UK locations has been quantified in this chapter. The case study was based on the Drake Landing Solar Community in Okotoks, Canada, which has a relatively high solar fraction. In supporting the techno-economic analysis, a TRNSYS model of DLSC was developed and validated using the publicly available annual monitoring data.

In general, a DLSC-like system installed in the UK will have a lower solar fraction and higher levelised cost of energy than the original system. Among the two studied locations, a system in Aberdeen has lower solar fraction than the one installed in Camborne. However, Aberdeen has better system efficiency and LCOE. The low system

efficiency in Camborne can be attributed to the unfavourable soil properties for borehole thermal energy storage. This signifies the importance of not only solar resource, but also soil properties in designing a solar district heating system with borehole thermal energy storage.

From the parametric study, it is evident that solar collector and long-term storage size have a more significant influence on the techno-economic metrics than the short-term storage. Furthermore, expanding the long-term storage size by increasing the borehole number is not only more feasible in the field, but can also produce a higher improvement in performance than increasing the borehole depth. It has also been shown that a system without long-term storage has little influence over the economic metrics, while it can reduce the solar fraction relative to the system with long-term storage.

Apart from equipment size, heat demand can also influence the techno-economic performance of the system. By modifying the specific annual heat demand of each house (kWh/m^2-year), it is clear that low energy demand houses will only improve the solar fraction of the system while worsening the remaining metrics. This is understandable since the system size remained constant, thus rendering the equipment to be oversized.

Due to the implementation of borehole thermal energy storage, soil properties have high relevance in determining the system performance. As shown in the case of Camborne, unfavourable soil thermal properties can lead to an excessive loss in the long-term storage, lowering the system efficiency despite the relatively high solar fraction. It has also been demonstrated that all major soil types in the UK have similar performance for DLSC system. Nevertheless, it should be noted that median values of soil properties were used in the simulation, and outliers such as in Camborne case do exist.

Although a system like DLSC is not eligible for either domestic or non-domestic RHI, it has been shown that the non-domestic RHI tariff has better capability to reduce the LCOE values. Furthermore, in order to significantly increase the financial competitiveness of DLSC-like system, the non-domestic RHI tariff needs to be increased up to the level of domestic one, and the payment has to be calculated based on the produced energy rather than a theoretical value.

Several options can be considered to improve the performance of a DLSC-like system and enhance its feasibility in UK locations. An example is to implement an operational optimisation in the operation of the system, using a Model Predictive Control approach as previously mentioned in Chapter 5. This is also an interesting possibility to test the interactions between optimisation and simulation models on a larger energy system than a single house. Another potential improvement is to use a ground source heat pump in combination with the solar collector as the energy conversion equipment. The heat pump can improve the utilisation of the boreholes by increasing the usable temperature

range of the thermal energy. These options should be considered in further studies of solar district heating feasibility in UK locations.

All in all, a solar district heating system such as DLSC is technically feasible to be implemented in the UK. The relatively lower solar fraction can be offset by installing long-term storage and implementing the system to supply new-built houses with better energy performance rather than older homes. Financially, the system still needs to be supported by encouraging policies, such as renewable heat incentive or carbon tax, in order to make it competitive with incumbent technologies.

The study in this chapter also illustrates a limitation of the simulation over optimisation approach, namely the relatively restrictive nature of the parametric study. Unlike the overall design space checking performed in an optimisation, a parametric study using a simulation model relies on the user to prescribe the values of the parameters.

Nevertheless, the more detailed nature of a simulation model makes it more accurate than a simplified model typically employed in an optimisation. This is particularly true when the simulation model can be validated against measurement data, as the case in this chapter.

Chapter 7

Conclusions

7.1 Conclusions

The aims of this thesis have been to (i) investigate the potential role of thermal energy storage in facilitating domestic heat decarbonisation in the UK, and (ii) evaluate two design tools, namely optimisation and simulation, in designing energy systems with thermal energy storage.

A review of previous work on energy systems and thermal energy storage was performed to identify knowledge gaps. The following research objectives were then derived from the identified gaps:

1. To explore how thermal energy storage contributes to improving the performance of renewable-based domestic heating systems in the UK.
2. To investigate the feasibility of long-term thermal energy storage to address the seasonal mismatch between solar energy and heat demand in the UK.
3. To examine the role of optimisation and simulation in designing thermal systems on a residential and community level.
4. To evaluate methods to manage increasing complexity in optimising and simulating energy systems with thermal energy storage.

These objectives have been achieved in the studies reported in Chapter 4, 5, and 6 of this thesis. Summaries of the achievements are given in the following paragraphs.

Thermal energy storage in renewable domestic heating systems

The first objective has been achieved by the study reported in Chapter 4. The contribution of TES was evaluated using a MILP optimisation model of a heat pump-based residential heating system. The case study was based on a typical annual heat demand of Scottish housing, with an assumed occupational profile of two adults working full-time. The influence of electricity tariff on the optimal sizing and operation of the system was explored further, along with the impact of Renewable Heat Incentive (RHI) subsidy on the total cost.

The optimisation results illustrate that in general, the influence of TES size over the total cost is minimal because the difference in investment cost is only slightly offset by the reduced operational cost. Furthermore, it can be concluded that HP-based heating systems, with or without TES, have significantly higher cost than a natural gas boiler heating system if the RHI subsidy was excluded. However, for cases with TES, the operational cost are lower than the HP-only scenario. Thus, the additional investment cost of TES is justified because it leads to a lower operational and total cost. It has also been shown that the new increased RHI-tariff can significantly reduce the consumer's total cost and make heat pumps a more attractive option for end users in the UK.

From a CO_2 equivalent emissions viewpoint, the optimal heating systems can reduce approximately 26% of CO_2e emissions relative to the natural gas boiler case. A further reduction up to 50% is possible when a lower heating flow temperature is implemented, e.g. under-floor heating. The lower operational cost of HP-TES scenarios relative to the HP-only case also illustrates the benefits of TES installation in reducing both operational cost and emission across all considered electricity tariffs.

The study in Chapter 4 has been focused on a heat pump residential heating system without considering its interaction with the electricity grid. On a broader scope of demand side management, this interaction is vital to assess the potential contribution of TES installation. Nevertheless, the focus of the optimisation and simulation study has been on the potential benefits of TES installation from the user viewpoint, rather than the network operator or other relevant parties. Therefore, the grid interaction can be neglected for this purpose.

Overall, the installation of TES in a residential heat pump system has both financial and environmental benefits from the perspective of the users. On a larger scale, the impact of the distributed TES in the system may even be larger than the sum of single house impacts. However, the grid side of the problem has to be carefully considered to avoid problem shifting in the form of, for example, excessive peak load.

Feasibility of long-term thermal storage in the UK

The second objective has been accomplished by the techno-economic study discussed in Chapter 6. The investigated long-term TES is a borehole storage and part of the solar district heating case study, namely the Drake Landing Solar Community (DLSC). The techno-economic performance of a DLSC system in two UK locations have been quantified in the chapter.

In general, a DLSC-like system installed in the UK will have a lower solar fraction and higher levelised cost of energy than the original system. The lower solar fraction is due to the lower solar irradiation in the UK. Furthermore, it has been shown that in addition

to the solar resource, soil properties also have significant influence in designing a solar district heating system with borehole thermal energy storage. Unfavourable soil thermal properties can lead to excessive heat loss, low system efficiency, and high LCOE. It has also been demonstrated that all major soil types in the UK have similar performance for a DLSC-like system. Nevertheless, it should be noted that median values of soil properties were used in the simulation, and outliers do exist. Thus, it is essential to perform on-site tests to determine the soil feasibility for borehole storage installation.

A solar district heating system with long-term TES such as DLSC is technically feasible to be implemented in the UK. The relatively lower solar fraction can be offset by installing long-term storage and implementing the system to supply new-built houses with better energy performance rather than older homes. Financially, the system still needs to be supported by encouraging policies, such as renewable heat incentive or carbon tax, to make it competitive with incumbent technologies.

Among different long-term TES solutions, borehole storage was considered in this thesis due to its lower investment cost relative to other technologies, as shown in Chapter 2. The utilisation of long-term TES in other scenarios, such as CHP-based district heating or industrial waste heat reuse, are also possible. However, its deployment in solar district heating systems remains the most developed application. This will arguably reduce the technological challenges in implementing it in the UK since various systems have been built and tested worldwide.

Optimisation and simulation tools in the design of residential and community heating system

Various aspects of the third objective have been addressed in Chapter 4, 5, and 6. In Chapter 4, optimisation and simulation models of a residential heating system were developed and utilised to analyse the influence of TES installation. The MILP optimisation results were used in discussing the technical and financial effects of TES in the heating system. The TRNSYS simulation model was developed specifically to illustrate one option of the comparative approach between optimisation and simulation, namely to use the resulting operational profile from MILP optimisation as an input of the TRNSYS simulation. Overall, the results of the TRNSYS simulations indicate that the MILP optimisation model is sufficiently accurate for design optimisation (i.e. equipment sizing) and deriving annual performance values. However, operational control algorithms cannot be derived directly from the optimisation model because the modelling simplifications could lead to unrealistic profiles.

In Chapter 5, the operational optimisation of a community solar district heating system, i.e. the DLSC, has been performed using a MILP formulation. Despite discrepancies in different metrics values between the optimisation results and measurement data, the

overall shares of energy flows are similar between them. The results of an operational optimisation of an energy system can also be viewed as the upper limit of the real operation. Although direct application of the resulting operational profile may not be possible, as shown in Chapter 4, useful insights can still be derived from the optimisation results. These include the trend of optimal operational control and the performance of a control assumption relative to the optimal one. Further analysis can then be performed by using a dynamic simulation approach.

In Chapter 6, a TRNSYS simulation model of DLSC was developed and validated using the publicly available annual monitoring data. Apart from addressing the feasibility of long-term storage installation in the UK, the study in this chapter also illustrates a limitation of simulation over optimisation approach, namely the relatively restrictive nature of the parametric study. Unlike the overall design space checking performed in optimisation, a parametric study using a simulation model relies on the user to prescribe the values of the parameters. However, the more detailed nature of a simulation model makes it more accurate than a simplified model typically employed in an optimisation. This is particularly true when the simulation model can be validated against measurement data, as is the case in Chapter 6.

Overall, it can be concluded that an optimisation model is better suited for reducing the number of potential system configurations, i.e. superstructure and equipment size, while a more detailed simulation model can be used to study these potential configurations in order to obtain a better understanding regarding their operational characteristics. The advantage of such approach is foreseen to be more apparent as the designed system becomes larger, i.e. from a single dwelling to a district and up to a city-wide energy system.

Complexity reduction technique in optimisation of energy systems with thermal energy storage

The fourth objective has been realised specifically in Chapter 5. It evaluates the benefits and trade-offs of using a temporal-based complexity reduction technique, namely the multiple time grids method, in the optimisation of an energy system which has thermal energy storage equipment with different temporal characteristics. The case study was modelled as a MILP optimisation problem and implemented with different time grids, i.e. single-uniform, multiple-uniform, and multiple-non-uniform.

It has been shown that the multiple time grids method can reduce the computational cost of energy system optimisation without significantly decreasing the results accuracy. Moreover, it has been shown that the benefits of using multiple time grids become more apparent as longer time horizon is considered. Although based on a specific case study,

the presented key points are quite general to be considered when using multiple time grids in energy systems optimisation.

While the computational time can be reduced by implementing the multiple time grids method, the problem formulation becomes more complex due to the tracking of equipment time grids. One potential solution is to implement a systematic algorithm to generate the time grids, as well as the general problem formulation. This is one of the recommendations for further work as discussed in the next section.

7.2 Recommendations for further work

The work presented in this thesis can be improved and extended in numerous ways. Several options with high potential impacts are discussed in the following paragraphs.

Inclusion of other energy vectors

All cases considered in this thesis have been focusing solely on thermal energy vector, while other vectors such as electricity and natural gas are considered only as inputs to the system. For instance, electricity is an input for the heat pump (Chapter 4) and pumps (Chapter 5 and 6), whereas natural gas is an input for the gas boiler (Chapter 5 and 6).

The inclusion of other energy vectors is not only relevant from the viewpoint of the optimisation results, but also from methodological aspects which have been detailed in this thesis. For example, equipment of different energy vectors may have various temporal characteristics which may benefit from the multiple time grids approach. Additional energy vectors will also increase the complexity of the optimisation and simulation, which may influence the relationship between the two methodologies.

As for the techno-economic study of solar district heating in Chapter 6, the consideration of other renewable-based technology, such as heat pump and CHP, may significantly change the results. The interaction of the district heating system with the electricity grid may improve the performance of the overall system.

Algorithms for multiple time grids generation

The time grids generation in Chapter 5 was based on empirical examination from typical LTS characteristics reported in the literature, e.g. charge/discharge rate. Thus, the next logical step is to develop generic algorithms capable of determining the multiple time grids systematically for a given system. Although algorithms for chemical processes are available in the literature (Velez and Maravelias, 2013, 2014), algorithms for energy systems are still unavailable.

The use of systematic algorithms is also foreseen to limit the increasing complexity in problem formulation as mentioned in the previous section. Furthermore, such algorithms can also be used inside a larger optimisation framework, increasing the ease of application of the multiple time grids method.

Physical decomposition of long-term TES equipment

The decomposition technique considered in this thesis is a time decomposition technique in the form of the multiple time grids method (Chapter 5), while physical decomposition can also be implemented to reduce the complexity of energy systems optimisation. It is particularly interesting to investigate a physical decomposition approach applied to, for example, the long-term storage in the solar district heating system.

A borehole TES can be modelled with different complexity orders. The simplest is the energy-based or capacity model employed in the MILP optimisation models in this thesis. Although it has low computational cost, it is limited regarding the capability to optimise different parameters. For example, borehole arrangements cannot be optimised with this model. A potential approach is to use a surrogate-based model to describe the behaviour of relatively complex components, such as a borehole storage.

Uncertainty consideration in optimisation and simulation

Uncertainty factors in different aspects, such as demand, weather, and prices, may have significant impacts on the results of energy systems optimisation and simulation. Therefore, considering uncertainty is another possible extension to the work presented in this thesis.

Although uncertainty factor in general has been studied considerably in energy systems optimisation, it is particularly interesting to investigate the relations between the uncertainty and multiple time grids or other complexity reduction techniques. On the one hand, the inclusion of uncertainty will increase the problem complexity and computational time; on the other hand, complexity reduction techniques can save the computational cost of the optimisation problem. Potential research questions include how the two sides interact with each other and whether it is beneficial to use them together.

Appendix A

Bilinear term reformulation

The MILP optimisation formulation of the case study in Chapter 4 contains a bilinear term in the heat pump output constraint, Eq. 4.8. The bilinear term is a product between the operational status of the heat pump, ζ_t^{HP}, and the nominal heat pump output, $\dot{Q}_{nom}^{HP}$. It represents a nonlinearity for the optimisation problem and can be linearised using a reformulation strategy (Glover, 1975). The strategy works by substituting the bilinear term with a single continuous decision variable. Extra constraints are then prescribed to ensure the behaviour of the bilinear term is reproduced correctly. The linearisation presented in the following paragraphs is based on the application of the reformulation strategy as implemented by Voll for a case in energy systems optimisation (Voll, 2013).

The original heat pump constraint is reproduced in Eq.A.1.

$$LF_{min}^{HP} \cdot \zeta_t^{HP} \cdot \dot{Q}_{nom}^{HP} \leq \dot{Q}_{out}^{HP} \leq \zeta_t^{HP} \cdot \dot{Q}_{nom}^{HP} \tag{A.1}$$

The bilinear product $\zeta_t^{HP} \cdot \dot{Q}_{nom}^{HP}$ is substituted by a continuous variable, ξ_t. Furthermore, another auxiliary variable, Ψ_t, is defined to reformulate $\dot{Q}_{nom}^{HP}$ into a time dependent variable, as stated in Eq. A.2.

$$\Psi_t = \dot{Q}_{nom}^{HP} \quad \forall t \tag{A.2}$$

In the final step, two extra constraints are formulated to guarantee that the behaviour of the original bilinear term is satisfied. These constraints are shown in Eq. A.3 and A.4.

$$\zeta_t^{HP} \cdot \dot{Q}_{nom,min}^{HP} \leq \xi_t \leq \zeta_t^{HP} \cdot \dot{Q}_{nom,max}^{HP} \tag{A.3}$$

$$\left(1 - \zeta_t^{HP}\right) \cdot \dot{Q}_{nom,min}^{HP} \leq \Psi_t - \xi_t \leq \left(1 - \zeta_t^{HP}\right) \cdot \dot{Q}_{nom,max}^{HP} \tag{A.4}$$

Appendix B

TRNSYS model: Residential heating system

The TRNSYS model developed in Chapter 4 contains two main loops: the heat pump and demand loop, which are connected by a hot water tank as the TES technology.

B.1 Heat Pump Loop

The heat pump loop is shown in Fig. B.1. The heat pump was modelled as a combination of Type 682 and Type 581b. The former is a load flow type which takes the rate of energy being transferred to the fluid flow as an input, while the latter is a Multi-Dimensional Data Interpolation component with 3 Independent Variables. The combination of these Types was used because the Mitsubishi Ecodan Air Source Heat Pump used as a reference in Chapter 4 is a multi-stage heat pump, while all heat pump Types in TRNSYS 17 are single-step implementation. Therefore, the performance tables of Ecodan ASHP (Mitsubishi Electric, 2013) were used as a reference in Type 581b, which then calculates the corresponding COP based on HP output, outlet temperature, and ambient temperature.

As described in Chapter 4, the heat pump operational profile as a result of the MILP optimisation was used as an input to the TRNSYS simulation. This is represented by a generic data reader Type 9a "MILP_HPout_Profile", which reads a text file containing the heat pump thermal energy output for every time step ($\dot{Q}^{HP}_{out,t}$). In addition to the heat pump model, this loop also contains a circulation pump, Pump_1, which is represented by a Type 977 Variable Speed Pump - Volumetric. The rated volumetric flowrate of the pump is taken from the rated flowrate of the heat pump, in this case 25 L/min. The pump was controlled to be active whenever there is a heat pump output power from the heat pump model.

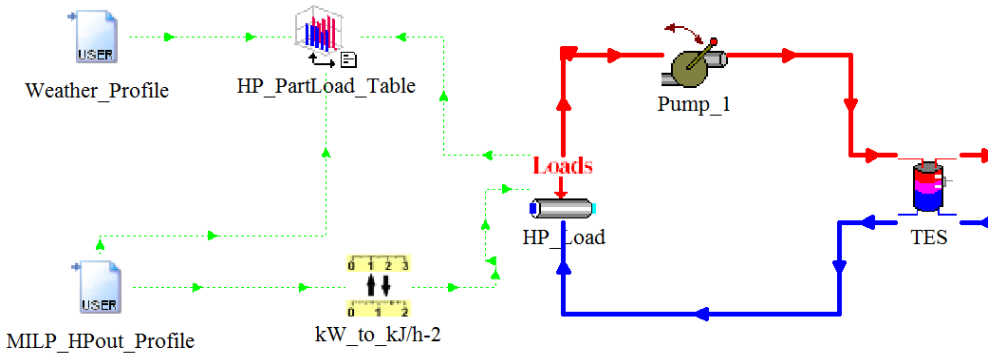

Figure B.1: Heat pump loop in the TRNSYS model.

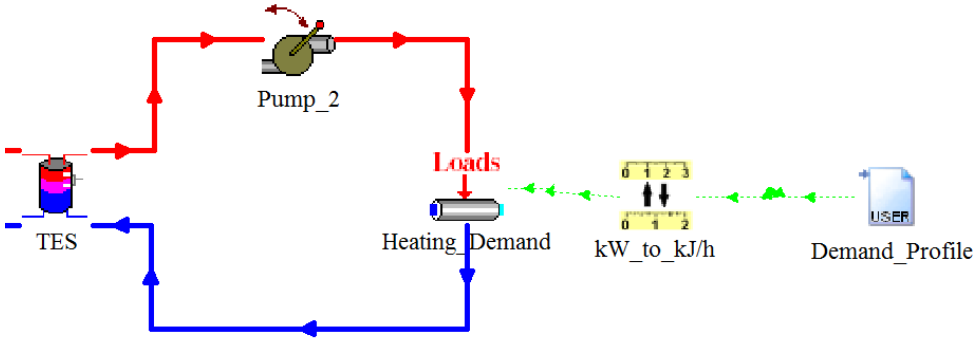

Figure B.2: Demand loop in the TRNSYS model.

B.2 Demand Loop

The demand loop is illustrated in Fig. B.2. The heating demand was modelled with Type 682, Heating Loads Imposed on a Flow Stream, which reads the heat demand values from an input file and applied them to the working fluid. In the case of heating, this will result in increasing working fluid temperature at the outlet of Type 682. The demand loop pump, Pump_2, was modelled with Type 977, Variable-Speed Pump - Volumetric. The rated volumetric flowrate of Pump_2 was assumed to be 15 L/min. It was controlled to be active whenever heating is requested.

The hot water tank TES was modelled with Type 60d Storage Tank; Fixed Inlets, Uniform Losses and Node Heights. It was selected among other storage tank types by considering a balance between a model which is as close as the real tank and data availability for the type's input. The storage tank parameters were gathered from manufacturer's data sheet (Kingspan Environmental, 2017).

Appendix C

Drake Landing Solar Community

C.1 Overview

The Drake Landing Solar Community (DLSC) is a solar district heating system located in Okotoks, Alberta, Canada. It supplies the space heating demand of 52 new-built single-detached homes. It has been operational since 2007 and managed to reach consistent solar fractions above 90% over the last 5 years (2011-2016). Information in this appendix was gathered from the DLSC website (www.dlsc.ca) and relevant publications (McDowell and Thornton, 2008; Sibbitt *et al.*, 2012; Quintana, 2013).

The aerial photo and schematic of DLSC are shown in Fig. C.1 and C.2, respectively. It can be seen in Fig. C.1 that the solar collectors are installed on the south-facing garage roof behind each house. The short-term storage is located inside the energy centre building (top right corner in Fig. C.1), while the long-term storage is located underground next to the energy centre building. The collected solar energy is sent to the short-term storage where it can either be stored, transferred to the long-term storage, or sent directly to the district loop. Natural gas boilers are available as back-up generation systems and working whenever the district set-point temperature (DLSP) cannot be achieved by the solar energy alone.

C.2 Main equipment

C.2.1 Solar collectors

The solar collector arrays consist of 800 flat plate panels with total net collector area of 2293 m^2. The working fluid is a mixture of water and glycol, which is pumped through the collectors and underground distribution pipes. These pipes connect the collector with the short-term storage through a heat exchanger.

Fig. C.3 shows the collector efficiency curve from both tested and measured results. It is clear from this figure that the selection of 50% as the constant efficiency in Chapter 5 is justifiable, as the measured efficiency fluctuates between 40-60%.

Figure C.1: Aerial view of DLSC (www.dlsc.ca)

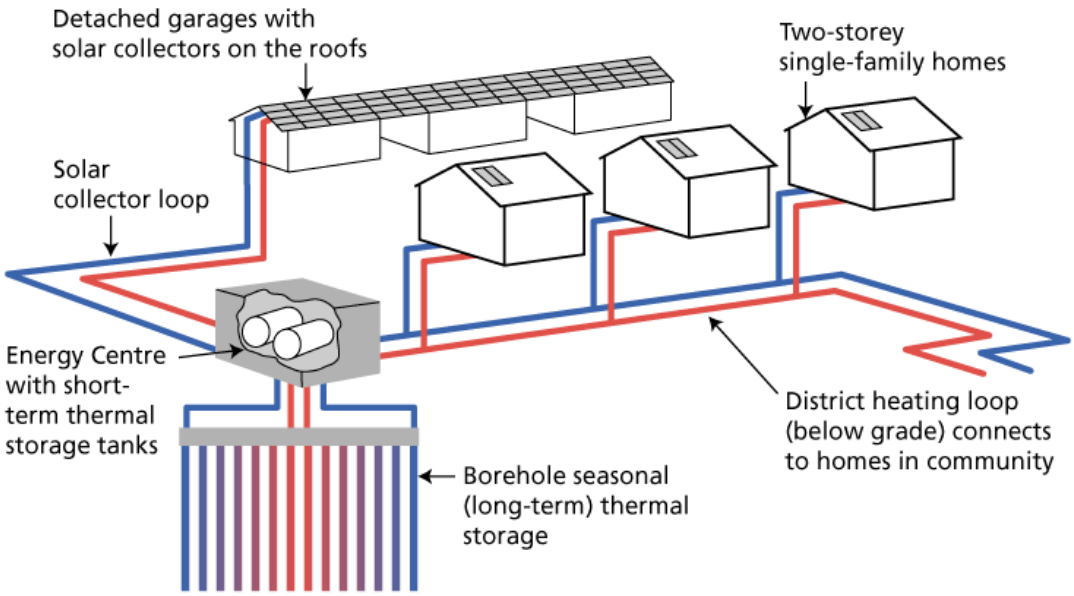

Figure C.2: Schematic of DLSC (www.dlsc.ca)

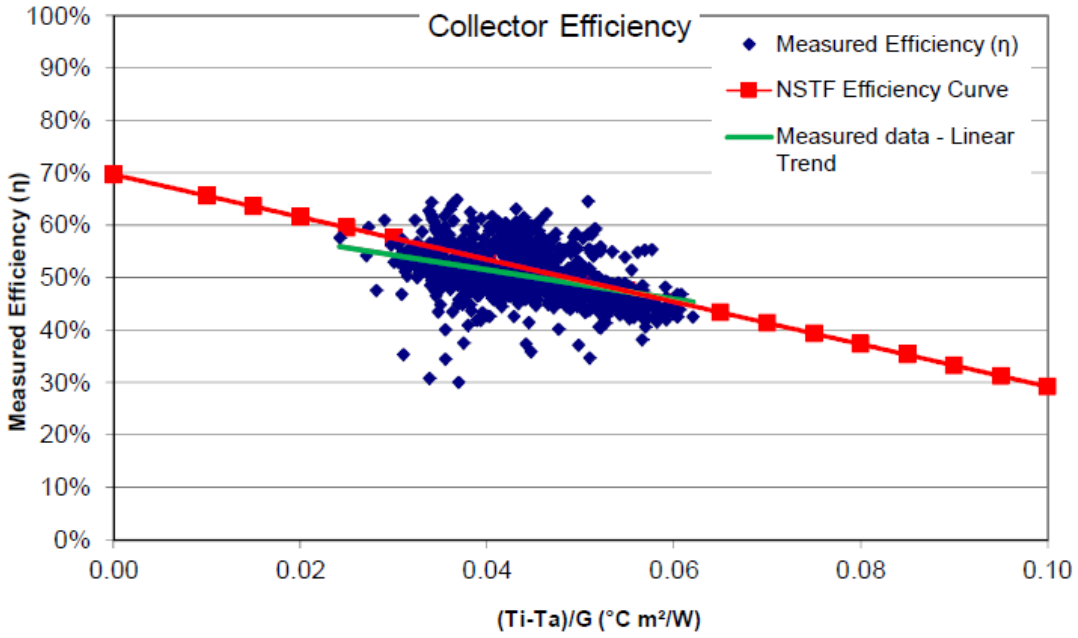

Figure C.3: Solar collector efficiency curve: test and measured curve (Leidos Canada, 2014)

C.2.2 Short-term storage

The short-term storage (STS) is two horizontal steel water tanks with a volume of 120 m^3 each. The tanks are connected between the bottom of the hotter and the top of the colder tank, as illustrated in Fig. C.4. The STS acts as a hub that connects all the main loops in the systems: solar collector, long-term storage, and district loop.

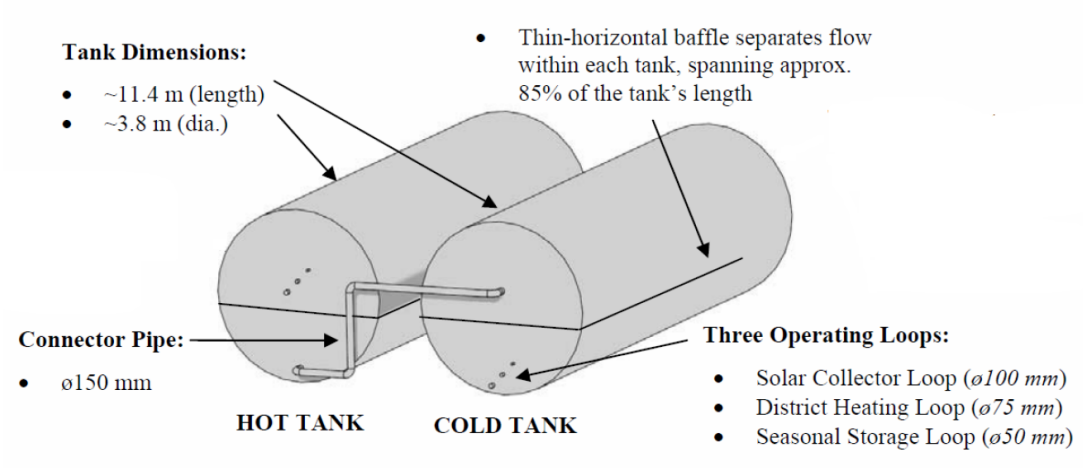

Figure C.4: DLSC Short-term Storage tanks (Rysanek, 2009)

C.2.3 Long-term storage

Borehole Thermal Energy Storage (BTES) is the implemented long-term storage in DLSC. It consists of 144 boreholes with 35 m depth. The boreholes are installed in mixed arrangement (parallel-series), with 24 parallel headers and 6 boreholes in series. The top view schematic of the long-term storage is shown in Fig. C.5.

The hot water from STS flows from the centre to the outer edge of the LTS during charging process, while the reverse flow with cold water from STS happens during discharging. This maximises the thermal stratification in the ground. On the other hand, it means that the LTS cannot be simultaneously charged and discharged.

C.2.4 Others

In addition to the aforementioned main equipment, other important parts of the system include pumps, distribution pipes, and auxiliary boilers. In the following description, the nomenclature in Fig. 6.5 is used as a reference. Pump1 and Pump2 are variable speed pumps and duplicated in the field for backup purposes. Pump3 and Pump3 are synchronised for simultaneous operation when there is heat demand. Furthermore, Pump5 is the pump for LTS charge and discharge operation and was a constant speed pump until replaced by a variable speed pump in 2012. The system utilises underground two-pipe district heating system with pre-insulated polyethylene pipes. The auxiliary boilers are 460 kW natural gas boilers.

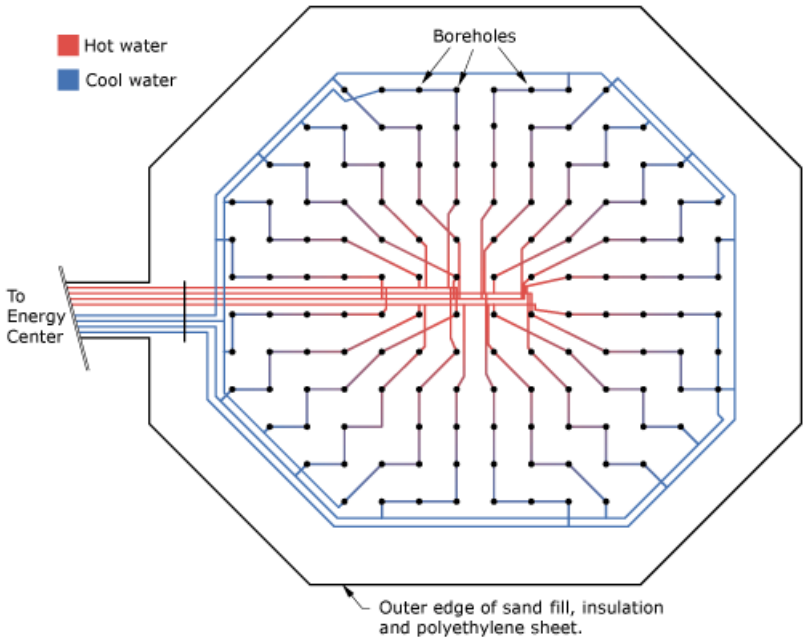

Figure C.5: Top view of the borehole thermal energy storage in DLSC (www.dlsc.ca)

C.3 System control

The DLSC control system has evolved over the operational period. In this thesis, two types of control system were considered based on publicly available information: original and latest control system. The former was partly applied in Chapter 5, while the latter was implemented in Chapter 6.

C.3.1 Original system control

The original system control briefly described in this section is mainly based on Ref. (Quintana, 2013). There are two modes of operation in the original control: winter and summer mode. The winter mode is fixedly activated between 1 September and 30 April, while the summer model is flexibly activated from May to August. During the summer months, it is possible to switch back and forth between the two modes depending on the weather condition.

Solar loop

Pump1 and Pump2 are controlled to keep a 15 °C difference between HX1 input and output on the solar collectors side. They are stopped when the average solar collector temperature is very close to the cold STS tank outlet temperature. In addition to this rule, two bypass rules are also implemented during the warming up of the solar collectors and if the STS is already full.

District loop

The overall aim of the district loop control rules is to satisfy the heating demand by providing hot water at the set-point temperature, the Drake Landing Set Point (DLSP). The value of DLSP is between 37 and 55 °C, depending on the time of the day and the ambient temperature. It is calculated according to Eq. C.1.

$$DLSP_t = \begin{cases} 55\ ^\circ\text{C} & \text{if } T_{amb} \leq -40\ ^\circ\text{C} \\ -0.48 \cdot T_{amb} + 35.8 & \text{if } -40\ ^\circ\text{C} < T_{amb} < -2.5\ ^\circ\text{C} \\ 37\ ^\circ\text{C} & \text{if } T_{amb} \geq -2.5\ ^\circ\text{C} \end{cases} \tag{C.1}$$

Pump3 is modulated so that the hot water temperature on the district side of HX2 is close to the required DLSP temperature. Pump4 is running to fulfill the heating demand and compensate the corresponding pressure losses in the district loop. Furthermore, the auxiliary boilers are activated when DLSP temperature cannot be met solely by the solar energy from STS through HX2.

STS loop

The main control parameter from the STS is its state-of-charge (SOC^{STS}). In the original control, this is calculated from DLSP and the temperature of two nodes in each of the STS tanks. However, since in this thesis the original system control was implemented in the energy-based optimisation (Chapter 5), the SOC was calculated according to Eq. 5.9. The SOC of STS is mainly used in the control of LTS loop, i.e. charging and discharging of the LTS.

LTS loop

The LTS loop control has different objectives depending on the overall control mode. In the winter mode, the main objective is to reduce natural gas consumption due to boiler operation. This is achieved by trying to maintain sufficient energy in the STS, so that the DLSP can be reached easily. In the summer mode, the main objective is to store as much solar as possible in the LTS.

Only the winter mode control rule is reported in Ref. (Quintana, 2013). In this mode, the LTS is charged if SOC^{STS} is higher than a charge factor multiplied by the required SOC^{STS} ($SOC^{STS}_{req,t}$). The LTS is dischargd if SOC^{STS} is lower than a discharge factor multiplied by the required $SOC^{STS}_{req,t}$. The values of $SOC^{STS}_{req,t}$ are given in the control rules and summarised in Table C.1.

C.3.2 Latest system control

The latest implemented control rules were based on those reported in Ref. (Yang *et al.*, 2017). Although it was not explicitly mentioned in the publication, the control rules were assumed to be the latest implementation in DLSC, taking into account that the authors were affiliated with the project leader organisation in the design and monitoring of DLSC (CanmetENERGY-National Resource of Canada).

The rules are summarised in Table C.2. Subscript *top, ctr* and *btm* correspond to the top, center, and bottom layer of the thermal stratification in a storage, respectively. Subscript *avg* corresponds to the average value of a variable.

Table C.1: The values of $SOC_{req,t}^{STS}$ as derived from Fig. 2-5 in Ref. (Quintana, 2013)

Time	DLSP <= 38	38 < DLSP < 45	DLSP >= 45
00:00	0.5	0.5	1
01:00	0.45	0.45	0.92
02:00	0.42	0.42	0.82
03:00	0.37	0.37	0.75
04:00	0.32	0.32	0.67
05:00	0.28	0.28	0.58
06:00	0.25	0.25	0.5
07:00	0.25	0.28	0.5
08:00	0.25	0.32	0.5
09:00	0.25	0.37	0.5
10:00	0.25	0.42	0.5
11:00	0.25	0.47	0.5
12:00	0.25	0.5	0.5
13:00	0.25	0.5	0.5
14:00	0.28	0.58	0.58
15:00	0.32	0.67	0.67
16:00	0.38	0.75	0.75
17:00	0.42	0.82	0.82
18:00	0.47	0.92	0.92
19:00	0.5	1	1
20:00	0.5	0.92	1
21:00	0.5	0.82	1
22:00	0.5	0.75	1
23:00	0.5	0.67	1

C.4 Annual monitoring results

The annual performance of DLSC has been monitored by CanmetENERGY and reported in the DLSC website. The summary for the first six years of operation is given in Table C.4 (Leidos Canada, 2014). It should be noted that some of the measurement results are not physically possible due to imperfect sensors calibration.

C.5 Financial data

Table C.3 summarises the estimated investment cost of DLSC(Sibbitt *et al.*, 2011). The values exclude unusual first costs which occurred during the construction of DLSC, such as cost related to flooding of the site. Furthermore, it was also estimated that the unit cost of solar energy delivered over 40 years to be around 0.17 CAD$/kWh.

Table C.2: DLSC control (Yang *et al.*, 2017)

Equipment		ON	OFF
Solar loop pump		T_{out}^{SCO} - $T_{btm}^{STS} \geq 10$ °C	T_{out}^{SCO} - $T_{btm}^{STS} \leq 2$ °C OR $T_{top}^{STS} \geq 90$ °C
HX1 pump	Flow is controlled to maintain ΔT_{cold}^{HX1} at 12 °C		
HX2 pump	Flow is controlled to achieve $T_{cold,out}^{HX2} = T^{DLSP}$		
LTS charge	Winter	T_{btm}^{STS} - $T^{DLSP} \geq 10$ °C AND $T_{top}^{STS} > T_{ctr}^{LTS}$	T_{btm}^{STS} - $T^{DLSP} \leq 2$ °C OR $T_{top}^{STS} \leq T_{ctr}^{LTS}$
	Summer	T_{top}^{STS} - $T_{ctr}^{LTS} \geq 10$ °C AND $T_{avg}^{LTS} \leq 90$ °C	T_{top}^{STS} - $T_{ctr}^{LTS} \leq 3$ °C AND $T_{avg}^{LTS} > 90$ °C
LTS discharge		T_{ctr}^{LTS} - $T_{btm}^{STS} \geq 10$ °C AND $T_{top}^{STS} \leq 55$ °C	T_{ctr}^{LTS} - $T_{btm}^{STS} \leq 3$ °C OR $T_{top}^{STS} > 55$ °C
District loop pump	Flow is controlled to maintain $T_{return}^{DL} = 0.9588 \cdot T_{supply}^{DL}$-4.79 °C		
Backup boiler		T^{DLSP} - 2 °C	T^{DLSP} + 2 °C

Table C.3: Summary of DLSC Investment Cost

Item	**Cost (CAD$ 2005-2007)**
Solar collectors	710000
Installation of solar collectors	430000
Seasonal storage borehole field	620000
Diestrict heating & solar collection loops	1025000
Energy centre including STS Tanks	600000
Total	3385000

Table C.4: Summary of DLSC annual performance (Leidos Canada, 2014)

Metrics	2012-2013	2011-2012	2010-2011	2009-2010	2008-2009	2007-2008
Total Incident Solar Energy (GJ)	12702.9	12973.8	12480	12709.1	13902	13321.1
Total Solar Energy Collected (GJ)	4328.3	4428	4058.9	4274.5	4390.9	4468.7
Total Solar Energy Delivered to STTS (GJ)	4590.3 *	4590.9	3929.7	4042.6	4330.3	4855.3
Total Energy Delivered to BTES (GJ)	2566.2	2517.7	2262.7	2499.4	2713.3	2608.8
Total Energy Extracted from BTES (GJ)	1306.8	902.6	1218.7	863.7	561.7	152.1
Total Energy Delivered from STTS to HX-2 (GJ)	2719.9	2401.3	2754.4.	2555.5	1980.6	2345.7
Total Solar Energy to District Loop (GJ)	2434	2047.9	2455.9.	2026.1	1791.9	1670.7
Natural Gas Energy Used (GJ)	42.4	65.14	436.2	543.6	1194.3	1573.6
Boiler Thermal Energy Delivered (GJ)	58.6 *	67.6	403.3	519.5	1172.2	1365.2
Total Energy Delivered to District Loop (GJ)	2493.6	2118.6	2859.3	2545.1	2964.2	3035.7
Average Solar Collector Efficiency	34%	34.1%	32.5%	33.6%	31.6%	33.5%
Average Efficiency of HX-1*	106.1%	103.7%	96.8%	94.6%	98.6%	92.0%
Average Efficiency of HX-2*	89.5%	85.3%	89.2%	79.3%	90.4%	71.2%
Average BTES Core Temperature	52.6 °C	55.6 °C	51.9 °C	44.3 °C	41.4 °C	39.7 °C
PV Energy Generated	82.6	71.07	39.89	12.81	13.66	10.72
Solar Fraction	97.6%	96.7%	85.9%	79.6%	60.4%	55.0%
Heating Degree Days (18°C ref.)	4579	4515	4911	5069	5393	5274

* Calculations were based on measurements using sensors with imperfect calibration.

Appendix D

TRNSYS model: Drake Landing Solar Community

D.1 Solar loop

The solar collector loop consists of solar collectors, supply and return pipes, a pump, and a heat-exchanger, as shown in Fig. D.1. The solar collectors arrays were modelled using Type 1a with the parameters as shown in Table D.1. The distribution pipes from the solar collector arrays to the first heat exchanger (HX1) were modelled as outdoor pipe (Type 31) and underground pipe (Type 952). The parameters for these pipes are shown in Table D.3 and D.2 (Verstraete, 2013). The pump in this loop was modelled with Type 110, with rated flow rate of 15 kg/s, and rated power of 6 kW. The heat exchanger between the solar loop and the short-term storage was modelled with Type 761, which was equipped with flow rate modulation signal to maintain temperature difference of 12 °C in the cold-side (see Table C.2).

Table D.1: Type 1a Parameters - Solar Loop

Parameter	Value	Unit
Collector area	2293	m^2
Fluid specific heat	3.64	kJ/kg·K
Intercept efficiency	0.693	
Efficiency slope	13.806	kJ/hr·m^2·K

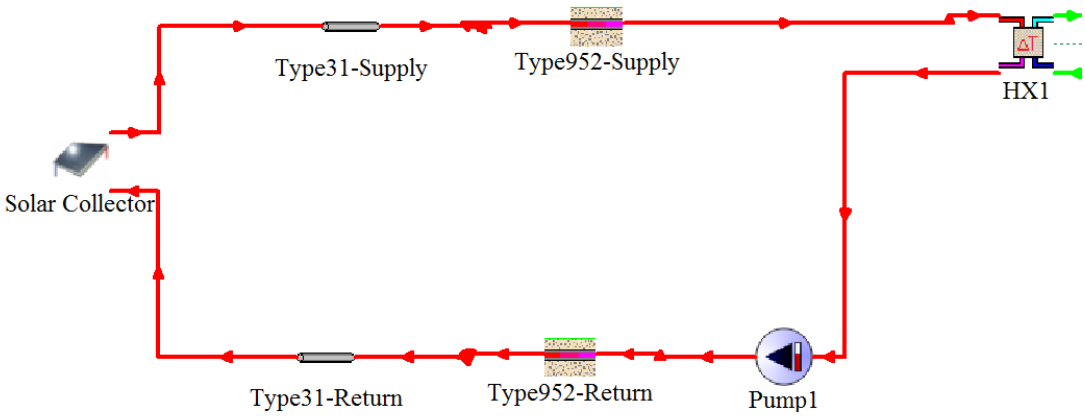

Figure D.1: TRNSYS model of the solar loop.

Table D.2: Type 952 Parameters - Solar Loop (Verstraete, 2013)

Parameter	Value	Unit
Pipe		
Length	255	m
Inner diameter	0.08606	m
Outer diameter	0.09243	m
Thermal conductivity	50	W/mK
Buried pipe depth	1.1	m
Insulation		
Thickness	0.05	m
Thermal conductivity	0.023	W/mK
Fluid		
Density	1025	kg/m^3
Thermal conductivity	0.37	W/mK
Specific heat	3.64	kJ/kgK
Viscosity	10.8	kg/mh
Initial temperature	20	°C
Soil		
Thermal conductivity	1.68	W/mK
Density	3406	kg/m^3
Specific heat	1	kJ/kgK
Average surface temperature	4.44	°C
Amplitude of surface temperature	12.14	°C
Day of minimum surface temperature	14.8	days

Table D.3: Type 31 Parameters - Solar Loop (Verstraete, 2013)

Parameter	Value	Unit
Inner diameter	0.05725	m
Length	632	m
Loss coefficient	2.283	W/m^2K
Fluid density	1025	kg/m^3
Fluid specific heat	3.64	kJ/kgK
Initial fluid temperature	20	°C

D.2 STS loop

The STS loop acts as a hub for the other loops in the system. Its main components are two horizontal storage water tank and two pumps, as illustrated in Fig. D.2.

The storage tanks were modelled using Type 534 with relevant parameters shown in Table D.4. The tank loss coefficients were prescribed according to the calibrated values (McDowell and Thornton, 2008). It was found that the manufacturer's value of loss coefficients (0.28 W/m^2K) lead to under prediction of heat loss. Thus, adjustments were performed, in which the top node coefficients were halved in both tanks and the bottom coefficient was doubled in the cold tank.

The pumps in the STS loop were modelled using Type 110 with rated flow rate of 15 and 6 kg/s for Pump2 and Pump3, respectively. Pump2 circulates the loop connected to the solar loop through HX1, while Pump3 manages the flow between the STS and district loop via HX2. Both heat exchangers types are equipped with flow modulation signal, which is transmitted to their corresponding pump. The signals were determined by the control rules, as stated in Table C.2.

Table D.4: Type 534 Parameters - Short Term Storage

Parameter	Value	Unit
Tank volume	120	m^3
Tank height	3.8	m
Loss coefficient	0.142 - 2.044	W/m^2K
Fluid density	1000	kg/m^3
Fluid specific heat	4.19	kJ/kgK

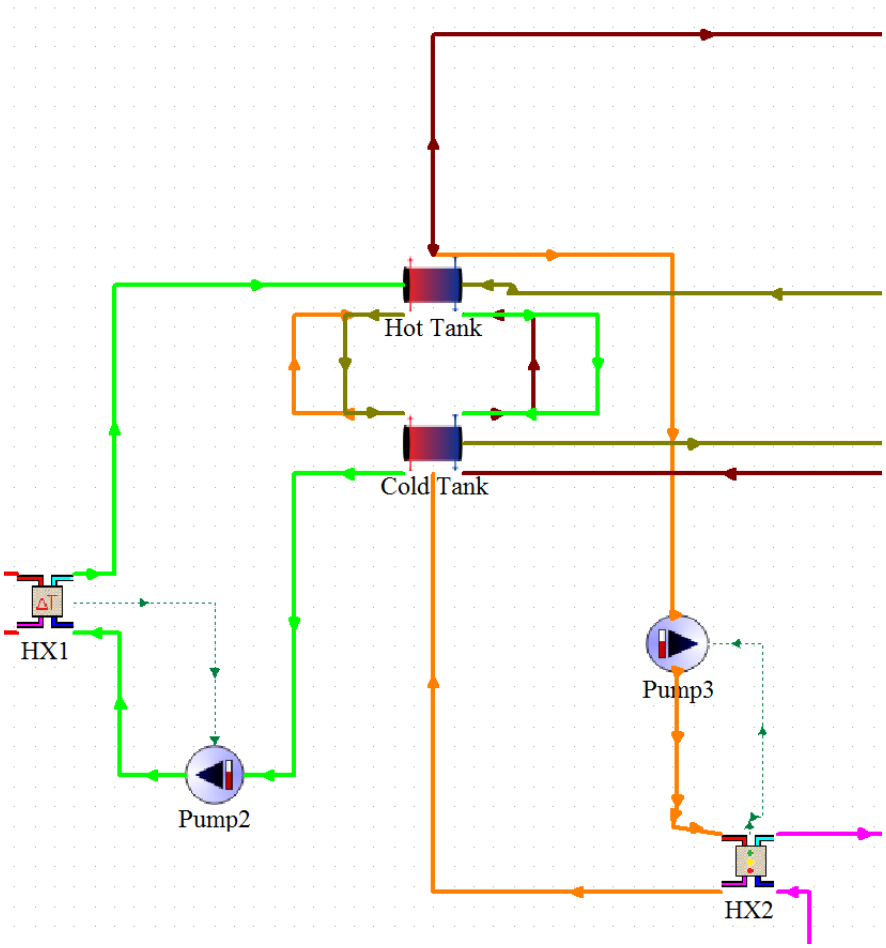

Figure D.2: TRNSYS model of the short-term storage.

D.3 LTS loop

The LTS loop consists of a borehole thermal energy storage, supply-return pipes, a pump, a mixing valve, and a diverter (Fig. D.3). The borehole storage was modelled by Type 557, which is based on the Duct Ground Heat Storage Model (Hellström, 1991). Essential Type 557 parameters used in the model are summarised in Table D.5

The underground piping in the long-term storage loop was modelled by Type 952. Furthermore, a mixing valve and a diverter were included in this loop. They were installed to assist in implementing the control of the BTES, i.e. the decision to charge, discharge, or store. The LTES control was based on the control rules reported in Ref. (Yang *et al.*, 2017) and are summarised in Table C.2. A controller implementing these rules was implemented as a separate type developed by the author.

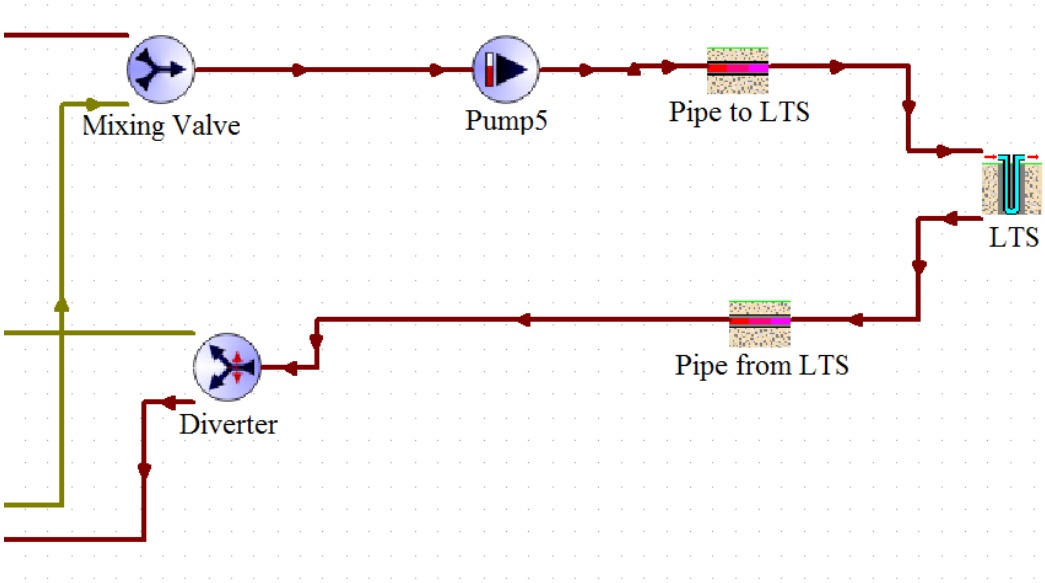

Figure D.3: TRNSYS model of the long-term storage loop.

Table D.5: Type 557 Parameters - Long Term Storage

Parameter	Value	Unit
Storage volume	33700	m^3
Borehole depth	35	m
Header depth	0.1	m
Number of boreholes	144	-
Borehole radius	0.075	m
Number of boreholes in series	6	-
Storage thermal conductivity	1.373	W/m·K
Storage heat capacity	3203	kJ/m^3·K
Outer Radius of U-Tube Pipe	0.0125	m
Inner Radius of U-Tube Pipe	0.01	m
Centre-to-Centre Half Distance	0.025	m
Fill Thermal Conductivity	0.89	W/m·K
Pipe Thermal Conductivity	0.41	W/m·K
Reference Borehole Flowrate	0.2	kg/s
Reference Temperature	30	°C
Fluid Specific Heat	4.182	kJ/kg·K
Fluid Density	990.2	kg/m^3
Number of simulation years	6	-
Initial Surface Temperature of Storage Volume	25	°C

D.4 District loop

As shown in Fig. D.4, the district loop contains the heating load, supply-return pipes, an auxiliary gas boiler, and a pump. The loop is connected to the STS through the

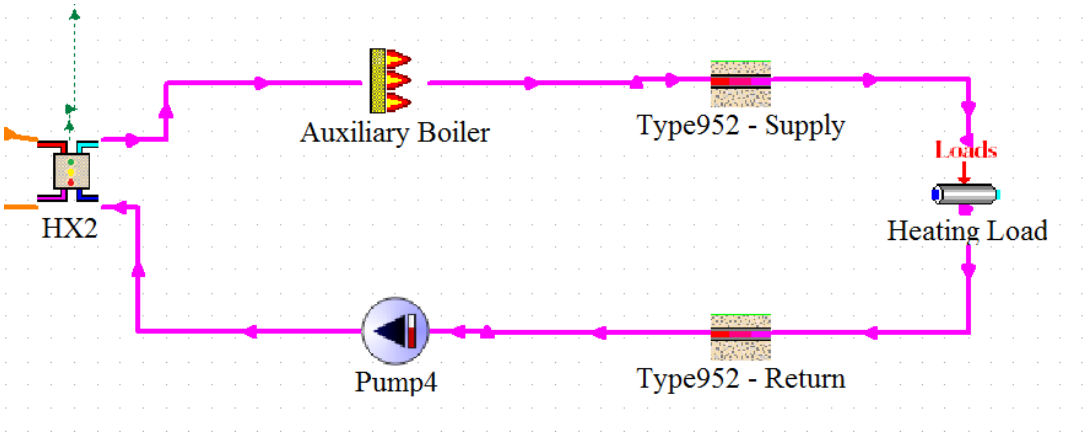

Figure D.4: TRNSYS model of the district loop.

second heat exchanger (HX2). This was modelled by a Type 512, which is a heat-exchanger model with hot-side flow rate modulation capability in order to maintain the cold-side outlet temperature above its set-point temperature (DLSP). A Type 659 was implemented to model the auxiliary gas boiler with rated capacity of 500 kW and 90% efficiency. The boiler was controlled to maintain the outlet water temperature based on the set-point temperature. As in the solar loop, the district loop distribution pipes are modelled with Type 952. The pipes parameters are shown in Table D.6. The heating load was represented as a lumped load flow using Type 682 with the heat demand values act as an input to the type.

D.5 Control rules

The implemented control rules were based on latest control system implementation as reported in Ref. (Yang *et al.*, 2017) and summarised in Appendix C.

Table D.6: Type 952 Parameters - District Loop (Verstraete, 2013)

Parameter	Value	Unit
Pipe		
Length	1000	m
Inner diameter	0.0514	m
Outer diameter	0.063	m
Thermal conductivity	0.38	W/mK
Buried pipe depth	1.1	m
Insulation		
Thickness	0.031	m
Thermal conductivity	0.0276	W/mK
Fluid		
Density	992.7	kg/m^3
Thermal conductivity	0.616	W/mK
Specific heat	4.182	kJ/kgK
Viscosity	2.406	kg/mh
Initial temperature	10	°C
Soil		
Thermal conductivity	1.68	W/mK
Density	3406	kg/m^3
Specific heat	1	kJ/kgK
Average surface temperature	4.44	°C
Amplitude of surface temperature	12.14	°C
Day of minimum surface temperature	14.8	days

Appendix E

List of publications

Parts of the work presented in this thesis have been published as journal articles and presented in conferences as follows:

E.1 Journal articles

1. Renaldi, R., and Friedrich, D. Multiple time grids in operational optimisation of energy systems with short-and long-term thermal energy storage. *Energy*, 133: 784-795, 2017.
2. Renaldi, R., Kiprakis, A., and Friedrich, D. An optimisation framework for thermal energy storage integration in a residential heat pump heating system. *Applied Energy*, 186: 520-529, 2017.

E.2 Conference proceedings

1. Renaldi, R., Kiprakis, A., and Friedrich, D. Optimisation of Thermal Energy Storage Integration in A Residential Heating System. Sustainable Thermal Energy Management Network. 2015, Newcastle, UK.

E.3 Conference presentations

1. Renaldi, R., and Friedrich, D. Solar District Heating in Scotland. 3$^{\text{rd}}$ International Conference on Smart Energy Systems and 4$^{\text{th}}$ Generation District Heating. 12-13 September 2017, Copenhagen, Denmark.
2. Renaldi, R., and Friedrich, D. Optimisation of Thermal Energy Storage Integration in A Residential Heating System. UK Energy Storage Conference. 2014, Warwick, UK.

E.4 Poster presentations

1. Renaldi, R., and Friedrich, D. Solar District Heating in Scotland. Scottish Renewables Solar Conference & Exhibition. 6 September 2017, Edinburgh, UK.
2. Renaldi, R., and Friedrich, D. Multiple time grids in operational optimisation of energy systems with short-and long-term thermal energy storage. UK Thermal Energy Storage Workshop. June 2016, London, UK.
3. Renaldi, R., Kiprakis, A., and Friedrich, D. Optimisation of energy systems with thermal energy storage. Workshop on the Mathematics of Demand Side Management and Energy Storage. 1-2 June 2015, Open University, Milton Keynes, UK.
4. Renaldi, R., and Friedrich, D. Computational modelling and optimisation of thermal energy storage. Solnet-SHINE PhD Course 13: Heat Storage for Solar Heating Systems. 17-23 May 2014, Technical University of Denmark, Lyngby.

Bibliography

Alberta Government. Utilities Consumer Advocate - Historic Rates, 2016. URL `https://ucahelps.alberta.ca/historic-rates.aspx`. Last accessed 13 October 2017.

Allegrini, J., Orehounig, K., Mavromatidis, G., Ruesch, F., Dorer, V., and Evins, R. A review of modelling approaches and tools for the simulation of district-scale energy systems. *Renewable and Sustainable Energy Reviews*, 52:1391–1404, 2015.

Andreas, W. and Biegler, L. T. On the implementation of an interior-point filter line-search algorithm for large-scale nonlinear programming. *Mathematical Programming*, 106:25–57, 2006.

Armstrong, P., Ager, D., Thompson, I., and McCulloch, M. Domestic hot water storage: Balancing thermal and sanitary performance. *Energy Policy*, 68:334–339, 2014a.

Armstrong, P., Ager, D., Thompson, I., and McCulloch, M. Improving the energy storage capability of hot water tanks through wall material specification. *Energy*, 78: 128–140, 2014b.

Arteconi, A., Hewitt, N., and Polonara, F. Domestic demand-side management (DSM): Role of heat pumps and thermal energy storage (TES) systems. *Applied Thermal Engineering*, 51(1-2):155–165, 2013.

Ashouri, A., Fux, S. S., Benz, M. J., and Guzzella, L. Optimal design and operation of building services using mixed-integer linear programming techniques. *Energy*, 59: 365–376, 2013.

Baldi, S., Le Quang, T., Holub, O., and Endel, P. Real-time monitoring energy efficiency and performance degradation of condensing boilers. *Energy Conversion and Management*, 136:329–339, 2017.

Banister, C. J. and Collins, M. R. Development and performance of a dual tank solar-assisted heat pump system. *Applied Energy*, 149:125–132, 2015.

Bauer, D., Marx, R., Nuß bicker Lux, J., Ochs, F., Heidemann, W., and Müller-Steinhagen, H. German central solar heating plants with seasonal heat storage. *Solar Energy*, 84(4):612–623, 2010.

Biegler, L. T. *Nonlinear programming: concepts, algorithms, and applications to chemical processes*. Society for Industrial and Applied Mathematics, 2010.

Biegler, L. T. and Grossmann, I. E. Retrospective on optimization. *Computers and Chemical Engineering*, 28(8):1169–1192, 2004.

Bonami, P., Biegler, L. T., Conn, A. R., Cornuéjols, G., Grossmann, I. E., Laird, C. D., Lee, J., Lodi, A., Margot, F., Sawaya, N., *et al.* An algorithmic framework for convex mixed integer nonlinear programs. *Discrete Optimization*, 5(2):186–204, 2008.

Bornatico, R., Pfeiffer, M., Witzig, A., and Guzzella, L. Optimal sizing of a solar thermal building installation using particle swarm optimization. *Energy*, 41(1):31–37, 2012.

British Gas. Gas and Electricity Tariff, 2017. URL `https://www.britishgas.co.uk/energy/gas-and-electricity.html`. Last accessed 13 October 2017.

Bros-Williamson, J., Garnier, C., and Currie, J. I. A longitudinal building fabric and energy performance analysis of two homes built to different energy principles. *Energy & Buildings*, 130:578–591, 2016.

Bruckner, T., Bashmakov, I., Mulugetta, Y., Chum, H., De la Vega Navarro, A., Edmonds, J., Faaij, A., Fungtammasan, B., Garg, A., Hertwich, E., *et al.* Energy Systems. In Edenhofer, O., Pichs-Madruga, R., Sokona, Y., *et al.*, editors, *Climate Change 2014: Mitigation of Climate Change. Contribution of Working Group III to the Fifth Assessment Report of the Intergovernmental Panel on Climate Change*. Cambridge University Press, 2014.

Busby, J. UK shallow ground temperatures for ground coupled heat exchangers. *Quarterly Journal of Engineering Geology and Hydrogeology*, 48(3-4):248–260, 2015.

Busby, J. Thermal conductivity and diffusivity estimations for shallow geothermal systems. *Quarterly Journal of Engineering Geology and Hydrogeology*, 49(2):138–146, 2016.

Cabeza, L. F. *Advances in thermal energy storage systems: Methods and applications*. Elsevier, 2014.

Cabrol, L. and Rowley, P. Towards low carbon homes – A simulation analysis of building-integrated air-source heat pump systems. *Energy and Buildings*, 48:127–136, 2012.

Castro, P. M. and Grossmann, I. E. New continuous-time MILP model for the short-term scheduling of multistage batch plants. *Industrial and Engineering Chemistry Research*, 44(24):9175–9190, 2005.

Chaudry, M., Abeysekera, M., Hosseini, S. H. R., Jenkins, N., and Wu, J. Uncertainties in decarbonising heat in the uk. *Energy Policy*, 87:623–640, 2015.

Cheng Hin, J. N. and Zmeureanu, R. Optimization of a residential solar combisystem for minimum life cycle cost, energy use and exergy destroyed. *Solar Energy*, 100: 102–113, 2014.

Christidis, A., Koch, C., Pottel, L., and Tsatsaronis, G. The contribution of heat storage to the profitable operation of combined heat and power plants in liberalized electricity markets. *Energy*, 41(1):75–82, 2012.

COIN-OR. COIN-OR Branch-and-Cut MIP Solver, 2017. URL `https://projects.coin-or.org/Cbc`.

Committee on Climate Change. Meeting Carbon Budgets: Closing the policy gap 2017 Report to Parliament. Technical report, Committee on Climate Change, 2017.

Crown. Climate Change Act 2008 chapter 27, 2008. URL `https://www.legislation.gov.uk/ukpga/2008/27/contents`. Last accessed 03 November 2017.

Department for Business, Energy & Industrial Strategy. Greenhouse gas reporting - Conversion factors 2016, 2016. URL `https://www.gov.uk/government/publications/greenhouse-gas-reporting-conversion-factors-2016`. Last accessed 03 November 2017.

Department of Business, Energy Industrial Strategy. Renewable sources of energy: Chapter 6, Digest of United Kingdom Energy Statistics (DUKES). Technical report, Department of Business, Energy & Industrial Strategy, 2016.

Department of Business, Energy Industrial Strategy. 2015 UK Greenhouse Gas Emissions, Final Figures. Technical report, Department of Business, Energy & Industrial Strategy, 2017a.

Department of Business, Energy Industrial Strategy. Energy Consumption in the UK. Technical report, Department of Business, Energy & Industrial Strategy, 2017b.

Department of Energy and Climate Change. Summary evidence on District Heating Networks in the UK. Technical report, Department of Energy & Climate Change, 2013.

Domínguez-Muñoz, F., Cejudo-López, J. M., Carrillo-Andrés, A., and Gallardo-Salazar, M. Selection of typical demand days for CHP optimization. *Energy and Buildings*, 43(11):3036–3043, 2011.

Dominković, D. F., Ćosić, B., Medić, Z. B., and Duić, N. A hybrid optimization model of biomass trigeneration system combined with pit thermal energy storage. *Energy conversion and management*, 104:90–99, 2015.

Duffie, J. A. and Beckman, W. A. *Solar Engineering of Thermal Processes*. Wiley, 2013. ISBN 0470873663.

Dunbabin, P., Charlick, H., and Green, R. *Detailed analysis from the second phase of the Energy Saving Trust's heat pump field trial*. Department of Energy and Climate Change, 2013.

Durão, B., Joyce, A., and Mendes, J. F. Optimization of a seasonal storage solar system using genetic algorithms. *Solar Energy*, 101:160–166, 2014.

Eames, P., Loveday, D., Haines, V., and Romanos, P. *The Future Role of Thermal Energy Storage in the UK Energy System: An Assessment of the Technical Feasibility and Factors Influencing Adoption - Research Report*. UKERC:London, 2014.

EDF Energy. Standard (Variable) Tariff Information, 2013. URL `https://my.edfenergy.com/product-closures-pdfs/SV-Tariff-Information.pdf`. Last accessed 14 September 2015.

Element Energy. Research on district heating and local approaches to heat decarbonisation. Technical report, Element Energy Ltd, 2015.

Evins, R. Multi-level optimization of building design , energy system sizing and operation. *Energy*, 90:1775–1789, 2015.

Evins, R., Orehounig, K., Dorer, V., and Carmeliet, J. New formulations of the 'energy hub' model to address operational constraints. *Energy*, 73:387–398, 2014.

Evins, R., Orehounig, K., and Dorer, V. Variability between domestic buildings: the impact on energy use. *Journal of Building Performance Simulation*, 9(2):162–175, 2016.

Fazlollahi, S. *Decomposition optimization strategy for the design and operation of district energy systems*. PhD thesis, École Polytechnique Fédérale de Lausanne, 2014.

Fazlollahi, S., Mandel, P., Becker, G., and Maréchal, F. Methods for multi-objective investment and operating optimization of complex energy systems. *Energy*, 45(1): 12–22, 2012.

Fazlollahi, S., Becker, G., and Maréchal, F. Multi-objectives, multi-period optimization of district energy systems: II–Daily thermal storage. *Computers & Chemical Engineering*, 71:648–662, 2014a.

Fazlollahi, S., Bungener, S. L., Mandel, P., Becker, G., and Maréchal, F. Multi-Objectives, Multi-Period Optimization of district energy systems: I-Selection of typical operating periods. *Computers & Chemical Engineering*, 65:54–66, 2014b.

Floudas, C. A. and Lin, X. Continuous-time versus discrete-time approaches for scheduling of chemical processes: a review. *Computers & Chemical Engineering*, 28(11):2109–2129, 2004.

Flynn, C. and Sirén, K. Influence of location and design on the performance of a solar district heating system equipped with borehole seasonal storage. *Renewable Energy*, 81:377–388, 2015.

Frangopoulos, C. A., Spakovsky, M. R. V., and Sciubba, E. A Brief Review of Methods for the Design and Synthesis Optimization of Energy Systems. *International Journal of Thermodynamics*, 5(4):151–160, 2002.

Fux, S. F., Benz, M. J., and Guzzella, L. Economic and environmental aspects of the component sizing for a stand-alone building energy system: A case study. *Renewable Energy*, 55:438–447, 2013.

Girardin, L., Marechal, F., Dubuis, M., Calame-Darbellay, N., and Favrat, D. EnerGis: A geographical information based system for the evaluation of integrated energy conversion systems in urban areas. *Energy*, 35(2):830–840, 2010.

Glover, F. Improved Linear Integer Programming Formulations of Nonlinear Integer Problems. *Management Science*, 22(4):455–460, 1975.

Government of Canada. Historical climate data, 2016. URL `http://climate.weather.gc.ca/`. Last accessed 13 October 2017.

Grossmann, I. E. and Biegler, L. T. Part II. Future perspective on optimization. *Computers & Chemical Engineering*, 28(8):1193–1218, 2004.

Grossmann, I. E. Advances in mathematical programming models for enterprise-wide optimization. *Computers and Chemical Engineering*, 47:2–18, 2012.

Grossmann, I. E. and Guillén-Gosálbez, G. Scope for the application of mathematical programming techniques in the synthesis and planning of sustainable processes. *Computers and Chemical Engineering*, 34(9):1365–1376, 2010.

Gueymard, C. A. and Wilcox, S. M. Assessment of spatial and temporal variability in the us solar resource from radiometric measurements and predictions from models using ground-based or satellite data. *Solar Energy*, 85(5):1068–1084, 2011.

Gurobi Optimization, Inc. Gurobi Optimization - The State-of-the-Art Mathematical Programming Solver, 2017. URL `http://http://www.gurobi.com/`. Last accessed 17 October 2017.

Harb, H., Reinhardt, J., Streblow, R., and Müller, D. Mip approach for designing heating systems in residential buildings and neighbourhoods. *Journal of Building Performance Simulation*, 9(3):316–330, 2016.

Hart, W. E., Laird, C., Watson, J.-P., and Woodruff, D. L. *Pyomo–optimization modeling in python*, volume 67. Springer Science & Business Media, 2012.

Hauer, A. Thermal Energy Storage: Technology Brief. Technical report, IEA-ETSAP and IRENA, 2013.

Hawkes, A. and Leach, M. Impacts of temporal precision in optimisation modelling of micro-Combined Heat and Power. *Energy*, 30(10):1759–1779, 2005.

Heat Network Partnership. Map - District Heating Scotland, 2017. URL `http://www.districtheatingscotland.com/map/`. Last accessed 22 October 2017.

Hedegaard, K. and Balyk, O. Energy system investment model incorporating heat pumps with thermal storage in buildings and buffer tanks. *Energy*, 63:356–365, 2013.

Hedegaard, K., Mathiesen, B. V., Lund, H., and Heiselberg, P. Wind power integration using individual heat pumps – Analysis of different heat storage options. *Energy*, 47 (1):284–293, 2012.

Heller, A. Heat-load modelling for large systems. *Applied Energy*, 72(1):371–387, 2002.

Hellström, G. *Ground heat storage: Thermal analyses of duct storage systems.* PhD thesis, Lund University, 1991.

Henze, G. P., Felsmann, C., and Knabe, G. Evaluation of optimal control for active and passive building thermal storage. *International Journal of Thermal Sciences*, 43 (2):173–183, 2004.

Hesaraki, A., Holmberg, S., and Haghighat, F. Seasonal thermal energy storage with heat pumps and low temperatures in building projects–A comparative review. *Renewable and Sustainable Energy Reviews*, 43:1199–1213, 2015.

Hewitt, N. J. Heat pumps and energy storage – The challenges of implementation. *Applied Energy*, 89(1):37–44, 2012.

Hoevenaars, E. J. and Crawford, C. A. Implications of temporal resolution for modeling renewables-based power systems. *Renewable Energy*, 41:285–293, 2012.

Holland, J. H. and Reitman, J. S. Cognitive systems based on adaptive algorithms. *Acm Sigart Bulletin*, (63):49–49, 1977.

Hsieh, S., Omu, A., and Orehounig, K. Comparison of solar thermal systems with storage : From building to neighbourhood scale. *Energy & Buildings*, 152:359–372, 2017.

IBM. IBM CPLEX Optimizer, 2017. URL `http://www-01.ibm.com/software/commerce/optimization/cplex-optimizer/index.html`. Last accessed 13 October 2017.

Ierapetritou, M. G. and Floudas, C. A. Effective Continuous-Time Formulation for Short-Term Scheduling. 1. Multipurpose Batch Processes. *Industrial & Engineering Chemistry Research*, 37(11):4341–4359, 1998a.

Ierapetritou, M. G. and Floudas, C. A. Effective continuous-time formulation for short-term scheduling. Part 2. Continuous and semicontinuous processes. *Industrial & Engineering Chemistry Research*, 37(11):4360–4374, 1998b.

Institution of Mechanical Engineers. Energy Storage: The Missing Link in the UK's Energy Commitments. Technical report, Institution of Mechanical Engineers, 2014.

Intergovernmental Panel on Climate Change. Mitigation of Climate Change. Contribution of Working Group III to the Fifth Assessment Report of the Intergovernmental Panel on Climate Change. *Cambridge University Press, Cambridge, UK and New York, NY*, 2014.

International Energy Agency. *Technology Roadmap Energy Storage*. International Energy Agency, 2014.

Jordan, U. and Vajen, K. DHWcalc: Program to generate domestic hot water profiles with statistical means for user defined conditions. In *ISES Solar World Congress*, Orlando, USA, 2005.

Kandiah, P. and Lightstone, M. F. Modelling of the thermal performance of a borehole field containing a large buried tank. *Geothermics*, 60:94–104, 2016.

Kane, T., Firth, S., and Lomas, K. How are UK homes heated? A city-wide, socio-technical survey and implications for energy modelling. *Energy and Buildings*, 86: 817–832, 2014.

Kargarian, A., Hug, G., and Mohammadi, J. A Multi-Time Scale Co-Optimization Method for Sizing of Energy Storage and Fast-Ramping Generation. *IEEE Transactions on Sustainable Energy*, 7(4):1351–1361, 2016.

Keirstead, J., Jennings, M., and Sivakumar, A. A review of urban energy system models: Approaches, challenges and opportunities. *Renewable and Sustainable Energy Reviews*, 16(6):3847–3866, 2012.

Kelly, N. J., Tuohy, P. G., and Hawkes, A. D. Performance assessment of tariff-based air source heat pump load shifting in a UK detached dwelling featuring phase change-enhanced buffering. *Applied Thermal Engineering*, 71(2):809–820, 2014.

Kelly, S., Shipworth, M., Shipworth, D., Gentry, M., Wright, A., Pollitt, M., Crawford-Brown, D., and Lomas, K. Predicting the diversity of internal temperatures from the English residential sector using panel methods. *Applied Energy*, 102:601–621, 2013.

Kensby, J., Trüschel, A., and Dalenbäck, J.-O. Potential of residential buildings as thermal energy storage in district heating systems – Results from a pilot test. *Applied Energy*, 137:773–781, 2014.

Kingspan Environmental. Kingspan Albion | Kingspan Hot Water, 2017. URL `https://www.kingspanenviro.com/kingspan-albion`. Last accessed 13 October 2017.

Klatt, K.-U. and Marquardt, W. Perspectives for process systems engineeringâĂŤpersonal views from academia and industry. *Computers & Chemical Engineering*, 33(3): 536–550, 2009.

Klein, S. *et al.* TRNSYS 18: A Transient Systems Simulation Program, Solar Energy Laboratory, University of Wisconsin, Madison, USA, 2017. URL `http://www.sel.me.wisc.edu/trnsys`.

Land, A. H. and Doig, A. G. An Automatic Method of Solving Discrete Programming Problems. *Econometrica*, 28(3):497–520, 1960.

Lauinger, D., Caliandro, P., Van herle, J., and Kuhn, D. A linear programming approach to the optimization of residential energy systems. *Journal of Energy Storage*, 7:24–37, 2016.

Leidos Canada. *Drake Landing Solar Community, Annual Performance Monitoring Report for 2012-2013*. Leidos Canada, 2014. URL `http://dlsc.ca/reports/JUL2015/2012-2013%20Annual%20Report%20v07%20FINAL.pdf`. Last accessed 13 October 2017.

Lindenberger, D., Bruckner, T., Groscurth, H.-M., and Kummel, R. Optimization of solar district heating systems : seasonal storage , heat pumps , and cogeneration. *Energy*, 25:591–608, 2000.

Lizana, J., Ortiz, C., Soltero, V. M., and Chacartegui, R. District heating systems based on low-carbon energy technologies in mediterranean areas. *Energy*, 120:397–416, 2017.

Lucon, O., Ürge-Vorsatz, D., Ahmed, A. Z., Akbari, H., Bertoldi, P., Cabeza, L., Eyre, N., Gadgil, A., Harvey, L., Jiang, Y., *et al.* Buildings. In Edenhofer, O., Pichs-Madruga, R., Sokona, Y., *et al.*, editors, *Climate Change 2014: Mitigation of Climate Change. Contribution of Working Group III to the Fifth Assessment Report of the Intergovernmental Panel on Climate Change*. Cambridge University Press, 2014.

Lund, H., Arler, F., Østergaard, P. A., Hvelplund, F., Connolly, D., Mathiesen, B. V., and Karnøe, P. Simulation versus optimisation: Theoretical positions in energy system modelling. *Energies*, 10(7):840, 2017.

Lund, P. Optimization of a community solar heating system with a heat pump and seasonal storage. *Solar Energy*, 33(3-4):353–361, 1984.

MacLean, K., Sansom, R., Watson, T., and Gross, R. Managing Heat System Decarbonisation – Comparing the impacts and costs of transitions in heat infrastructure. Technical report, Centre for Energy Policy and Technology, Imperial College London, 2016.

Makhorin, A. GLPK (GNU Linear Programming Kit), 2012. URL `https://www.gnu.org/software/glpk/`. Last accessed 17 October 2017.

Mauthner, F. and Herkel, S. Technology and Demonstrators. Technical Report Subtask C - Part C1. Technical report, Task 52 Solar Heat and Energy Economics in Urban Environments. IEA Solar Heating & Cooling Programme., 2016.

Mavrotas, G., Florios, K., and Vlachou, D. Energy planning of a hospital using Mathematical Programming and Monte Carlo simulation for dealing with uncertainty in the economic parameters. *Energy Conversion and Management*, 51(4):722–731, 2010.

McDowell, T. P. and Thornton, J. W. Simulation and model calibration of a large-scale solar seasonal storage system. *Third national conference of IBPSA-USA*, pages 174–181, 2008.

McTigue, J. D., White, A. J., and Markides, C. N. Parametric studies and optimisation of pumped thermal electricity storage. *Applied Energy*, 137:800–811, 2015.

Met Office. *MIDAS: UK Hourly Weather Observation Data*. NCAS British Atmospheric Data Centre, 2006. URL `http://catalogue.ceda.ac.uk/uuid/916ac4bbc46f7685ae9a5e10451bae7c`. Last accessed 13 October 2017.

Meteotest. Meteonorm: Irradiation data for every place on Earth, 2017. URL `http://www.meteonorm.com/`. Last accessed 22 October 2017.

Miró, L., Gasia, J., and Cabeza, L. F. Thermal energy storage (TES) for industrial waste heat (IWH) recovery : A review. *Applied Energy*, 179:284–301, 2016.

Misener, R. and Floudas, C. A. ANTIGONE: Algorithms for coNTinuous / Integer Global Optimization of Nonlinear Equations. *Journal of Global Optimization*, 59 (2-3):503–526, 2014.

Mitra, S., Pinto, J. M., and Grossmann, I. E. Optimal multi-scale capacity planning for power-intensive continuous processes under time-sensitive electricity prices and demand uncertainty. Part I: Modeling. *Computers & Chemical Engineering*, 65:89–101, 2014.

Mitsubishi Electric. ecodan Renewable Heating Technology Data Book, 2013. URL `http://library.mitsubishielectric.co.uk/pdf/book/Ecodan_PUHZ_Databook_FTC4`. Last accessed 13 October 2017.

Murat Sen, S., Dumesic, J. a., and Maravelias, C. T. A Superstructure-Based Framework for Simultaneous Process Synthesis, Heat Integration, and Utility Plant Design. *Computer Aided Chemical Engineering*, 37:1391–1396, 2015.

National Resources Canada. Drake landing satellite solar resource data, 2015. URL `ftp://ftp.nrcan.gc.ca/energy/SOLAR/DrakeLanding_SatteliteSolarResourceData/`. Last accessed 13 October 2017.

Nordell, B., Scorpo, A. L., Andersson, O., Rydell, L., and Carlsson, B. Long-term Long Term Evaluation of Operation and Design of the Emmaboda BTES.: Operation and Experiences 2010-2015. Technical report, Luleå Tekniska Universitet, 2016.

Novo, A. V., Bayon, J. R., Castro-Fresno, D., and Rodriguez-Hernandez, J. Review of seasonal heat storage in large basins: Water tanks and gravel-water pits. *Applied Energy*, 87(2):390–397, 2010.

Nuytten, T., Claessens, B., Paredis, K., Van Bael, J., and Six, D. Flexibility of a combined heat and power system with thermal energy storage for district heating. *Applied Energy*, 104:583–591, 2013.

Ochs, F., Heidemann, W., and Müller-Steinhagen, H. Performance of Large-Scale Seasonal Thermal Energy Stores. *Journal of Solar Energy Engineering*, 131(4): 041005–1 – 041005–7, 2009.

Ofgem. Domestic Renewable Heat Incentive, 2017. URL `https://www.ofgem.gov.uk/environmental-programmes/domestic-renewable-heat-incentive`. Last accessed 13 October 2017.

Olsthoorn, D., Haghighat, F., and Mirzaei, P. a. Integration of storage and renewable energy into district heating systems: A review of modelling and optimization. *Solar Energy*, 136:49–64, 2016.

Omu, A., Hsieh, S., and Orehounig, K. Mixed integer linear programming for the design of solar thermal energy systems with short-term storage. *Applied Energy*, 180: 313–326, 2016.

Ortiga, J., Bruno, J., and Coronas, A. Selection of typical days for the characterisation of energy demand in cogeneration and trigeneration optimisation models for buildings. *Energy Conversion and Management*, 52(4):1934–1942, 2011.

Pan, W. and Cooper, M. Decision criteria for selecting air source heat pump technology in uk low carbon housing. *Technology Analysis & Strategic Management*, 23(6):623–637, 2011.

Papoulias, S. A. and Grossmann, I. E. A structural optimization approach in process synthesis–III. *Computers & Chemical Engineering*, 7(6):723–734, 1983.

Patteeuw, D., Bruninx, K., Arteconi, A., Delarue, E., D'haeseleer, W., and Helsen, L. Integrated modeling of active demand response with electric heating systems coupled to thermal energy storage systems. *Applied Energy*, 151:306–319, 2015.

Pavlov, G. K. and Olesen, B. W. Thermal energy storage – A review of concepts and systems for heating and cooling applications in buildings : Part 1 – Seasonal storage in the ground. *HVAC&R Research*, 18(3):515–538, 2012.

Perez-Mora, N., Bava, F., Andersen, M., Bales, C., Lennermo, G., Nielsen, C., Furbo, S., and Martínez-Moll, V. Solar district heating and cooling : A review. *International Journal of Energy Research*, pages 1–23, 2017.

Pinel, P., Cruickshank, C. a., Beausoleil-Morrison, I., and Wills, A. A review of available methods for seasonal storage of solar thermal energy in residential applications. *Renewable and Sustainable Energy Reviews*, 15(7):3341–3359, 2011.

Prasanna, A. and Dorer, V. Optimisation of a district energy system with a low temperature network. *Energy*, pages 1–17, 2017.

Quintana, H. J. A Practical Approach to Model Predictive Control (MPC)for Solar Communities. Master's thesis, École Polytechnique de Montréal, 2013.

Quintana, H. J. and Kummert, M. Optimized control strategies for solar district heating systems. *Journal of Building Performance Simulation*, 8(2):79–96, 2015.

Rad, F. M. and Fung, A. S. Solar community heating and cooling system with borehole thermal energy storage - Review of systems. *Renewable and Sustainable Energy Reviews*, 60:1550–1561, 2016.

Radcliffe, J. and Li, Y. Thermal energy storage in Scotland. Technical report, University of Birmingham, 2015.

Rager, J. M. F. *Urban Energy System Design from the Heat Perspective using mathematical programming including thermal storage.* PhD thesis, École Polytechnique Fédérale de Lausanne, 2015.

Raine, R. D., Sharifi, V. N., and Swithenbank, J. Optimisation of combined heat and power production for buildings using heat storage. *Energy Conversion and Management*, 87:164–174, 2014.

Renaldi, R. and Friedrich, D. Multiple time grids in operational optimisation of energy systems with short- and long-term thermal energy storage. *Energy*, 133:784–795, 2017.

Renaldi, R., Kiprakis, A., and Friedrich, D. An optimisation framework for thermal energy storage integration in a residential heat pump heating system. *Applied Energy*, 186:520–529, 2017.

Rieder, A., Christidis, A., and Tsatsaronis, G. Multi criteria dynamic design optimization of a small scale distributed energy system. *Energy*, 74:230–239, 2014.

Robineau, J., Page, J., and Marechal, F. A Method for Taking Into Account Seasonal Storage in a District Energy System Optimisation Problem. In *The 15th International Symposium on District Heating and Cooling*, 2016.

Rogers, J., Cooper, S., O'Grady, A., McManus, M., Howard, H., and Hammond, G. The 20% house – An integrated assessment of options for reducing net carbon emissions from existing UK houses. *Applied Energy*, 138:108–120, 2015.

Rysanek, A. M. Second law performance analysis of a large thermal energy storage vessel using CFD. Master's thesis, Queen's University, 2009.

Samsatli, S. and Samsatli, N. J. A general spatio-temporal model of energy systems with a detailed account of transport and storage. *Computers & Chemical Engineering*, 80: 155–176, 2015.

Schütz, T., Streblow, R., and Müller, D. A comparison of thermal energy storage models for building energy system optimization. *Energy and Buildings*, 93:23–31, 2015.

Schütz, T., Schiffer, L., Harb, H., Fuchs, M., and Müller, D. Optimal design of energy conversion units and envelopes for residential building retrofits using a comprehensive milp model. *Applied Energy*, 185:1–15, 2017.

Shaarawy, M. Numerical Analysis of Thermal Stratification in Large Horizontal Thermal Energy Storage Tanks. Master's thesis, McMaster University, 2014.

Shaarawy, M. and Lightstone, M. Numerical analysis of thermal stratification in large horizontal thermal energy storage tanks. *Journal of Solar Energy Engineering*, 138 (2):021009–1 – 021009–13, 2016.

Shiba, T., Yokoyama, R., and Ito, K. Optimal sizing of a heat pump/thermal storage system based on the linear programming method. *International journal of energy research*, 19(8):665–674, 1995.

Sibbitt, B., Mcclenahan, D., Djebbar, R., Thornton, J., Wong, B., Carriere, J., and Kokko, J. Measured and simulated performance of a high solar fraction district heating system with seasonal storage. *Proceedings of 30th Ises Biennial Solar World Congress 2011, Swc 2011*, pages 3037–3048, 2011.

Sibbitt, B., McClenahan, D., Djebbar, R., Thornton, J., Wong, B., Carriere, J., and Kokko, J. The performance of a high solar fraction seasonal storage district heating system - Five years of operation. *Energy Procedia*, 30:856–865, 2012.

Singh, H., Muetze, A., and Eames, P. C. Factors influencing the uptake of heat pump technology by the UK domestic sector. *Renewable Energy*, 35(4):873–878, 2010.

Soares, N., Costa, J., Gaspar, A., and Santos, P. Review of passive pcm latent heat thermal energy storage systems towards buildings' energy efficiency. *Energy and buildings*, 59:82–103, 2013.

Söderman, J. and Pettersson, F. Structural and operational optimisation of distributed energy systems. *Applied Thermal Engineering*, 26(13):1400–1408, 2006.

Solargis. Free download of global and regional solar resource maps / Overview | Solargis, 2017. URL `http://solargis.com/products/maps-and-gis-data/free/overview/`. Last accessed 22 October 2017.

Solites. Saisonalspeicher.de - das wissensportal für die saisonale wärmespeicherung, 2014. URL `http://www.saisonalspeicher.de/`. Last accessed 13 October 2017.

Stadler, P., Ashouri, A., and Maréchal, F. Model-based optimization of distributed and renewable energy systems in buildings. *Energy and Buildings*, 120:103–113, 2016.

Staffell, I., Brett, D., Brandon, N., and Hawkes, A. A review of domestic heat pumps. *Energy & Environmental Science*, 5(11):9291, 2012.

Stinner, S., Huchtemann, K., and Müller, D. Quantifying the operational flexibility of building energy systems with thermal energy storages. *Applied Energy*, 181:140–154, 2016.

Summerfield, A. J., Lowe, R., Bruhns, H., Caeiro, J., Steadman, J., and Oreszczyn, T. Milton keynes energy park revisited: Changes in internal temperatures and energy usage. *Energy and Buildings*, 39(7):783–791, 2007.

Swan, L. G. and Ugursal, V. I. Modeling of end-use energy consumption in the residential sector: A review of modeling techniques. *Renewable and Sustainable Energy Reviews*, 13(8):1819–1835, 2009.

Tassou, S., Marquand, C., and Wilson, D. Energy and Economic Comparisons of Domestic Heat Pumps and Conventional Heating Systems in the British Climate. *Applied Energy*, 24:127–138, 1986.

Tawarmalani, M. and Sahinidis, N. V. A polyhedral branch-and-cut approach to global optimization. *Mathematical Programming*, 103:225–249, 2005.

Taylor, P., Bolton, R., Stone, D., Zhang, X.-P., Martin, C., and Upham, P. *Pathways for energy storage in the UK*. Centre for Low Carbon Futures, 2012.

The Green Age. How much energy does my home use? - TheGreenAge, 2015. URL `https://www.thegreenage.co.uk/how-much-energy-does-my-home-use/`. Last accessed 23 October 2017.

The Scottish Government. Heat Policy Statement - Towards Decarbonising Heat: Maximising the Opportunities for Scotland. Technical report, The Scottish Government, 2015.

Thomas, J. and Charlick, H. Analysis of data from 23 Mitsubishi heat pump properties. Technical report, Energy Saving Trust in partnership with Kiwa GASTEC at CRE, 2013.

Tulus, V., Boer, D., Cabeza, L. F., Jiménez, L., and Guillén-Gosálbez, G. Enhanced thermal energy supply via central solar heating plants with seasonal storage: A multi-objective optimization approach. *Applied Energy*, 181:549–561, 2016.

Tveit, T.-M., Savola, T., Gebremedhin, A., and Fogelholm, C.-J. Multi-period MINLP model for optimising operation and structural changes to CHP plants in district heating networks with long-term thermal storage. *Energy Conversion and Management*, 50(3):639–647, 2009.

UK Energy Research Centre. UKERC Energy Data Centre, 2015. URL `http://ukedc.rl.ac.uk/`. Last accessed 13 October 2017.

Velez, S. and Maravelias, C. T. Multiple and nonuniform time grids in discrete-time MIP models for chemical production scheduling. *Computers and Chemical Engineering*, 53:70–85, 2013.

Velez, S. and Maravelias, C. T. Theoretical framework for formulating MIP scheduling models with multiple and non-uniform discrete-time grids. *Computers & Chemical Engineering*, 72:233–254, 2014.

Verhelst, C., Degrauwe, D., Logist, F., Van Impe, J., and Helsen, L. Multi-objective optimal control of an air-to-water heat pump for residential heating. *Building Simulation*, 5(3):281–291, 2012a.

Verhelst, C., Logist, F., Van Impe, J., and Helsen, L. Study of the optimal control problem formulation for modulating air-to-water heat pumps connected to a residential floor heating system. *Energy and Buildings*, 45:43–53, 2012b.

Verstraete, A. Étude d'une communauté solaire avec stockage thermique saisonnier par puits géothermiques. Master's thesis, Polytechnique Montréal, 2013.

Vesterlund, M., Toffolo, A., and Dahl, J. Optimization of multi-source complex district heating network , a case study. *Energy*, 126:53–63, 2017.

Voll, P. *Automated optimization-based synthesis of distributed energy supply systems*. PhD thesis, RWTH Aachen, 2013.

Wakui, T. and Yokoyama, R. Optimal structural design of residential cogeneration systems in consideration of their operating restrictions. *Energy*, 64:719–733, 2014.

Wakui, T. and Yokoyama, R. Impact analysis of sampling time interval and battery installation on optimal operational planning of residential cogeneration systems without electric power export. *Energy*, 2015.

Walker, S. Energy Use in the Home - Measuring and Analysing Domestic Energy Use and Energy Efficiency in Scotland. Technical report, Scottish House Condition Survey, 2012.

Wallerand, A. S., Selviaridis, A., Ashouri, A., and Maréchal, F. Targeting Optimal Design and Operation of Solar Heated Industrial Processes: A MILP Formulation. *Energy Procedia*, 91:668–680, 2016.

Wang, S. and Baldea, M. Temperature Control and Optimal Energy Management using Latent Energy Storage. *Industrial & Engineering Chemistry Research*, 52(9): 3247–3257, 2013.

Weiss, W., Spörk-Dür, M., and Mauthner, F. Solar heat worldwide: Global market development and trends in 2016 | detailed market figures 2015. *IEA Solar Heating and Cooling Programme*, 2017.

Werner, S. International review of district heating and cooling. *Energy*, 137:617–631, 2017.

Westaway, R. Repurposing of disused shale gas wells for subsurface heat storage: preliminary analysis concerning uk issues. *Quarterly Journal of Engineering Geology and Hydrogeology*, 49(3):213–227, 2016.

White, A., Parks, G., and Markides, C. N. Thermodynamic analysis of pumped thermal electricity storage. *Applied Thermal Engineering*, 53(2):291–298, 2013.

Winkelman, J. R., Chow, J. H., Allemong, J. J., and Kokotovic, P. V. Multi-Time-Scale Analysis of a Power System. *Automatica*, 16:35–43, 1980.

World Energy Council. World Energy Resources E-Storage | 2016. Technical report, World Energy Council, 2016.

Xu, J., Wang, R., and Li, Y. A review of available technologies for seasonal thermal energy storage. *Solar Energy*, 103:610–638, 2014.

Yang, L., Entchev, E., Rosato, A., and Sibilio, S. Smart Thermal Grid with Integration of Distributed and Centralized Solar Energy Systems. *Energy*, 122:471–481, 2017.

Yao, R. and Steemers, K. A method of formulating energy load profile for domestic buildings in the UK. *Energy and Buildings*, 37(6):663–671, 2005.